DakoCytomation

CyAn™ ADP User Guide

Document Number 0000050

Revision B

September 2004

Copyright © 2004 DakoCytomation. All rights reserved.

This document may not be copied in whole or in part or reproduced in any other media without the express written permission of DakoCytomation. Please note that under copyright law, copying includes translation into another language.

The CyAn Advanced Digital Processing (ADP) High-Performance Flow Cytometer is a research tool engineered for precision analysis of cells, bacteria, and other similarly sized particles. With CyAn ADP, DakoCytomation sets a new industry standard with a combination of features never before available on a bench-top analyzer. CyAn ADP gives users three excitation lines with independent, alignment-free focusing optics, simultaneous 9 color and 2 scatter parameters, analysis rates of 50,000 events per second, a full 9 × 9 interlaser compensation matrix, and high sensitivity. The result is stable, user-friendly, and flexible technology. The instrument is optimized for cell cycle, kinetics, fluorescent protein work, and multi-color immunophenotyping. Rare-event analysis, such as MHC Dextramers (Tdex™) studies, and no-lyse whole blood applications are easily performed on the CyAn ADP. The instrument also provides simplified compensation before, during, and after acquisition with unequaled sensitivity in all fluorescent channels.

Contacting DakoCytomation

DakoCytomation should be contacted immediately for assistance in the event of any instrument malfunction. For further information please contact your local DakoCytomation office.

Australia
Tel. 2 9316 4633
Fax 2 9316 4773

Austria
Tel. 0800 0800 7153
Fax 0800 0800 7154

Belgium
Tel. 016 38 72 20
Fax 016 38 72 21

Canada
Tel. 905 858 8510
Fax 905 858 8801

Czech Republic
Tel. 420 541 423 710
Fax 420 541 423 711

Denmark
Head Office
Tel. 44 85 95 00
Fax 44 85 95 95

Sales
Tel. 44 85 97 56
Fax 44 85 84 29

France
Tel. 1 30 50 00 50
Fax 1 30 50 00 11

Germany
Tel. 040 69 69 470
Fax 040 69 52 741

Italy
Tel. 02 58 078 1
Fax 02 58 078 292

Japan
Tel. 075 211 3655
Fax 075 211 1755

The Netherlands
Tel. 020 42 11 100
Fax 020 42 11 101

Norway
Tel. 23 14 05 40
Fax 23 14 05 42

Poland
Tel. 058-661 1879
Fax 058-661 3390

Spain
Tel. 93 499 05 06
Fax 93 499 02 08

Sweden
Tel. 08 556 20 600
Fax 08 556 20 619

Switzerland
Tel. 041 760 11 66
Fax 041 760 11 77

United Kingdom
Tel. (0)1 353 66 99 11
Fax (0)1 353 66 89 89
Technical Support
Tel. (0) 1 353 66 99 65

United States of America
Carpinteria, California
Tel. 805 566 6655
Fax 805 566 6688

Technical Support
Tel. 800 424 0021

Customer Service
Tel. 800 235 5763

United States of America
Fort Collins, Colorado
Flow Instrumentation
Tel. 800 822 9902
Fax 970 226 0107

User Resources

For the latest information on DakoCytomation products and services, please visit the DakoCytomation Web site at http://www.dakocytomation.com.

Scope

This guide provides a detailed discussion of the architecture and operating procedures for the CyAn™ ADP High-Performance Flow Cytometer. Detailed operating instructions for Summit® software can be found in the Summit® online help system. The information contained in this document can be applied to all CyAn products.

Disclaimers

This document is not a substitute for the detailed operator training provided by DakoCytomation or for other advanced instruction in general cytometric techniques. It is essential that the operator have a working knowledge of Microsoft® Windows XP® or current Operating System prior to using this guide. DakoCytomation also recommends the use of all of the networking services provided in the individual operator's laboratory. Although daily maintenance and routine instrument adjustments are discussed here, your local DakoCytomation Technical Service Group should be contacted immediately for assistance in the event of any instrument malfunction.

Trademarks

Microsoft® and Windows XP® are registered trademarks of Microsoft Corporation. Macintosh™ is a registered trademark of Apple, Inc. MoFlo® is a registered trademark of DakoCytomation. CyAn™, Summit™, SpectrAlign™, and SpectraComp™ are trademarks of DakoCytomation. All other trade names and trademarks are the property of their respective holders.

Table of Contents

User Resources v
Scope v
Disclaimers v
Trademarks v
Table of Contents vii
Section 1 1
Safety 1
Laser Safety 2
Section 2 5
Installation 5
CyAn ADP Installation Requirements 5
General Laboratory Information 5
CyAn ADP Installation Requirements (UV Model) 6
General Laboratory Information 6
CyAn ADP (UV Model) Coherent Enterprise Laser Power Requirements 7
CyAn ADP (UV Model) Coherent Enterprise Laser Ambient Air and Cooling Water Specifications 8
CyAn ADP (UV Model) Heat Exchanger 8
Section 3 9
System Overview 9
CyAn ADP Features 9
CyAn ADP Subsystems 10
Fluidics 11
Optics 12
Electronics 16
Peripheral Devices 16
Software 16
Summit Features 18
Section 4 21
Startup and Shutdown Procedures 21
Startup Procedure 21
Required Reagents 21
CyAn ADP Startup 21
CyAn ADP Approved Cleaners and Disinfectants 24
Shutdown Procedure 25
Section 5 27
Fluids Management 27
Sheath Management System Indicators 27
Changing Out Sheath and Waste Containers 33
Replacing Cleaner Fluid 34
Section 6 35
CyAn™ ADP Maintenance 35
Daily Preventive Maintenance 35
Weekly Preventive Maintenance 35
SMS Clean & Rinse Cycle 35
Monthly Preventive Maintenance 35
Laser Interlock Maintenance Procedure 35
Annual Maintenance Procedure 36
Section 7 37
Troubleshooting 37
Section 8 39

Tutorials 39
Using Compensation 39
The argument against compensation 39
The argument for compensation 39
Hardware vs. Software Compensation 40
Hardware Compensation 40
Software Compensation 41
Digital Signal Processing (DSP) Compensation 42
Fluorescent Compensation 43
Background: Use in Flow Cytometry 43
Fluorescent "Cross-Contamination" in the Raw Measure 43
Compensation Preparation 45
Preparation Summary: 45
Completing the Compensation Matrix: Helpful Tips 46
Historical Compensation Calculation 46
Negative Compensation 47
Why Negative Compensation? 47
A Negative Compensation Example 48
An Alternative to Negative Compensation 51
Absolutely Perfect Compensation? 52
2-Color Compensation 54
Calculating Compensation Values 54
Justifying a Different Compensation Algorithm: Two-Color Example 55
2-Color Compensation Experiment 57
Goal of Compensation 58
How does this work with Dot Plots? 59
An Example Using Fluorescent Beads 64
Compensating the Data 64
Advanced Issues 67
3-Color Compensation 68
Calculating 3-Color Compensation Values 69
Proper Compensation: Pragmatics 70
5-Color Compensation Experiment 71
Background 71
Setting Up Histograms for Compensation 72
Running the First Sample 76
Setting Compensation 77
Running the Second Sample 78
Running the Remaining Samples 81
Running the "All Stains" Sample 87
Putting Compensation Into Practice 87
Pan Leucocytes + B-cells 88
Helper subset of the T-cell subset of white cells 89
Suppressor subset of the T-cell subset of white cells 89
White cells that are neither T or B cells. i.e. NK cells 90
Contour Plots 92
Contour Methods 93
Summary 94
Outlier Events 96
Display "All" Events 97
Data Resolution 98
The Analog Particle or Cell Signal 98
The Digital Signal and Software Data Display 99
Doublet Discrimination 105
Doublet Handling 105
Integrated Signal 105

Pulse Width ... 106
Finding Doublets using Color Gating ... 106
Methods of Doublet Discrimination ... 107
Histogram Scaling ... 108
Manual Scaling ... 109
Manual Scaling Options ... 109
Increment By ... 109
Set Fixed Scale ... 110
Auto Scaling ... 111
Auto Scaling Options ... 112
Subtraction Histograms ... 114
Controls Versus Samples ... 114
Subtraction Methods ... 116
Experimental and Biological Relevance ... 120
Appendix A ... 123
CyAn ADP Consumables ... 123
Appendix B ... 125
Technical and Instrument Specifications ... 125
Appendix C ... 133
Flow Cytometry References ... 133

SECTION 1

SAFETY

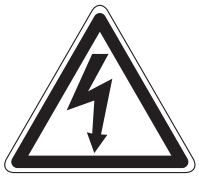

Electrical Safety

The DakoCytomation instrument product line conforms to international regulations encompassing the accessibility of high voltages by the user. In the United States, each flow cytometer is manufactured to comply with applicable regulations from the American National Standards Institute (ANSI), the Occupational Safety and Health Administration (OSHA), and various state regulatory organizations. Internationally, each CyAn™ ADP High-Performance Flow Cytometer is manufactured to comply with the International Electrotechnical Commission's Standard for Safety Requirements for Electrical Equipment for Measurement, Control and Laboratory Use (IEC 61010-1) and subsequent amendments.

Biohazard Safety

The CyAn ADP instrument may be used for the analysis of pathogenic or other harmful agents. These operations can constitute a biohazard for the operator as well as bystanders in the surrounding laboratory space. DakoCytomation does not certify any instrumentation for use with any hazardous organism or agent. DakoCytomation strongly recommends explicit guidance be obtained from the institutional or company biosafety officer prior to operating this instrument with any potentially hazardous organism or agent.

WARNING

If any biohazardous organism or agent is used in this instrument, the user must inform DakoCytomation in writing prior to any field service visit or the return of any part to DakoCytomation, or its vendors, for service. Safety of the CyAn ADP user and of all DakoCytomation employees is of primary concern. Proper decontamination procedures must be followed for returned parts.

WARNING

Wear Personal Protective Equipment in accordance with your laboratory safety procedures when operating or maintaining this instrument. Use of this instrument in a manner other than that specified in this manual may cause impairment of equipment and result in injury. Use of controls or adjustments or performance of procedures other than those specified in this manual may result in hazardous radiation exposure. This radiation will be in the UV or visible regions of the electromagnetic spectrum. Do not attempt to defeat the interlocks or open covers or panels retained with screws.

Laser Safety

The CyAn ADP instrument conforms to international regulations encompassing laser safety. The CyAn ADP is a Class 1 laser device.

CLASS 1 LASER PRODUCT
IEC/EN 60825 -1/A2:2001

This designation indicates no hazardous laser energy is accessible to the user during normal operation or during a failure mode.

Note Because the CyAn ADP has been designed to operate as a Class 1 Laser Device, the instrument must be operated with all light containment tubes in place and all protective light seals intact. Most laser components of the CyAn ADP flow cytometer are Class IIIB to Class IV. As such, these lasers have the potential to cause injury.

Certification of regulatory compliance of these lasers often requires significant involvement from the institutional or company laser-safety officer. DakoCytomation does not provide regulatory certification for the individual lab.

All access plates and other user accessible points of potential laser exposure are clearly designated on the CyAn ADP instrument with the labels illustrated in figures 1.1, 1.2, and 1.3 below. Interlocks are designed to prevent accidental irradiation of the operator. The user should not defeat these interlocks.

Figure 1.1: Laser Warning Label

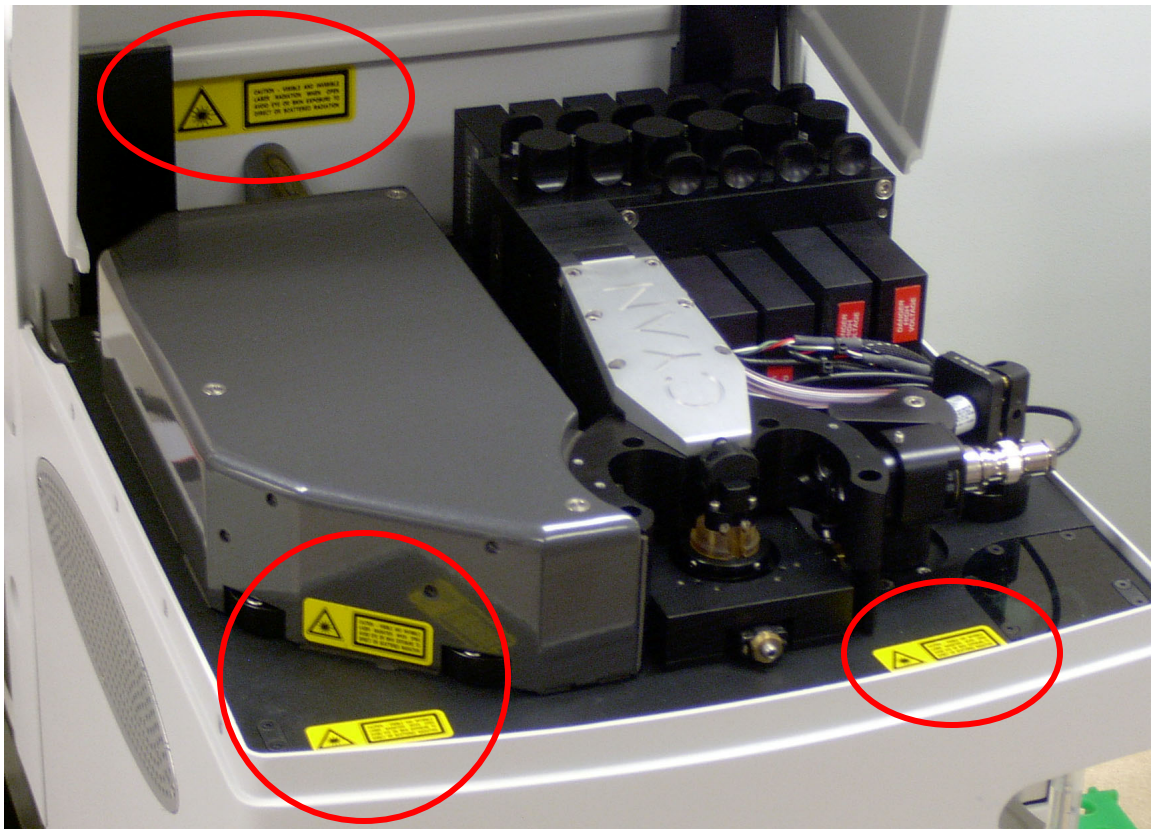

Figure 1.2: Interior Laser Warning Label Locations

Figure 1.3: Laser Warning on Rear of CyAn Unit

SECTION 2

INSTALLATION

CyAn ADP Installation Requirements

IMPORTANT
Your DakoCytomation representative is responsible for uncrating, installing, and initial set up of the CyAn ADP.

General Laboratory Information

Heating and air conditioning vents or fans are not recommended directly above the CyAn ADP because of the resulting temperature fluctuation, vibration, and possible dust.

Table 2.1: CyAn ADP Installation Requirements

General Requirements	
Power Requirements	100V – 240V, 600VA(W), 50/60 Hz
Lab Bench	Stable bench/table top to support the CyAn ADP, one or two monitors, keyboard, and a mouse pad
Service Access	45.7 cm (18 in) minimum around instrument components
Phone	Location near CyAn ADP for contacting technical support
Internet Access	Internet Service Provider or LAN connection for downloading software updates
Dimensions (not including Auxiliary Components)	Height front cover closed - 39.1 cm (15.4 in) front cover open – 72.1 cm (28.4 in) Width - 33.3 cm (13.1 in) Depth - 49.8 cm (19.6 in) with clearance for cables – 62.5 cm (24.6 in) Weight - 36.3 kg (80 lbs)
Auxiliary Components	

Sheath Management System (with casters): Houses sheath container, waste container, cleaner fluid container, air compressor, and vacuum	Height – 61.3 cm (24.2 in) Width - 73.3 cm (28.9 in) Depth – 61.9 cm (24.4 in) Weight – 22.6 kg (50 lbs)
Summit Workstation	Height – 42.9 cm (16.9 in) Width – 19.1 cm (7.5 in) Depth – 45.7 cm (18.0 in) Weight – 10.5 kg (23 lbs)
Uninterruptible Power Supply	Height – 20.3 cm (7.9 in) Width – 14.7 cm (5.7 in) Depth – 44.5 cm (17.5 in) Weight – 20 kg (44 lbs)
Operating Environment	
Ambient Temperature	15 to 30°C (59 to 86°F) For optimum performance maintain at +/- 2°C
Relative Humidity	20 to 80% RH (non-condensing)

CyAn ADP Installation Requirements (UV Model)

General Laboratory Information

Heating and air conditioning vents or fans are not recommended directly above the CyAn ADP because of the resulting temperature fluctuation, vibration, and possible dust.

Table 2.2: CyAn ADP Installation Requirements (UV Model)

General Requirements	
Power Requirements	100V – 240V, 600VA(W), 50/60 Hz
Lab Bench	Stable bench/table top to support the CyAn ADP, one or two monitors, keyboard, and a mouse pad
Service Access	45.7 cm (18 in) minimum around instrument components
Phone	Location near CyAn ADP for contacting technical support

General Requirements	
Internet Access	Internet Service Provider or LAN connection for downloading software updates
Dimensions (not including Auxiliary Components)	Height front cover closed - 39.1 cm (15.4 in) front cover open – 72.1 cm (47.0 in) Width – 119.4 cm (13.1 in) Depth – 59.2 cm (23.3 in) with clearance for cables – 132.1 cm (52.0 in) Weight – 86.5 kg (190 lbs)
Auxiliary Components	
Sheath Management System (with casters): Houses sheath container, waste container, cleaner fluid container, air compressor, and vacuum	Height – 61.3 cm (24.2 in) Width - 73.3 cm (28.9 in) Depth – 61.9 cm (24.4 in) Weight – 52 kg (115 lbs)
Summit Workstation	Height – 42.9 cm (16.9 in) Width – 19.1 cm (7.5 in) Depth – 45.7 cm (18.0 in) Weight – 10.5 kg (23 lbs)
Uninterruptible Power Supply	Height – 20.3 cm (7.9 in) Width – 14.7 cm (5.7 in) Depth – 44.5 cm (17.5 in) Weight – 20 kg (44 lbs)
Operating Environment	
Ambient Temperature	15 to 30°C (59 to 86°F) For optimum performance maintain at +/- 2°C
Relative Humidity	20 to 80% RH (non-condensing)

CyAn ADP (UV Model) Coherent Enterprise Laser Power Requirements

A dedicated 208-240V single phase 50 amp circuit is required. The laser is hardwired into a junction box with fused disconnect. The junction box must be within 6 feet of the CyAn ADP. An electrician must be available to connect and ensure adequate power for the Enterprise laser on the first day of CyAn ADP installation.

CyAn ADP (UV Model) Coherent Enterprise Laser Ambient Air and Cooling Water Specifications

The Enterprise laser is a water-cooled laser that requires very stable temperatures of the ambient air and the cooling water.

CyAn ADP (UV Model) Heat Exchanger

The CyAn ADP UV model comes with a Coherent Laser Pure 5 (LP5) water-to-air heat exchanger. The LP5 generates 17,000 BTU/hour that needs to be dissipated as efficiently as possible. Laser stability is dependent on the constant temperature of the water circulating through the laser cavity.

Because the water is cooled through a water-to-air heat exchanger, the ambient temperature and humidity must be constant. Heating and air conditioning vents or fans are not recommended directly above the CyAn ADP UV model because of the resulting temperature fluctuation. Table 2.3 lists some helpful guidelines for optimum laser performance.

Table 2.3: Coherent LP5 Optimum Conditions

Item	Description
Ambient Temperature Specification	+/- 2°C
Heat Dissipation	One meter (3 ft) of clearance on all sides for proper air flow. If the laboratory containing the CyAn ADP is too small or the air conditioning not adequate to maintain +/- 2°C, the LP5 comes with 25 ft of hose that allows for the heat exchanger to be placed in an adjacent room. The adjacent room must have thermal stability. The water hoses to the heat exchanger cannot be greater than 50 ft long.
Other Options	The cooling hoses can be hooked up to a variety of heat exchange systems or “chillers.” The water system cooling the laser should be 10-35°C with stability of +/- 1%.

Section 3

System Overview

The CyAn ADP™ is a state-of-the-art flow cytometer that utilizes one or more laser excitation sources to analyze biological cells, beads, or other microscopic particles as they are transported through an interrogation point in single file. Information can be gathered from large numbers of particles in a relatively short time so that populations can be studied or differentiated from other populations using simple to complex statistical methods. Physical and biochemical characteristics that can be measured using this instrument include but are not limited to forward scatter (size-related), side scatter (morphology-related), fluorescence from tagged (stained) cells/particles, and auto fluorescence from non-stained cells/particles.

CyAn ADP Features

The CyAn ADP High-Performance Flow Cytometer is a research tool engineered for precision analysis of cells, bacteria, and other similarly sized particles. With CyAn ADP, DakoCytomation sets a new industry standard with a combination of features never before available on a bench-top analyzer. CyAn ADP gives users three excitation lines with independent, alignment-free focusing optics, simultaneous 9 color and 2 scatter parameters, analysis rates of 50,000 events per second, a full 9 × 9 interlaser compensation matrix, and high sensitivity. The result is stable, user-friendly, and flexible technology. The instrument is optimized for cell cycle, kinetics, fluorescent protein work, and multi-color immunophenotyping. Rare-event analysis, such as MHC Dextramers (Tdex™) studies, and no-lyse whole blood applications are easily performed on the CyAn ADP. The instrument also provides simplified compensation before, during, and after acquisition with unequaled sensitivity in all fluorescent channels.

The main features of CyAn ADP include:

Walk-Up Operation
CyAn ADP offers walk-up, push-button operation that puts even a novice user at ease. With no optical alignment necessary, the user simply places a 5 mL sample tube in the tube holder and chooses the desired protocol in Summit Software. The software is used to control instrument settings.

Bench-Top Configuration
The CyAn ADP was designed with today's laboratories in mind. The CyAn ADP measures 30 cm wide x 45 cm deep x 40 cm high and the CyAn UV Model measures 120 cm wide x 60 cm deep x 40 cm high.

Summit Software
Summit Software, DakoCytomation's premier cytometry software product, offers full control of all CyAn ADP functions, coupled with robust user- and application-specific data acquisition, analysis, storage, reduction, and retrieval. Summit controls all instrument parameters in an intuitive MS

Windows®-based drag-and-drop environment using simple protocol-based menus. Summit also provides high-content data acquisition, database capabilities, and open architecture for data exchange. Additional features include off-line analysis and easy page layout.

Safety
The CyAn ADP High-Performance Cell/Bead Analyzer has been designed to incorporate the highest level of laboratory and operator safety.

CyAn ADP Subsystems

CyAn ADP has four key subsystems that form a powerful research tool. The four subsystems are:

Fluidics
Optics
Electronics
Software

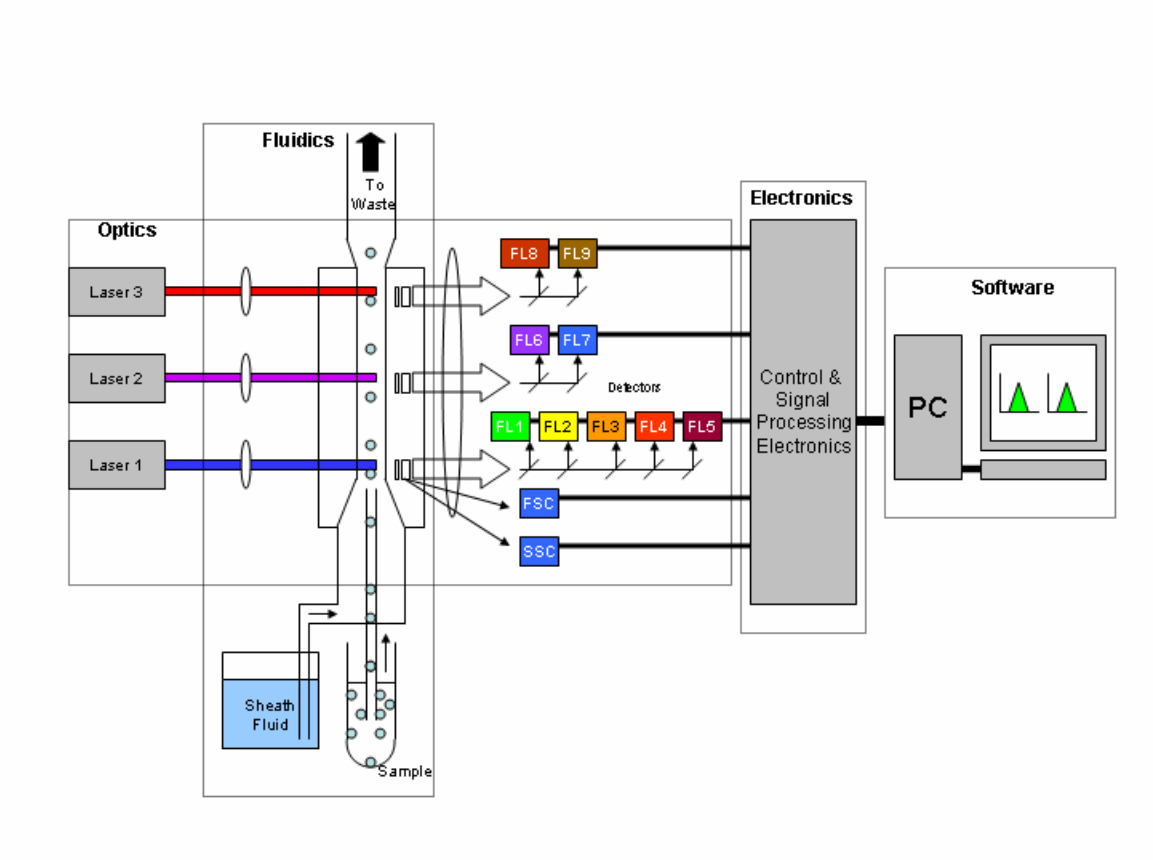

Figure 3.1: CyAn ADP Functional Block Diagram

A functional block diagram for the CyAn ADP High-Performance Flow Cytometer is shown in figure 3.1. The fluidics system pressurizes the system and transports particles to the interrogation point. Lasers are used as excitation sources and their beams, along with the ensuing scatter and fluorescence, are directed within the optical system. Electronics are used to power and control the instrument functions. The software provides the user interface for the above fluidics, optical,

and electronic hardware, and the functions to acquire, analyze, and store data associated with the particles.

Fluidics

The Sheath Management System controls the transfer of sheath fluid, waste, and cleaner fluid throughout the CyAn ADP system. Sheath fluid is housed in either a replaceable 20 liter cubitainer or 20 liter plastic carboy. Waste is contained in a 20 liter plastic carboy. Cleaner fluid is contained in a 5 liter cubitainer. The Sheath Management System provides improved sheath pressure stability and prevents bubbles from entering the system when the sheath container is changed. The built-in cleaner fluid cubitainer allows the user to easily clean and rinse the sheath path using DakoCytomation Clean and Rinse solution and sheath or DI water as rinsing fluid. The 20 liter sheath and waste containers provide approximately 24 hours of system run time.

Figure 3.2 outlines the key fluidics components of CyAn ADP. In general, flow of air and fluids follows a path left to right in the diagram. An air compressor provides pressure for propulsion of the sample, cleaner, and sheath fluids. Air regulators condition and stabilize the pressure source prior to sheath and cleaner reservoirs and sample vessel. A number of electrically controlled valves control the flow state of the system and provide a means for cleaning and debubbling, in addition to routine flow conditions for sample analysis.

Sample is forced through tubing, is introduced to the flow cell, and is fluidically focused by sheath fluid. This hydrodynamic focusing effect causes individual particles to be introduced in single file to each of the sequential laser beams. While a pinch valve is used to allow the flow of sample, the rate of sample flow is controlled by adjusting the over-pressure (differential pressure) of an electrically controlled air regulator relative to sheath pressure. Waste is drawn by a vacuum pump to a holding container for disposal.

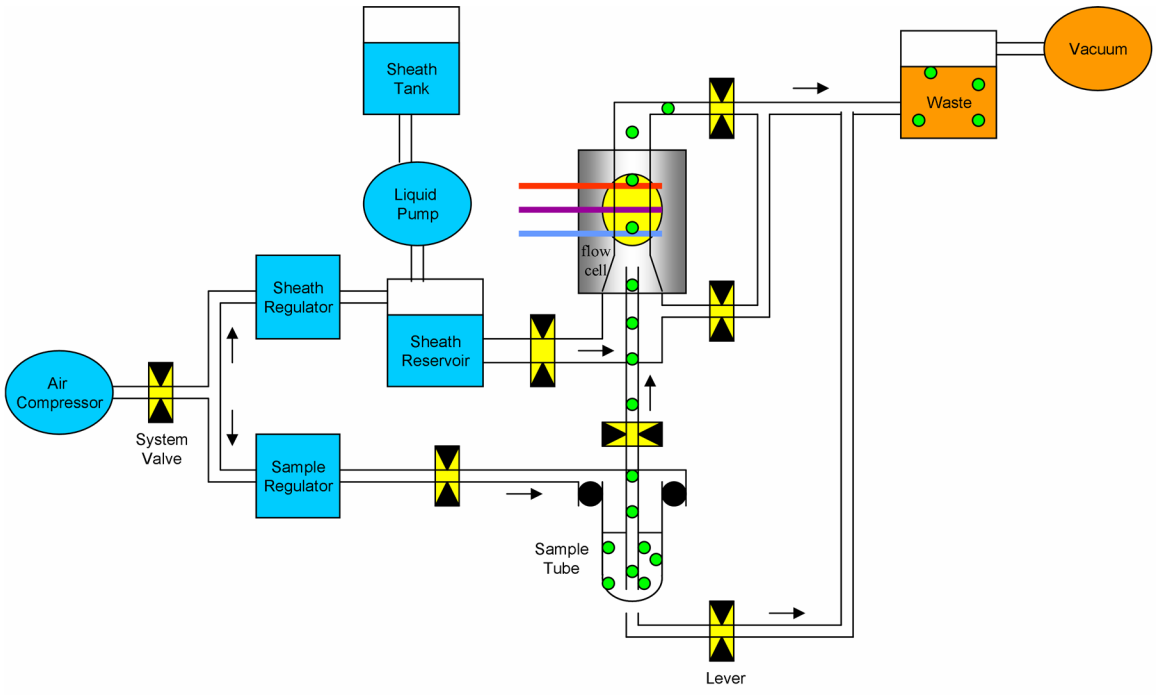

Figure 3.2: CyAn ADP Fluidics Block Diagram

Optics

Figure 3.3 is an illustration of the optical geometry of the CyAn ADP UV model. Up to three excitation sources can be accommodated on the optical bench. Each path has its own independent, unique steering and focusing elements to provide optimal excitation of particles at the interrogation point. Shown in the figure are laser paths for a 488 nm line (blue), a UV line and a 635 nm line (red). Each laser beam is focused to the quartz flow cell, where particles are transported past the laser beams.

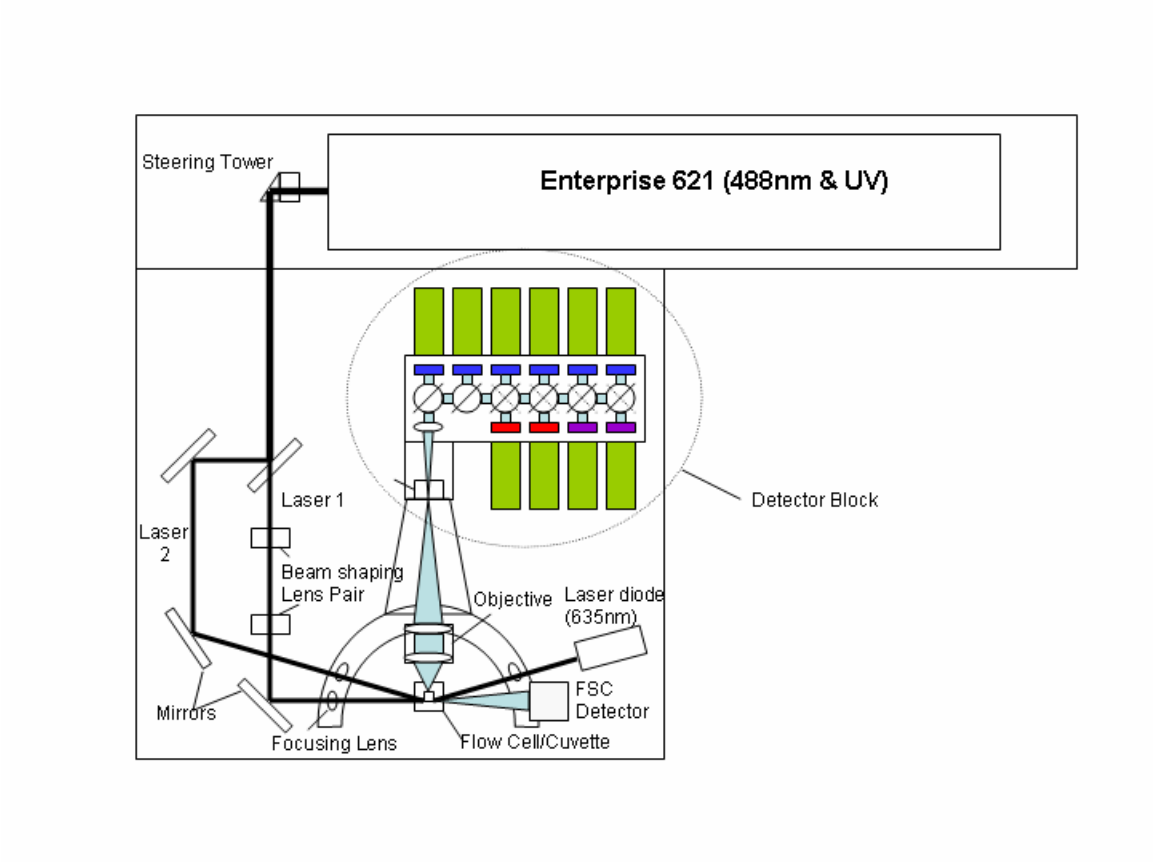

Figure 3.3: CyAn ADP UV Model Optical Block Diagram and Location of Laser Apertures

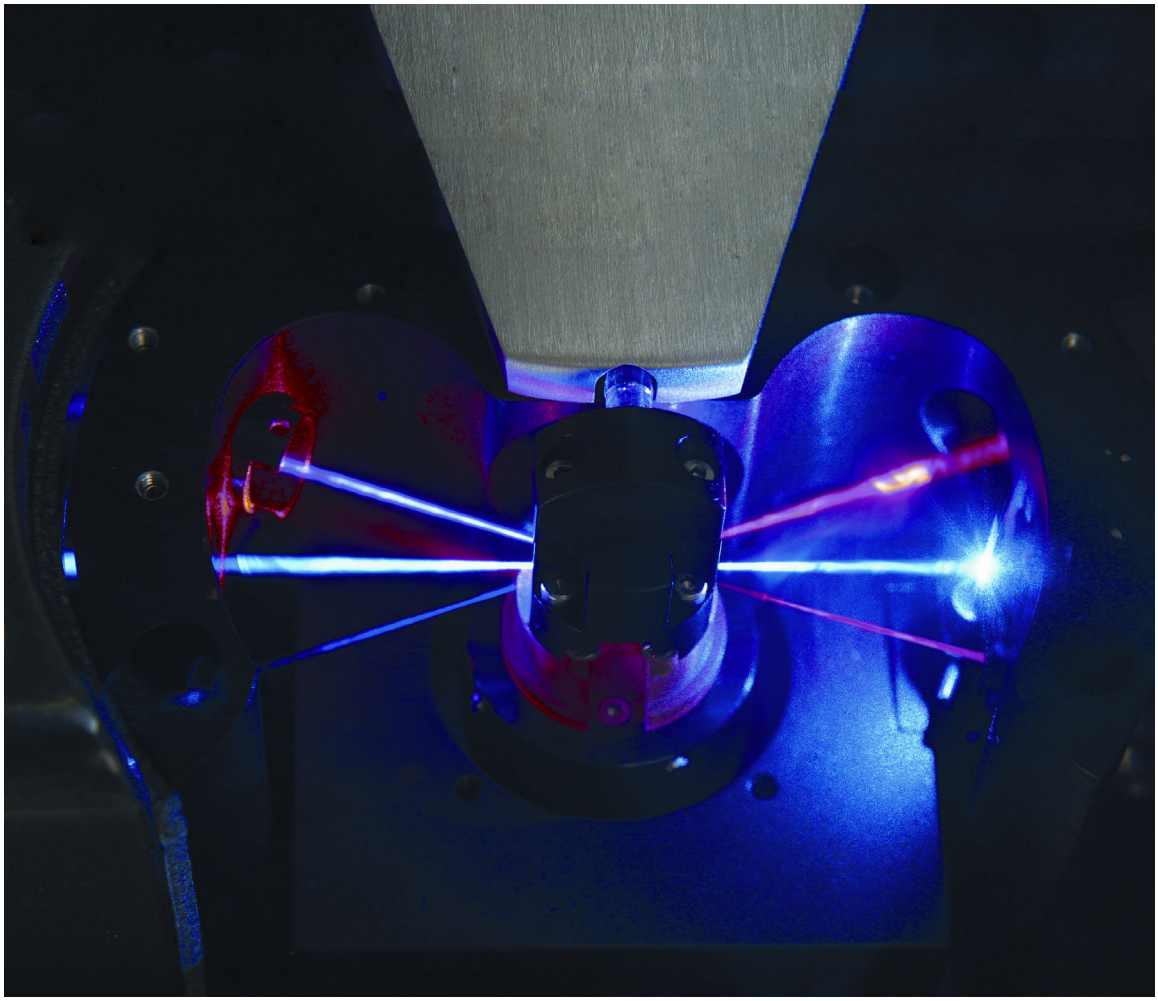

The focused beams are separated vertically to ensure minimal optical crosstalk between detection paths. Further, the signals that are detected as particles that traverse the beams are electronically gated to reduce unwanted signal interference between channels. A high numerical aperture microscope objective is used to collect scatter and fluorescence and to generate an image of the interrogation point for each of three apertures (spatial filters). The apertures improve signal to noise by preventing unwanted scatter around the excitation region from entering the detector block. Light that transmits through the spatial filters is reflected and spectrally filtered on its way to the appropriate photomultiplier tubes (PMT) for detection.

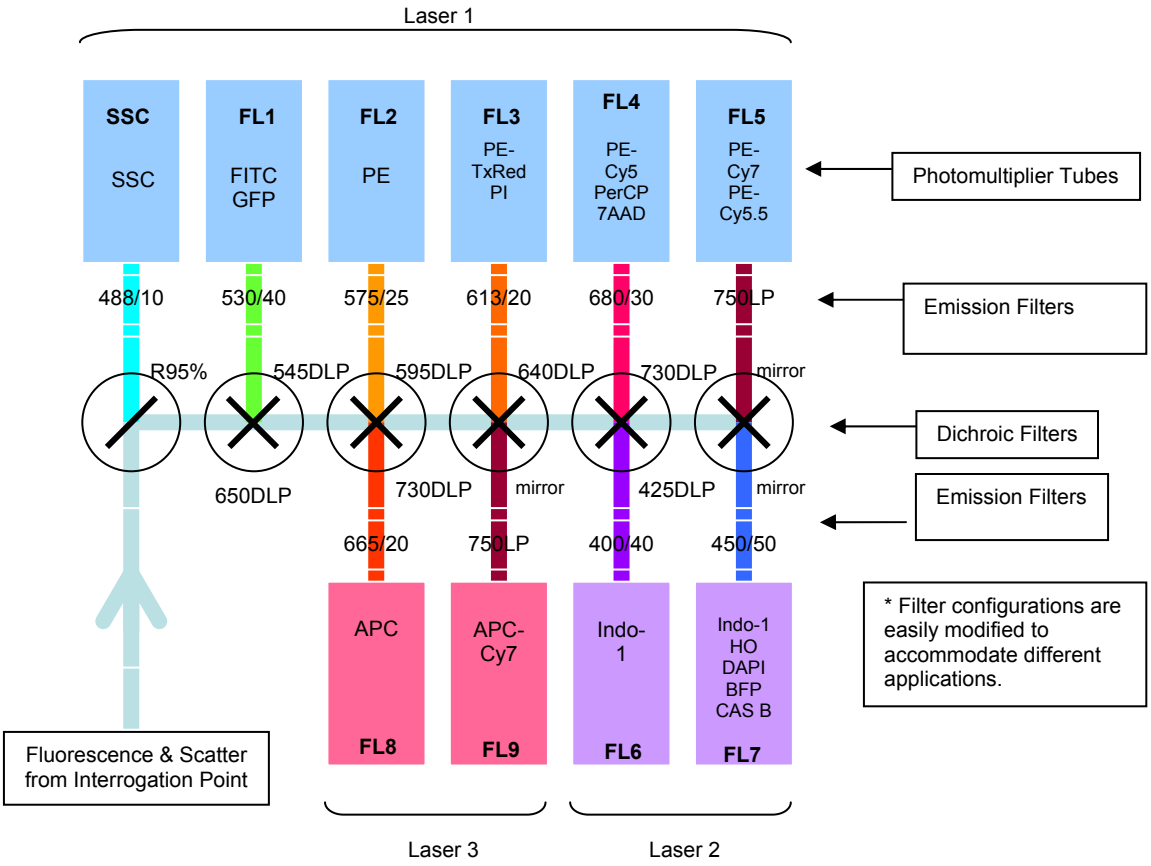

Figure 3.4: CyAn ADP UV Model Detector Block and Optical Filter Layout

Figures 3.4 and 3.5 illustrate the location, position, and orientation of the optical filters and PMTs within the detection block assembly of the CyAn ADP UV Model and CyAn ADP respectively. Dichroic filters are located at 45° to the direction of light propagation, while emission filters are located at 90° to the light path. Filter sticks are interchangeable, thus allowing custom configurations to be implemented. Please contact DakoCytomation to order dichroic filter sets.

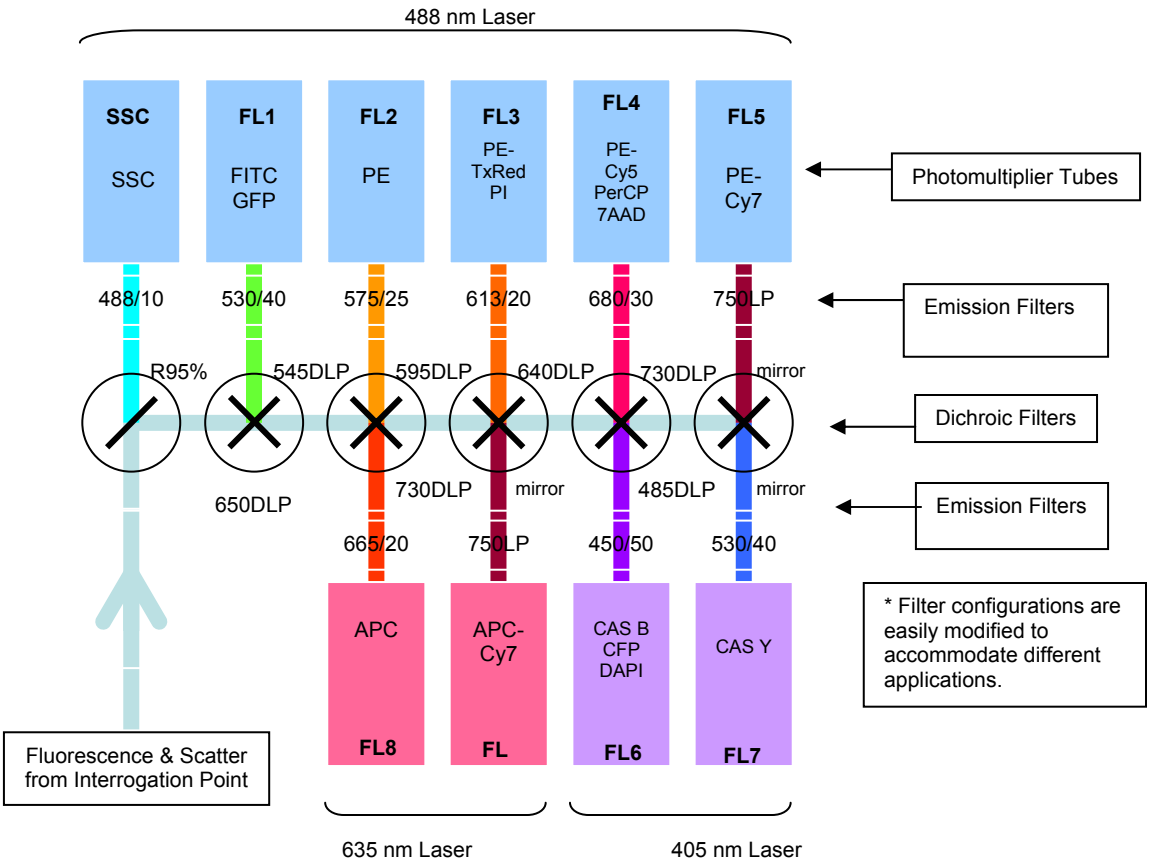

Figure 3.5: CyAn ADP Detector Block and Optical Filter Layout

Electronics

CyAn ADP has an array of electronic components. The PC/workstation is used for instrument control, status, and data acquisition functions and communicates with the CyAn ADP instrument through a high-speed serial link. Housed within the instrument is a state-of-the-art electronic chassis that provides a communication backplane/bus with a number of available card slots to allow modular connection of key electronic control and sensing components. These components include trigger and signal processing, and multi-function input/output. Peripheral to the electronic chassis, but within the instrument are a number of devices that can be grouped as fluidics control and sense (pumps, regulators, valves, and sensors), laser/shutter control and sense, PMT voltage control, and PMT signal. The multifunction I/O card is used for controlling these peripheral devices and sensing instrument status. The PMT and photodiode detectors convert light emitted from particles excited at the interrogation point, into electrical signals. These signals are input to the trigger and signal processing cards. Amplification, analog to digital conversion, and sampling techniques provide quantitative measurements including peak, area/integral, log, and pulse width for a given triggered particle event.

Peripheral Devices

The CyAn ADP instrument has the following peripheral devices: Summit Workstation, two Monitors, a printer, and Sheath Management System (SMS). The SMS houses sheath container, waste container, cleaner cubitainer, level indicators, in-line sheath filter, and compressor/vacuum pump.

Software

CyAn ADP uses Summit Data Acquisition and Analysis Software for instrument control, data acquisition, and subsequent data analysis. Summit is the Windows user interface for the entire DakoCytomation flow cytometry product line.

Summit software offers users complete control of the CyAn ADP instrument at varying levels of complexity, depending on their needs. The instrument control panel (figure 3.6) provides access to laser control, event rate settings, system maintenance functions such as clean and rinse, and Sheath Management System functions. The sample parameters panel (figure 3.7) has software controls for adjusting parameter settings such as threshold, PMT voltage, and gain.

User documentation for Summit is available from the **Help** menu.

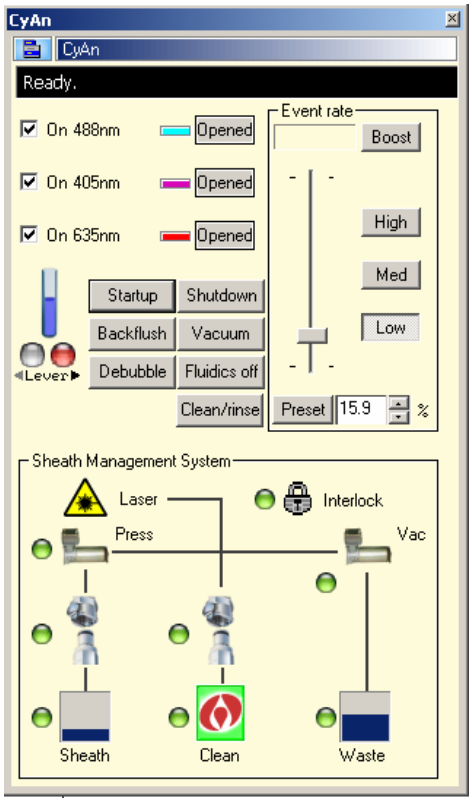

Figure 3.6: Instrument Control Panel

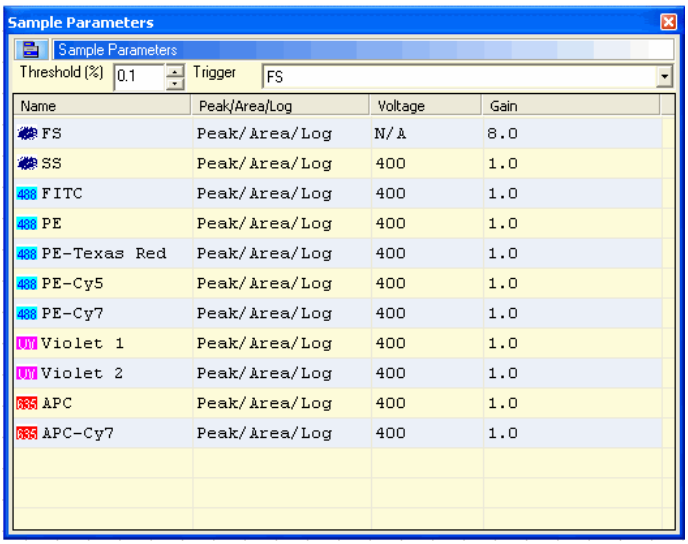

Figure 3.7: Sample Parameters Panel

Summit Features

Summit software offers the compensation, flexibility, intelligence, organization, and intuitiveness essential for today's advanced flow cytometry applications.

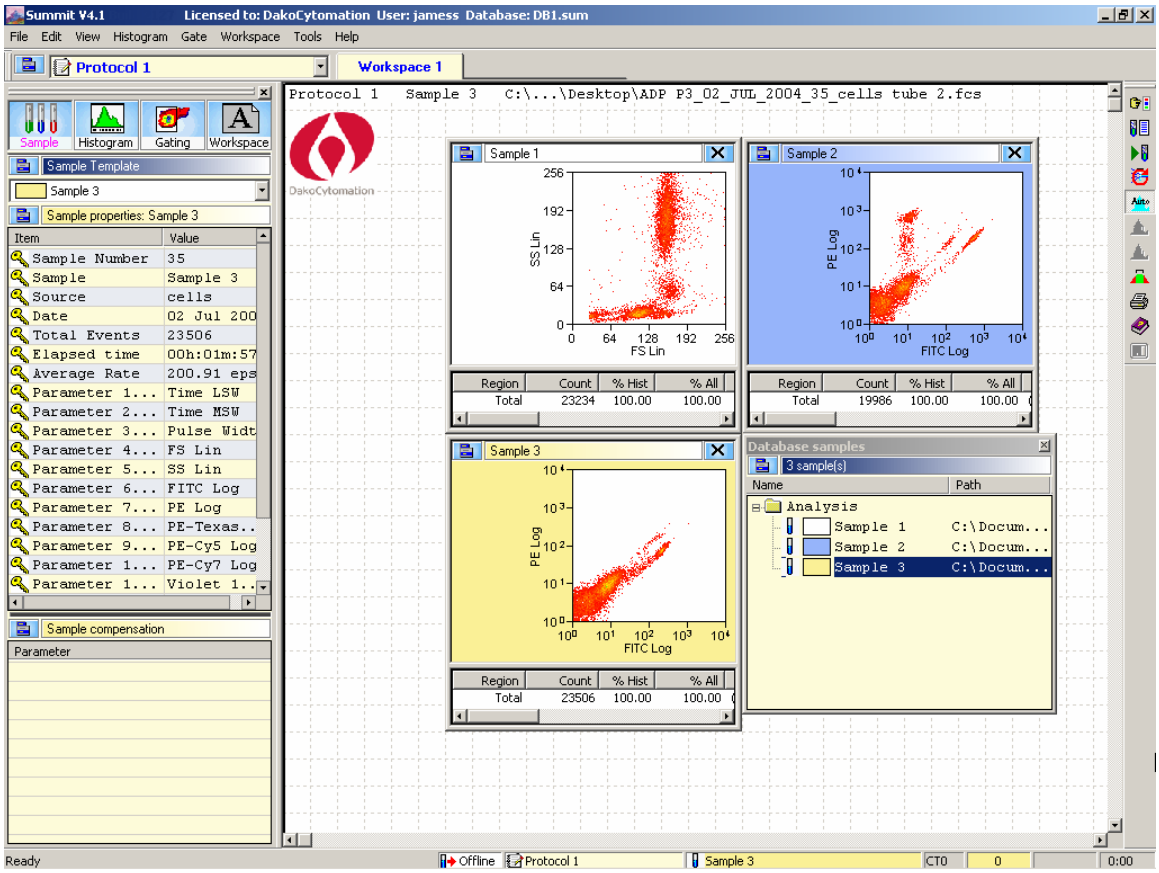

Compensation

Summit Software performs full 9 × 9 inter-laser compensation of fluorescence parameters. Data saved as a sample file in Summit will retain all compensation values as well as the uncompensated data for each parameter.

Flexibility

Summit Software offers flexibility throughout the program to allow the data to be gathered and manipulated in ways that best suit the application and user. For example, virtually any logical expression can be defined using any number of regions in "AND" and "NOT" combinations for generating statistics, including non-rectangular regions with an almost limitless number of vertices. In addition, any and all parameters available with the CyAn ADP High-Performance Flow Cytometer can be selectively stored, including the ability to disable non-contiguous groups of parameters. Eliminating unnecessary parameters increases the display performance during acquisition and reduces data storage needs.

Intelligence

While performing batch analysis, Summit Software's intelligent parameter matching feature dynamically determines the correct parameter to display for a sample based on antibody, stain, name, parameter type, channel, or a combination of these. This feature works regardless of the type of instrument that generated the FCS listmode file for the sample.

Organization

Summit’s sample viewer tracks samples in user-definable folders. Tests and controls with different parameters can be grouped, and samples can be dragged and dropped between folders to help organize information. Statistics for each gate or region are automatically available under each histogram, or may be detached for placement anywhere on the desktop.

Summit's Real-world Desktop

With Summit’s “real-world” desktop, the user doesn't have to remember to load-and-save protocols. Summit remembers everything the user does in a given session, and the next time Summit is opened, the desktop appears exactly as the user left it. Every window, color, size, and placement is the same as it was at the end of your last session. No saving is required. With Summit software, you focus on the science.

SECTION 4

STARTUP AND SHUTDOWN PROCEDURES

Startup Procedure

Required Reagents

DakoCytomation Decontamination Solution, catalog # S2324
DakoCytomation Clean and Rinse Solution, catalog # S2323

CyAn ADP Startup

Note The Quick Start Guides for the CyAn ADP (Document Numbers. 0000023 and 0000022) are available for a quick reference for Startup and Shutdown procedures.

CyAn ADP UV Model users:

Turn on the power to the Laser Power Supply by turning the key to the **On** position and turning the switch to the **On** position.

All CyAn ADP users:

1. Log on to the Summit workstation.
2. Open Summit by double-clicking the Summit icon on the Windows desktop.
3. Select an existing database or create a new one, and then click **OK**.

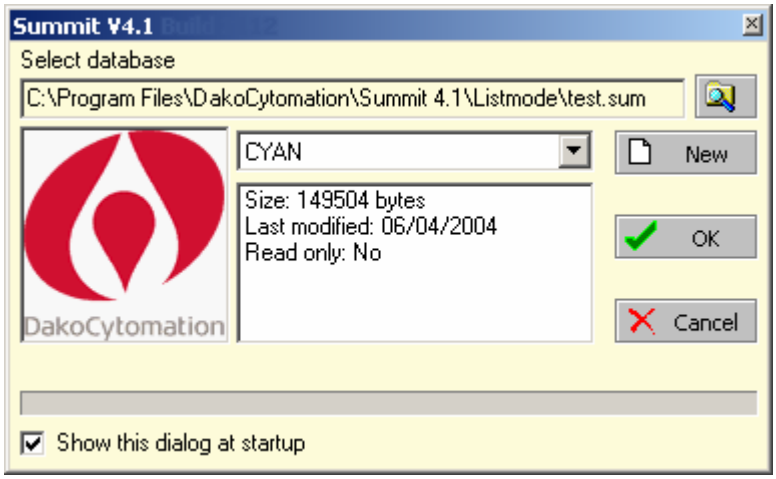

4. Click the **Instrument** tab to view the CyAn Control Panel.

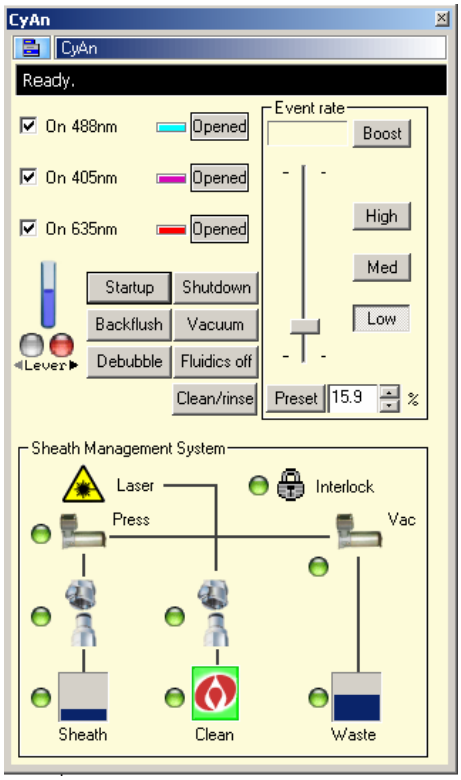

5. Check the status of the sheath container and the waste container by viewing the **Sheath** and **Waste** levels in the CyAn Control Panel. Make sure the sheath container is at least half full and the waste container is at least half empty. If necessary, fill the sheath container and empty the waste container as described in **Section 5: Fluids Management**.

WARNING
Remove the waste container and the sheath container from the cart before emptying or filling. Dispose of the contents of the waste container in accordance with local, state, and federal regulations.

WARNING
Do not drop the waste or sheath container on the Sheath Management System. Doing so may result in improper calibration of the load cells.

6. Click **Startup** on the Cyan Control Panel.

7. On the CyAn Control Panel, make sure the desired lasers are checked **On**.

   For UV model users:

   - Make sure the LP5 or in-house cooling system is turned on before turning on the 488nm UV laser.
   - If your CyAn is equipped with a remote control for the 488nm UV laser, press the **On** button.

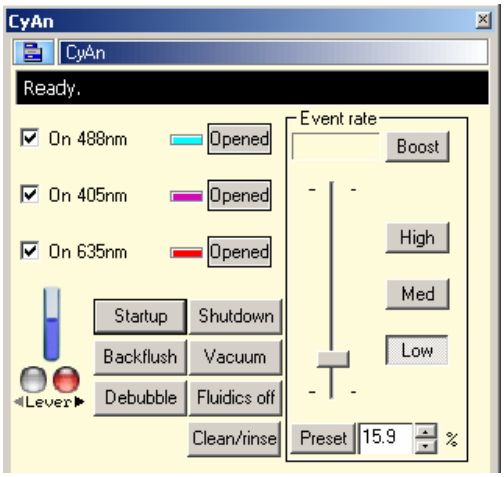

8. Open the required laser shutters by clicking the **Closed** buttons.

9. On the **Instrument** menu, point to **CyAn**, and then click **Clean** to run the clean cycle with a tube of DakoCytomation Clean and Rinse solution or your choice of cleaner from the approved cleaner list (see **CyAn ADP Approved Cleaners and Disinfectants** below).

10. Repeat the clean cycle using a tube of DI water.

11. Allow a minimum of 30 minutes for the lasers to stabilize.

12. Open your QC file protocol generated by your laboratory, place a tube with SpectrAlign beads (10^6 concentration) on the sample probe, and acquire (F2) at a low event rate (~100 eps). Verify that the data is within your daily QC specification. DakoCytomation recommends the following CV specifications for instrument calibration.

Parameter	Target CV
FL1	3.0
FL2	3.0
FL3	3.5
FL4	4.5
FL5	6.5
FL6	6.0 (UV model: 3.0)
FL7	6.0 (UV model: 3.0)
FL8	6.0
FL9	6.0

13. If QC data is within specification, you are ready to run samples. If not, click **Debubble** on the CyAn Control Panel. Rerun the SpectrAlign beads. If necessary, repeat **Debubble** and then recheck SpectrAlign beads.

IMPORTANT
If you have problems with the CyAn ADP or maintenance questions, please contact your local DakoCytomation Technical Service Group.

CyAn ADP Approved Cleaners and Disinfectants

DakoCytomation Clean and Rinse
DakoCytomation Decontamination Solution
70% Ethanol in DI water
0.1% Triton-X100 in DI water
0.5N NaOH (Sodium Hydroxide) in DI water
10% Solution of household bleach in DI water

Shutdown Procedure

DakoCytomation recommends that **Clean** and **DI Water Clean** are enabled for shutdown.

1. On the **Edit** menu, click **Preferences**.
2. Expand the **Instrument** list item by clicking the + sign.
3. Click **CyAn**.
4. In the **Command Options** list, select **Shutdown**, check the **Clean** and **DI Water Clean** check boxes, and then click **Save and Close**.

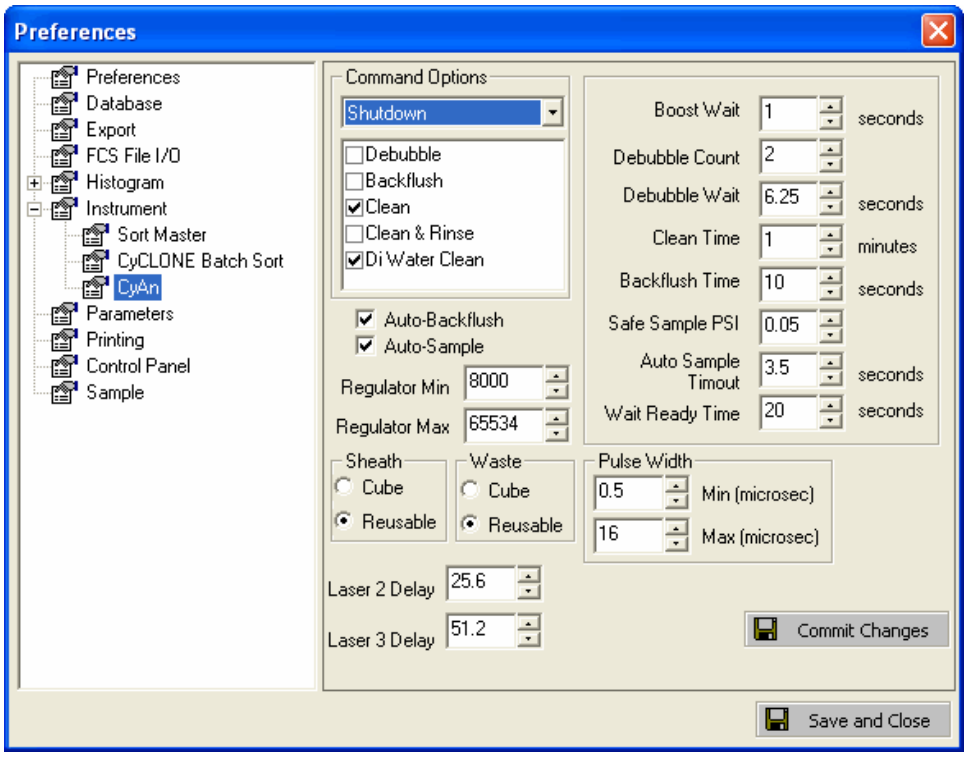

5. Click **Shutdown** on the CyAn Control Panel. When prompted, place a tube full of cleaner on the sample probe and close the lever.

Note Clicking **Shutdown** will automatically shut down the lasers and close the laser shutters. If your CyAn is equipped with a remote control for the 488nm UV laser, press the **Off** button.

6. When prompted, remove the tube, replace with a tube of DI water and move the sample lever in.
7. Check the status of the sheath container and the waste container by viewing the **Sheath** and **Waste** levels in the CyAn Control Panel. Make sure the sheath container is at least half full and the waste container is at least half empty. If necessary, fill the sheath container and empty the waste container as described in **Section 5: Fluids Management**.
8. Fill the test tube with DI water, place it on the sample probe and leave the lever out.

9. **For CyAn ADP UV model users only:** Turn the laser power supply key to the **Off** position and then turn the power switch to the **Off** position. If desired, secure the laser key. On the LP5, check that the **Cool Down Cycle** indicator is illuminated. If the indicator for the **Cool Down Cycle** is not illuminated, make sure that the main power on the LP5 is off and the **Cool Down Cycle** is on.

   Note With the **Cool Down Cycle** switch on, the LP5 unit will remain on until the laser has sufficiently cooled down.

10. Close Summit.

Note DakoCytomation recommends waiting 30 seconds after closing Summit before logging off of the workstation in order to allow all data sources to close.

11. Log off of the workstation and turn off the computer.

12. Turn off the computer monitor(s).

SECTION 5

FLUIDS MANAGEMENT

Sheath Management System Indicators

The Sheath Management System provides 20 - 24 hours of sample run time. As the level of sheath fluid decreases and the level of waste fluid increases, both Summit software and Light Emitting Diodes (LED) indicators on the Sheath Management System front panel will provide fluid level status information and alerts to the user.

SMS indicators can be viewed in the **Sheath Management System** section of the **Instrument** tab in the Control Panel. There are nine indicator lights in the SMS area. When all nine indicator lights are green, all components of the SMS are functioning properly.

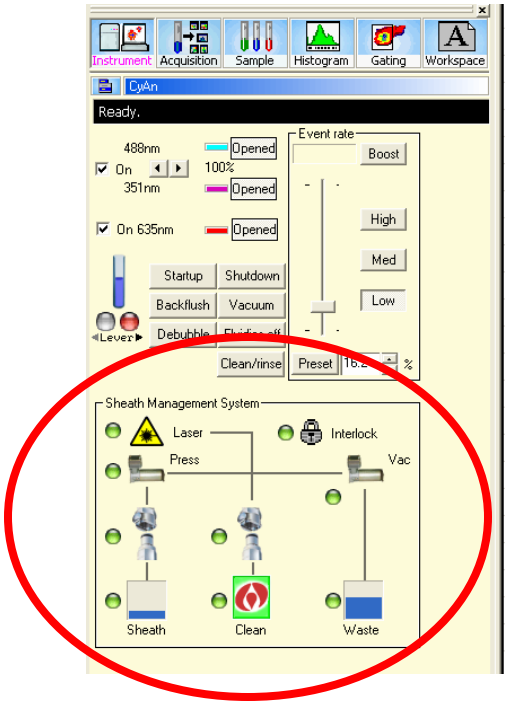

Figure 5.1 – SMS section of Control Panel

If an error condition occurs or status changes for a subsystem, an indicator light will change from green to amber or red. When you place your cursor over the indicator light, a message appears that provides a description of the warning and instructions for how to fix the problem.

The following figures illustrate some of the possible error conditions in the SMS.

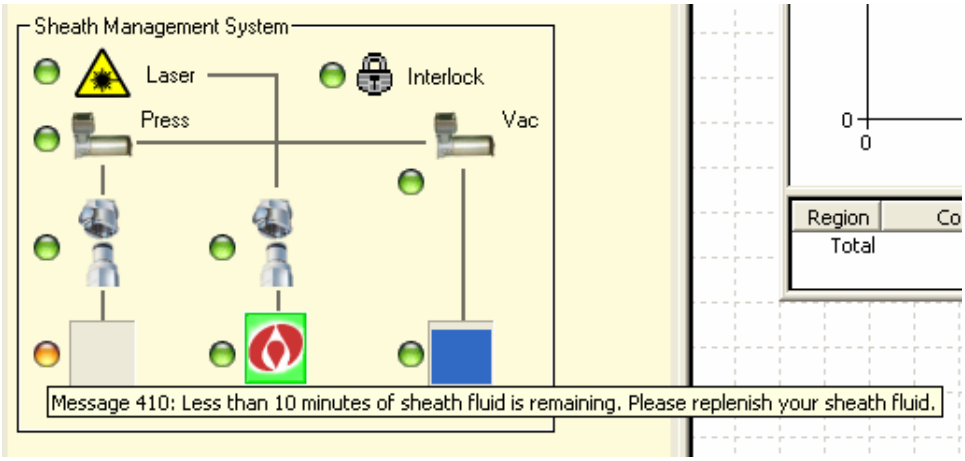

Figure 5.2 – Low sheath fluid warning

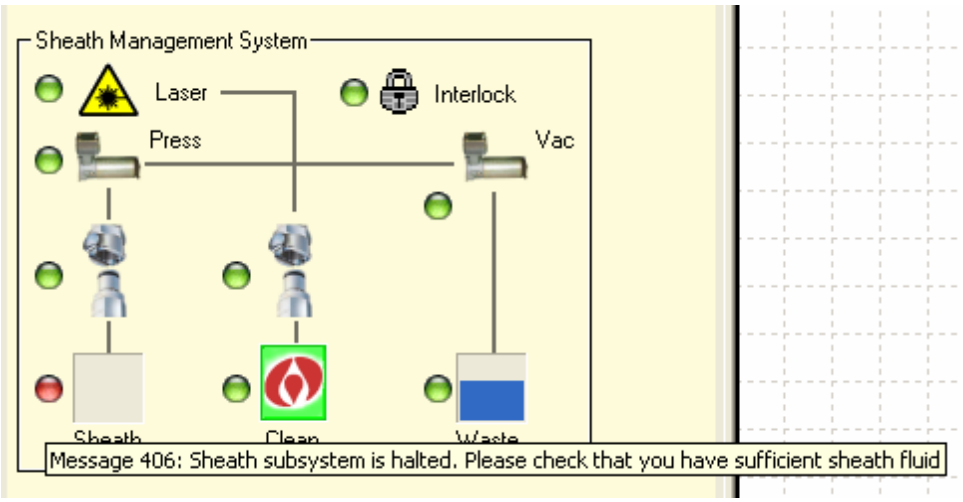

Figure 5.3 – Empty sheath fluid message

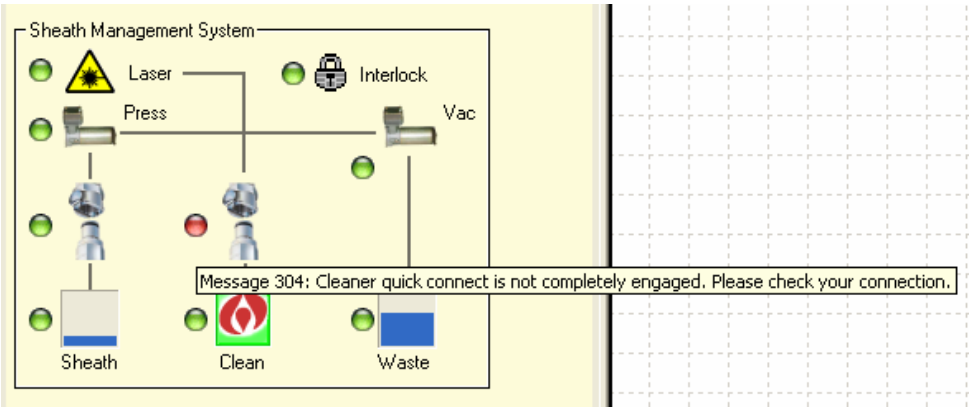

Figure 5.4 – Cleaner quick connect error message

The LED indicators on the front panel of the Sheath Management System also change when fluid levels change in the SMS. Three fluid levels are monitored on the SMS panel: **SHEATH LEVEL**, **CLEANER LEVEL**, and **WASTE LEVEL**.

When all fluids are at suitable levels for proper operation of the CyAn ADP, the **SHEATH LEVEL**, **CLEANER LEVEL**, and **WASTE LEVEL** LEDs appear green beside the **OK** label:

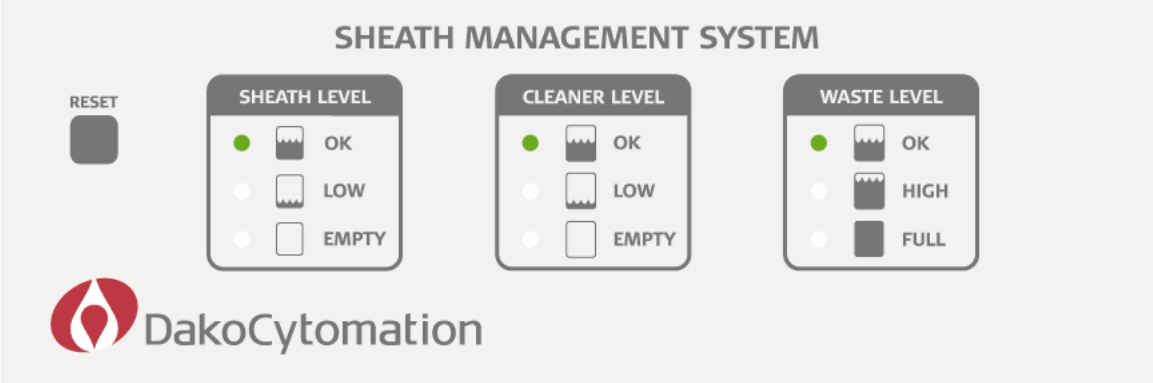

When the sheath level or cleaner fluid level is low, the green **OK** LED changes to a flashing amber or a solid amber LED beside the **LOW** label:

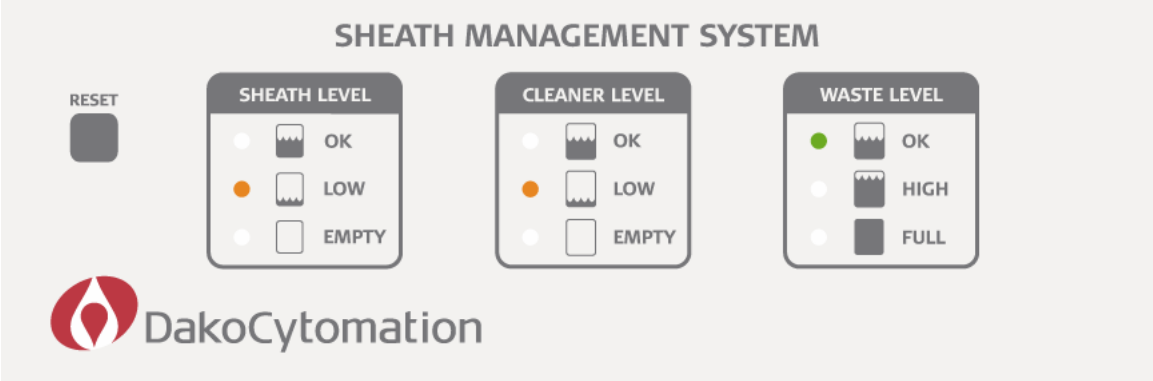

When the waste fluid level is high, the green **OK** LED changes to a flashing amber LED beside the **HIGH** label:

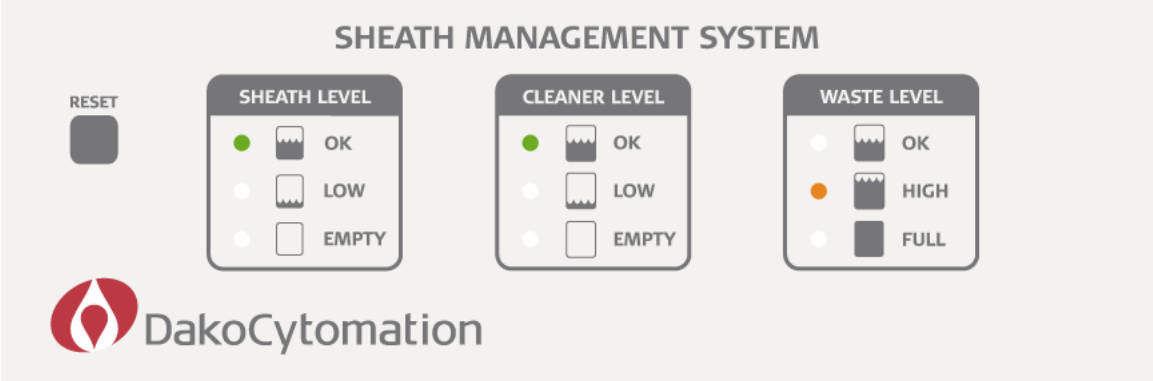

When the sheath or cleaner level changes from low to empty, the flashing amber LED changes to a red LED beside the **EMPTY** label:

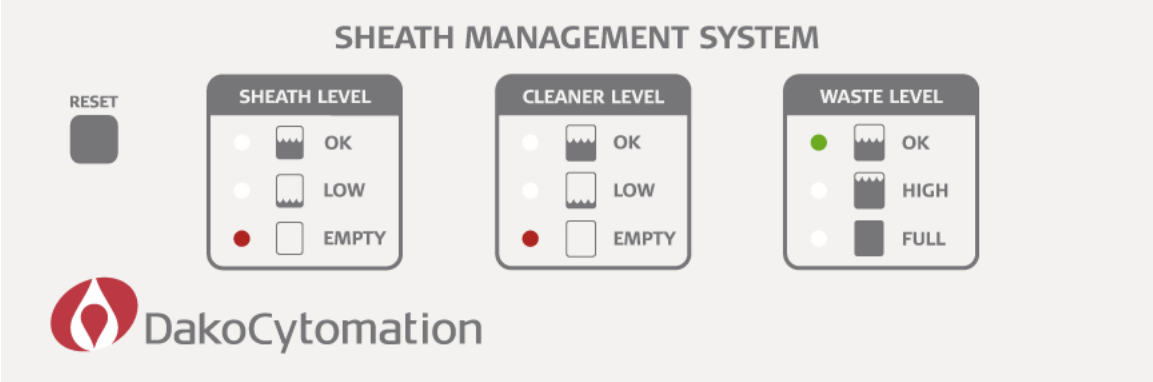

When the waste fluid level changes from high to full, the flashing amber LED changes to a red LED beside the **FULL** label:

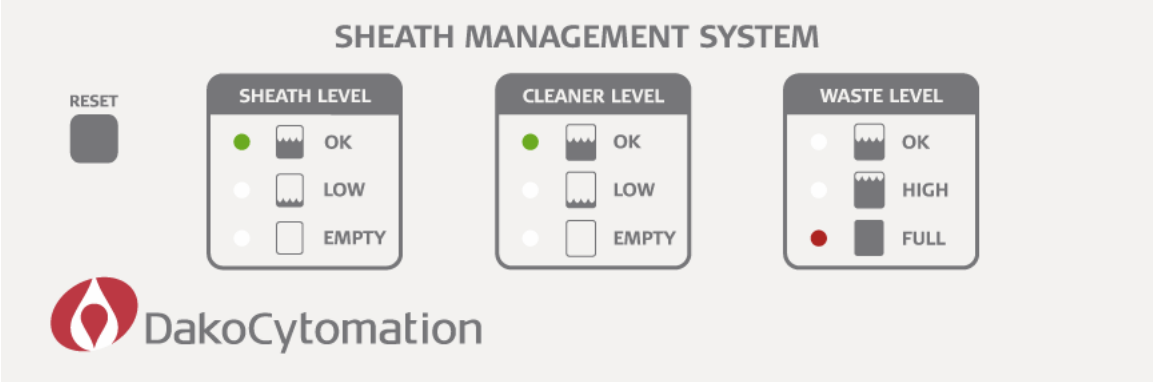

Table 5.1 lists the indicators in the CyAn Control Panel user interface and the message text for each error or status condition.

Table 5.1: CyAn ADP Control Panel Indicators

CyAn Control Panel	Message Text
	Message 101: The 621 Laser has reported a fault. Please check the cooling lines and interlocks on the 621 Laser.
	Message 102: Your CyAn cover is open. The laser shutters have been closed and fluidic system is shutdown. Please close your cover and restart.
	Message 301: Cleaner fluid is low. Please replace the cleaner solution and press the Startup button on the CyAn Control Panel.
	Message 302: Cleaner fluid is empty. Please replace the cleaner solution and press the Startup button on the CyAn Control Panel.
	Message 304: Cleaner quick connect is not completely engaged. Please check your connection.
	Message 305: Internal reservoir overfilled. This will not prevent operation of the instrument but may require future service.
	Message 306: Clean subsystem is halted. Please check that you have sufficient cleaner fluid.
	Message 307: Cleaner subsystem switch error. This will not prevent operation of the instrument but may require future service.
	Message 430: Less than 30 min of sheath fluid is remaining.
	Message 410: Less than 10 minutes of sheath fluid is remaining. Please replenish your sheath fluid.

CyAn Control Panel	Message Text
	Message 401: Internal sheath reservoir level is low. CyAn will stop soon. Please replenish your sheath fluid.
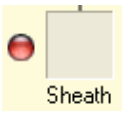	Message 402: Out of sheath fluid. Replenish sheath and press the Startup button on the CyAn Control Panel.
	Message 404: Sheath quick connect is not completely engaged. Please check your connection.
	Message 405: Internal reservoir overfilled. This will not prevent operation of the instrument but may require future service.
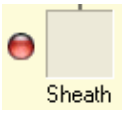	Message 406: Sheath subsystem is halted. Please check that you have sufficient sheath fluid.
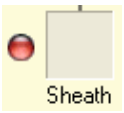	Message 407: Sheath subsystem switch error. Service maybe required.
	Message 705: Waste subsystem is halted. Please check waste tank level.
	Message 730: Less than 30 min until the waste container is full.
	Message 710: Less than 10 min until the waste container is full. Please empty the waste container.
	Message 700: Waste container is full. Please empty the waste container.
	Message 905: Low sheath pressure inside CyAn. Check connection between the CyAn and SMS.
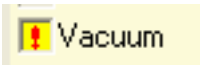	Message 906: Low vacuum inside CyAn. Check connection between CyAn and SMS.

CyAn Control Panel	Message Text
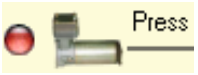	Message 997: Low sheath pressure in SMS.
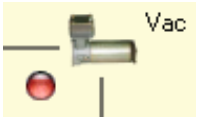	Message 998: Waste subsystem halted due to loss of vacuum. If during operation, please check vacuum pump, waste quick connect or waste tank level.
<Message in top portion of Control Panel>	Message 999: SMS Power fault. Reset SMS to continue. If this problem reoccurs, please call DakoCytomation for technical support.

Changing Out Sheath and Waste Containers

Use the shutdown fluidics procedure to fill and empty sheath and waste containers when running samples.

1. Click **Fluidics Off** on the CyAn Control Panel.

WARNING
Remove the waste container and the sheath container from the cart before emptying or filling. Dispose of the contents of the waste container in accordance with local, state, and federal regulations.

WARNING
Do not drop the waste or sheath containers on the Sheath Management System. Doing so may result in improper calibration of the load cells.

2. At the waste container, release the quick-connects.

3. Remove the waste container from the cart, remove the lid, and empty. Dispose of the contents of the waste container in accordance with local, state, and federal regulations.

4. Place 40mL of regular household bleach into the bottom of the container.

Note This will provide 100ppm available chlorine when the tanks full capacity of 20L has been reached. If the samples you are running will not be effectively killed by this concentration of sodium hypochlorite solution, a larger amount of bleach should be used to achieve effective disinfection concentration.

5. Replace the lid and tighten, place the container back in its position on the cart, and reconnect the waste container using the quick-connects.

6. Restore the sheath fluid by either replacing the entire sheath cubitainer or refilling the plastic carboy, depending on which type of sheath container is used with your Sheath Management System:

    - If you are using the sheath cubitainer, release the quick-connects. Dispose of the entire cubitainer in accordance with local, state, and federal regulations. Place a new sheath cubitainer back in its position on the cart. Reconnect the cubitainer by using the quick-connect.

    - If you are using the plastic carboy, release the quick-connects by pulling up on the collar. Remove the carboy from the cart, loosen the lid, and fill with particulate-free deionized water (dH2O) or a suitable sheath fluid. Seal the lid, and place the container back in its position on the cart. Reconnect the sheath container using the quick-connects.

7. Click **Startup** on the Cyan Control Panel.

8. Run SpectrAlign beads in accordance with your laboratory QC procedure.

Replacing Cleaner Fluid

1. Release the cleaner cubitainer quick-connect.

2. Unscrew the cap from the spent cleaner cubitainer. Retain this cap for use on the new cubitainer.

3. Dispose of the entire cleaner cubitainer in accordance with local, state, and federal regulations.

4. Remove the cardboard punch-out on a new cleaner cubitainer. Holding onto the ring around the cap, pull up on the lid so that the lid extends up to the cardboard.

5. Remove the cap and replace it with the cap from the previous cubitainer.

6. Place a new cleaner cubitainer back in its position on the cart. Reconnect the cubitainer quick-connect.

SECTION 6

CYAN™ ADP MAINTENANCE

Regular maintenance of the CyAn ADP instrument is recommended as described in this section. In addition to performing preventive maintenance procedures, we also recommend that you establish and perform other laboratory procedures for routine operations such as backing up your data and experimental protocols.

Daily Preventive Maintenance

Follow the decontamination and cleaning procedures in Section 4 for daily preventive maintenance.

Weekly Preventive Maintenance

SMS Clean & Rinse Cycle

Note Before running the clean & rinse cycle, make sure you have enough sheath fluid and cleaner fluid to complete the cycle.

- On the CyAn Control Panel, click the **Clean and Rinse** button.

A message box will warn you that the Clean and Rinse process will take 10-15 minutes. Click **OK** to continue. The clean cycle takes seven minutes to complete and the rinse cycle takes seven minutes to complete.

Monthly Preventive Maintenance

Laser Interlock Maintenance Procedure

1. Follow the instrument startup procedure. Make sure the lasers are on and the laser shutters are open.
2. Visually inspect the housing on the instrument to verify that panels or covers are fitted and tight so that all laser energy is contained in the interior.
3. Facing the instrument, lift the lid approximately one inch. The LED light(s) on the right front of the cover should go out, verifying that the laser shutters are closed.
4. Close the lid.
5. If the LED light(s) did not go out when the lid was opened, contact your local DakoCytomation Support Representative.

Annual Maintenance Procedure

A DakoCytomation Field Service Representative should perform an annual maintenance check on the CyAn ADP. To schedule an annual maintenance check, contact your local DakoCytomation Support Representative.

SECTION 7

TROUBLESHOOTING

There are no operator-replaceable fuses in the CyAn ADP. Contact your local DakoCytomation Field Service Representative immediately for assistance with any instrument malfunction or service need.

WARNING
Do not attempt any maintenance on the CyAn ADP laser components. Laser maintenance should only be performed by specially trained, certified DakoCytomation Field Service Representatives.

The following table is a guide for troubleshooting CyAn ADP problems.

Table 6.1: CyAn ADP Troubleshooting Guide

Problem	Action
Vacuum pressure on the waste container is low. 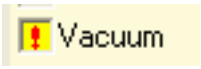	Make sure the quick-connects are connected. If still low, contact customer service.
No sheath pressure. 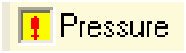	Make sure that the quick-connects are fully engaged. If there is still no pressure, contact customer service.
CyAn has no power	Make sure that the power plug is firmly attached to the wall. Make sure that the power switch on the back of the CyAn is on.
Acquiring data, but no display	Make sure that the lasers are on. Make sure that the laser shutters are open on the CyAn Control Panel.

SECTION 8

TUTORIALS

Using Compensation

The term "compensation" as applied to flow cytometry typically refers to a mathematical manipulation that subtracts or otherwise minimizes the effect of a spectral overlap across colors, thereby better resolving sub-populations. More accurately, compensation is the process by which the physical observation is mathematically manipulated to better observe biological significance.

A common problem in resolving events that are positive in one color from events in another color is that the spectrum may be very close together. Worse yet, the spectrums may actually overlap. For example, if you have a "yellow" dye and a "green" dye in the same sample, it's possible that some events are only positive for "yellow", but they actually look a little "green" because "yellow" and "green" overlap a little bit in their spectrums.

As with any tool, compensation is a not useful to a user that does not understand it. While some would argue that properly performed compensation better identifies populations of biological significance, almost all would agree that improper compensation is worse than no compensation. It distorts data, leads to inaccurate results, and can even be considered fraudulent if done intentionally.

Still, among very educated users that know the issue well, there is little agreement over the acceptable use of compensation.

The argument against compensation

Those who are against the use of compensation argue that it is a mathematical manipulation against observed reality. It can be considered falsification of data, just as any "arbitrary" mathematical manipulation of results would be considered false. It is improper to base research on anything other than the "actual" or "observed" reality.

This assertion is heightened by the fact that many users do not fully understand the issue of compensation, how it is being performed, and how compensated data is to be interpreted. For example, even though two populations can be mathematically be separated on the screen, the overlap of the observed signal is the actual reality; cell sort purities on a population identified by an experienced operator on raw data should be the same as cell sort purities on a population identified on compensated data, no matter how good your compensation.

The argument for compensation

Those who favor the use of compensation argue that it is a mathematical manipulation to bring the physical observation of reality in line with a biologically significant reality. Thus, compensation is merely a tool to assist the researcher in viewing the data in a format where biologically significant populations are more easily identified, as opposed to relying on the researcher to perform the same conversion in his or her head.

This can be likened to the argument of "estimating" the next digit of precision when you can see a little further than the scale offers. For example, what is the width of the component below?

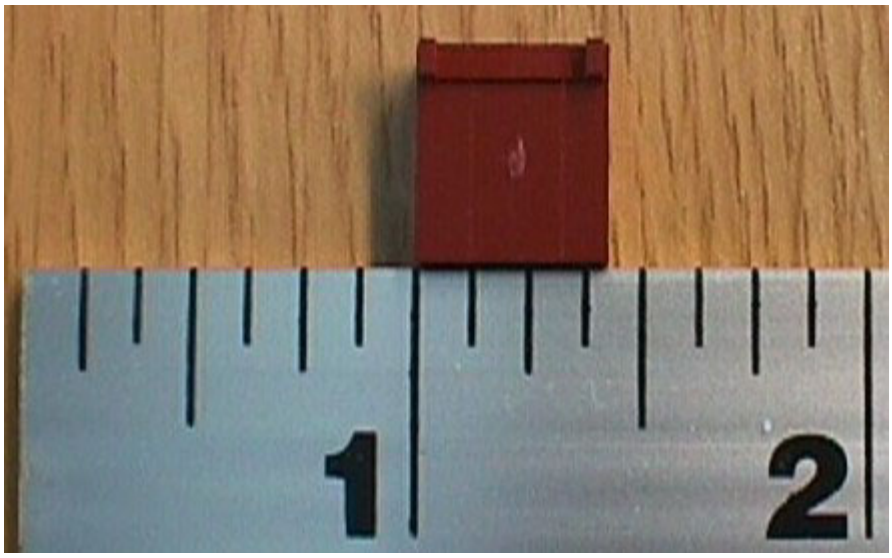

One person might argue that your measurement is simply restricted to the resolution of your scale, and you must pick 3/16" or 4/16" only. In this case, you'd probably round down to 3/16" because the width appears to be closer to that mark than the next. This same person would argue that you cannot "make up" new digits of precision, because they simply do not exist at this scale.

However, another individual may argue that you know it is in fact greater than 3/16", and less than 4/16". Further, you can estimate the location in that range between the two marks. In this case, you are not actually "making up" new digits of resolution, you simply take advantage of the resolution that is present in the measurement but not present in the current scale being used. If the "exact" location were 4/16 of the way between the two marks and your guess was in fact 3/16 or 5/16 (or even 2/16 or 6/16) between the two marks, you would still be closer to the "true" measurement of the item and therefore this estimation of the "next digit" will actually increase the resolution of the measurement.

In terms of compensation, the researcher is mathematically manipulating the data to better approximate the biological significance of the populations. Where one scientist may consider it fabrication, another may consider it enhanced resolution.

Hardware vs. Software Compensation

Historically, there have been two approaches to performing compensation: hardware compensation and software compensation.

Hardware Compensation

The colors are first observed in analog, because photons and the "real world" are in analog. Before these signals or values are converted to digital (the computer manipulates everything in digital format, and event data is always stored in digital format), colors can be subtracted from each other to bring the "observed" signal in line with what the researcher believes to be the "true" signal.

Advantages:

The computation is very close to the "ideal" computation. The data looks very good.
The electronics are relatively easy to implement.

Disadvantages:

The "observed" signal is usually lost. Only the mathematically manipulated signal (what the researcher believed at the time to be "true") is actually stored. Because of this, you can't re-create your experiment from the data or change your mind later if your compensation constants were incorrect.

Because of hardware path limits, you only have a fixed number of color paths that you are permitted to compensate. For many hardware platforms, this usually means you cannot compensate all your colors against each other, even if you only have three colors.

The algorithm is still only approximate, and the actual result is data distortion and over-compensation (subtracting too much). This opens the topic of negative compensation.

Software Compensation

If the analog signal of the observed light (the observed photons) is permitted to convert to a digital signal (a numerical representation of how much light in a given spectrum was seen for that event), then we have succeeded in getting the "real" or "observed" value into the computer and even saved in the data file. Then, because the "real" signal is preserved, the researcher can play "what-if" scenarios to compensate the data in various ways on the raw data to generate what the researcher believes to be the "true" signal.

Advantages:

The "observed" signal is not lost. Compensation can be re-applied in the future with different values for "what-if" scenarios or to re-create the experiment or generate in different ways what the researcher believes to be the "true" signal.

The computation can be the "ideal" computation, where more than one color can be considered in compensating another color.

No restrictions are imposed for what colors may be compensated against other colors.

No specialized hardware is required.

Disadvantages:

The compensation algorithm is difficult to implement properly for both log and linear data, but it can be done.

As technology continues to advance on so many levels, an additional tool has been developed to address the historical weaknesses for sorting based on software or hardware compensation: Digital Signal Processing (DSP) Compensation.

Digital Signal Processing (DSP) Compensation

If the "real" or "observed" signal is still converted to digital and all the benefits of software compensation are maintained, there only needs to be a hardware component that can make real-time sort decisions based on other parameters without going through the (possibly flawed) multi-dimensional re-map from "true" to "real" space, as is done with software compensation for sorting. That's the job of DakoCytomation's Computed Parameter Board, which uses a DSP processor.

Compensation is still performed in software, and both the raw and compensated values can be saved to the data file for all the benefits of "no data or precision loss". However, the hardware makes the exact same calculation that is made by the software, so real-time sort decisions are made with the "ideal" algorithm.

Advantages:

All the benefits of hardware compensation.
All the benefits of software compensation.

By removing restrictions in a new flexible hardware architecture, and maintaining all the advantages of software manipulation, the user can apply software compensation with hardware real-time sort decisions to get the best of both worlds.

In fact, the implication states that almost any computation can be made on a per-event basis to decide whether or not an event is sorted. This wasn't possible for the thirty years prior to DSP technology being released in 1999. Of course, if you don't need to sort (you simply analyze), then software compensation is probably what you are after and the DSP solution providing you real-time computation won't be necessary, except to speed your data display during acquisition.

Fluorescent Compensation

Background: Use in Flow Cytometry

Flow cytometry performs measurement of multiple parameters on an individual particle, usually as that particle passes one or more lasers at one or more interrogation points. An individual sample may contain many particles, and these particles are analyzed individually with many parameters for each particle. Thus, a tremendous amount of flow cytometric data is typically created for each sample (for each collection of particles). Some measurements such as particle size and shape can be determined from pulse width and light scatter patterns as the particle passes a laser. However, it is common to treat particles with reagent markers that bind with some level of selectivity to proteins, large molecules, or other cell structures; when these markers fluoresce after excitation by a laser with a given power and frequency range, the resulting measure is used to indicate particle attributes.

Fluorescent "Cross-Contamination" in the Raw Measure

Commonly more than one fluorescent marker is used in a single experiment, and an individual particle will express more or less of one or the other or both markers. Below is an example of the spectral emission wavelength for two such markers commonly used together, FITC and PhycoErithryn (PE). It is clear to see that some spectral overlap exists between the two, should a given particle express both markers:

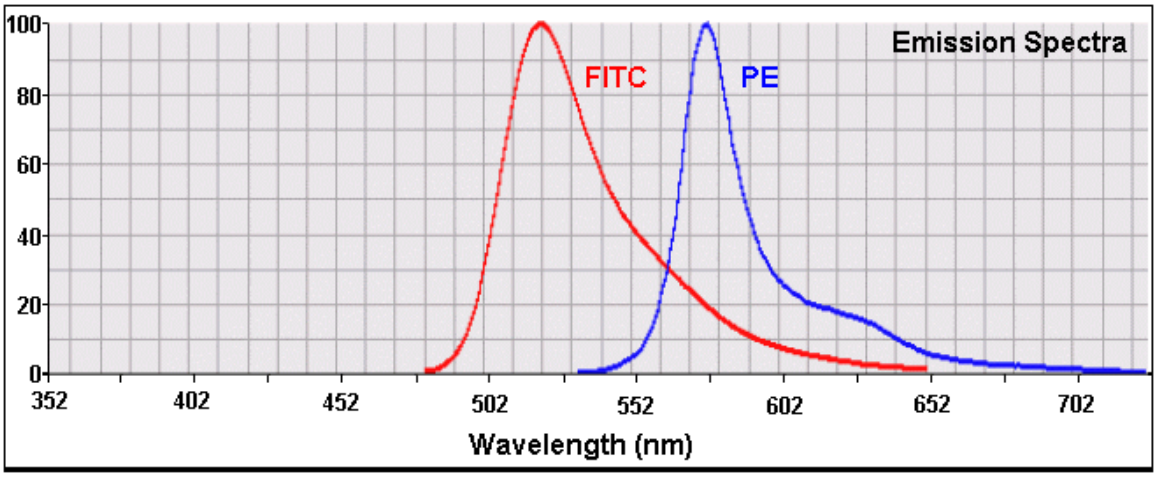

One of the reasons these markers are used together is that each is adequately excited by a 488nm laser. For example, many flow cytometers have one or two lasers, but two or three detectors may exist on each laser path. If many markers can be sufficiently excited by a single laser, but fluoresce in different wavelengths, they can be properly resolved on relatively inexpensive cytometers (because only one laser is needed for multiple markers). Below is the relative excitation efficiencies for FITC and PE, including a line identifying the commonly used 488nm laser line used to excite these markers:

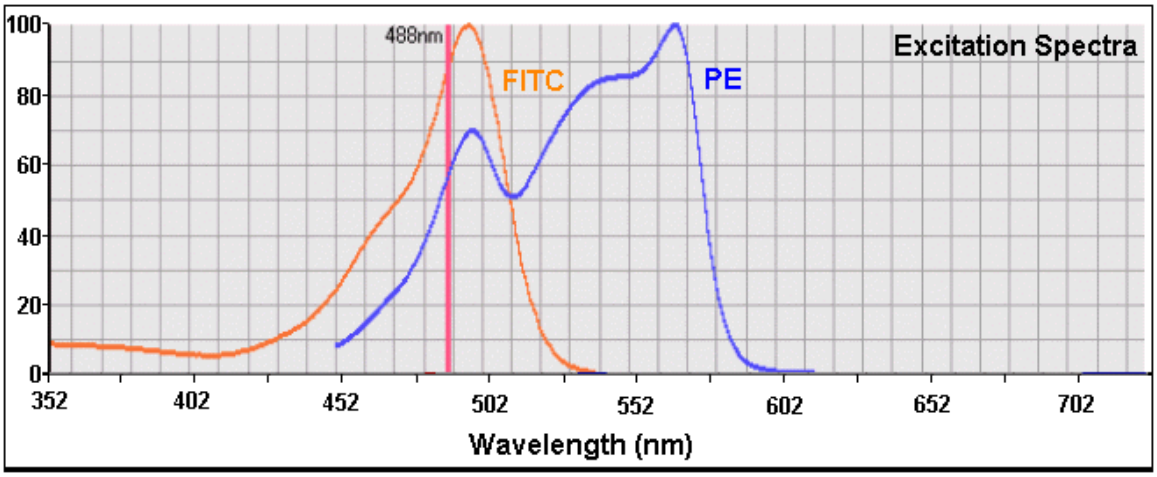

As seen on the graph, each is excited at 488nm (FITC at approximately 90% efficiency, and PE at approximately 60% efficiency.) As previously shown, FITC and PE will fluoresce at different spectra. Therefore, it is possible to resolve both FITC and PE, even though each was excited by the same laser (because of differences between their spectral emission properties.) Further, as shown by comparing the emission graph with the excitation graph, it is common for the excitation wavelength to be higher energy (shorter wavelength) than the fluorescence (which is lower energy, longer wavelength.)

With the addition of filters, we can reduce "noise" (or cross-contamination) from other spectrums that are not of interest and thus determine a "rough" FITC measure and a “rough” PE measure. By "rough", we mean that this is only an approximate measure because some contamination remains from other fluorescence (beyond the fluorescence from the single marker of interest). For example, let’s again look at the FITC and PE emission spectra, but also use filters and dichroics to isolate a frequency band to measure FITC, and another frequency band to measure PE:

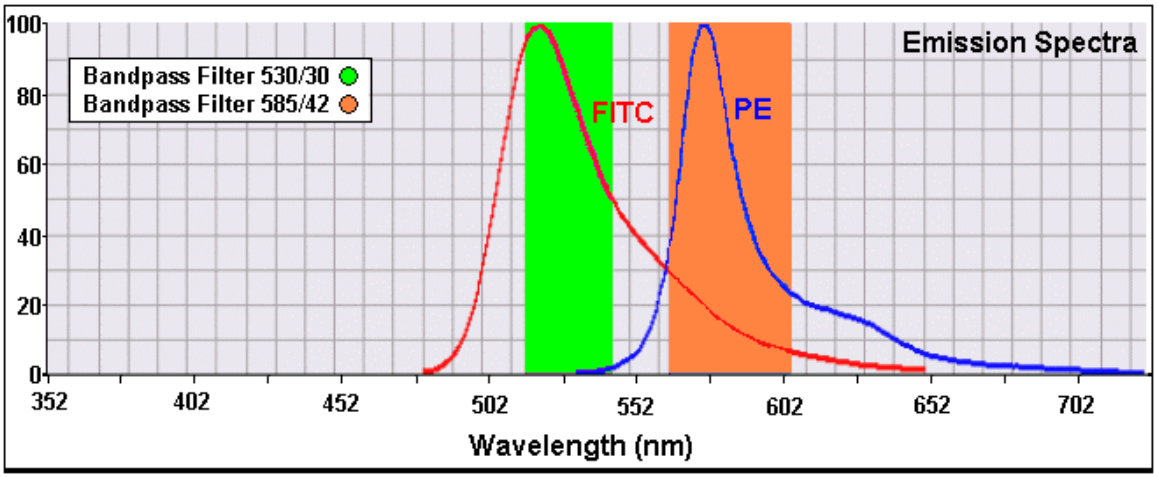

As shown in the graph, the FITC measure will be based on the area under the FITC curve within the 530/30 band, but will also include a small amount of contamination from the lower end of the PE curve that also extends into this 530/30 band. Similarly, the PE measure will be based on the area under the PE emission curve within the 585/42 band, but with a (relatively large) amount of contamination from the upper end of the FITC emission curve that similarly extends into the 585/42 band. The contamination of PE into FITC and FITC into PE is cross-contamination, and poses a potentially large basis for error in our measure. This contamination in the measured range is termed, "spectral overlap".

Compensation Preparation

Preparation Summary:

In order for compensation to be properly defined, an n-color experiment will require preparation of n+2 tubes. The tubes for a 4-color experiment are defined above. [n + unstained (nonspecific isotype is best) + all stains sample]

Autofluorescence is a background level of fluorescence emitted from unstained and stained cells that is primarily due to intracellular flavins. The effects of autofluorescence can be minimized by defining a region in the light scatter (FSC vs. SSC) bivariate histogram and gating all of the fluorescence histograms from this population. You should always gate on cells using light scatter before adjusting compensation to prevent autofluorescence.

After the tubes have been prepared, proceed by running the unstained cells to set the PMT voltages as outlined below.

Using the negative isotype or unstained cells, set the PMT voltages for each fluorescence channel so the population falls in the first decade log scale.

Always set Fluorescence ADC's to Log mode when setting up compensation and analyzing.

- Using the negative tube, plot a univariate (Log scale) histogram of the first stain channel and adjust the PMT voltage until the peak appears centered in the first log decade of the histogram.

- Once this PMT voltage is set and compensation has been optimized, it should not be changed throughout the experiment.

- Now you can select a second parameter by simply right-clicking on the X-axis of the same histogram and selecting a different parameter. Adjust the PMT of this parameter in the same way as the first and continue through all channels to be used in this experiment.

The following plot shows the proper settings for negative population in PE channel.

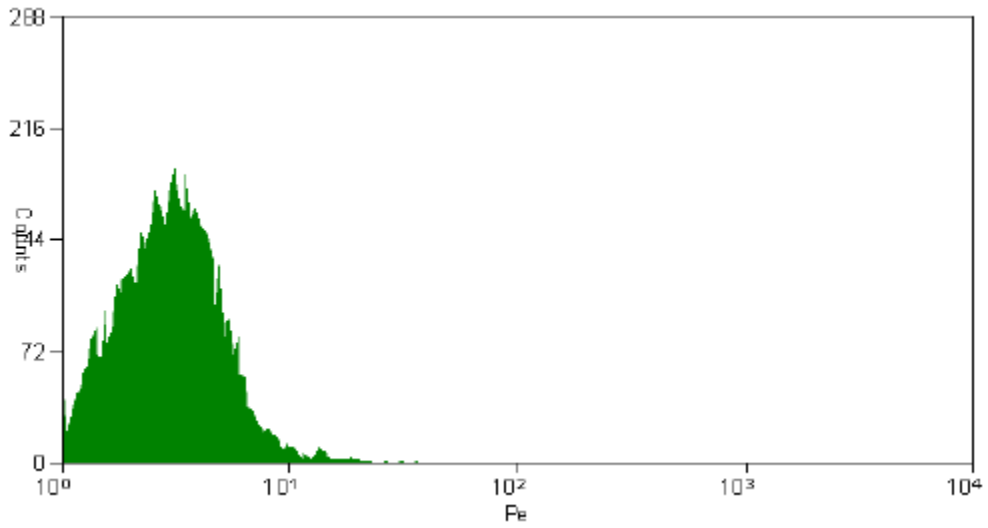

Completing the Compensation Matrix: Helpful Tips

It is a good idea to be aware of the emission spectra of your fluorochromes before you set up compensation and run the experiment. Consult a fluorochrome guide or reference to research the extent of spectral overlap. The greater the overlap between two fluorochromes, the greater the error will be in the analysis or sort.

1. Start by placing the first fluorescence channel (FITC) data on the x-axis and the second fluorescence channel compensated (PE Comp) on the y-axis. (If compensation has not yet been applied to PE, PE Comp will not appear. Select PE and then compensate.) Left click the mouse pointer in the FITC column and the PE Comp row. This will alter the value in the box so it can be adjusted. Adjust compensation appropriately. Plot each fluorochrome on the x-axis and sequentially go through each of the other fluorochromes in the experiment along the y-axis.

2. Proceed by moving on to the next fluorochrome. To do this, you need to do two things: right click on the y-axis label and select PE-TR Comp from the list, and left click in the PE-TR Comp row of the FL1 column in the Compensation Matrix. There is no need to plot the same fluorochrome on both the x and y-axis.

3. Move on to the next fluorochrome (PE) by either running the PE-stained only tube or by selecting the PE-single stained data from the Data Navigator if the data has been previously stored in Summit. Change the x-axis on the histogram to reflect the PE data and change the data on the y-axis to FITC Comp. Optimize compensation for FITC Comp and then move on to PE-TR Comp, PE-Cy5 Comp, and so on.

4. In general, only fluorochromes with neighboring emission spectra need to be considered for compensation. FITC and PE used in the same experiment require compensation for the FITC fluorescence in the PE channel. FITC and Cy5-PE, however, do not overlap in their respective bandpass filter channels. No compensation is required between these two channels.

Historical Compensation Calculation

The problems with the historical compensation calculation include:

Homogeneous populations are mathematically divided into sub-populations that do not biologically (or physically) exist. (Computation of the "true" value is arbitrary, and based on per-particle values of other markers.)

Amplitude of the error is cumulative across additional colors and markers, decreasing the sensitivity of experiments with additional markers. (Markers are mathematically [arbitrarily] correlated with markers that are physically unrelated.)

Attempts to correct for the formulae deficiencies create additional ambiguities and error, and may be difficult to explain (i.e., negative compensation; compensation constants on markers that are physically not correlated.)

The only advantage of this historical calculation is ease of implementation in analog circuitry on older flow cytometers.

The historical calculation for compensation can be described as a "reasonable approximation", albeit one that introduces error and creates anomalous mathematical sub-populations that do not biologically (or physically) exist.

Pragmatic justifications for this technique fade with the advancement of new hardware and software, and this approach can be completely replaced with the proper compensation algorithm

that has no such side effects. Benefits include increased sensitivity on all experiments using fluorescent compensation, and most especially with experiments utilizing an increasing number of colors. Further, pragmatic approaches to implementing proper compensation including iterative determination of compensation constants and compensation matrix inversion make proper compensation very reasonable to implement in both hardware and software.

Negative Compensation

The Stanford Laboratories first broached the subject of negative compensation, which remains quite controversial. Just as many (even experienced) researchers and operators have a misunderstanding of compensation in general, there remains a widespread misunderstanding of negative compensation and why it may be considered necessary by some scientists.

In short, negative compensation may be used to make up for inherent overcompensation resulting from hardware compensation.

You can refer to Stanford's published paper on 8-Color compensation which addresses the issue of negative compensation:

8 Color, 10-Parameter Flow Cytometry to Elucidate Complex Leukocyte Heterogeneity.
Mario Roederer, Stephen De Rosa, Rachel Gerstein, Michael Anderson, Marty Bigos, Richard Stovel, Thomas Nozaki, David Parks, Leonore Herzenberg, and Leonard Herzenberg. Department of Genetics, Stanford University, Palo Alto, California. Cytometry 29:328-339(1997).

Why Negative Compensation?

On its surface, it would seem illogical to have negative compensation. Compensation is usually a mathematical manipulation to remove the influence of an overlapping color on a given parameter. Thus, "negative" compensation would be "adding back" a color to a parameter. Why would you ever want to do this?

Stanford's initial work on this subject was performed with Beckton-Dickinson FACScan units, where compensation was provided at the hardware level, and the analog signals were subtracted prior to conversion to a digital signal (this was hardware compensation). Further, they were working with many overlapping colors (the paper listed above mentions 8 colors).

While their paper suggested several things, two points are key:

Fluorescent colors overlap more than you might first think; the asymptotic tails extend quite far into other spectra.

Analog compensation at the hardware level is flawed in that it over-compensates the data.

The first point suggests that the spectral overlap can be larger than the user first anticipates, especially when considering the theoretical spectral curves for each color. The second point suggests that additional colors, other than those with "expected" spectral overlap, may influence the compensation of a given color. This influence results in overcompensation that must later be "undone". However, if the overcompensation took place on analog data at the hardware level, the original data is no longer available to correct for the initial overcompensation at the time the data was collected.

A Negative Compensation Example

As a specific example, consider the following event data, where we have three colors, "Yellow", "Green", and "Blue". Further, consider that each color overlaps the neighboring color by 30%, but that non-neighboring colors do not overlap at all. (Note that in reality it is likely that non-neighboring colors do actually overlap, but that only complicates the math in this example; the principle is the same.)

Thus, if you were to build a compensation matrix, it would look like the following:

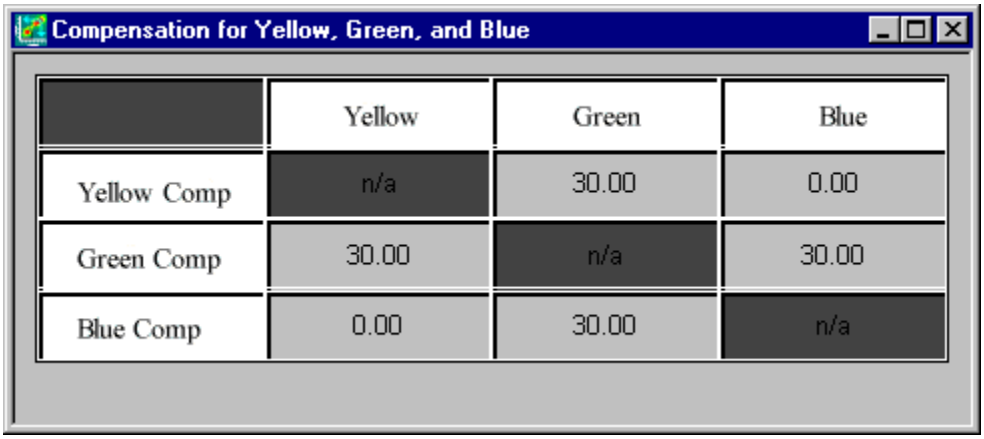

	Yellow	Green	Blue
Yellow Comp	n/a	30.00	0.00
Green Comp	30.00	n/a	30.00
Blue Comp	0.00	30.00	n/a

We now generate a list of every possible combination for a particle with positive/negative response for each of the three colors. Assume that "10" is the value for a positive response (we saw those photons for that color), and "0" is the value for a negative response (we did not see any photons for that color):

	Real Values (if no spectral overlap)		
Event	Yellow	Green	Blue
1	0	0	0
2	10	0	0
3	0	10	0
4	0	0	10
5	10	0	10
6	10	10	0
7	0	10	10
8	10	10	10

The table above notes biological reality: there is truly no Green response on Event #2, because that event was negative for Green.

However, because we stated that there is a 30% spectral overlap for neighboring colors, we will actually observe the following table, where a little of each "positive" color washes into the next color. For example, Note that Event #2 now shows a small amount of Green, because it was positive for Yellow, and there was 30% carry-over to the Green spectrum (the other events behave similarly):

	Observed Values		
Event	Yellow	Green	Blue
1	0	0	0
2	10	3	0
3	3	10	3
4	0	3	10
5	10	6	10
6	13	13	3
7	3	13	13
8	13	16	13

Note Typically the operator will run controls for each color and adjust the PMTs to obtain some "positive" value for a given color; thus, it will be tuned to provide a positive "10" for each color. Thus, any carry-over to the next color (30% in this example), does not detract from the "positive" value that was set when the PMTs were calibrated for the experiment.

We now have the typical problem where we might want to use compensation to manipulate the observed responses to be more in line with what we know to be truly (biologically) significant.

Using the compensation matrix we defined above, the value for computing the compensated values are the following:

Yellow[comp] = Yellow - (0.3 * Green) - (0.0 * Blue)
Green[comp] = Green - (0.3 * Yellow) - (0.3 * Blue)
Blue[comp] = Blue - (0.0 * Yellow) - (0.3 * Green)

For this example, we only want to compute Yellow. The results are the same if you compute Green or Blue.

Doing the math for Yellow compensation on each of our events we get the following:

#1: Yellow[comp] = 0 - (0.3 * 0[Green]) - (0.0 * 0[Blue]) = 0.0
#2: Yellow[comp] = 10 - (0.3 * 3[Green]) - (0.0 * 0[Blue]) = 9.1
#3: Yellow[comp] = 3 - (0.3 * 10[Green]) - (0.0 * 3[Blue]) = 0.0
#4: Yellow[comp] = 0 - (0.3 * 3[Green]) - (0.0 * 10[Blue]) = -0.9 ??
#5: Yellow[comp] = 10 - (0.3 * 6[Green]) - (0.0 * 10[Blue]) = 8.2 ??
#6: Yellow[comp] = 13 - (0.3 * 13[Green]) - (0.0 * 3[Blue]) = 9.1
#7: Yellow[comp] = 3 - (0.3 * 13[Green]) - (0.0 * 13[Blue]) = -0.9 ??
#8: Yellow[comp] = 13 - (0.3 * 16[Green]) - (0.0 * 13[Blue]) = 8.2 ??

Remember that events #2, #5, #6, and #8 were positive for Yellow, but the other events were negative for Yellow. However, we're starting to get some strange results (some spreading) from our calculations. For example, both events #2 and #5 had the same originally observed value (10), but after compensation, they have different values (9.1 and 8.2, respectively). The similar problem exists with events #6 and #8 that shared an original (observed) value of 13, but after compensation have 9.1 and 8.2, respectively. In fact, the problem even occurs with Yellow-negative event pairs like #1 and #4, and #3 and #7, where values even calculate to a negative number. This, of course, would "crash" the events into the axis on a histogram plot (a typical problem for compensated data).

The problem for compensating Yellow in this example is the spectral overlap from Blue to Green, where Green is artificially high on Blue-positive events. Because Blue makes Green artificially

high, we're subtracting too much Green from our Yellow, but only on the Blue-positive events. This is an unfortunate problem for hardware compensation, leading to population spreading as classical compensation is introduced (Blue-positive and Blue-negative events separate when considering Yellow, even though there is theoretically no spectral overlap from Blue to Yellow.)

This is the anomaly for analog subtraction (compensation) in hardware, and why some (not all) of the data is actually over-compensated. If you perform this calculation and never save the raw event data, your population ends up being distorted. This stretching isn't real; it's a mathematical anomaly.

As Stanford pointed out, this can be corrected with a mathematical adjustment to correct after-the-fact for the mathematical anomaly introduced as a result of the analog hardware compensation.

To resolve this problem, negative compensation suggests "putting back" a little bit of Yellow based on the amount of Blue for that event that was accidentally subtracted. This should give us a better approximation of the biological reality, and should help to minimize the spreading in a Yellow compensated parameter for Blue-positive and Blue-negative events. In other words, add the Blue color to the equation using a negative compensation constant (negative compensation).

Because we know that Blue overlaps Green by 30% in this example, we know that Green is artificially high by 30% of Blue. Of that 30%, we know that there will be another 30% carry-over to Yellow, because we also stated that Green carries over 30% to Yellow. This suggests the Blue should be "added back" at 0.3 * 0.3, which is 0.09 (or 9%).

Performing negative compensation for Blue on these events produces the following result:

#1: Yellow[comp] = 0 - (0.3 * 0[Green]) - (-0.09 * 0[Blue]) = 0.0
#2: Yellow[comp] = 10 - (0.3 * 3[Green]) - (-0.09 * 0[Blue]) = 9.1
#3: Yellow[comp] = 3 - (0.3 * 10[Green]) - (-0.09 * 3[Blue]) = 0.27
#4: Yellow[comp] = 0 - (0.3 * 3[Green]) - (-0.09 * 10[Blue]) = 0.0
#5: Yellow[comp] = 10 - (0.3 * 6[Green]) - (-0.09 * 10[Blue]) = 9.1
#6: Yellow[comp] = 13 - (0.3 * 13[Green]) - (-0.09 * 3[Blue]) = 9.37
#7: Yellow[comp] = 3 - (0.3 * 13[Green]) - (-0.09 * 13[Blue]) = 0.27
#8: Yellow[comp] = 13 - (0.3 * 16[Green]) - (-0.09 * 13[Blue]) = 9.37

By "adding back" some of the Blue that we over-subtracted from Yellow, we are getting better approximations. Events #2 and #5 both move from values of 10 to values of 9.1, and events #6 and #8 both move from values of 13 to values of 9.37. Similarly, events #1 and #4 both keep their original values of zero (#4 does not become negative), and events #3 and #7 both move from values of 3 to values of 0.27.

Thus, spreading as a result of compensation is removed. Negative compensation may be a viable way to improve the compensation of data.

This brings up a couple of points:

Negative coefficients look strange. At first glance, it looks like something that shouldn't be done. Many experienced researchers and operators (even those that believe in compensation) don't like the idea that these coefficients are negative.

We now have a non-zero constant for the "Blue" color in our equation to calculate the "Yellow" compensated value, where the "Blue" value should have dropped out of the equation (after all, we stated from a physics perspective that Blue and Yellow do not spectrally overlap, so Blue should never be considered when calculating the compensated value for Yellow.) In essence, we modify

the proper equation with a "work-around" constant to handle a mathematical anomaly. It's not ideal, but may be the best we can do to correct for errors introduced by analog compensation in hardware.

An Alternative to Negative Compensation

In response to these criticisms, it turns out that there is a mathematically equivalent operation to bring about the same result.

Recall that historically, compensation is performed on the raw data, because the relatively simple analog compensation done in hardware has only the raw signal to work with. However, software compensation allows more flexibility in that it can do any amount of analysis in determining the compensated value for any given event, and because no loss of resolution exists when parts of the signal are lost as a result of hardware compensation.

If we accept the fact that compensation on the raw signal results in over-compensation and may even justify a negative-compensation correction, that leaves the possibility that compensating against a non-inflated value (against a compensated parameter) may actually be a better approximation of biological significance. This means we may want to consider compensating against compensated parameters, instead of compensating against raw parameters (whose signals may be artificially inflated).

Consider our original compensation equations:

Yellow[comp] = Yellow - (0.3 * Green) - (0.0 * Blue)
Green[comp] = Green - (0.3 * Yellow) - (0.3 * Blue)
Blue[comp] = Blue - (0.0 * Yellow) - (0.3 * Green)

If we were to compensate against compensated values, the equations become:

Yellow[comp] = Yellow - (0.3 * Green[comp]) - (0.0 * Blue[comp])
Green[comp] = Green - (0.3 * Yellow[comp]) - (0.3 * Blue[comp])
Blue[comp] = Blue - (0.0 * Yellow[comp]) - (0.3 * Green[comp])

However, that introduces an interesting recursion because compensated Yellow is dependent on compensated Green, which is dependent on compensated Yellow. However, if you disallow the recursion, you can substitute out the equations and get the following (without performing negative compensation):

Yellow[comp] = Yellow - (0.3 * (Green - (0.3 * Yellow) - (0.3 * Blue))) - (0.0 * (Blue - (0.0 * Yellow) - (0.3 * Green)))
Green[comp] = Green - (0.3 * (Yellow - (0.3 * Green) - (0.0 * Blue))) - (0.3 * (Blue - (0.0 * Yellow) - (0.3 * Green)))
Blue[comp] = Blue - (0.0 * (Yellow - (0.3 * Green) - (0.0 * Blue))) - (0.3 * (Green - (0.3 * Yellow) - (0.3 * Blue)))

Performing the calculation for compensated Yellow on the same events for this example would yield the following results:

#1: Yellow[comp] = 0 - (0.3 * (0 - (0.3 * 0) - (0.3 * 0))) - (0.0 * (0 - (0.0 * 0) - (0.3 * 0))) = 0.0
#2: Yellow[comp] = 10 - (0.3 * (3 - (0.3 * 10) - (0.3 * 0))) - (0.0 * (0 - (0.0 * 10) - (0.3 * 3))) = 10
#3: Yellow[comp] = 3 - (0.3 * (10 - (0.3 * 3) - (0.3 * 3))) - (0.0 * (3 - (0.0 * 3) - (0.3 * 10))) = 0.54
#4: Yellow[comp] = 0 - (0.3 * (3 - (0.3 * 0) - (0.3 * 10))) - (0.0 * (10 - (0.0 * 0) - (0.3 * 3))) = 0.0
#5: Yellow[comp] = 10 - (0.3 * (6 - (0.3 * 10) - (0.3 * 10))) - (0.0 * (10 - (0.0 * 10) - (0.3 * 6))) = 10
#6: Yellow[comp] = 13 - (0.3 * (13 - (0.3 * 13) - (0.3 * 3))) - (0.0 * (3 - (0.0 * 13) - (0.3 * 13))) = 10.54
#7: Yellow[comp] = 3 - (0.3 * (13 - (0.3 * 3) - (0.3 * 13))) - (0.0 * (13 - (0.0 * 3) - (0.3 * 13))) = 0.54
#8: Yellow[comp] = 13 - (0.3 * (16 - (0.3 * 13) - (0.3 * 13))) - (0.0 * (13 - (0.0 * 13) - (0.3 * 16))) = 10.54

The user may notice that we are getting negative values of 0.0 and 0.54 in this example, and positive values of 10 and 10.54, as opposed to negative compensation yielding negative values of 0 and 0.27 and positive values of 9.1 and 9.37. However, we have actually performed the same mathematical manipulation, but with the anomaly that the scale is compressed for negative compensation. The range and spread (in fact, the validity of the result), is actually identical when you perform the mathematical proofs.

This clears up the two disconcerting points for some researchers:

The user doesn't see negative constants. Compensation is calculated only from the "real" signal, not the artificially inflated signal.

The "Blue" color is still not (directly) considered when compensating against "Yellow", and correctly "drops out" of the equation.

Additionally, the researcher only needs to identify the constants for colors with actual spectral overlap (in this case one constant) instead of constants for every color that may indirectly affect compensation (in this case two constants). This minimizes user error and data misinterpretation.

Absolutely Perfect Compensation?

In this example we've illustrated how we can perform traditional compensation, or correct for mathematical anomalies with negative compensation or compensating from the compensated, as opposed to compensating from the raw signal. However, is it possible to perform compensate "perfectly" to achieve "perfect" results, regardless of other spectra that may be present whether it overlaps a given color or not?

Remember that in our example we started with negative values at 0 and 3, and positive values at 10 and 13. While our mathematical corrections in performing compensation eliminated population spread that's found in traditional compensation, we still have the problem that we never get all negative events to exactly 0, and all positive events to exactly 10. That's what we would expect from a "perfect" compensation algorithm, since that's exactly the biological reality.

There's actually a little more going on when we stated that negative compensation or compensating on compensated (not raw) signals are mathematically equivalent. That's still true (both approaches are mathematically equivalent), other than the fact that the negative compensation compresses the scale a little bit. The real problem relies in the recursive nature of compensating-on-compensated (not raw), where we stated that compensated Yellow depends on

compensated Green, which depends on compensated Yellow. For our example above, we eliminated recursion by stopping at the first level, where we substituted all raw events.

However, if we did not stop at the first level of recursion, we would ever-more-closely better approximate the biological reality.

For example, consider our example event #3:

	Observed Values		
Event	Yellow	Green	Blue
1	0	0	0
2	10	3	0
3	3	10	3
4	0	3	10
5	10	6	10
6	13	13	3
7	3	13	13
8	13	16	13

We see that event #3 is positive for Green, but should be negative for both Yellow and Blue. However, because of our one-step computation of compensated from compensated parameters, we end up subtracting 0.3 (30%) of the "one-step" compensated Green (which is 8) from our Yellow value of 3, leaving 0.54 instead of the expected 0.0. (Remember that the "one-step" compensated Green will subtract 0.3*3[Yellow] and 0.3*3[Blue] from the original Green value of 10, leaving 8.)

However, what if we permit this recursion? What if we allow some level of recursion to take place where we actually do calculate compensated Yellow from compensated Green from compensated Yellow from compensated Green, and so on?

The first approach is to see if the recursive nature of the operation will approach some limit that we can discreetly determine. Unfortunately, this is not the case (please contact DakoCytomation directly if you want to understand the math theory as to why this cannot be solved.) However, failing some limit optimization, we can actually perform this calculation in software on each event until the incremental value of the next recursive iteration is insignificant. In short, this can be done.

For each event in this example, the values for each event asymptotically approach the expected result:

#1: Yellow[comp] = 0 - (0.3 * 0[Green[comp]]) - (0.0 * 0[Blue[comp]]) = 0
#2: Yellow[comp] = 10 - (0.3 * 3[Green[comp]]) - (0.0 * 0[Blue[comp]]) = 10
#3: Yellow[comp] = 3 - (0.3 * 10[Green[comp]]) - (0.0 * 3[Blue[comp]]) = 0
#4: Yellow[comp] = 0 - (0.3 * 3[Green[comp]]) - (0.0 * 10[Blue[comp]]) = 0
#5: Yellow[comp] = 10 - (0.3 * 6[Green[comp]]) - (0.0 * 10[Blue[comp]]) = 10
#6: Yellow[comp] = 13 - (0.3 * 13[Green[comp]]) - (0.0 * 3[Blue[comp]]) = 10
#7: Yellow[comp] = 3 - (0.3 * 13[Green[comp]]) - (0.0 * 13[Blue[comp]]) = 0
#8: Yellow[comp] = 13 - (0.3 * 16[Green[comp]]) - (0.0 * 13[Blue[comp]]) = 10

Is this realistic? Yes. Given today's hardware, this computation is realistic on every event, even in very large files.

2-Color Compensation

Fluorescent compensation is the process by which the cross-contamination error from spectral emissions from other than the marker of interest is mathematically removed. In other words, it is the process by which the "true' value of each marker is computed from the "measured" value of each marker by removing the contamination from other markers.

This is illustrated in the following graph:

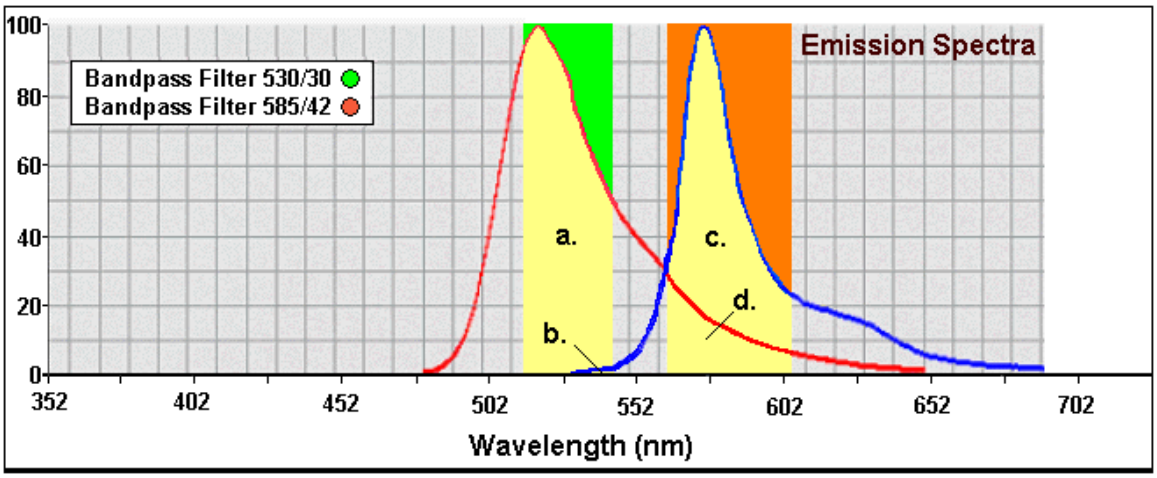

Based on the labeled regions, the "true" and "measured" values for each marker would be:

FITC true = a
FITC measured = a + b
PE true = c
PE measured = c + d

Calculating Compensation Values

Historically, fluorescent compensation to deduce the "true" from the "measured" for a two-color experiment using FITC and PE was defined incorrectly as:

FITC true = FITC measured - (C1% * PE measured)
PE true = PE measured - (C2% * FITC measured)

The constants C1 and C2 are proposed to either be "spillover coefficients" (based on the area percentage that PE fluorescence contributes to the measure in the FITC band above, and the area percentage that FITC fluorescence contributes to the measure in the PE band above, respectively), or "compensation coefficients" (based on the area percentage that other markers [in addition to PE] contributes to the measure in the FITC band above, and the area percentage that other markers [in addition to FITC] contributes to the measure in the PE band above, respectively.)

Unfortunately, this calculation is incorrect. It is technically inappropriate and mathematically ambiguous to consider "contamination" from other colors as part of the computation for the "true" marker value. Rather, these equations should read:

FITC true = FITC measured - (C1 * PE true)
PE true = PE measured - (C2 * FITC true)

The premise of the historical compensation formula is based on pragmatics, including real time processing constraints (decisions during acquisition), available hardware and technical hardware limitations, and software availability. For example, fluorescent compensation has been achieved through analog subtraction in hardware (where complex computation is not possible, and only the computed value is reported, not the raw value), and in software (where the input is the raw values reported by the instrument, and software calculates the compensated value.) In extreme cases, some users have performed both hardware and software compensation (which can produce an apparently reasonable approximate "compensated" value, although the validity of such a dual-approach is always mathematically ambiguous.)

Further, simply correcting the constants as "compensation coefficients" or "spillover coefficients" is not sufficient: The compensated value remains ambiguous unless the "true" value of the contaminating marker is used, not the "measured" value. This ambiguity is based on the fact that two particles with the same "true" value will have very different measured values, cumulatively dependant on the presence of other markers on that particle. The result of this mathematical ambiguity is population spread after compensation (as illustrated in the example below.)

Justifying a Different Compensation Algorithm: Two-Color Example

It is mathematically ambiguous and technically incorrect to subtract a percentage from an "unknown". If we merely relied upon the "measured" value of a marker with an unknown percentage of cross-contamination, then we deliberately introduce an unknown degree of error into the result. However, this is entirely unnecessary: We can empirically compute the amount of cross-contamination (indeed, that's the purpose of compensation), and we can subtract a known value from a "true" value, thus eliminating this error. Failure to use the "true" values as operands in calculating compensation results in population "spread" so clearly documented in the literature and introduction of mathematically anomalous sub-populations that never existed in the real world.

Consider the following example:

An arbitrary range exists from "0" (no fluorescence) to "1024" (bright beyond our detector).
"+" means "positive" for that marker (measure ³ 500).
"-" means "negative" for that marker (measure < 500).
Instrument is aligned for the negative population at 100.
Instrument is aligned for the positive population at 1000.
The "spillover" from PE to the FITC measure is 5% (of the "true" PE).
The "spillover" from FITC to the PE measure is 30% (of the "true" FITC).
Calculated "spillover" is the "spillover" constant times the fluorescent value above negative (above 100). [Since the instrument's PMTs are arbitrarily aligned to "negative" populations at 100, a population negative for all markers should have all markers reporting that population at 100.]

This provides us with the following compensation matrix:

	FITC	PE
FITC	n/a	5.00%
PE	30.00%	n/a

Assuming perfect expression, the following particles represent all possibilities for FITC and PE expression within a population:

Particle	FITC	PE	FITCmeasure	FITCtrue	PEmeasure	PEtrue
1	-	-	100	100	100	100
2	+	-	1000	1000	370	100
3	-	+	145	100	1000	1000
4	+	+	1045	1000	1270	1000

Using the "historical" calculation of compensation where we subtract percentages from the measured values (not the true values) we incorrectly reach:

FITC true = FITC measured - (0.05 * PE measured)
PE true = PE measured - (0.30 * FITC measured)

					Historical	Historical			Historical	Historical
Particle	FITC	PE	FITCmeasure	FITCtrue	FITCcomp	Diff(true-comp)	PEmeasure	PEtrue	PEcomp	Diff(true-comp)
1	-	-	100	100	100	0	100	100	100	0
2	+	-	1000	1000	986.5	13.5	370	100	100	0
3	-	+	145	100	100	0	1000	1000	986.5	13.5
4	+	+	1045	1000	986.5	13.5	1270	1000	986.5	13.5

Here we see differences between the computed value and the true value, which is entirely based on subtracting an percentage from a "dirty" value (the raw, measured value). We term this "dirty" because it varies for each particle: While particles #2 and #4 both have a "true" value of 1000, one measured at 1000 and the other at 1045 (a 4.5% shift).

This suggests one reason why uncompensated histograms show population spreading that aren't biologically (or physically) true. However, in this case, the compensated values for both particles were the same: Both were determined at channel 986.5 instead of their true channel 1000, (a 1.35% shift), but the population was not further distorted (indeed, the population was tighter since both ended up in the same channel.) Using the proper calculation, we correctly reach:

FITC true = FITC measured - (0.05 * PE true)
PE true = PE measured - (0.30 * FITC true)

					Proper	Proper			Proper	Proper
Particle	FITC	PE	FITCmeasure	FITCtrue	FITCcomp	Diff(true-comp)	PEmeasure	PEtrue	PEcomp	Diff(true-comp)
1	-	-	100	100	100	0	100	100	100	0
2	+	-	1000	1000	1000	0	370	100	100	0
3	-	+	145	100	100	0	1000	1000	1000	0
4	+	+	1045	1000	1000	0	1270	1000	1000	0

As seen in this calculation, the computed value resolved to the "true" value with no population spreading, and no population shift.

2-Color Compensation Experiment

(A 2-Color Experiment involving FITC and PE)

The requirement for compensation arises from spectral overlap between fluorescence detectors. Dyes such as fluorescein (FITC) and phycoerythrin (PE) which are excited at 488 nanometers will fluoresce optimally at 520 and 576 nanometers respectively. Filters with bandwidths of 20 or 30 nanometers are typically used to allow photodetectors to respond to either a FITC or PE fluorochrome. However, the emission wavelengths of these dyes are sufficiently broad that light from a PE fluorochrome will leak through the filter of the FITC detector and vice versa. Compensation is a method to remove this spectral overlap. This makes the data orthogonal, simplifying human interpretation and separating distinct populations that may overlap on the dot plot.

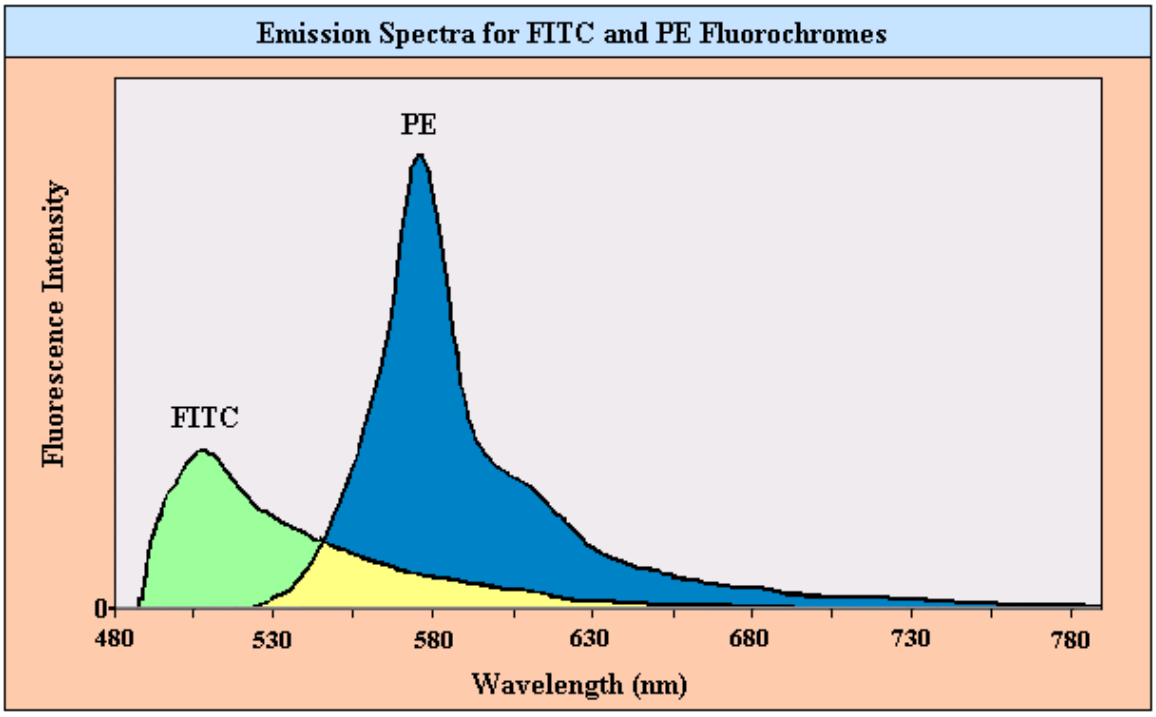

The diagram above shows the emission spectra for both FITC and PE. It is common for a fluorochrome's emission distribution to have a steep intensity rise on the shorter wavelength side and a gradual decline in intensity on the longer wavelength side. This usually means that spectral overlap is less a concern for the shorter wavelength fluorochrome than for the longer wavelength fluorochrome (usually we worry about emissions from the shorter wavelength fluorochrome spilling into the bandpass filter range and PMT of the longer wavelength fluorochrome, not the other way around). In this case, FITC contaminates PE more than PE contaminates FITC in the range we use to measure the fluorochrome.

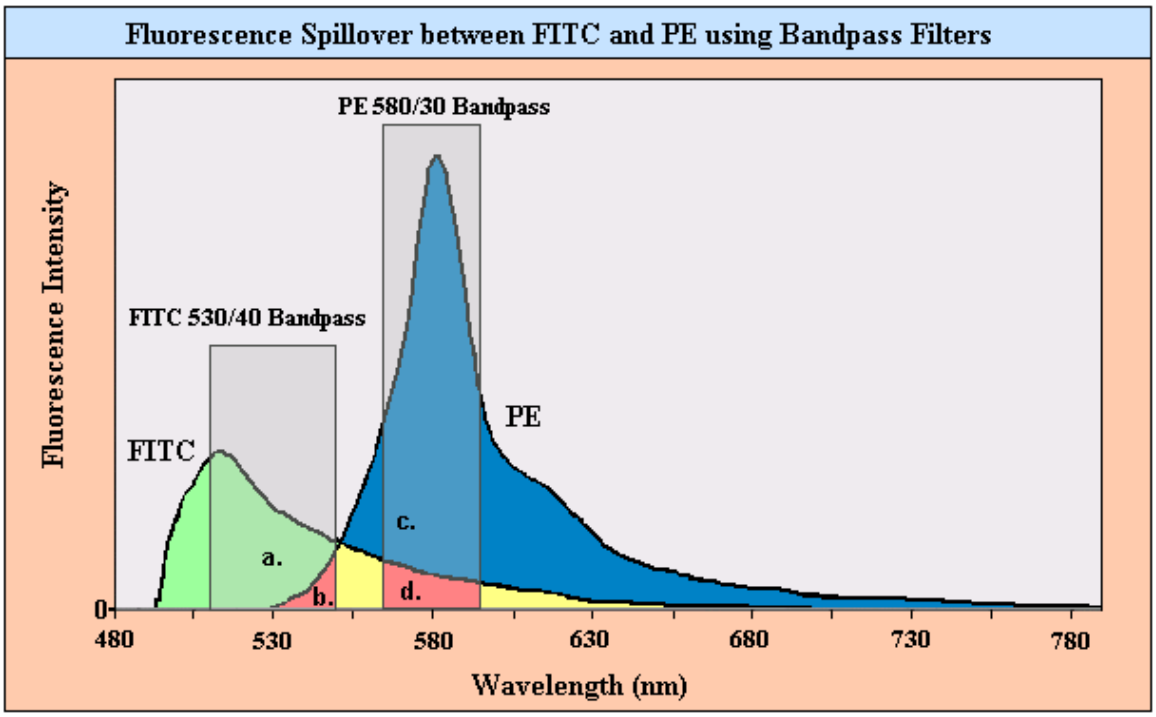

As seen when using a 580/30 bandpass filter to detect PE signal, this spectral overlap of FITC within the filter's wavelength range causes a falsely high accounting of PE. In the range of the bandpass filter, a small percentage of the total (collected) PE signal will be from FITC fluorescence (the contribution of area "d" to the PE measure). Consequently, we must compensate the observed PE signal by subtracting out a percentage of the observed FITC signal. The same is true for our need to compensate the observed FITC signal by subtracting out a percentage of the observed PE signal (we subtract out the contribution of area "b" to the FITC measure). This is explained in the following equations:

$$FITC_{measured} = a + b \qquad PE_{measured} = c + d$$

$$FITC_{real} = a \qquad PE_{real} = c$$

If multiple colors are being measured simultaneously, there can be a cascading need for compensation across several measured fluorescent values. This can be accomplished by creating a Compensation Matrix in the Summit Software program to mathematically correct for the multiple combinations of fluorescent overlap.

Goal of Compensation

The goal of compensation is to apply the proper correction factor to each parameter so that the median fluorescence in the stained population is equivalent to the median fluorescence in the unstained population. If a specimen is stained with only FITC, then ideally we should not see any fluorescent intensity in the PE channel. However, this is not the case because of the overlap in emission (around 575nm) between the two fluorochromes. Once the proper compensation value is applied, the median fluorescent intensity for PE in a sample stained with only FITC is equivalent to the PE median in cells not stained with FITC.

How does this work with Dot Plots?

For example, when setting compensation using FITC and PE beads or for a 2-color experiment, unstained events that are FITC - and PE - would appear within the lower left portion of the FITC versus PE dot plot.

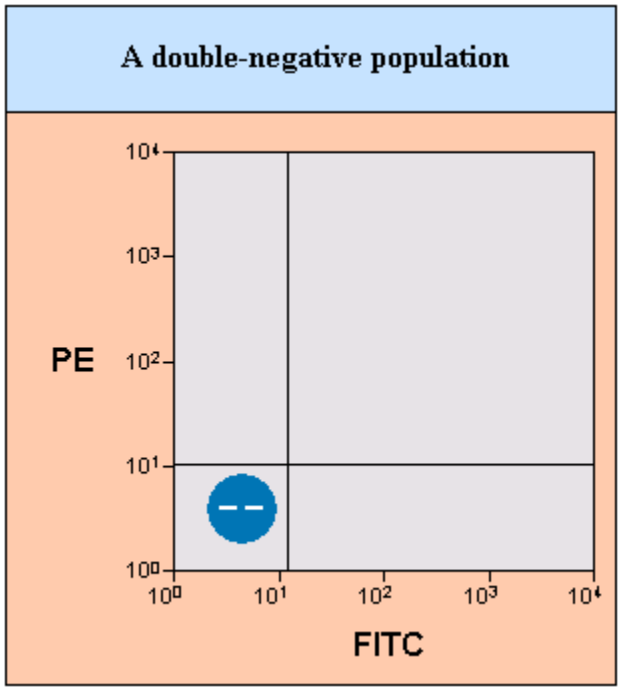

A double positive population would appear somewhere within the upper right-hand portion of the dot plot, indicating both FITC and PE signal. This population may appear along any fluorescent intensity range within the histogram based on factors such as FITC and PE fluorochrome density, filters used, or PMT voltage settings.

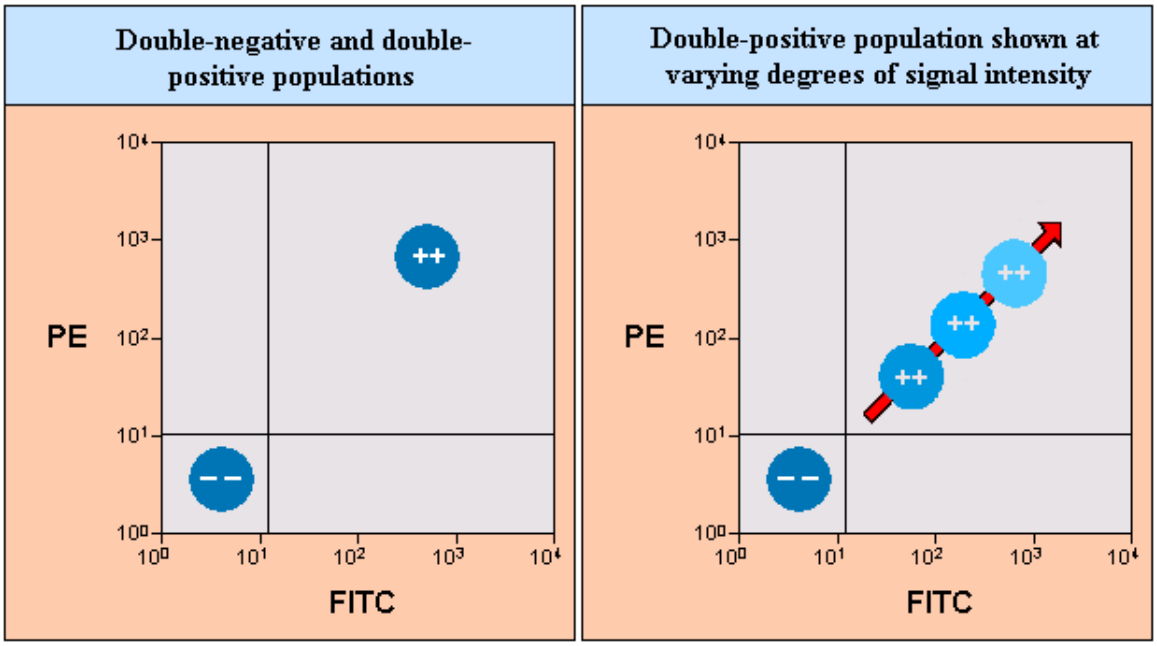

In an “ideal world" where no compensation would be needed, both the FITC and PE positive populations would fall along the appropriate axis and have the same median fluorescence as the negative population.

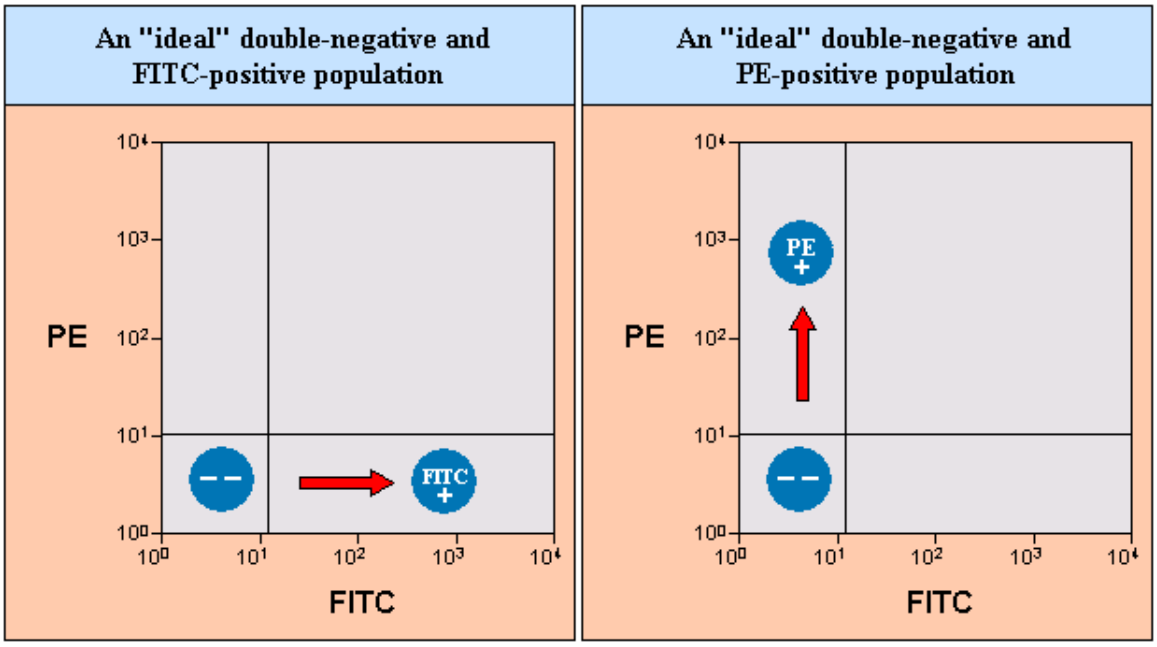

The positive populations may appear anywhere along the corresponding axis. The range of florescence intensity is based on factors such as antigen density, the quantum fluorochrome excitation and emission efficiency, filter differences, or PMT voltage settings.

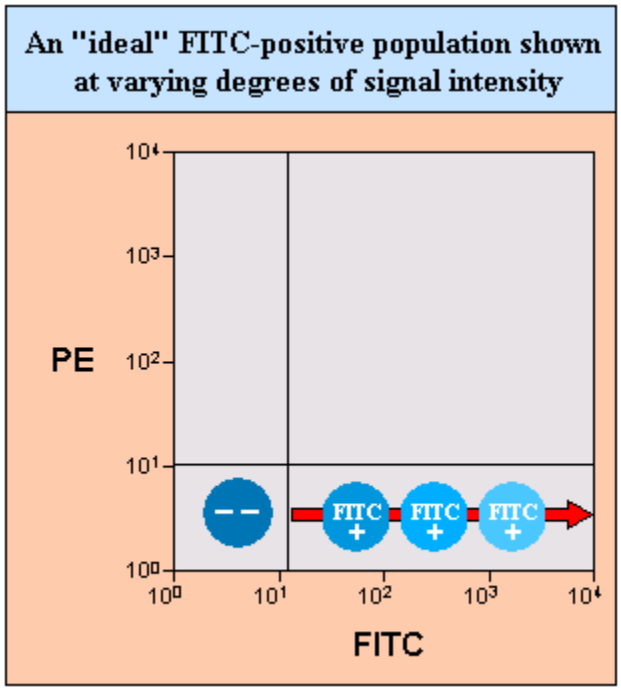

In reality, because there is spectral overlap between the two signals, the FITC and PE positive populations will appear offset (that is, to have a different median fluorescence from the negative population). A FITC-positive population which is not stained with PE will still appear slightly brighter in the PE parameter because of the spectral contamination from the FITC. The same is true for FITC when running a PE single-positive control. This spectral overlap is what is physically observed by the cytometer (by the photodetectors for each parameter).

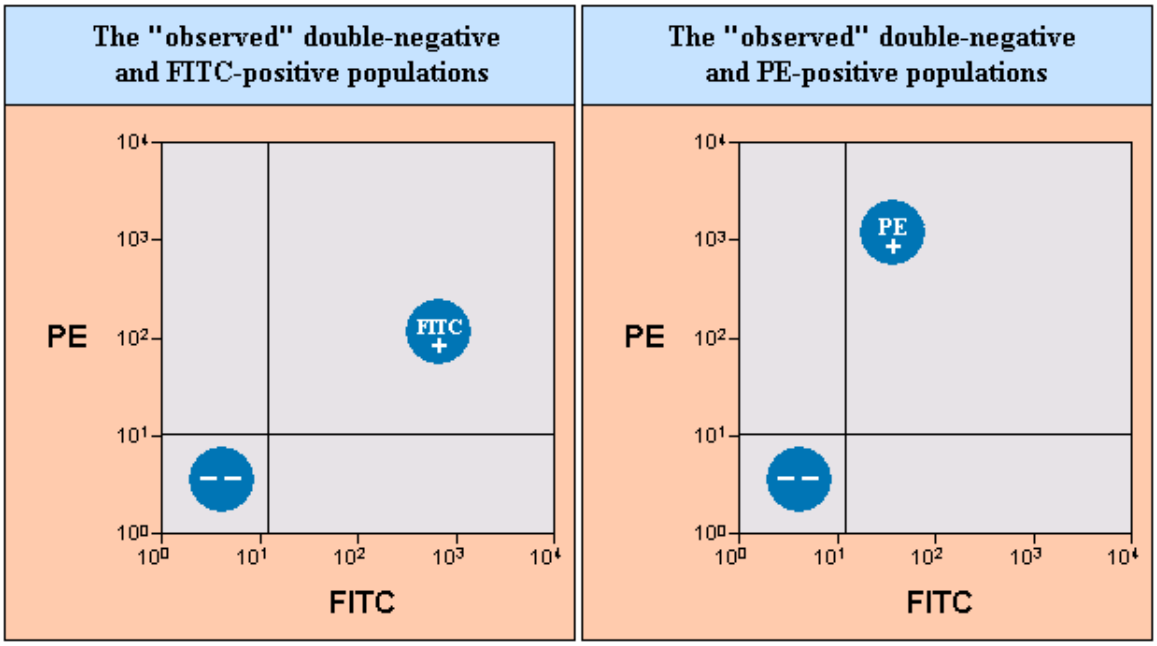

The degree that both populations are offset with regard to the ideal position represents the spectral overlap from one fluorescent signal into the other.

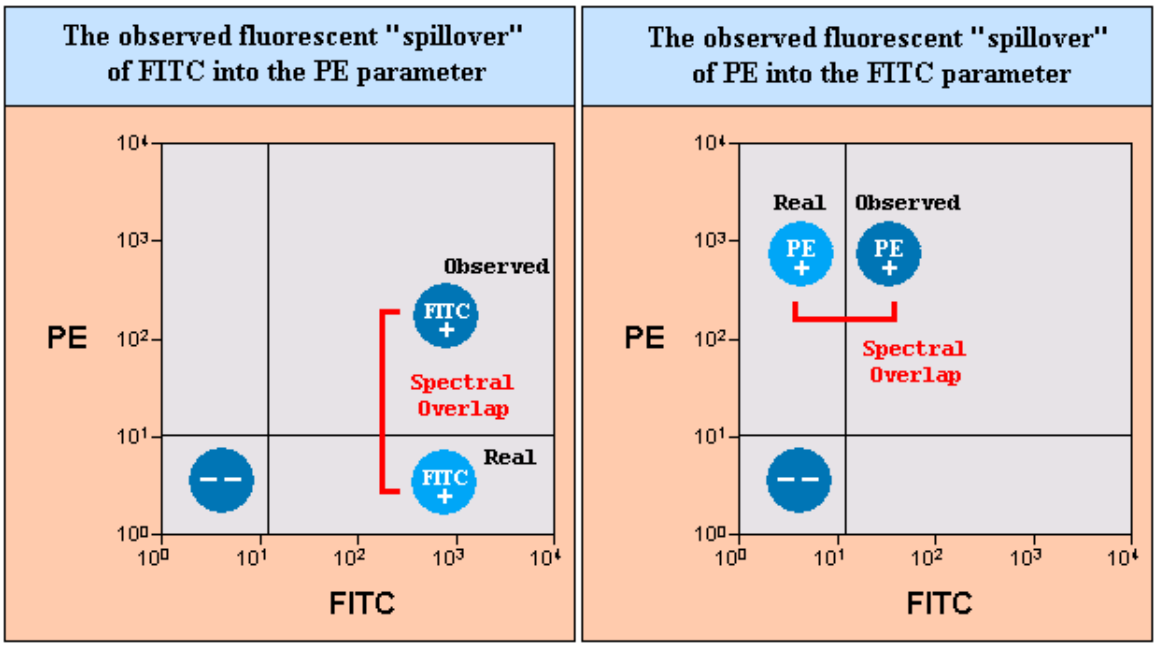

Keep in mind that the degree of spectral overlap for the two populations is not identical. This is accounted for by the fact that the degree of overlap between the emission spectra of the two fluorescent compounds is not symmetrical.

Because of the spectral overlap between the FITC and PE signals, compensation is needed to correct for the unwanted overlap (or spectral cross-contamination). Compensation controls allow you to adjust or shift the data to mathematically remove the fluorescent overlap.

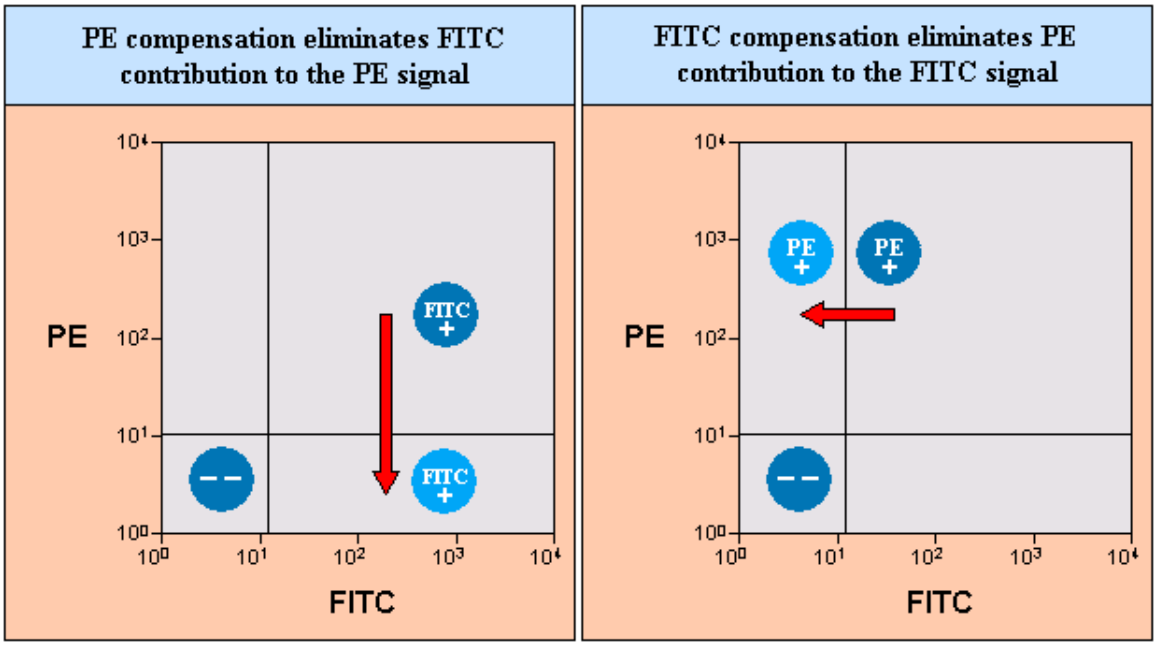

Compensation is adjusted to align populations so that the median fluorescence in the stained population is equivalent to the median fluorescence in the unstained population. Positioning of the data is performed with respect to the negative control population: A PE-negative population should have the same median value as all the other PE-negative populations, regardless of the presence of FITC receptors on that population.

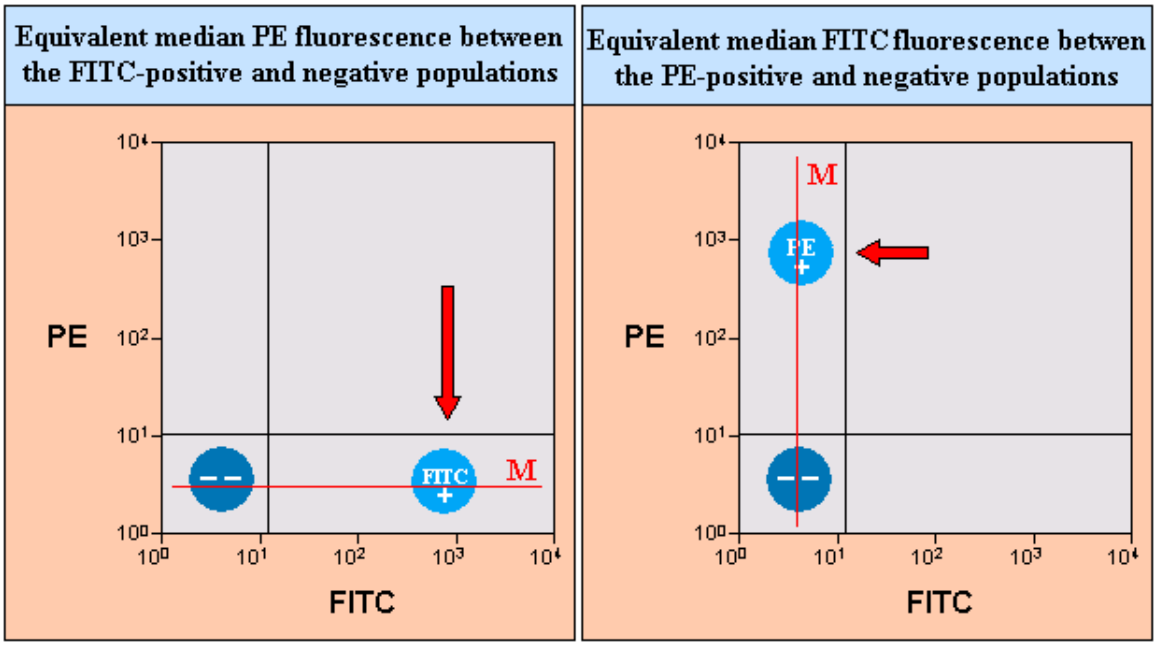

Typically, after the data is compensated, the populations will appear more stretched or oblong because the population is moving along a logarithmic axis. For example, on a logarithmic scale, the difference between two channels at the beginning of the first decade is "one", the difference between two channels at the beginning of the second decade is "ten", and the difference between two channels at the beginning of the third decade is "one hundred". When the population is pulled "lower" on the axis, the population retains the same resolution, but the data appears to stretch.

Further, compensation algorithms used by some software may stretch the population because of the compensation math involved. In this case, this phenomenon is amplified depending upon the amount of compensation applied (based on the degree of overlap between the two signals).

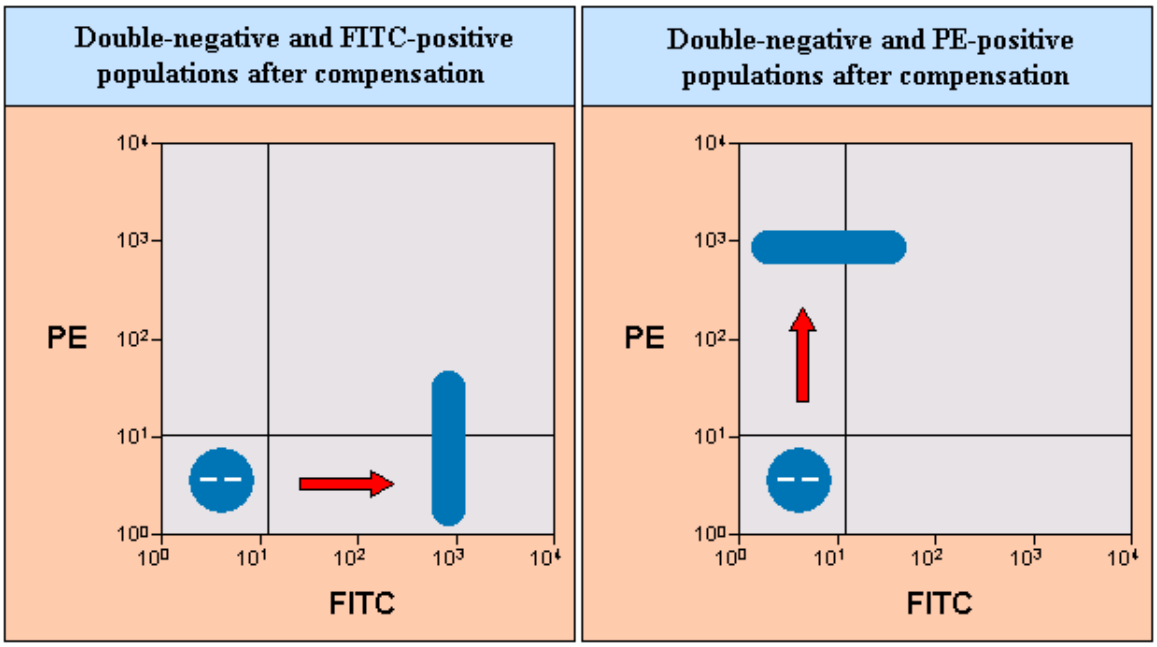

An Example Using Fluorescent Beads

The following illustrates an example of bead data using FITC and PE stained beads. The dot plot below shows three populations: an unstained population, a FITC-positive population, and a PE-positive population. Data was collected using DakoCytomation's FloComp™ beads.

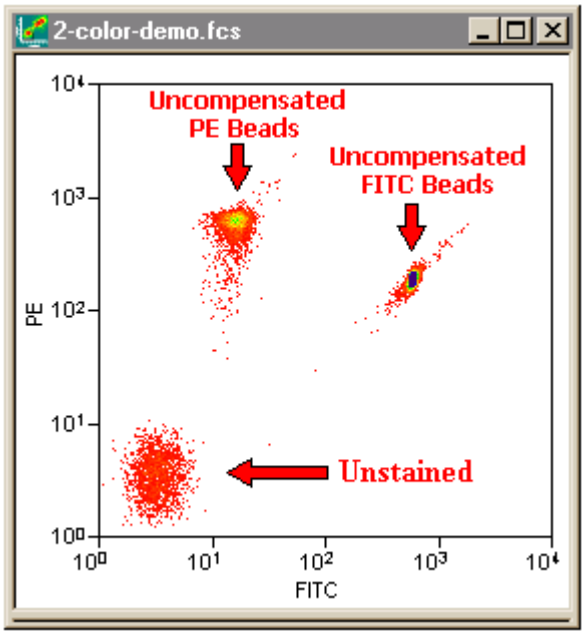

Compensating the Data

Within the dot plot, you will want to create a quad region. The statistics (median fluorescence) generated from the quad region will be used to align the median fluorescence of the unstained

and stained populations. Actual placement of the quadrants depends on the data and on the scientist's preference, but placement at one decade on a four-decade resolution axis is common.

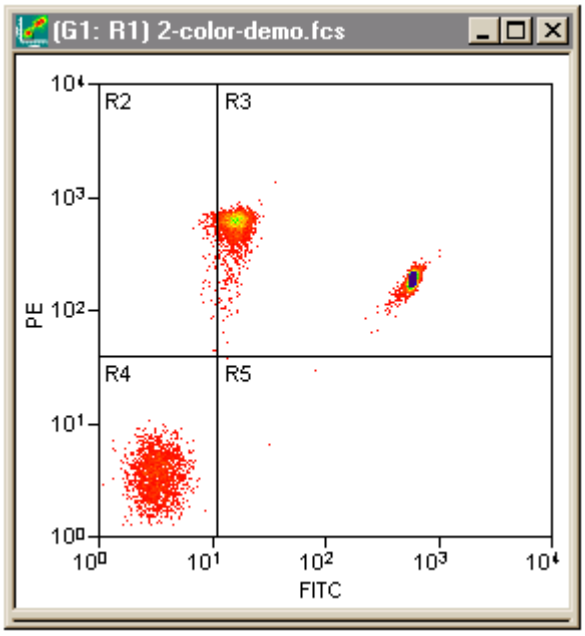

Using Summit, you can right-click along a dot plot axis and select the "Adjust Compensation" option. When the adjust compensation feature is activated, red slider arrows will appear along both the X and Y-axis. These sliders can be used to adjust compensation.

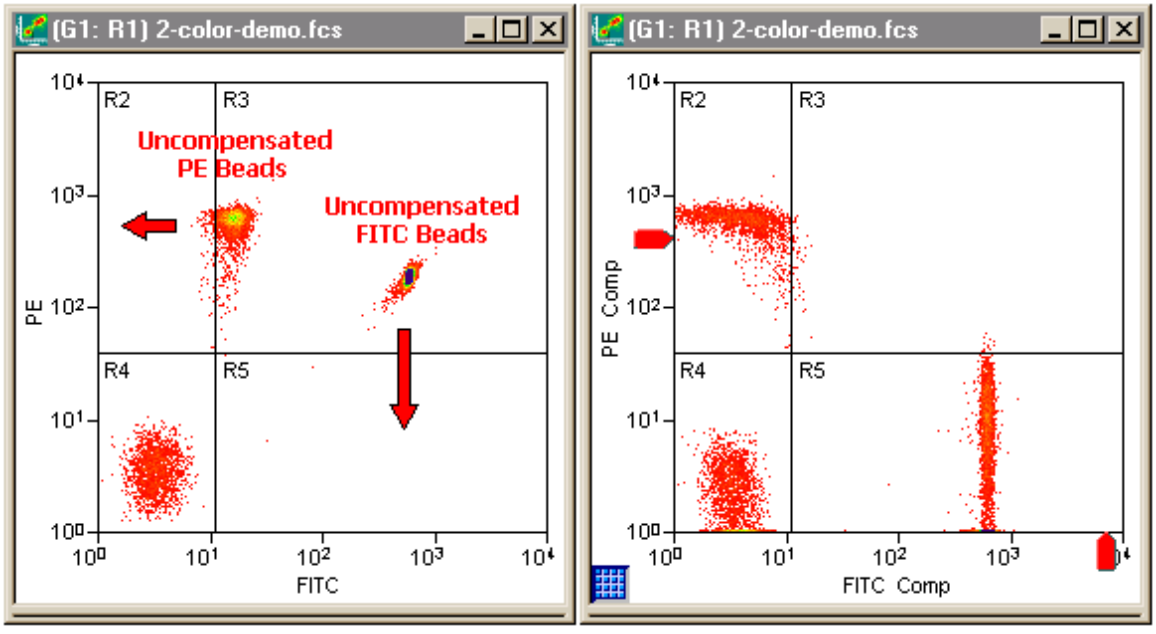

To properly set compensation, adjust the X and Y-axis sliders such that the median fluorescent channel of the positive population is nearly equivalent to the median fluorescent channel of the unstained population. For example, to set compensation for the FITC bead population, align the FITC bead population within Region 5 so that the median fluorescent channel is nearly equal to

the Region 4 population. (Within 1.0 is typically acceptable, but more accuracy is usually obtained when performing compensation post-acquisition.)

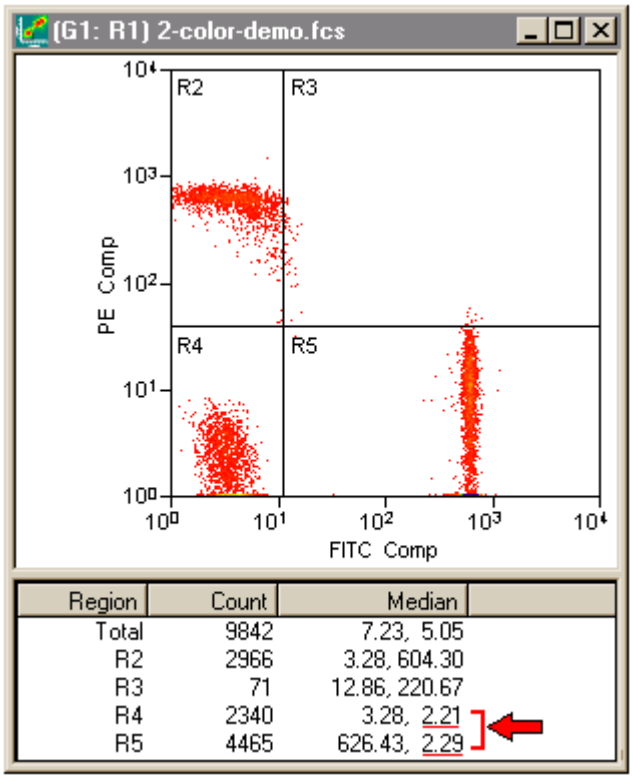

Region	Count	Median
Total	9842	7.23, 5.05
R2	2966	3.28, 604.30
R3	71	12.86, 220.67
R4	2340	3.28, 2.21
R5	4465	626.43, 2.29

To set compensation for the PE bead population, align the PE bead population within Region 2 so that the median fluorescent channel is nearly equal to the Region 4 population.

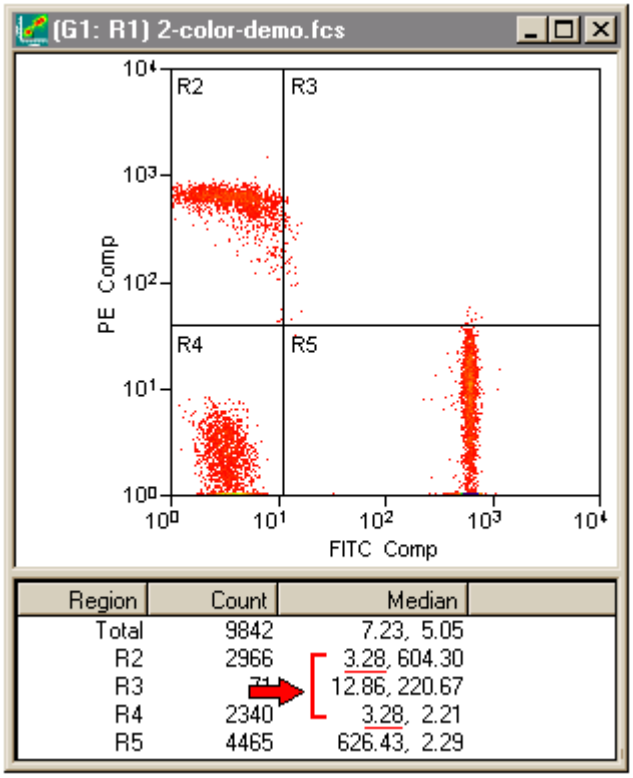

Advanced Issues

This topic discusses the basic principle of spectral overlap between fluorescence detectors which creates a need for compensation. An example of spectral overlap, both in theory and in practice, is shown for FITC and PE.

A number of compensation topics exist which are well beyond the scope of this topic. These include issues and differences in hardware versus software compensation, online and post-acquisition compensation, different compensation algorithms and approaches (mathematical anomalies that exist with some algorithms), compensation for experiments with more fluorescent parameters (five to seven parameters are common, with some research at twelve or more simultaneous colors), procedures to run single- and multi-color controls, and procedural and operational considerations. The latter includes various types of fluorochrome interaction (competition, background noise, quantum fluorochrome excitation and emission efficiency, filter differences, PMT voltage settings, etc.) While conceptually simple, the need for proper fluorescent compensation plays a significant role in research advances involving instrumentation, reagents, and sample preparation or measure.

3-Color Compensation

The issue of compensation is dramatically amplified with additional markers in the same experiment. We now consider the following excitation curves for FITC, PE, and Cy5-PE (a tandem dye where excitation is in a PE molecule, but fluorescence is transferred to the Cy5 molecule for emission in a lower-energy wavelength), including the 488nm laser line used to excite each:

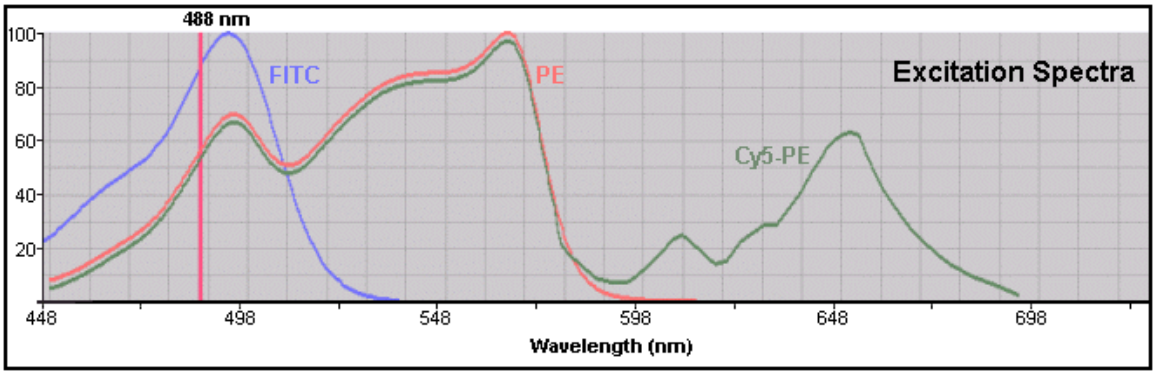

FITC, PE, and Cy5-PE will fluoresce at the following wavelengths, and we use the indicated bands for their respective measures:

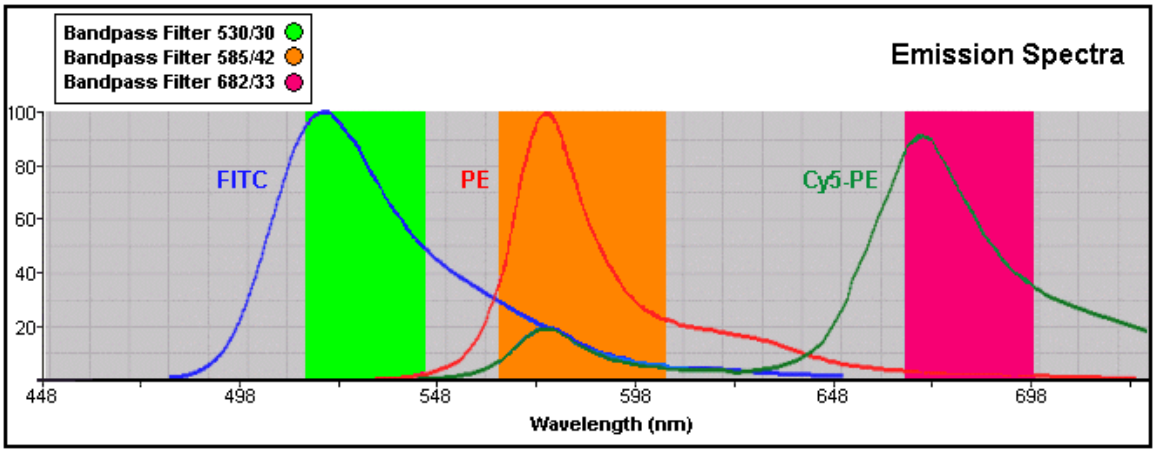

The "spillover" from PE to the FITC measure is 5% (of the "true" PE).
The "spillover" from Cy5-PE to the FITC measure is 1% (of the "true' Cy5-PE).
The "spillover" from FITC to the PE measure is 30% (of the "true" FITC).
The "spillover" from Cy5-PE to the PE measure is 25% (of the "true" Cy5-PE).
The "spillover" from FITC to the Cy5-PE measure is 0% (of the "true" FITC).
The "spillover" from PE to the Cy5-PE measure is 8% (of the "true" PE).

This yields the following compensation matrix:

	FITC	PE	Cy5-PE
FITC	n/a	5.00%	1.00%
PE	30.00%	n/a	25.00%
Cy5-PE	0.00%	8.00%	n/a

The "true" and measured values are:

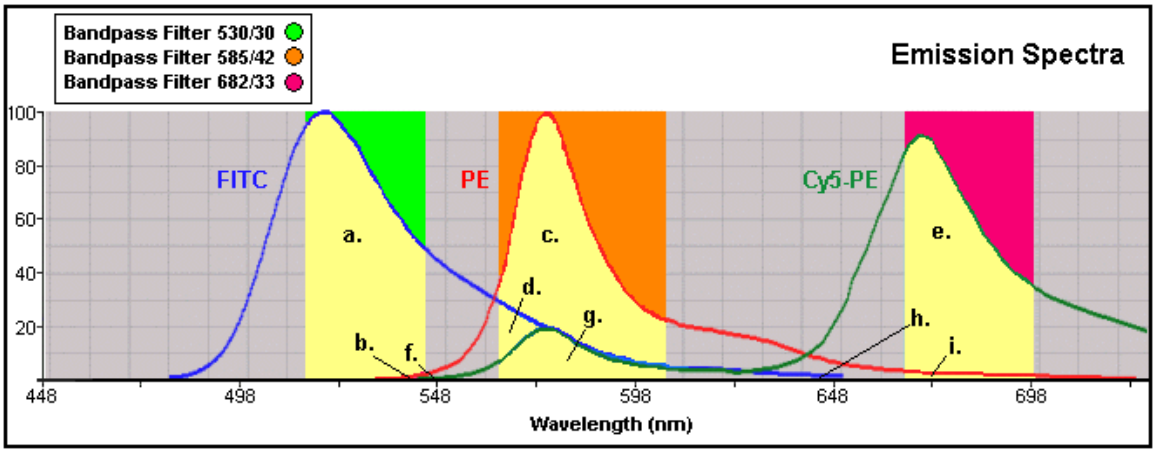

FITC true = a
FITC measured = a + b + f
PE true = c
PE measured = c + d + g
Cy5-PE true = e
Cy5-PE measured = e + i + (h)

Please note that for completeness we include "h" in our calculations, but we state in this example that there is no "spillover" from FITC to Cy5-PE (represented by the area of "h"). Assuming perfect expression, the following particles represent all possibilities for FITC and PE and Cy5-PE expression within a population:

Particle	FITC	PE	Cy5-PE	FITCmeasure	FITCtrue	PEmeasure	PEtrue	Cy5-PEmeasure	Cy5-PEtrue
1	-	-	-	100	100	100	100	100	100
2	+	-	-	1000	1000	370	100	100	100
3	-	+	-	145	100	1000	1000	172	100
4	+	+	-	1045	1000	1270	1000	172	100
5	-	-	+	109	100	325	100	1000	1000
6	+	-	+	1009	1000	595	100	1000	1000
7	-	+	+	154	100	1225	1000	1072	1000
8	+	+	+	1054	1000	1495	1000	1072	1000

Calculating 3-Color Compensation Values

Using the "historical" calculation of compensation where we subtract percentages from the measured values, not the true values, we incorrectly reach:

FITC true = FITC measured - (0.05 * PE measured) - (0.01 * Cy5-PE measured)
PE true = PE measured - (0.30 * FITC measured) - (0.25 * Cy5-PE measured)
Cy5-PE true = Cy5-PE measured - (0.00 * FITC measured) - (0.80 * PE measured)

						Historical	Historical			Historical	Historical			Historical	Historical
Particle	FITC	PE	Cy5-PE	FITCmeasure	FITCtrue	FITCcomp	Diff(true-comp)	PEmeasure	PEtrue	PEcomp	Diff(true-comp)	Cy5-PEmeasure	Cy5-PEtrue	Cy5-PEcomp	Diff(true-comp)
1	-	-	-	100	100	100	0	100	100	100	0	100	100	100	0
2	+	-	-	1000	1000	986.5	13.5	370	100	100	0	100	100	78.4	21.6
3	-	+	-	145	100	99.28	0.72	1000	1000	968.5	31.5	172	100	100	0
4	+	+	-	1045	1000	985.78	14.22	1270	1000	968.5	31.5	172	100	78.4	21.6
5	-	-	+	109	100	88.75	11.25	325	100	97.3	2.7	1000	1000	982	18
6	+	-	+	1009	1000	975.25	24.75	595	100	97.3	2.7	1000	1000	960.4	39.6
7	-	+	+	154	100	88.03	11.97	1225	1000	965.8	34.2	1072	1000	982	18
8	+	+	+	1054	1000	974.53	25.47	1495	1000	965.8	34.2	1072	1000	960.4	39.6

Differences between the computed and the true values are much more significant in this example, beyond what was seen in the two-color example. For example, even though the FITC and PE interaction remains constant, the introduction of the Cy5-PE marker changes our error shift of 1.35% in our determination of the "true" value of PE from the two-color example to as high as 3.42% for PE in the three-color example (more than doubling). Further, the contribution of both FITC and Cy5-PE to PE amplifies the same error, resulting in a calculated error of 3.96% for Cy5-PE. In other words, too much PE is subtracted from Cy5-PE, because that PE measure was arbitrarily inflated by both FITC and Cy5-PE. Moreover, the erroneous calculation essentially subtracts FITC from Cy5-PE even though we state that there is no physical association (rather, the historical calculation introduces a faulty mathematical association between FITC and Cy5-PE.)

One anomaly deserves specific attention: Population spreading. While particles #5, #6, #7, and #8 all have the same "true" value, the historical calculation striates that group into two sub-populations: One with a 1.8% error, and one with a 3.96% error. This is entirely a mathematical anomaly that creates population spreading, or at high resolution, population striation (since these sub-populations have a 2.16% shift from each other). All three markers exhibit this shift for both positive and negative populations, including a four-level gradient of error for the FITC negatives and a four-level gradient of error for FITC positives.

We now repeat the calculation with the proper compensation formulae:

FITC true = FITC measured - (0.05 * PE true) - (0.01 * Cy5-PE true)
PE true = PE measured - (0.30 * FITC true) - (0.25 * Cy5-PE true)
Cy5-PE true = Cy5-PE measured - (0.00 * FITC true) - (0.80 * PE true)

						Proper	Proper			Proper	Proper			Proper	Proper
Particle	FITC	PE	Cy5-PE	FITCmeasure	FITCtrue	FITCcomp	Diff(true-comp)	PEmeasure	PEtrue	PEcomp	Diff(true-comp)	Cy5-PEmeasure	Cy5-PEtrue	Cy5-PEcomp	Diff(true-comp)
1	-	-	-	100	100	100	0	100	100	100	0	100	100	100	0
2	+	-	-	1000	1000	1000	0	370	100	100	0	100	100	100	0
3	-	+	-	145	100	100	0	1000	1000	1000	0	172	100	100	0
4	+	+	-	1045	1000	1000	0	1270	1000	1000	0	172	100	100	0
5	-	-	+	109	100	100	0	325	100	100	0	1000	1000	1000	0
6	+	-	+	1009	1000	1000	0	595	100	100	0	1000	1000	1000	0
7	-	+	+	154	100	100	0	1225	1000	1000	0	1072	1000	1000	0
8	+	+	+	1054	1000	1000	0	1495	1000	1000	0	1072	1000	1000	0

As before, we have no such mathematical anomalies with the proper compensation approach.

Proper Compensation: Pragmatics

Consider again the formulae for "proper" compensation in our three-color example:

FITC true = FITC measured - (0.05 * PE true) - (0.01 * Cy5-PE true)
PE true = PE measured - (0.30 * FITC true) - (0.25 * Cy5-PE true)
Cy5-PE true = Cy5-PE measured - (0.00 * FITC true) - (0.80 * PE true)

At first blush, this appears to be a recursive calculation. For example, FITC true is calculated from PE true which is similarly calculated from FITC true . If these circular dependencies exist, can the value be calculated?

First, the calculations could be made if each operation was theoretically taken to infinity, and the results were propagated back to the highest level. Similarly, today's hardware could compute the value at one level of recursion, and then a second level, and if those levels are different to a significant digit, the process could continue until a third level, comparing with the second level. This is a practical approach that would take only a handful of iterations, and is quite reasonable on a per-particle basis (even real time during acquisition) on today's hardware

5-Color Compensation Experiment

The following 5-color experiment involves compensation and uses the following fluorochromes: FITC, PE, PE-Cy5, APC, and APC-Cy7. Whole blood is drawn from a donor and partitioned into 7 tubes. Tube #1 is not stained with any fluorochrome (a "no stain" control). Tubes #2-6 are each stained using one of the 5 colors. Cells within tube #7 are stained using all 5 fluorochromes. Below is a table listing the 7 tubes, fluorochromes used for each, and the respective cell surface marker targeted.

Sample	Target	Stain
Tube #1	None	None
Tube #2	CD3	FITC
Tube #3	CD19	PE
Tube #4	CD45	PE-Cy5
Tube #5	CD4	APC
Tube #6	CD8	APC-Cy7
Tube #7	All	All

Background

When performing a multi-color experiment on your instrument, the forward and side light scatter parameters should be set to linear; all fluorescent parameters should be set to log. Create a forward versus side scatter dot plot and run the non-stained sample. This allows identification of the cell populations that will be used for gating. Below is a dot-plot showing unstained whole blood using both the forward and side scatter parameters. The lymphocyte, monocyte, and granulocyte populations have been color coded for easy recognition.

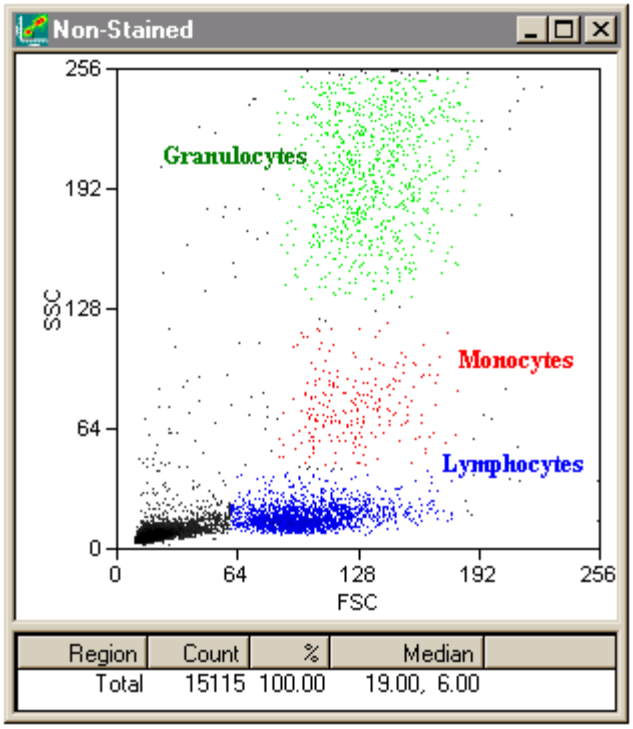

Within the forward-side scatter plot, create a region around the lymphocyte population. This region will be used to gate the lymphocytes into additional histograms.

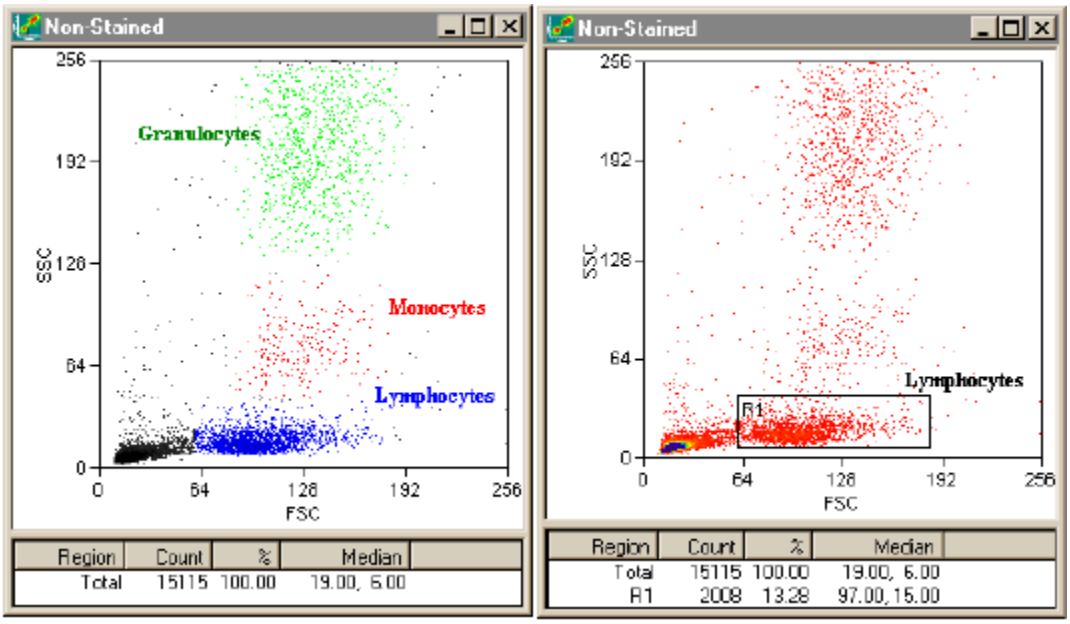

Setting Up Histograms for Compensation

When performing a multi-color experiment, a non-stained sample is run followed by the first "single color" stain to be analyzed (e.g. FITC). Create a series of plots such that this parameter is paired with each of the other colors in the experiment. For example, this 5 color experiment involves FITC, PE, PE-Cy5, APC, and APC-Cy7. If FITC is the first "single color" to be run, 4

plots should be created: FITC versus PE, FITC versus PE-Cy5, FITC versus APC, and FITC versus APC-Cy7. Typically, we recommend that you plot FITC along the X-axis and the other 4 colors along the Y. If a 7-color experiment is being conducted, 6 plots need to be created: color 1 versus. 2, 1 versus 3, 1 versus 4, 1 versus 5, 1 versus 6, and 1 versus 7.

Additionally, you will want to create a quadrant within each of the dot plots. Statistics from the quad regions will be used in setting compensation from the control samples and identifying positive and negative populations in the "all stains" sample. In general, we recommend that you position the quadrants to encompass the 1st log decade. Although this is not essential when setting and adjusting compensation, when the "all stains" sample is run, the quadrant will need to be aligned along the 1st decade mark to properly identify the positive and negative populations.

The graphic below shows 4 plots that have been created for the 5-color data. Notice that FITC has been paired against the other 4 fluorochromes used in the experiment.

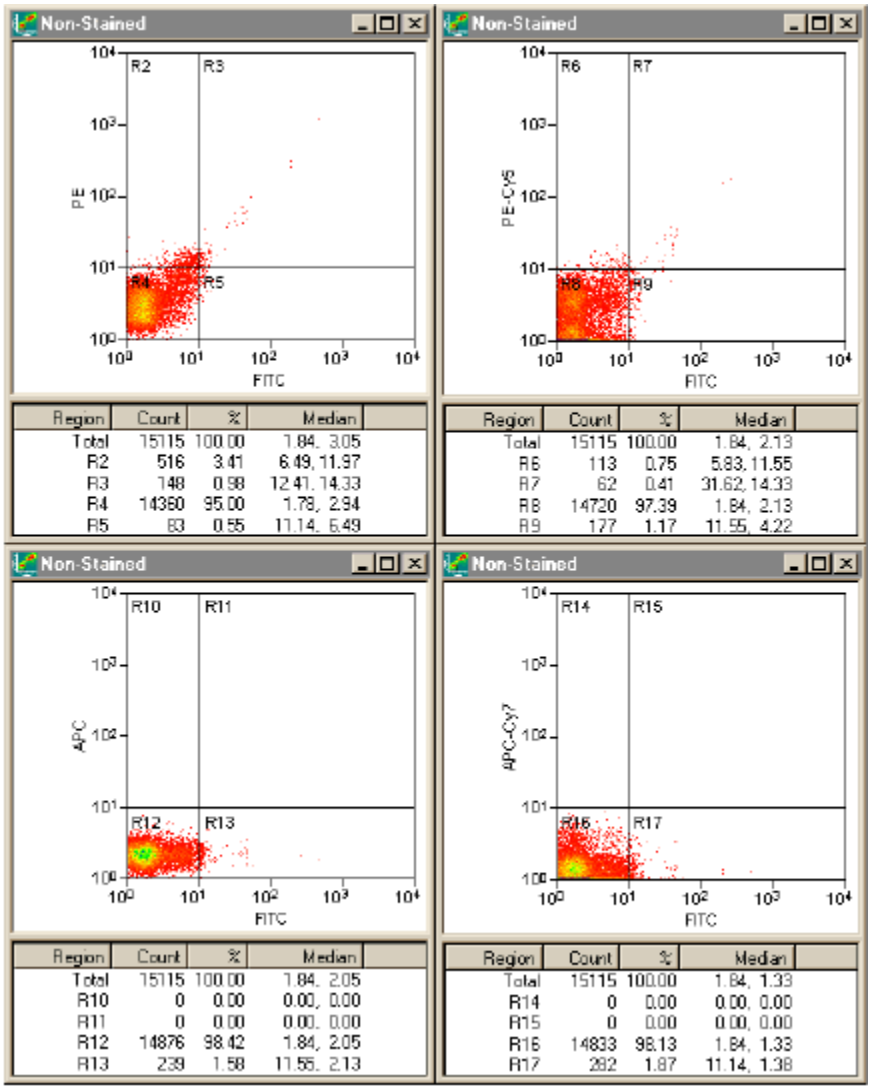

After creating the necessary histograms and quad regions, gate the lymphocyte population from region (R1) to the 4 dot plots.

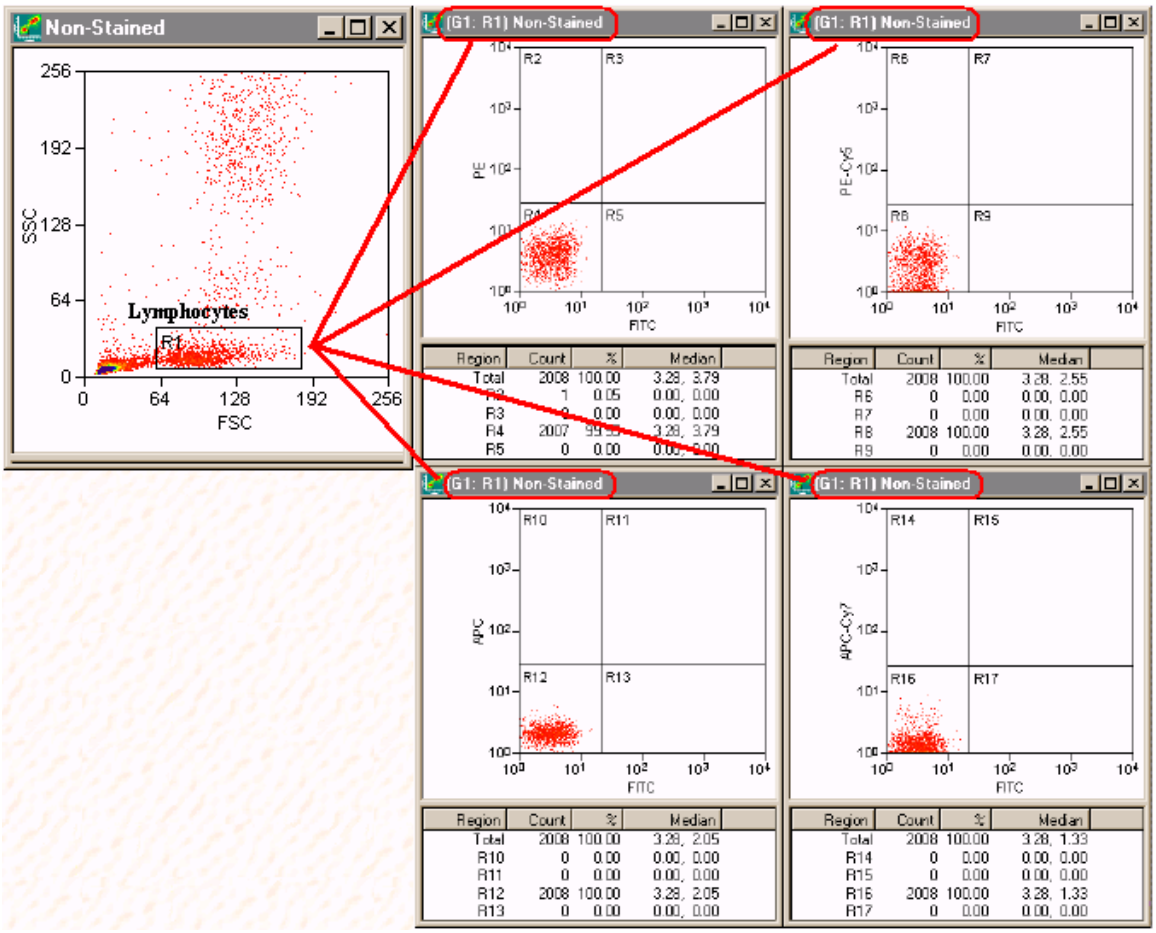

Run the non-stained sample. If necessary, use the PMT controls to set the negative population for each fluorescent channel within the first log decade.

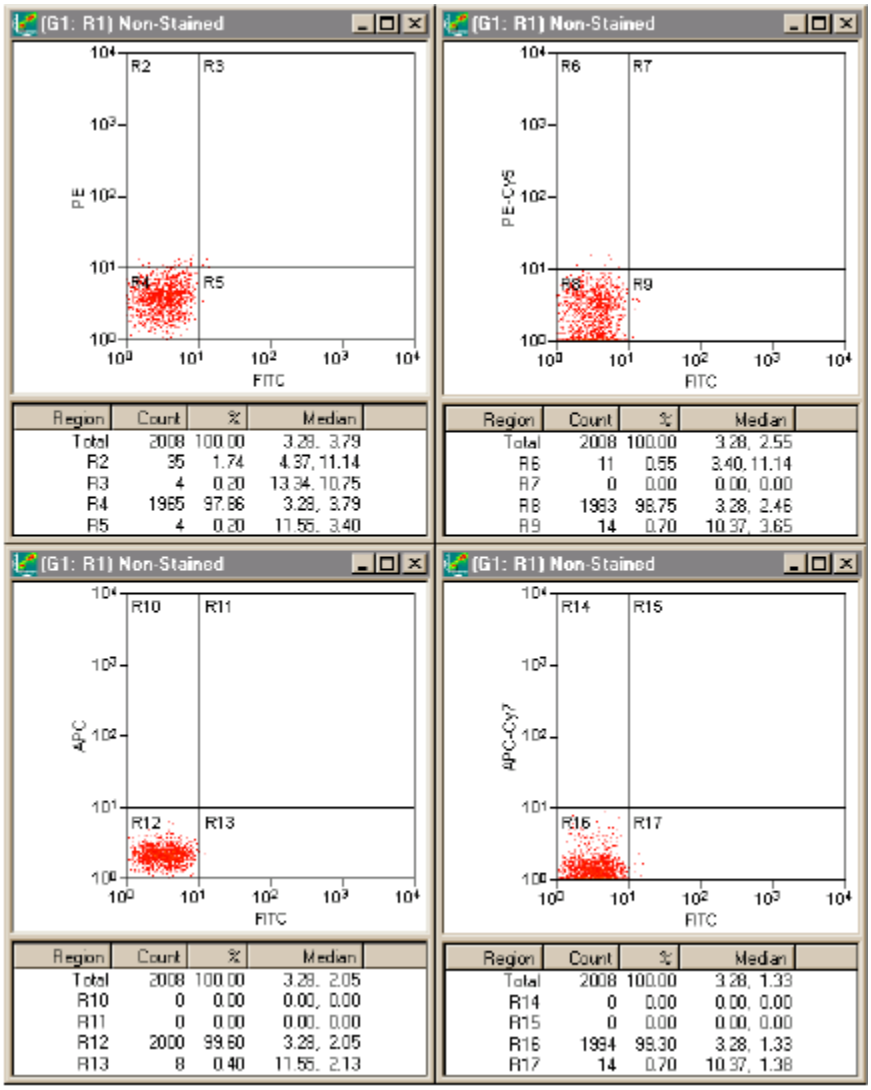

Running the First Sample

After gating the dot plots for the lymphocyte population within region (R1), run the first "single color" sample. In theory, it does not matter which of the 5 "single color" samples you begin with, although in this example we are starting with FITC. When the first "single color" sample is run, you will notice a negative population within the lower left quadrant with the FITC positive population occurring in the lower right quadrant. The negative population occurs because not all cells within the lymphocyte population express the CD3 marker, and thus will report as FITC - .

Also, you will notice that in the FITC versus PE plot, the positive population is shifted into the upper right quadrant. This means that the signal from the FITC population is also being detected by the PE channel. The degree to which signal is being detected for the PE parameter represents the % spillover of PE into the FITC signal.

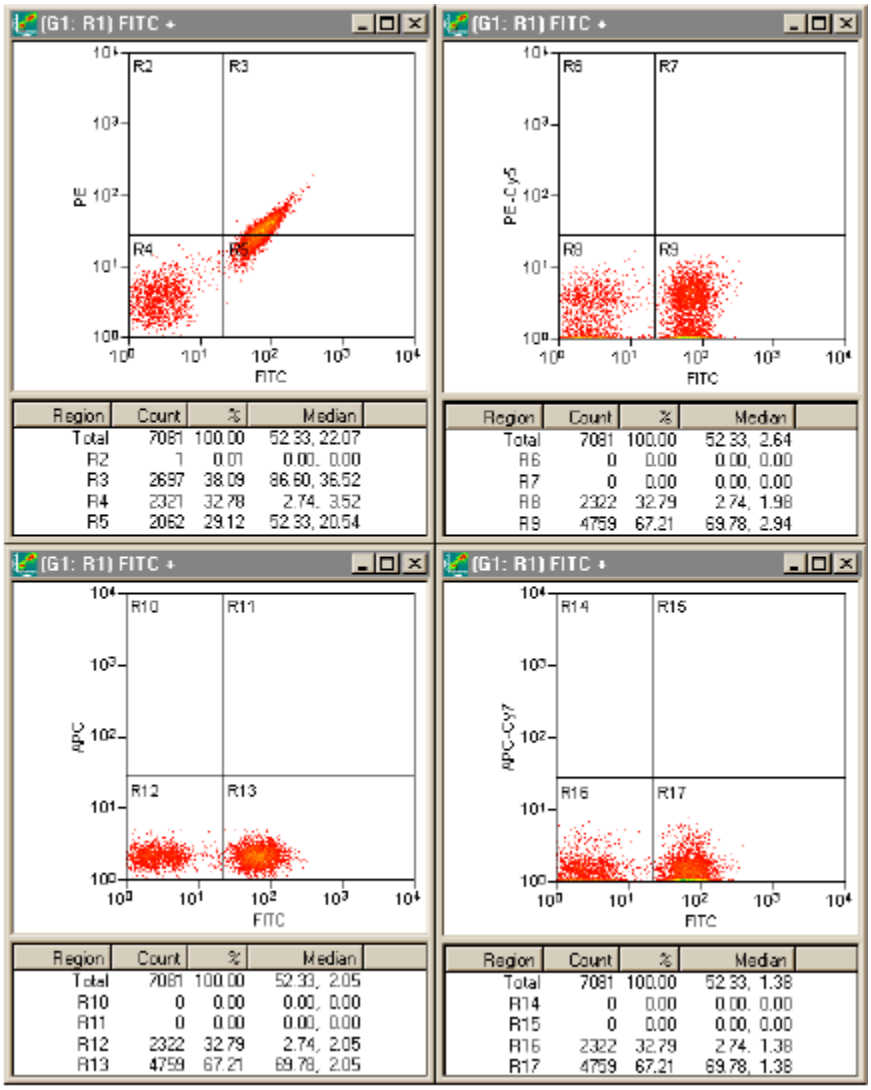

Setting Compensation

For proper compensation, check to see that the median fluorescence for the populations within the lower two quadrants are equivalent. (Within 1.0 is typically acceptable, but more accuracy is usually obtainable when performing compensation post-acquisition). If the values are not almost identical, adjust the compensation settings such that the median fluorescent values of the FITC negative and positive populations are almost identical. For this example, compensation needed to be applied for the FITC versus PE plot. A slight adjustment was also needed for the FITC versus PE-Cy5 plot. Notice that the median values between the two populations is now within 1.0 for all 4 plots.

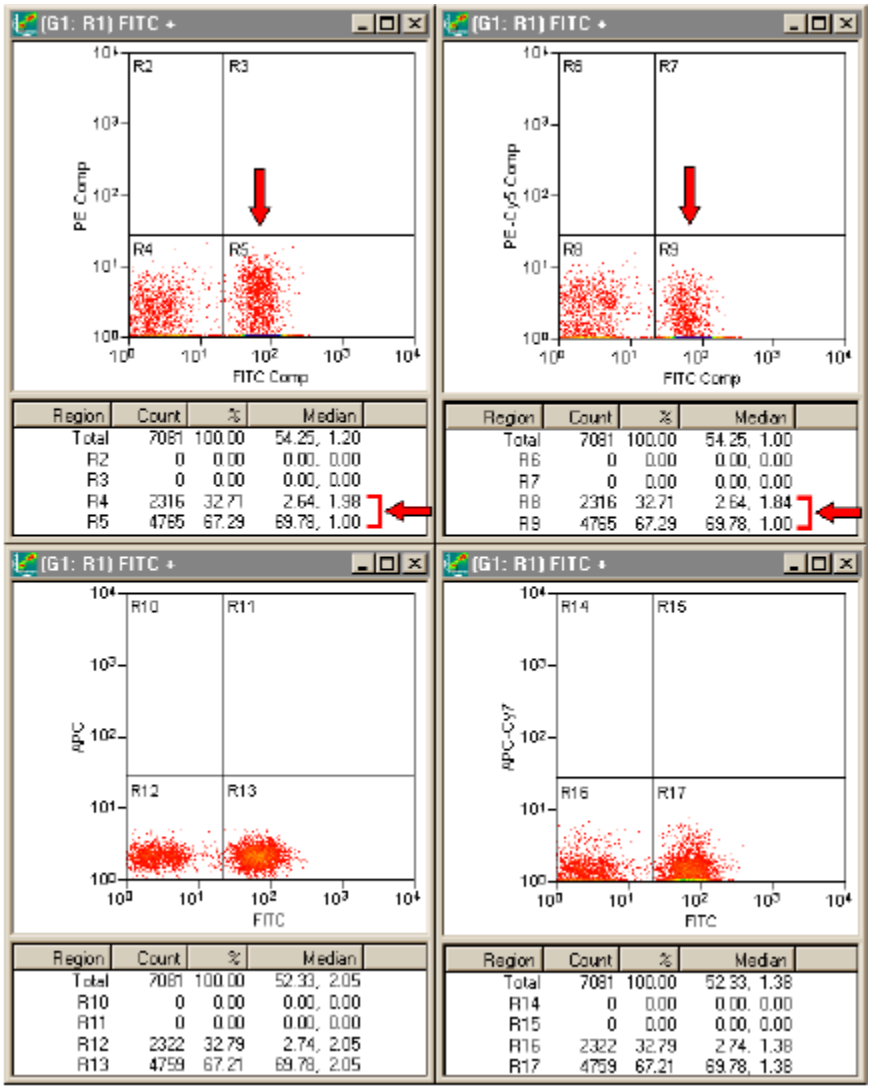

Running the Second Sample

Next, run the second "single color" sample. Before doing this, change the parameters of each of the histograms such that the second color (in this case PE) is plotted against the other 4 colors: PE vs. FITC, PE vs. Cy5, PE vs. APC, and PE vs. APC-Cy7. As the sample is run, two populations will be delineated, PE negative and positive.

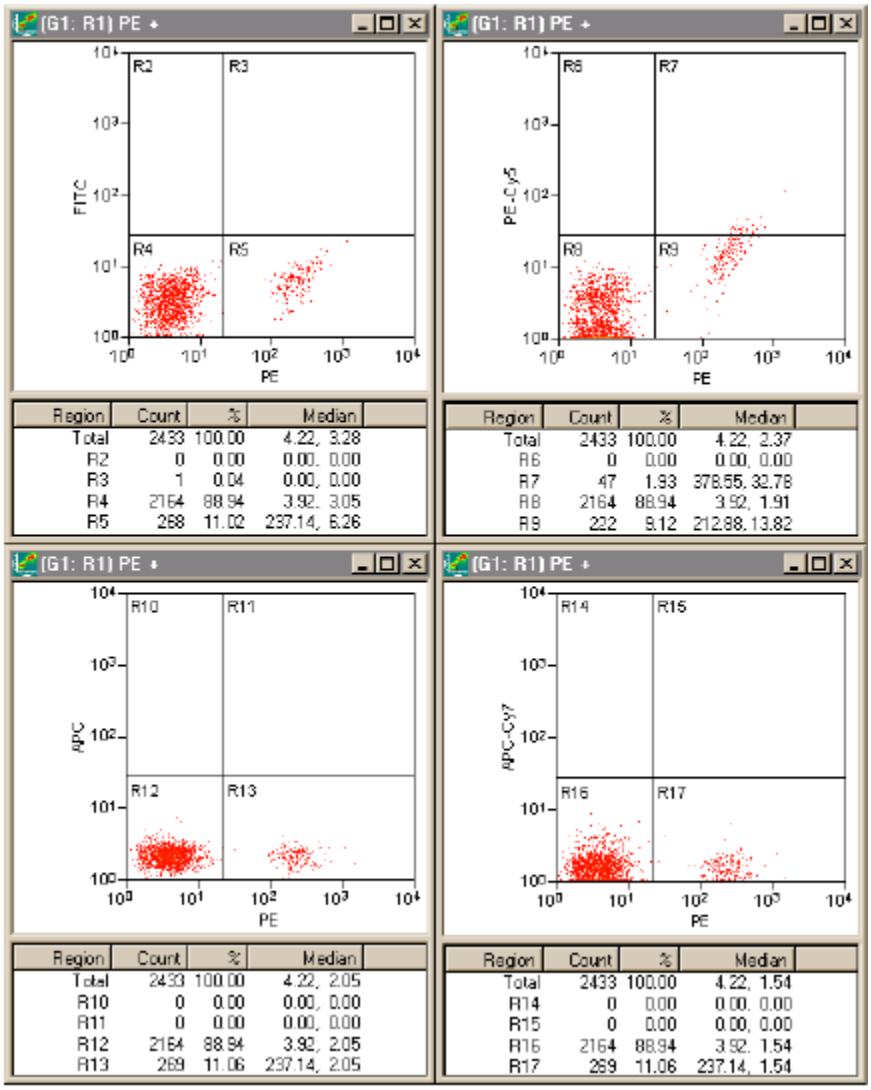

Again, compare the median fluorescence among the negative and positive PE populations and adjust compensation as needed. Below, compensation was adjusted for both the PE versus FITC and PE versus PE-Cy5 plots.

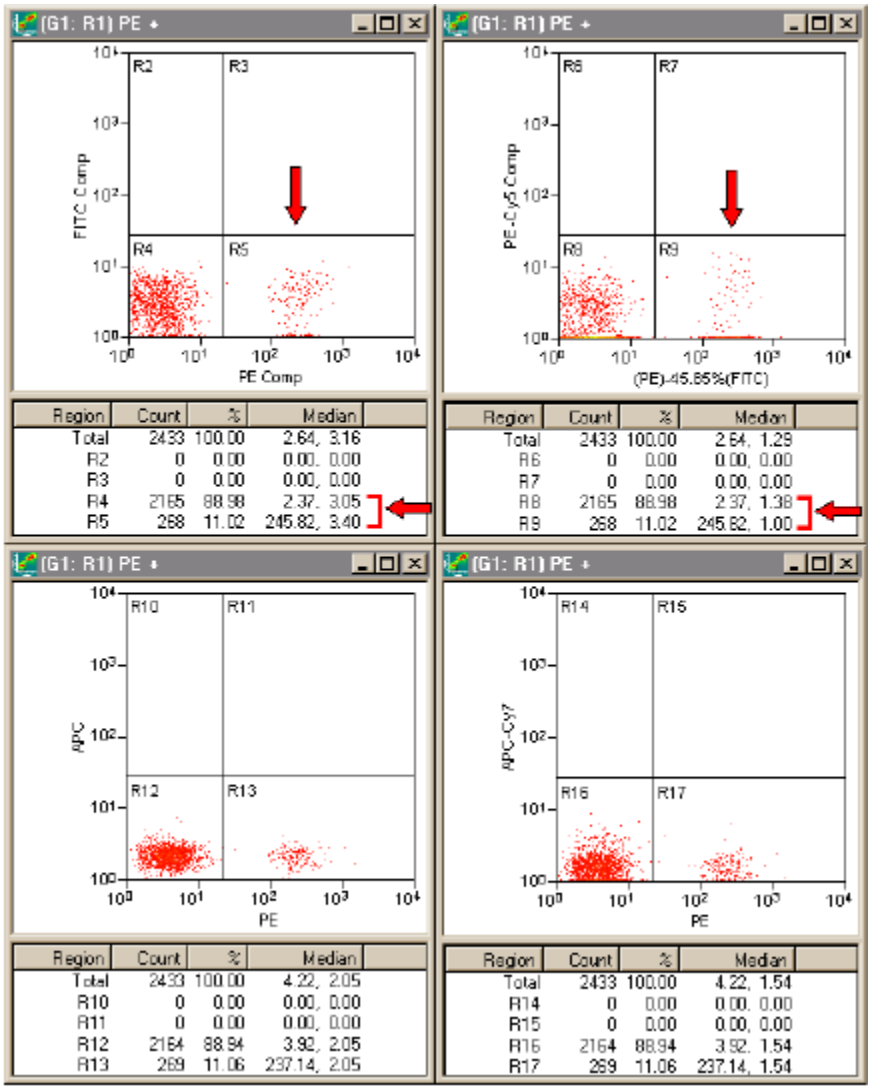

Why adjust compensation for the PE versus FITC plot when FITC versus PE was compensated for the FITC sample? This is because the % fluorescent spillover occurs both ways, FITC into the PE channel and PE into the FITC channel. Look at the spectral emission curves for both fluorochromes, you will notice that the degree of spillover between the two fluorochromes actually differs. This is why compensation must be adjusted based on both the FITC and PE "single color" samples.

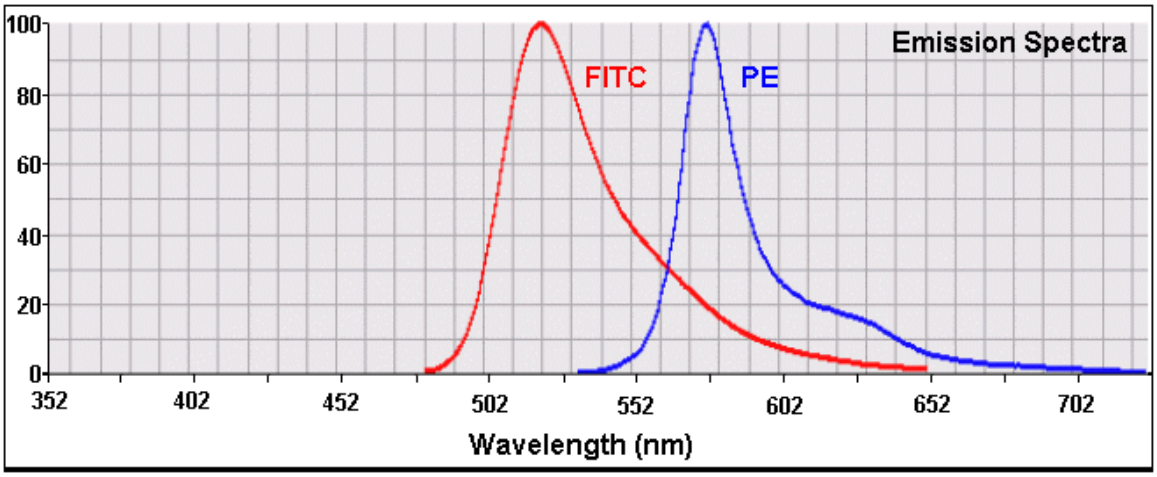

Running the Remaining Samples

Now run the third "single color" sample, in this case PE-Cy5. Again, remember to reset the parameters along the dot plot axes so that PE-Cy5 is plotted against the other 4 colors: PE-Cy5 vs. FITC, PE-Cy5 vs. PE, PE-Cy5 vs. APC, and PE-Cy5 vs. APC-Cy7. Note, these steps will be repeated for the remaining "single color" samples.

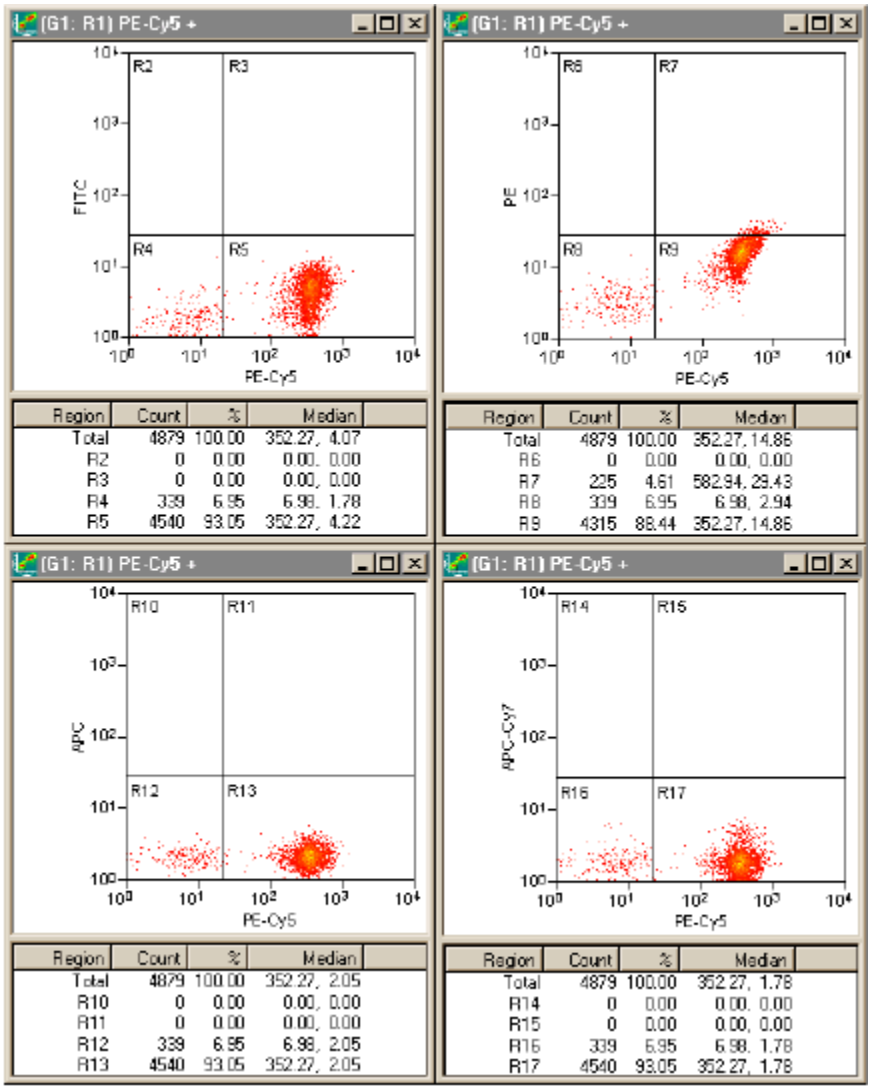

Where necessary, adjust compensation to align the median fluorescence (relative to the other 4 colors) between the PE-Cy5 negative and positive populations.

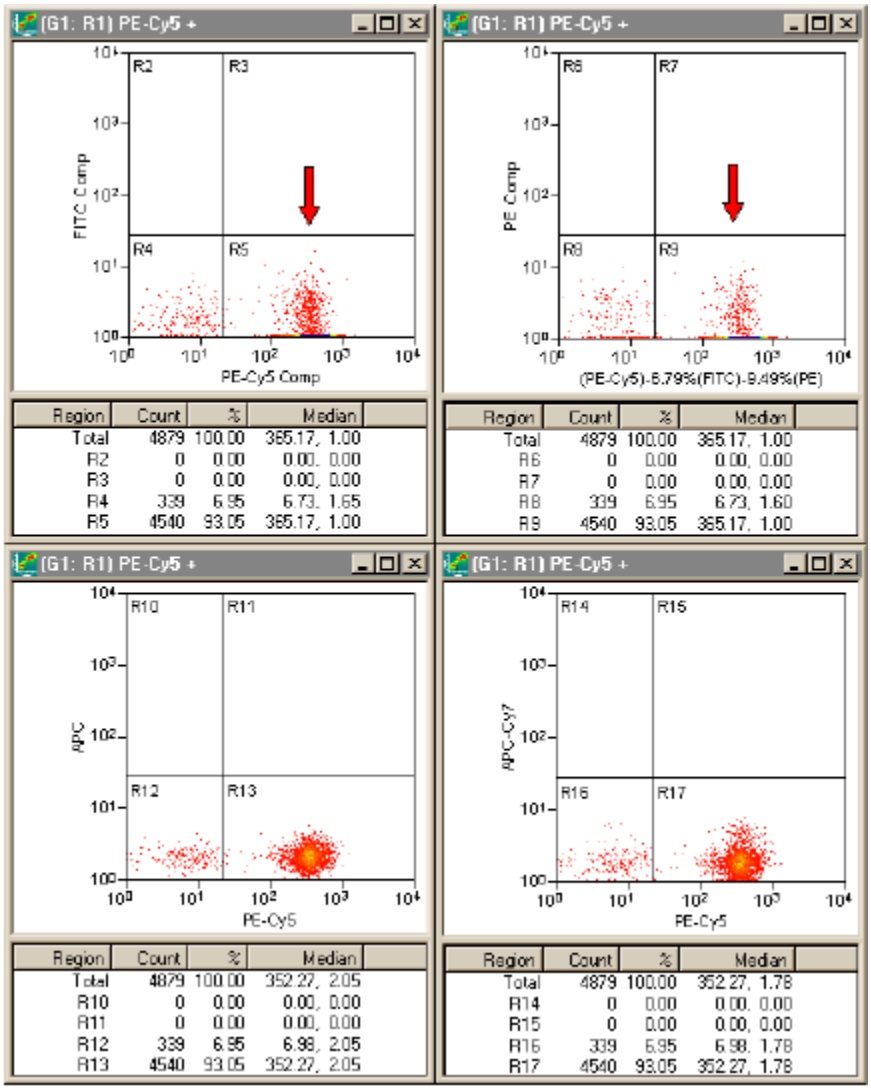

Run the 4th sample (APC). Pair the APC parameter against FITC, PE, PE-Cy5, and APC-Cy7 for the dot plots.

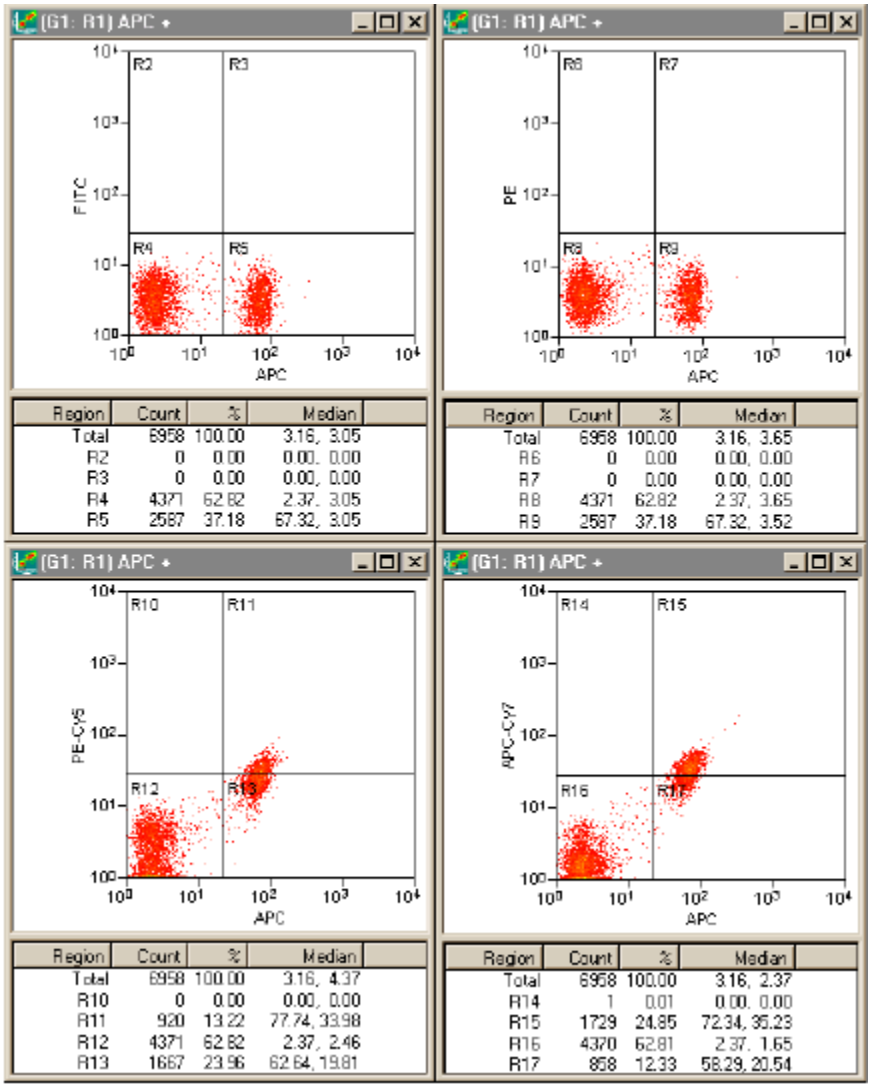

Where necessary, adjust compensation to align the median fluorescence (relative to the other 4 colors) between the APC positive and negative populations.

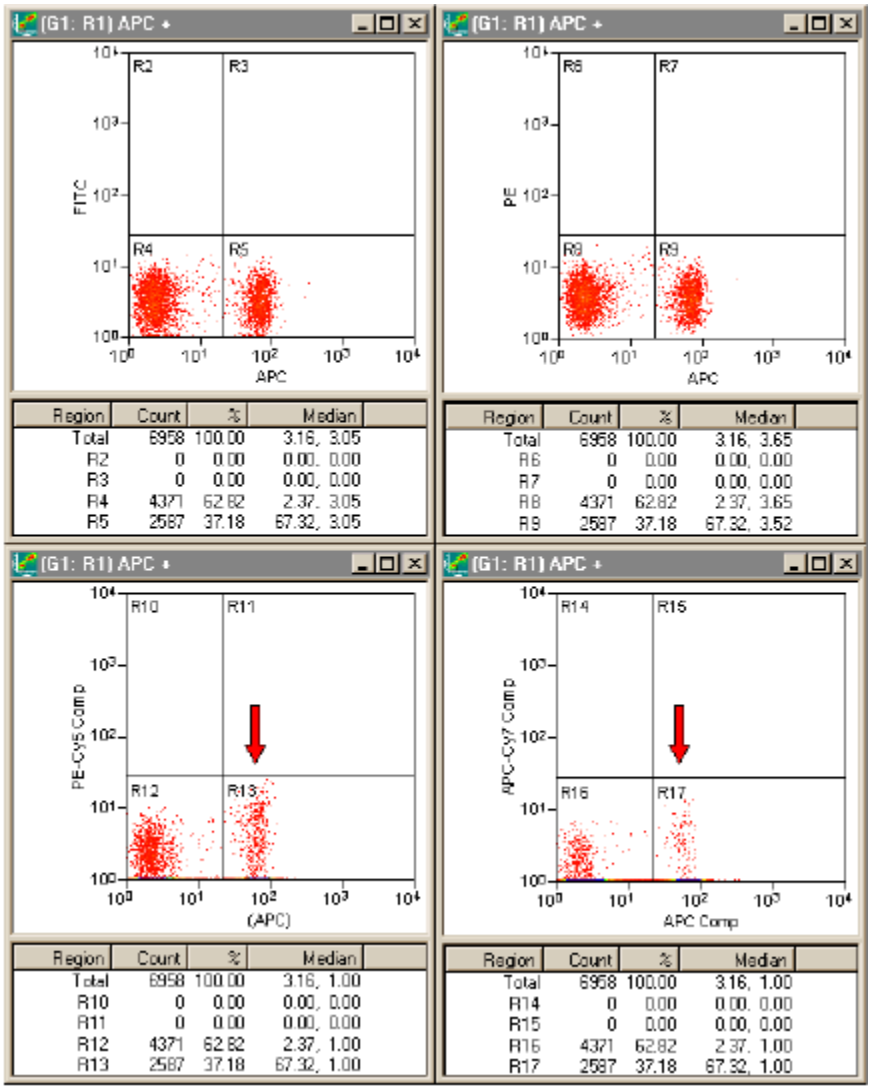

Run the 5th and final "single color" sample (APC-Cy7). Pair the APC-Cy7 parameter against FITC, PE, PE-Cy5, and APC for the dot plots.

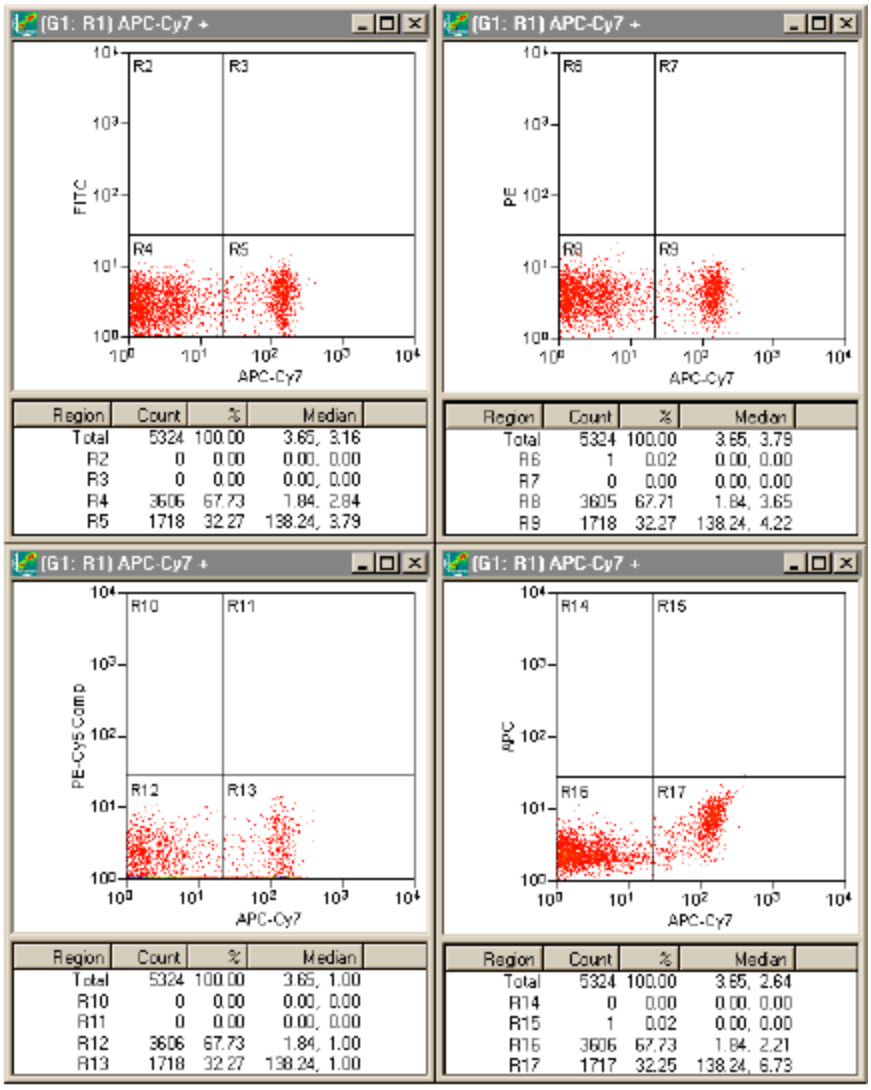

Where necessary, adjust compensation to align the median fluorescence (relative to the other 4 colors) between the APC positive and negative populations. Notice that for this sample, compensation only needed to be adjusted for the APC-Cy7 versus APC plot.

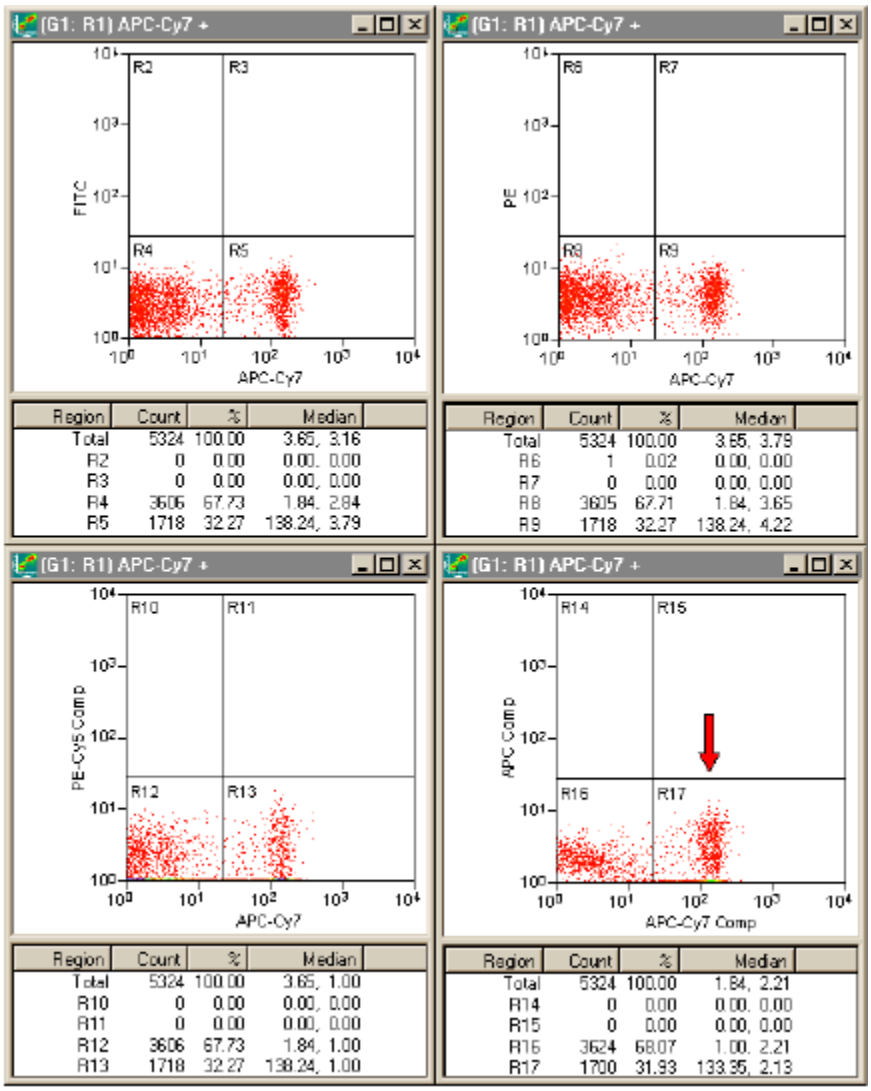

Running the "All Stains" Sample

Finally, run the "all stains" or experimental sample. This sample can be analyzed using dot plots containing any combination of the 5 parameters: FITC, PE, PE-Cy5, APC, and APC-Cy7. If compensation has been properly set, the populations will be aligned so that the positive and negative populations can be easily identified. Again, when running the "all stains" sample, verify that the quad regions are aligned along the first log decade marks.

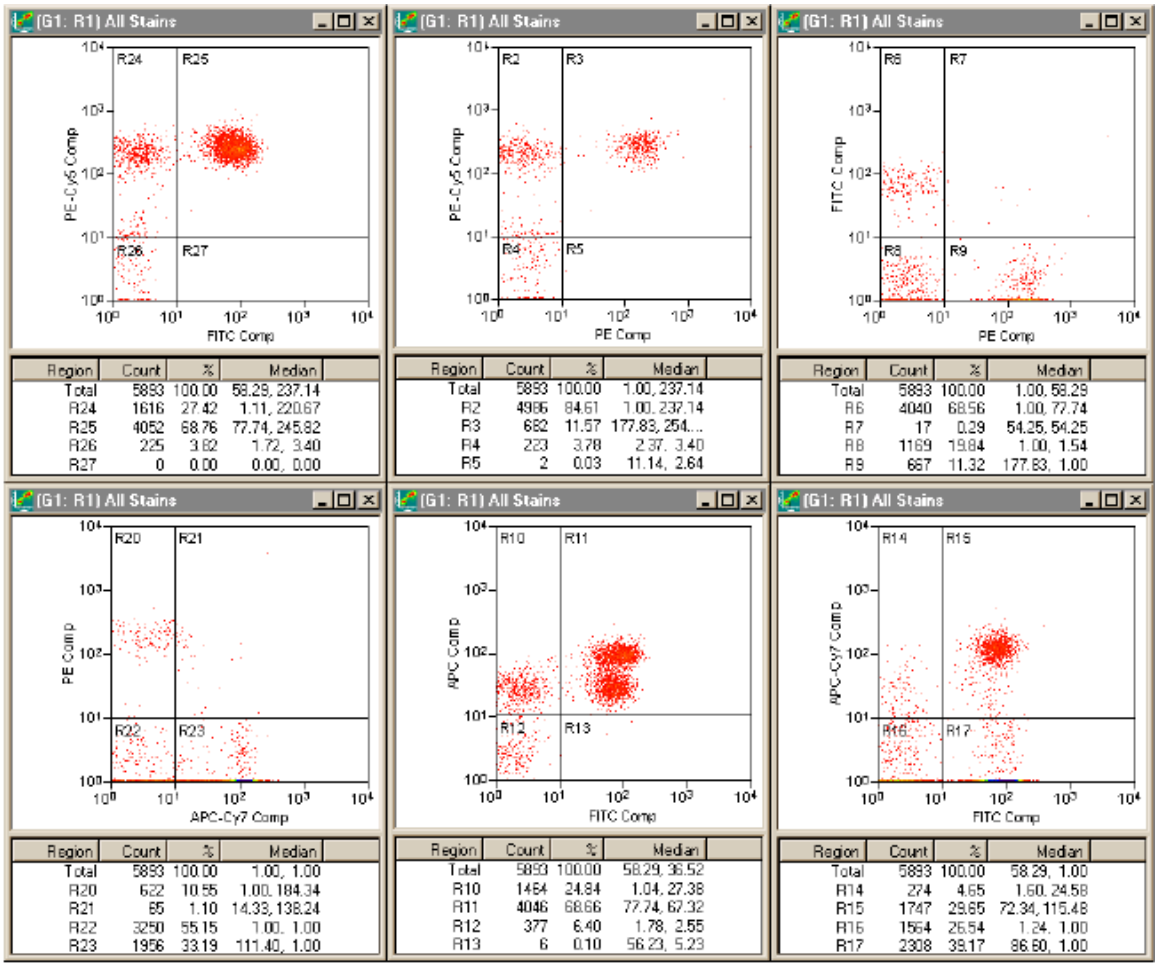

Putting Compensation Into Practice

This tutorial has demonstrated how to perform a 5-color experiment involving compensation. However, after running the "all stains" sample, how does one make sense of and use the compensated data from the "all stains" sample? The following illustrates 4 different cell populations that can be identified, analyzed, and/or sorted based on the 5-color experiment. For each of the cell populations below, identification is based upon the presence or absence of specific cell surface markers. To recall which marker correlates to which fluorochrome, refer to the original tube setup table below.

Sample	Target	Stain
Tube #1	None	None
Tube #2	CD3	FITC
Tube #3	CD19	PE
Tube #4	CD45	PE-Cy5
Tube #5	CD4	APC
Tube #6	CD8	APC-Cy7
Tube #7	All	All

Pan Leucocytes + B-cells

Pan Leucocytes and B-cells are both CD45 + (PE-Cy5) and CD19 + (PE). Using the "all stains" sample, when a dot plot of compensated "PE versus PE-Cy5" is created (as seen below), the pan leucocytes and B-cells appear in the upper left quadrant (indicating a positive signal for both PE-Cy5 and PE).

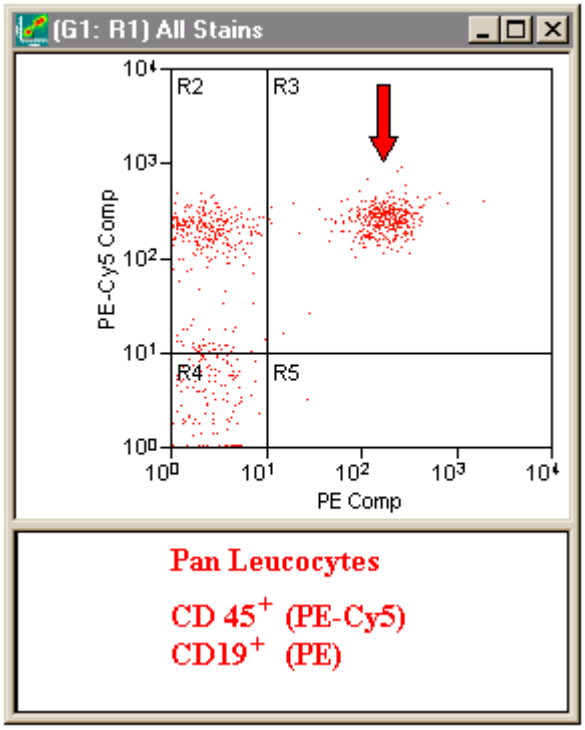

Helper subset of the T-cell subset of white cells

Helper cells, a subset of the T-cell population of white cells, are CD45 + (PE-Cy5), CD3 + (FITC), and CD4 + (APC). Using the "all stains" sample, when 3 dot plots are created with compensated "FITC versus PE-Cy5", "APC versus PE-Cy5", and "APC versus FITC", the helper cells will appear in the right upper quadrant of all plots (indicating a positive signal for both parameters).

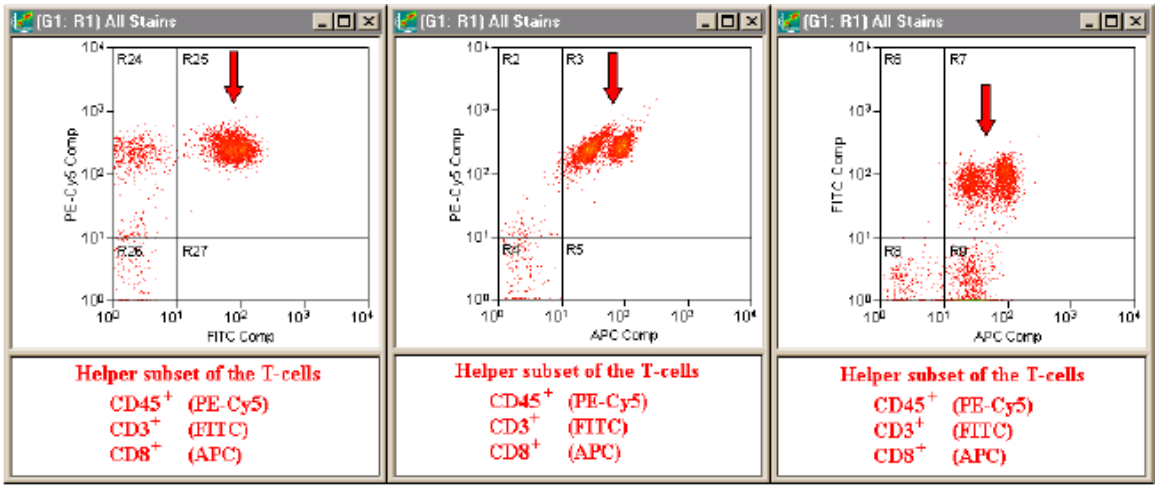

Suppressor subset of the T-cell subset of white cells

Suppressor cells, a subset of the T-cell population of white cells, are CD45 + (PE-Cy5), and CD3 + (FITC), and CD8 + (APC-Cy7). Using the "all stains sample, when 3 dot plots are created with compensated "FITC versus PE-Cy5", "APC-Cy7 versus PE-Cy5", and "APC-Cy7 versus FITC", the suppressor cells will appear within the right upper quadrant of all plots (indicating a positive signal for both parameters).

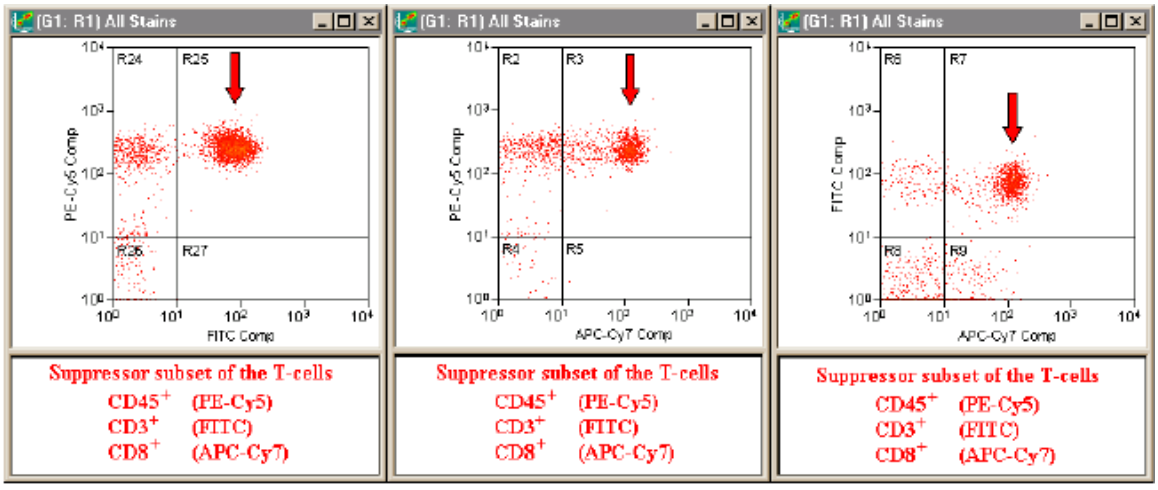

To better identify the "true" suppressor cells, a complex gating strategy can be used. Because the suppressor cells should appear within the upper right quadrant of all three plots, a gate can be set to include all three regions. By applying this gate to all three plots, only those cells that occur in all 3 regions will be displayed within each of the plots. Additionally, the gate for region R1 is also included. Below illustrates how, by applying a gate that includes regions R1, R25, R3, and R7, the suppressors can be separated from other lymphocyte cells.

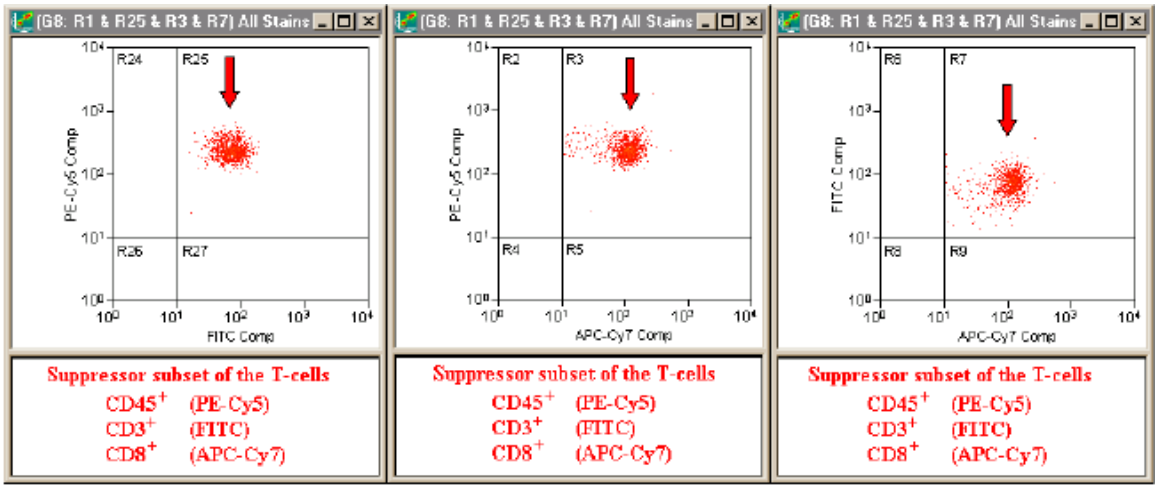

White cells that are neither T or B cells. i.e. NK cells

Non- T or B-cells (i.e. NK cells), are CD45 + (PE-Cy5), CD3 - (FITC), and CD19 - (PE). Using the "all stains" sample, 3 plots can be created with compensated "FITC versus PE-Cy5", "PE versus PE-Cy5", and "PE versus FITC". In the "FITC versus PE-Cy5" and "PE versus PE-Cy5" plots these cells will run in the upper left quadrant (indicating a positive signal for PE-Cy5). In the "PE versus FITC" plot these cells run in the lower left quadrant (indicated that they are negative for both FITC and PE).

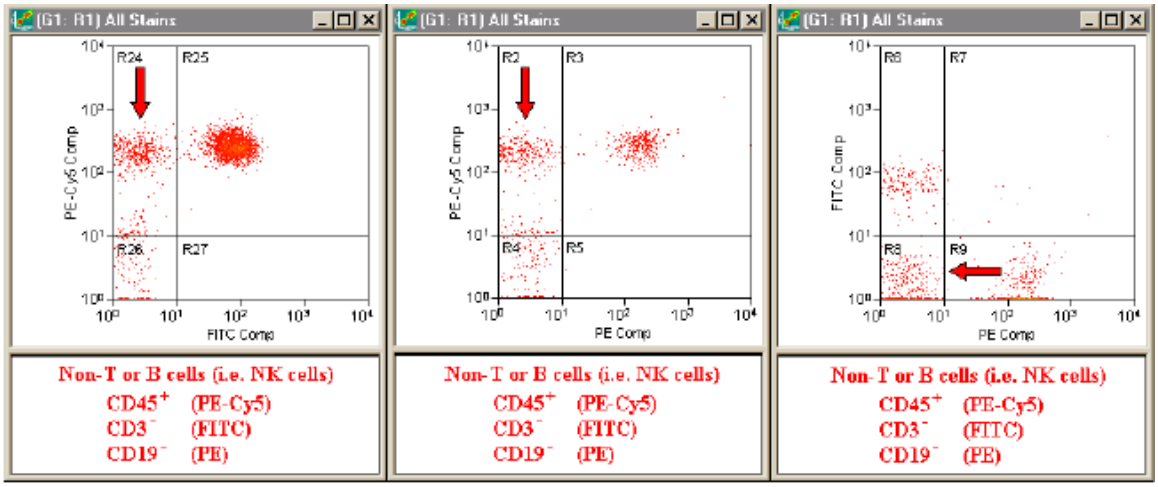

To better identify those cells that are not T or B cells, a complex gating strategy is used. A gate can be created to include the quadrants where these cells should fall, the upper left quadrant for the "FITC versus PE-Cy5" and "PE versus PE-Cy5" plots, and the lower left quadrant for the "PE versus FITC" plot. By applying this gate to all three plots, only those cells that occur in all 3

regions will be displayed. Additionally, the gate for region R1 is also included. Below illustrates how, by applying a gate that includes regions R1, R24, R8, and R2, the non T and B cells (i.e. NK cells) can be separated from other lymphocyte cells.

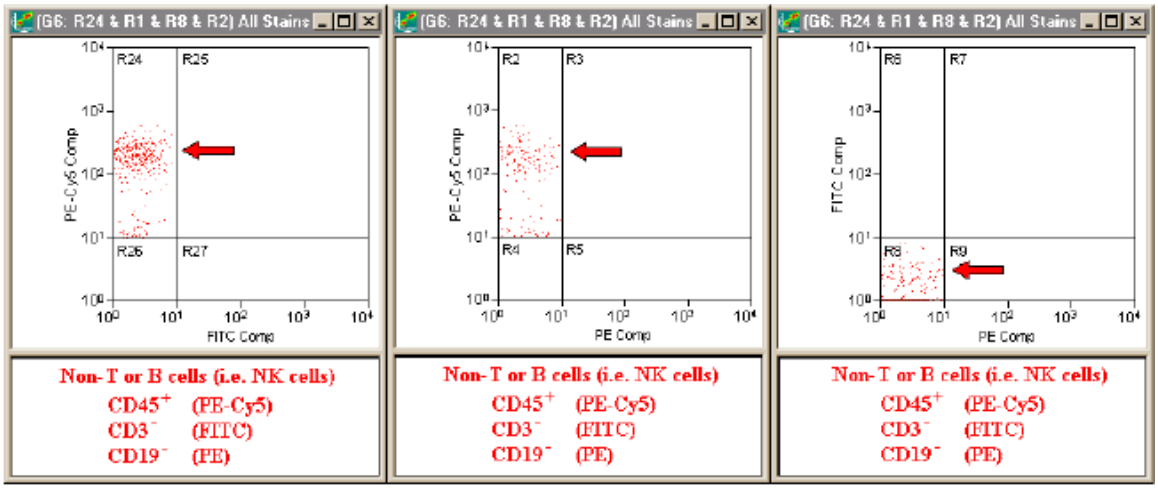

Contour Plots

Contouring is a alternate method of data display available for 2-parameter histograms or plots. When applied, this option displays the data as a series of lines (similar to what is observed with topographical maps) based on the distribution and density levels of events in the plot. Contour patterns will correlate to the density plot display, but more importantly, they can provide further insight into the distribution and number of events at various locations in the dot plot. This property of contouring is useful for data analysis or for publication purposes.

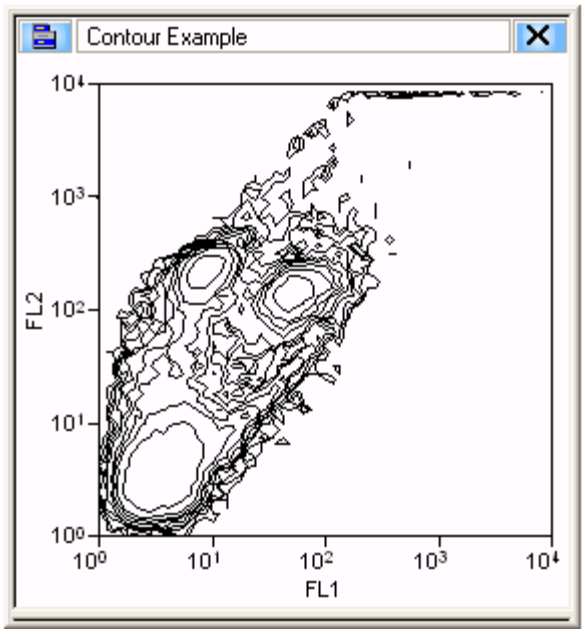

In Summit, there are four contour algorithms available for displaying data. Each of these methods contains a number of options where the assignment and mapping of lines can be adjusted. As contour line patterns are modified, the raw data values of the sample are not changed- thus contouring only represents an alternative way to view and analyze the data.

Below is a listing of the available contour methods in Summit and a description of each.

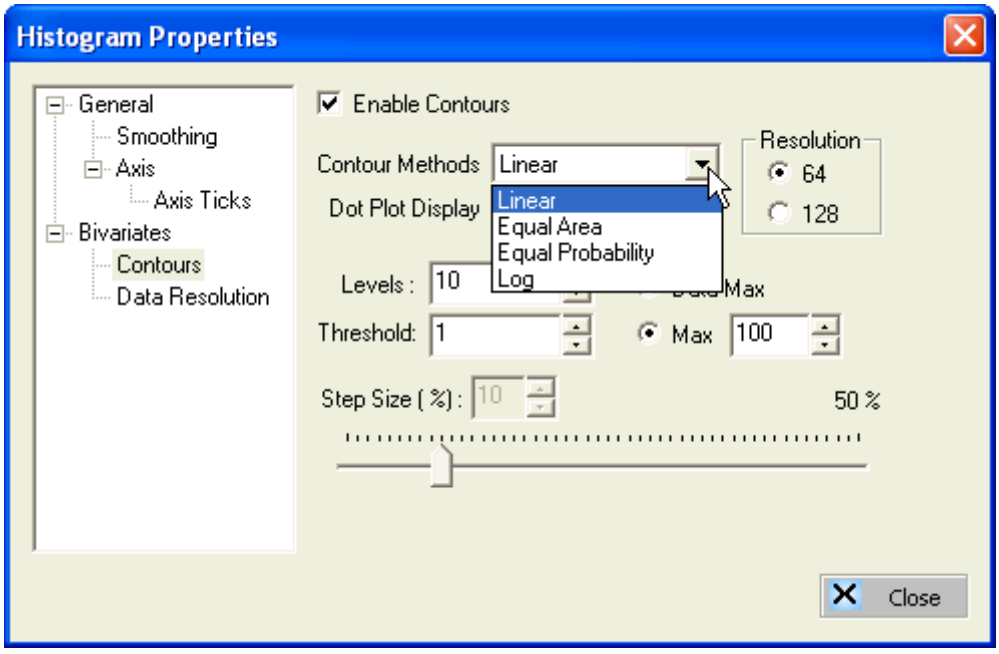

Contour Methods

Linear

Contour lines are plotted as a function of the maximum event number. Lines are equally spaced and are uniformly distributed based on the number of events per contour area. This method emphasizes high-density portions of the data while minimizing low-density areas. As such, peak areas will typically contain high concentrations of contour lines, whereas contour detail may be lost for low density populations.

Keep in mind that linear plots can be misleading when comparing overall count numbers between populations. For example, a dot plot may contain two populations with equal numbers of cells: one population is defined as a tall, tightly distributed peak, and the second as a short, broad peak. In this case, the number of contour lines for the first population will be more numerous, thus giving the overall impression that the first population has a greater number of cells.

Log

Contour lines are plotted as a function of the maximum event number but with the lines logarithmically spaced. For example, the first contour line (C) is set at a population's highest density point. The next contour line (C2) is mapped at "half height" of the original (or C/2). The next contour (C3) is again mapped at "half height" of the second line or C2/2. Contour lines are plotted until a value below 1/"X" is reached.

This method is useful for enhancing low-density areas of data while maintaining some emphasis on high event areas (emphasis on low event populations is less than with the equal area algorithm). One way to counter this method's reduced focus on low event populations is to use the "outlier" option. This adds dots or small lines in the plot to represent those events that fall outside the lowest contour.

Equal Area

Contour lines are calculated for the entire data set and are plotted such that an equal area space occurs between contour lines. This method tends to emphasize low-density, sparsely populated portions of the data and while under representing high concentration areas of the data. Although this method is useful for highlighting rare and low event populations, when applied to most plots, the data can be difficult to interpret. In general, this method should be used sparingly.

Equal Probability

Contour lines are plotted as a percentage (%) of the total events. With this method, a "percentage" can be defined which determines the percentage of a population that will fall outside the contour areas. The area or space between contour lines can vary and is equivalent to the corresponding (%) of total events (i.e. contour lines are closer together in high density areas). Because the area between contour lines represents a "fixed percentage" of the total population, an equal number of events will appear between each pair of contour lines. The algorithm derives it's name from the fact that each event has an equal probability to fall between any pair of adjacent contours.

Overall, this method provides a good representation of the total number of events in a population, since in a given area, the number of visible contour lines are fairly proportional to the number of events. This is because events that fall between pairs of contour lines correspond to a certain percentage of events in the sample (i.e. high concentration = narrow lines; low concentration = wide lines). Like linear density contouring, this algorithm emphasizes high-density areas. However, unlike the linear method, equal probability provides a better portrayal of low event populations.

If necessary, one way to increase the emphasis on low event populations is to use the "outlier" option. This adds dots or small lines in the plot to represent those events that fall outside the lowest contour.

Summary

The chart below presents a comparison between the different contouring algorithms (Linear, Log, Equal Area, and Equal Probability) and how effective each is for emphasizing both high and low density events. Below and Above refer to the under or over emphasis of a population type.

Event Count	Linear	Logarithmic	Probability	Equal Area
High-Density Area	Above	Average-Below	Average-Above	Below
Low-Density Area	Below	Average-Above	Average-Below	Above

Data Example

The following is a example to illustrate the various contour methods. A density plot displays the sample using the parameters FL1 versus FL2.

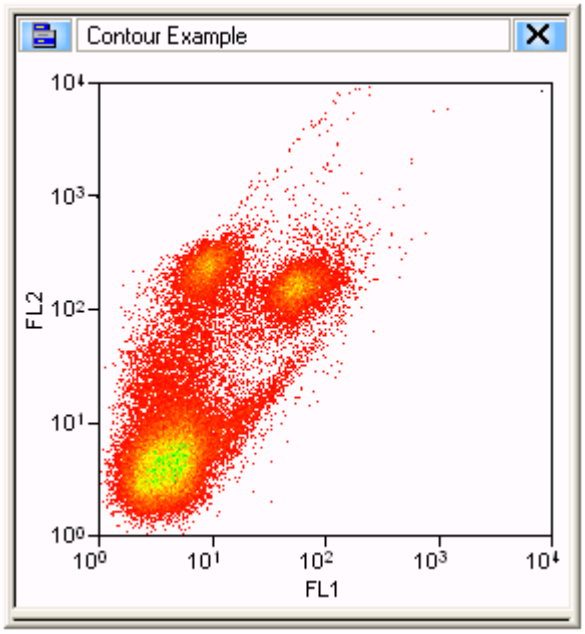

Using the same two parameters (FL1 and FL2), the data is now displayed and compared using the four different contour methods. Although data sets do vary, the following is meant as a general guideline to illustrate how sample data is displayed using each contour method. Notice how the linear method tends to highlight the peak data areas, the log and equal area algorithms emphasize low-density areas (in comparison to the peak areas), while equal probability provides the best overall representation of total events and their distribution.

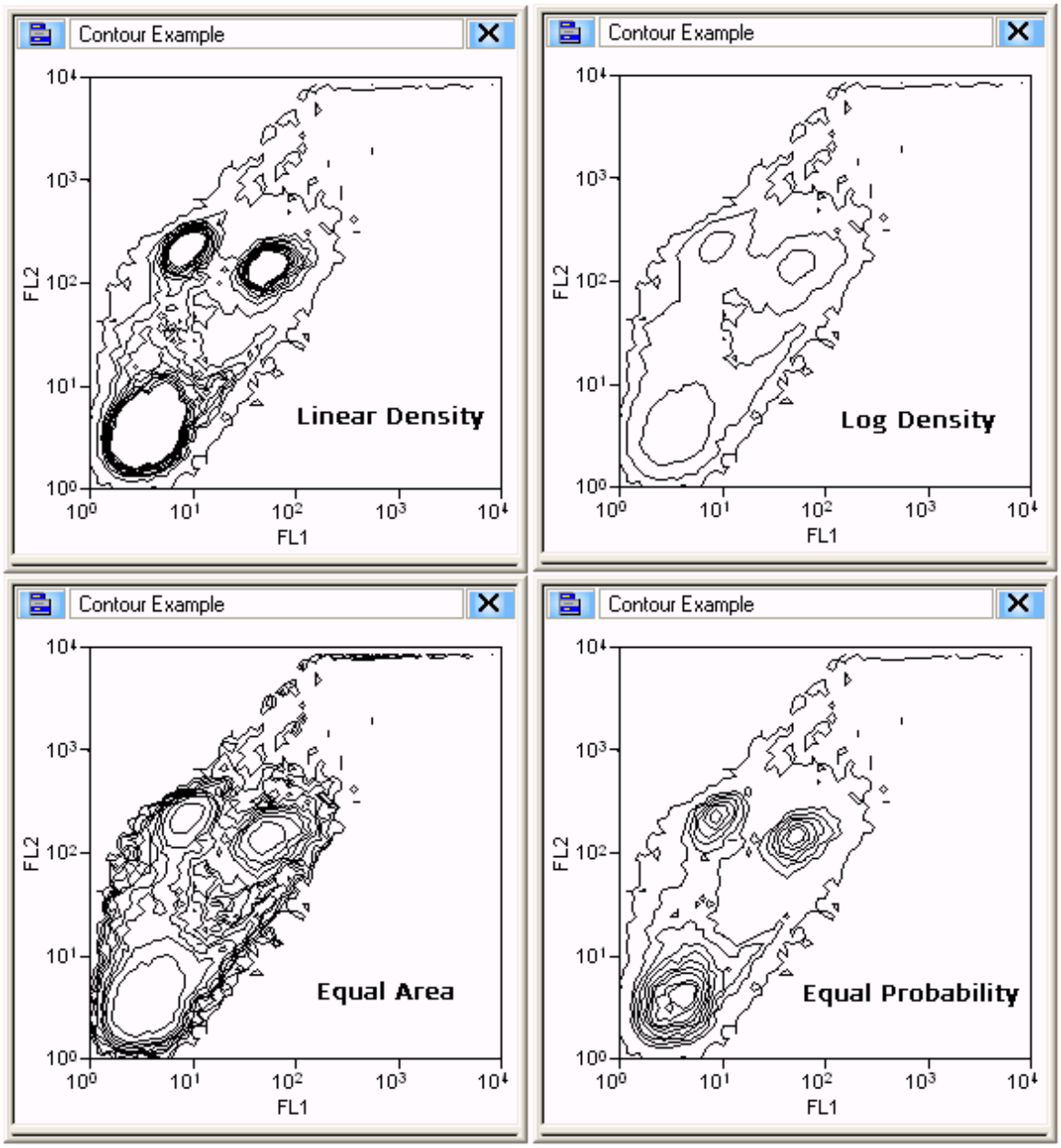

Outlier Events

Outliers refer to low-density or low-frequency populations. When using various contour algorithms, these populations can be lost or underrepresented in the dot plot. The contour "outlier

option" provides a mechanism to add dots or small lines in the plot to represent those events. This option is useful when using either the Equal Probability or Linear Density contour method.

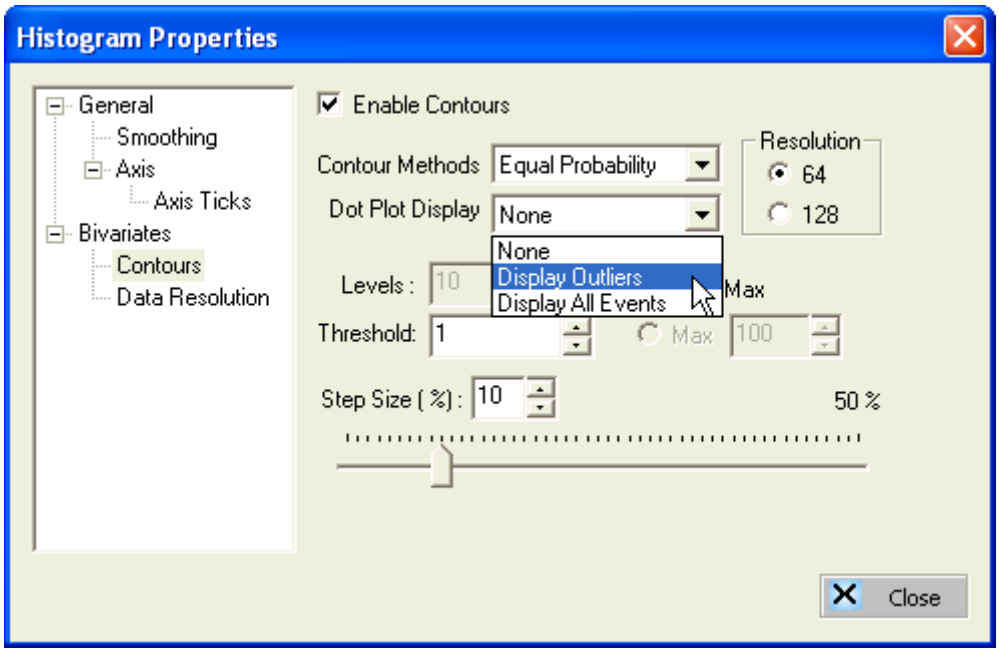

Display "All" Events

One option in Summit that deserves special mention is the ability to simultaneously display data using both a contour and density plot. To activate this feature, use the "dot plot display" drop-down menu and select "Display all events". The data will then be displayed as a density plot overlayed with contour lines based on the selected contouring method. Below shows a density plot with Equal Probability contouring applied.

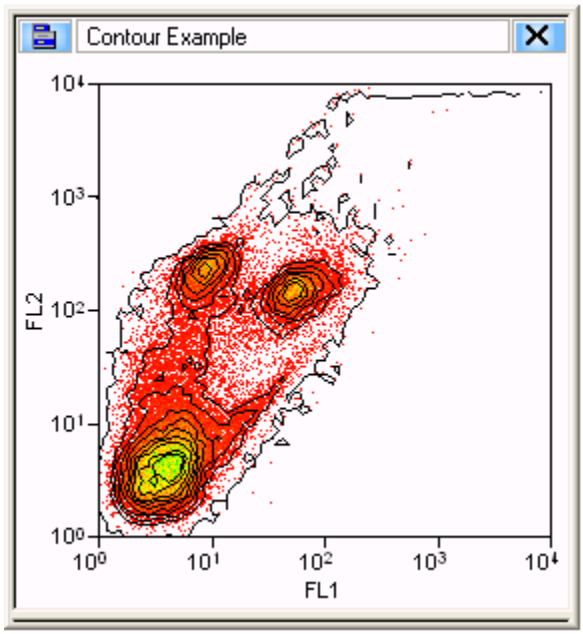

Data Resolution

The Analog Particle or Cell Signal

Cells or particles are suspended in a fluid medium and passed though the cytometer. Carried by the stream, the individual cells or particles pass sequentially through specific laser illumination zones. At these "interrogation points", information is obtained on each cell including the real-time detection of reflected and refracted light and laser-stimulated emission of the fluorescent markers.

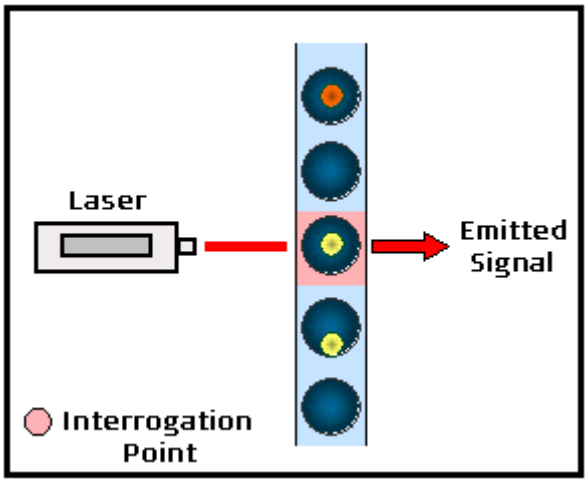

The emitted light and fluorescent signals are then passed to detectors or photomltiplier tubes (PMTs) using various combinations of filters, for example bandpass (BP), shortpass (SP), or longpass (LP), and dichroic mirrors. The filters are designed and configured to provide the best optical resolution of the signals elicited from each cell or particle. Because the filters are configured to allow only certain wavelengths of light to reach a given detector, each PMT becomes specific for detecting fluorescent compounds with compatible emission spectra such as FITC, PE, PE-Cy5, GFP, or Texas Red.

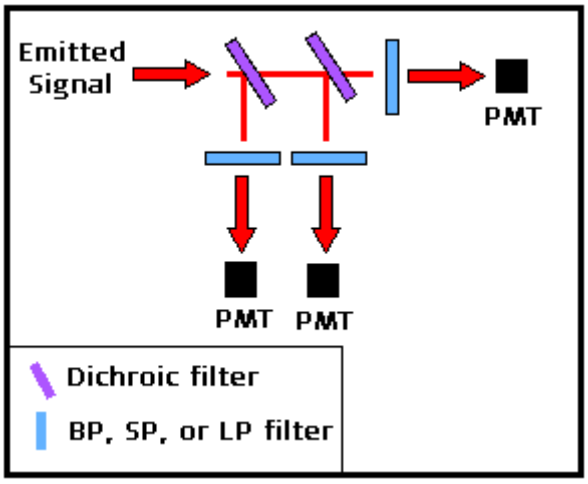

With the aid of an amplifier, PMTs convert this reflected or fluorescent light into an electrical signal (voltage) which describes the intensity of light from each cell. Signals are usually quantified and reported within the range of 0-10 volts. Keep in mind, the number of possible values within this range is infinite (For example, cells can elicit signals with values of 2.3, 2.456, 4.56897... volts, etc.) Analog values recorded along this "continuous distribution" are later assigned to a

specific channel number or "bin" with the aid of an Analog to Digital Converter (ADC). The end result is a digital description of a single event that contains an intensity value for each fluorescent or light scatter "color". The data's digital signal can then be visualized and analyzed using a number of methods such as a histogram or dot plot.

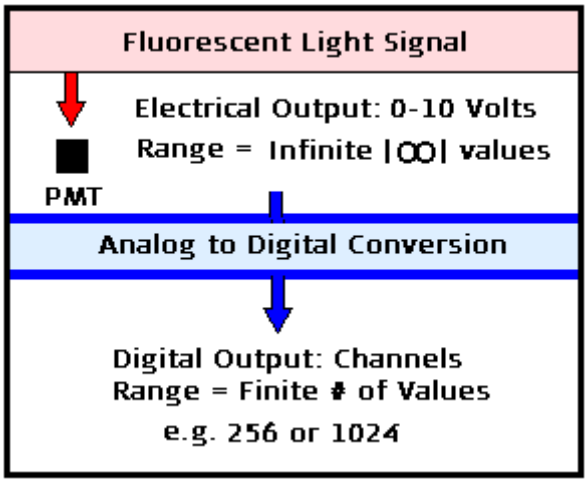

The Digital Signal and Software Data Display

The number of possible channels to which a particle's signal can be assigned is a finite amount (a discrete, as opposed to a continuous distribution) and is dependent upon the resolution of the ADC. For example, a 10-bit ADC can bin the electronic signal (or voltage) into one of 1024 possible channels (or 2 n , where n=10). A 12-bit ADC has a range up to 4096 channels (or 2 10). This range of available channels determines the visual resolution of the data when analyzed within a histogram or dot plot.

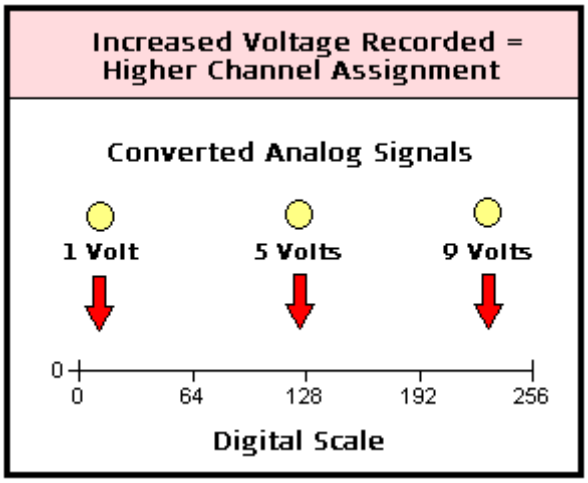

Based on the analog signal recorded from a particle or cell, the digital output will be assigned to a particular channel. Resolution of the data, or the potential to distinguish between two events, is partially dependent upon the number of channels available. For example, if only a single channel were available, events within a histogram would be digitally or visually indistinguishable since they would all fall within the same channel. For a gaussian or a symmetrically distributed population, a two channel situation would show half the events within the first (or lower) channel and the other half within the second (or upper) channel. For a symmetrically distributed

population, four channels would bin events equally among all 4 channels. By increasing the channel number, the granularity by which events can be distinguished from one another increases.

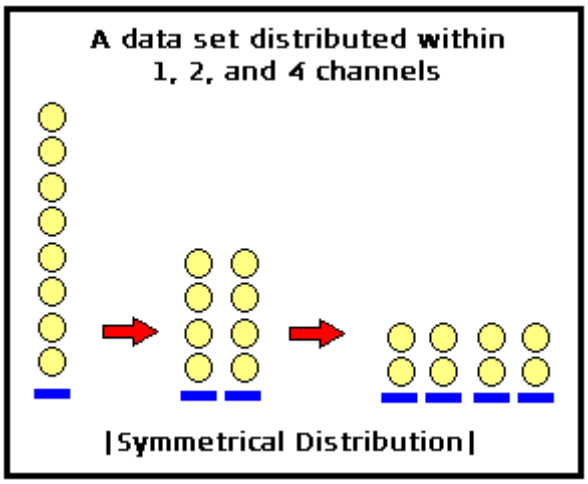

In reality, when samples are run through a cytometer, individually recorded signals are not likely to represent a perfect, symmetrical distribution. Individual events are assigned a channel based on the detected signal for that parameter, and as such, may not be displayed equally in all channels. The example below illustrates how events from a single channel may be binned according to the actual detected signal intensities. In the 2-channel situation, rather than dividing up the signals equally (i.e. half in one channel and half in the other), a greater number of events may be assigned to one channel. This distribution is based on the actual recorded signals. In this case, more appear in the left-most channel since more of the events were detected with a lower signal intensity. This unequal distribution is carried over and seen when the same events are distributed into 4 channels.

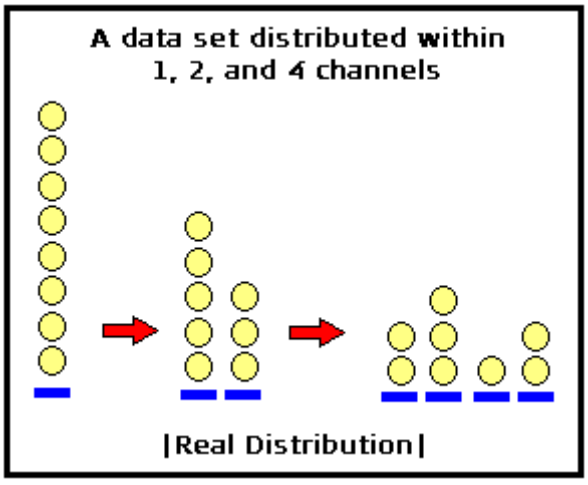

The same logic of binning data and channels applies to histograms and dot plots in Summit, only the number of channels is greater (256-4096 channels for histograms and 64-1024 channels for dot plots). When data is initially acquired and saved, the maximum resolution is imposed, and the channel value is determined by the resolution of the instrument's analog to digital converter (ADC). The FCS file is saved as 10-bit data (1024 channels maximum), 12-bit data (4096 channels maximum), etc. After the data is saved, Summit allows it to be viewed and analyzed at

various resolutions (but not exceeding the resolution at which the data was collected, analog to digitally converted, and saved).

For example, during analysis, data from a 12-bit data file can be binned and displayed within a histogram using 4096, 1024, or 256 channels. A 12-bit data file can be analyzed using 256 or 1024 channels, but not 2048 or 4096 since the later two cases exceed the resolution of the collected data. The following illustrates this concept with a 2-bit data set (4 channels) and 1-bit data set (2 channels). The 2-bit data can be displayed and analyzed within either 2 or 4 channels, but the 1-bit data set is limited to 2 channels (You cannot exceed the maximum resolution of the raw data by binning extrapolation).

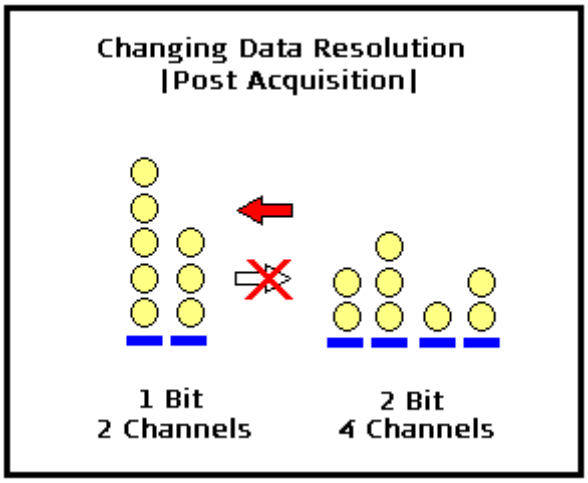

The following shows the data resolution settings available for histograms within Summit. Data can be binned and displayed using 256, 512, 1024, 2048, or 4096 channels. These settings are available in the **Histogram Properties** dialog.

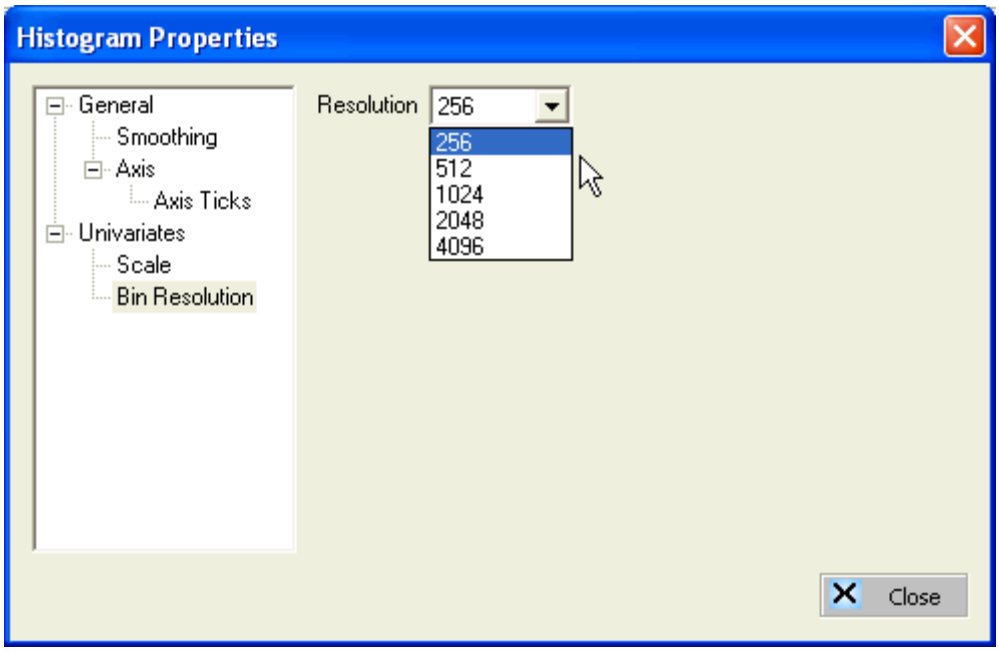

As the channel resolution for a histogram is increased, the data becomes dispersed within more channels along the axis and the Y-axis is rescaled to reflect the reduced event count per channel. This can result in the data profile appearing more "jagged".

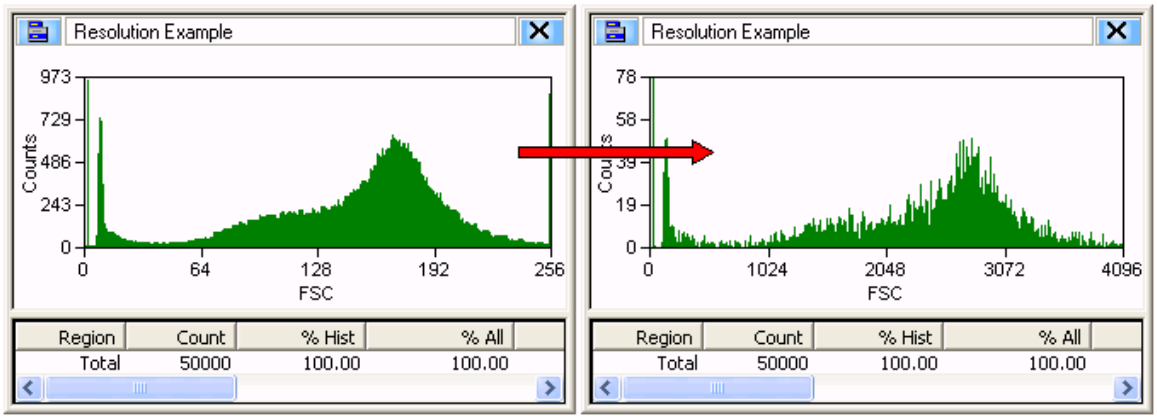

When the resolution is changed, auto scaling is performed which maintains the "overall" data profile. Although useful, this can be visually misleading unless the counts along the Y-axis are taken into consideration.

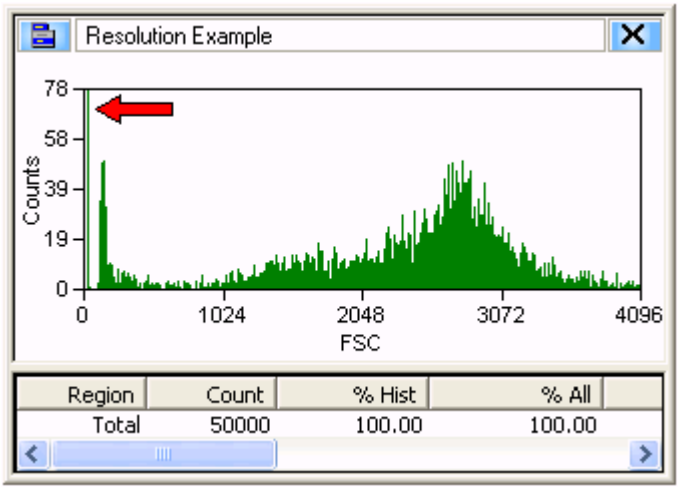

As the resolution on the same histogram is changed using a fixed count scale, the data will "flatten" along the X-axis. This is expected since the same number of events is now distributed within an increased number of channels in the histogram- increased number of channels for better resolution of the data set, but with fewer events per channel. Ultimately, the advantage of a having a higher channel number within a histogram or dot plot is better resolution of the data. This means that a group of events that were indistinguishable from one another because they were binned within the same channel are now distributed as subgroups within several channels. Increased resolution is useful when distinguishing between populations with "similar" signal intensities (e.g. chromosomes) The major drawback to having an increased number of channels is that many more events must be collected for the sample to achieve nice "Gaussian" curves or peaks within the data (versus having a "flat" data profile).

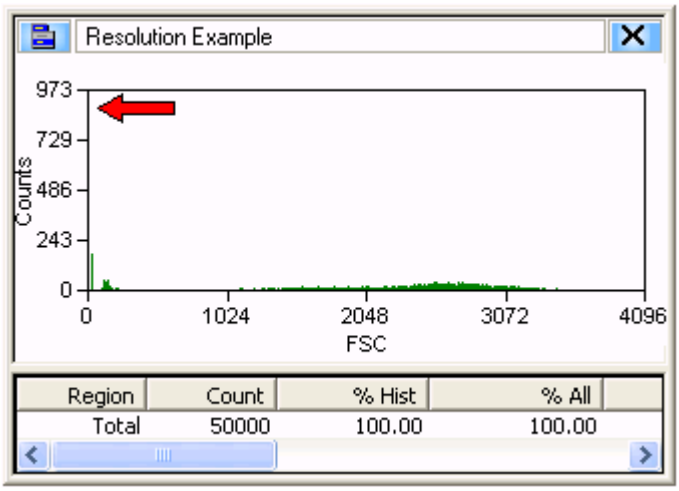

When increasing the resolution within dot plots, the data will become more disperse due to the greater number of channels along both the X and Y-axis. When decreasing the resolution within dot plots, the data will become intensified due to the reduced number of channels along the X and Y-axis. Both of these effects can be seen in the set of dot plots below.

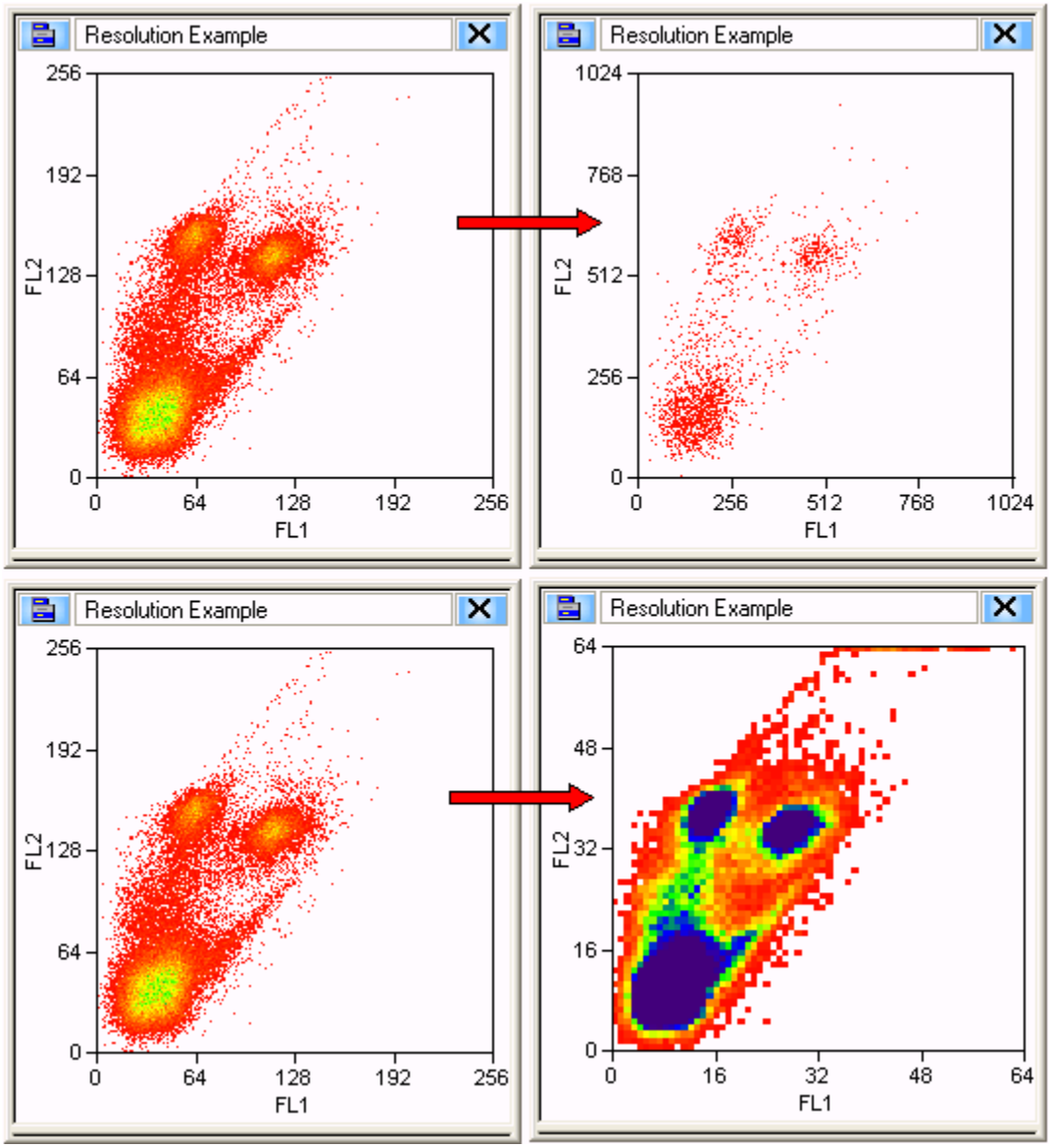

Doublet Discrimination

Doublets are an inevitable element in flow cytometry. The probability of doublets increases when analyzing cells that tend to stick together or when flowing at high event rates or a high pressure differential.

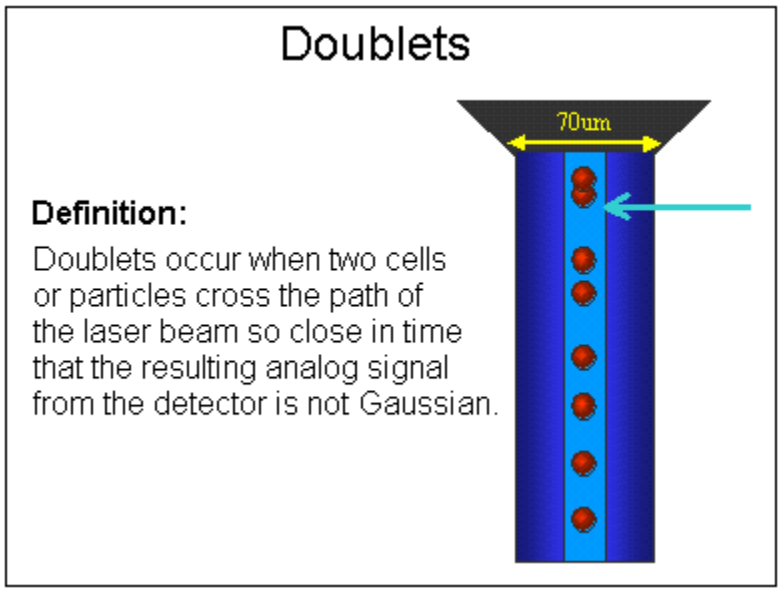
Doublets
70um
Definition:
Doublets occur when two cells or particles cross the path of the laser beam so close in time that the resulting analog signal from the detector is not Gaussian.

Tip Proper sample preparation and pre-filtering of the sample can minimize doublets or clumps of cells. Beads can be sonicated to minimize doublets.

Doublet Handling

Integrated Signal

The Integrated Signal of a doublet will yield a greater value than a singlet. On the contrary, Peak (height) selection on the ADC would not provide any information that would distinguish between a singlet and a doublet.

Note Area signal processing is only available in Linear amplification. Make sure the desired ADC is set to **Area**.

Pulse Width

The pulse width is defined as the time it takes for the signal to go above and back below the threshold. Doublets will stay above the threshold longer than a singlet, and will therefore provide a measurement and a means of discriminating against doublets.

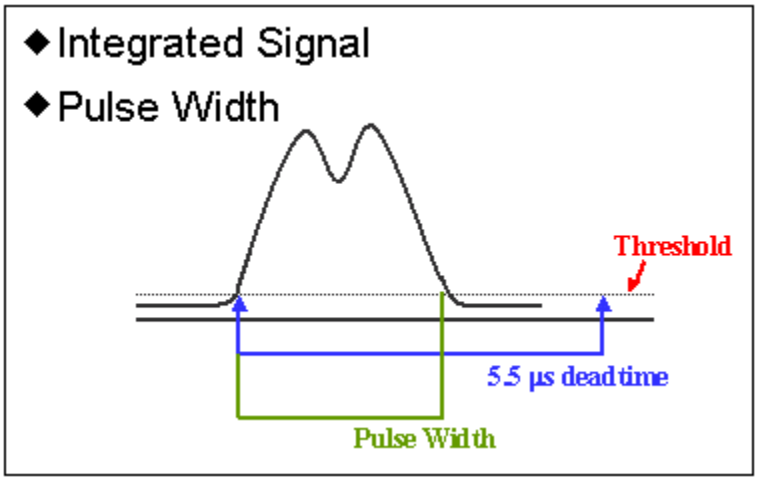

Finding Doublets using Color Gating

Color Gating is an excellent way to help find the doublet population in your histograms. Use the color gating feature in Summit to define and help set up sorting regions for doublet discrimination.

1. Define a region around the suspected doublets.

2. Right-click in the region and then click **Select Gate Color** from the menu.

3. If necessary, create other regions to identify doublets.

4. Move the regions around to help identify the doublet population.

5. Set your sort decisions so that doublets are eliminated from the sort.

Below are some histograms that show an example of color gating in Summit. This data was gathered by analyzing a bead lot that had been centrifuged to create a preponderance of doublets. They are spherical beads with one size and one fluorescent intensity. In a perfect world, with no doublets, we would see one population in scatter and fluorescence plots. Instead, we see the doublets shown below in purple.

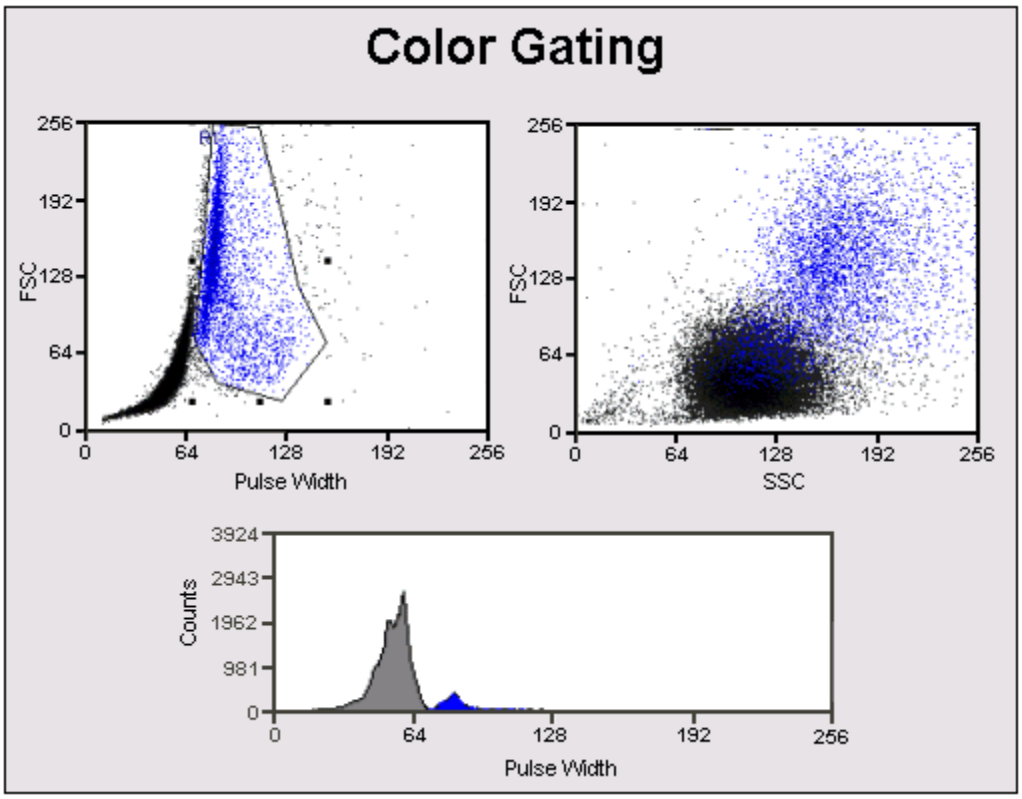

Methods of Doublet Discrimination

There are many ways to perform doublet discrimination that involve integrated signals and the pulse width parameter. In fact, it's possible and often helpful to combine two or more means through gating on multiple histograms. Below are some of the more common methods.

FSC (Area) versus Pulse Width - FSC ADC is set to Area. Create FSC area versus PW histogram in Summit.
FSC (Area) versus SSC (Integrated) - Both FSC and SSC ADC's are set to Area.
FLX (Area) versus FLX (Peak) - Change BNC wiring to enable the same parameter to be processed on two different ADC's.
FSC (Area) versus Pulse Width - The FSC(Area) vs. PW method provides doublet information on both axes of the dual parameter histogram. To set it up, you simply select **Area** on the FSC analog to digital converter (ADC). In Summit, create a dual parameter histogram plotting FSC area vs. Pulse Width. Define a gated region on the main singlet population and include this region in your Boolean logic sort decision.
FSC (Area) versus SSC (Area) - The FSC(Area) vs. SSC(Area) also provides doublet information on both axes. To set it up, make sure both FSC and SSC ADC's are set to **Area**. Create a FSC area vs. SSC area histogram in Summit and gate on the main singlet population.

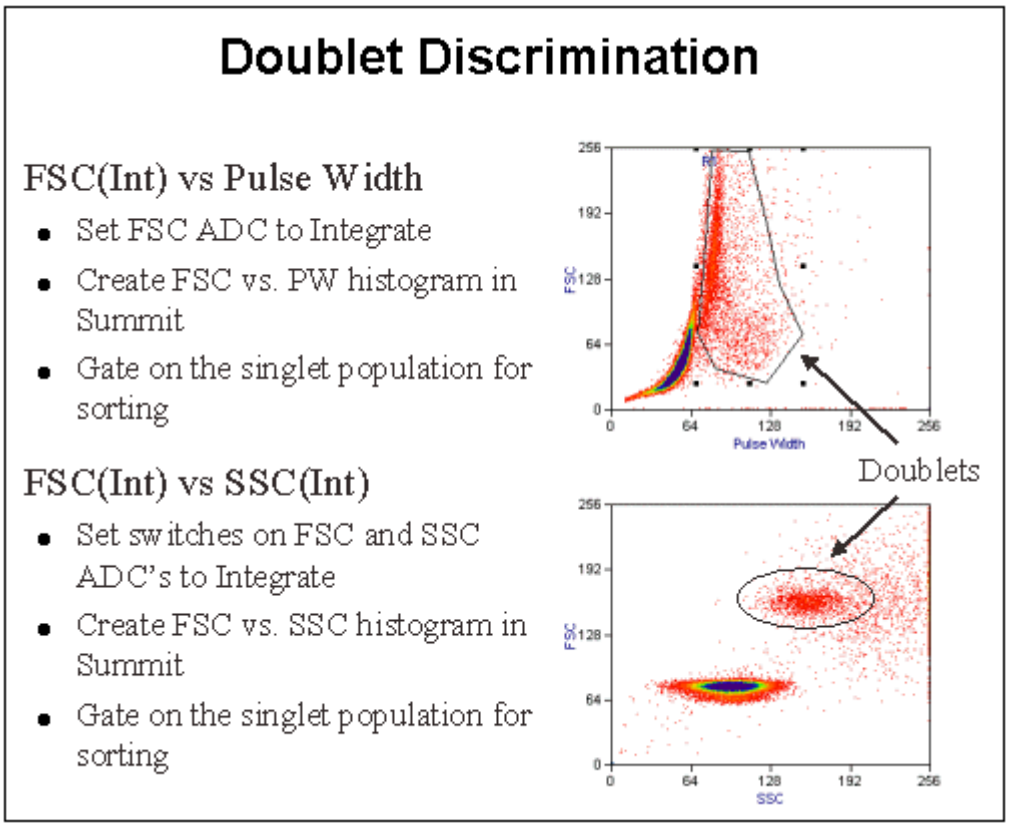

Histogram Scaling

A number of manual and auto-scaling features are available for histograms in Summit. The following tutorial explains the various scaling options and how each functions to enhance data display and analysis.

In the **Histogram Properties** dialog, the **Scale** list item provides access to all the manual and auto-scale options.

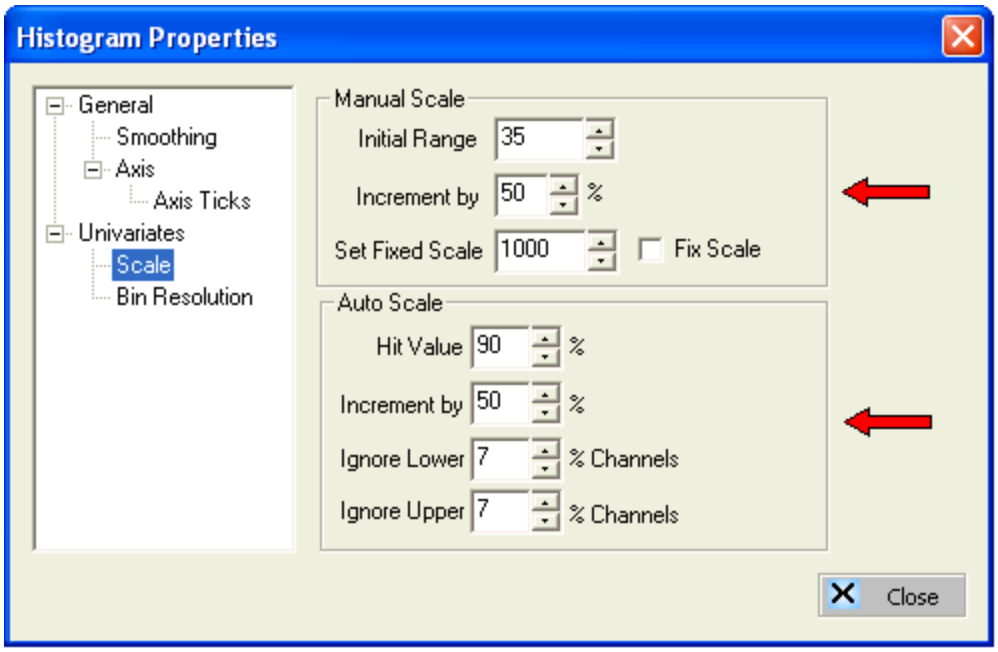

Manual Scaling

Data can be manually re-scaled in any histogram. Simply select the histogram of interest and click the or icon.

Manual Scaling Options

There are also a number of settings that can be adjusted for manually scaling the data.

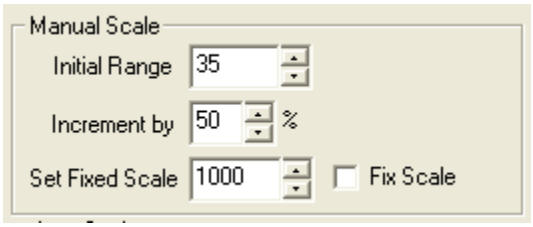

Increment By

The **Increment by** value determines the degree to which the Y-axis scale is changed when histogram data is manually re-scaled using either the or icon. For example, suppose the manual scale "increment" value is set to 50%. When histogram data is re-scaled, the Y-axis value will increment by a factor of 50% or 1/2 depending on where the data is scaled up or down. Below shows a histogram with the Y-axis set to 1000 counts.

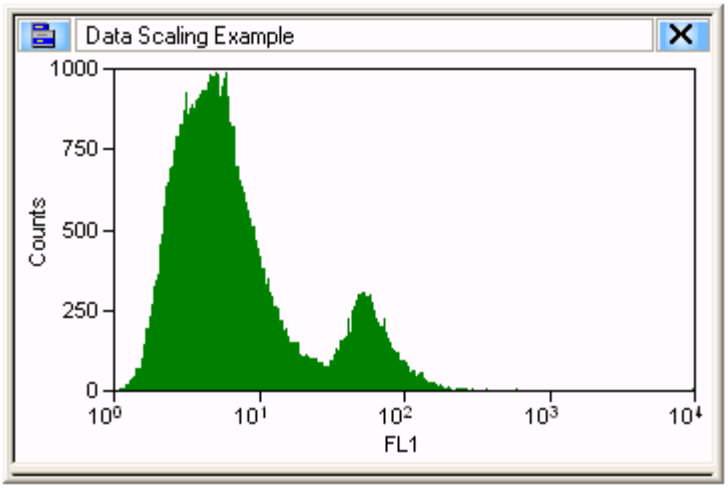

When the icon is clicked, the histogram data is manually reduced in size in the histogram. This increases the Y-axis scale by 50% (in this case from 1000 to 1500) to reflect the visual "scaling down" of the data. When the icon is clicked, the data increases in size in the histogram. As the data is scaled up, the count value along the axis "increments" by 1/2 (or is reduced or scaled down by 50% to illustrate the "scaled up" data).

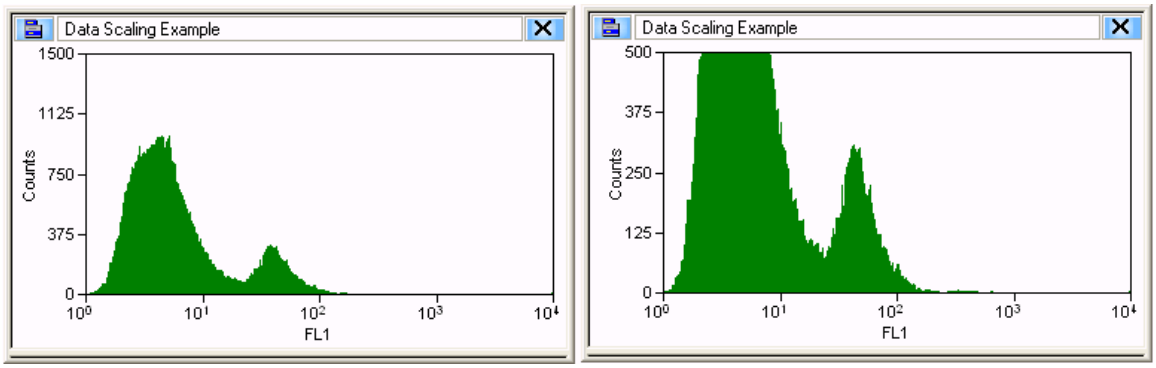

Set Fixed Scale

The **Set Fixed Scale** option allows you to determine an exact count value for the Y-axis. Simply select the checkbox to activate and enter a value for the scale.

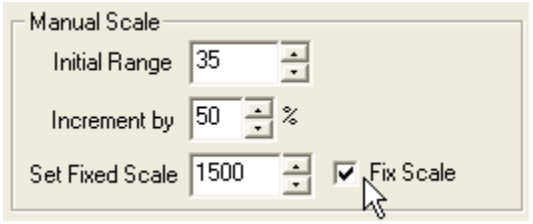

The histogram and corresponding data will be set to the defined count value.

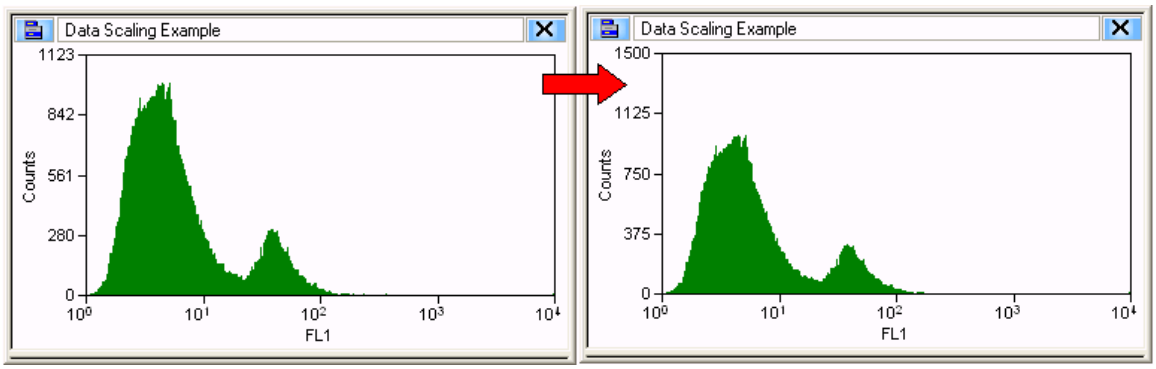

Auto Scaling

During acquisition and for offline data analysis, this feature is automatically performed in all histograms. Users have the option to manually scale data in any histogram, but by default, auto scaling is initially activated. Auto scaling ensures that the display of data in a histogram, based on count number, is visually proportional relative the scale of the Y-axis based on the distribution and count number of the data.

Auto scaling also provides a proper visual display of events during acquisition. For example, if acquisition were performed without auto scaling, the Y-axis count value would be arbitrarily set. As a result, collected data for the sample would be initially displayed and confined to the histogram's visual area. However, as more events are collected, the data's event count in various channels would eventually exceed the set Y-axis count. At that point, peak values in the data are not visible and the data would be defined as "offscale".

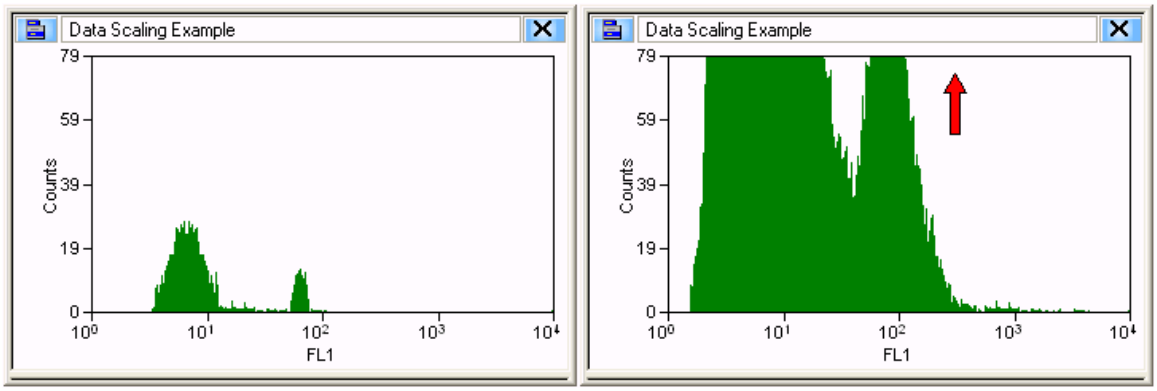

With auto scaling, when the number of events in the peak data channel approach the histogram's "count limit", the Y-axis is automatically rescaled to encompass a greater count range. In turn, the displayed data is resized based on the new Y-axis count. As acquisition continues, the process of rescaling the Y-axis and resizing the data is repeated each time the data reaches the histogram's count limit. This ensures that the full data display remains in the histogram and does not drift "offscale".

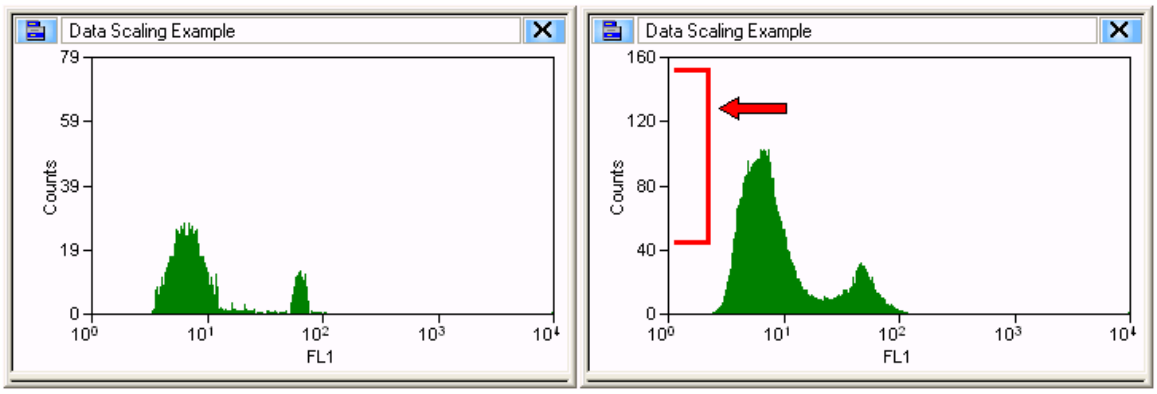

Auto Scaling Options

There are a number of settings that can be adjusted for auto scaling.

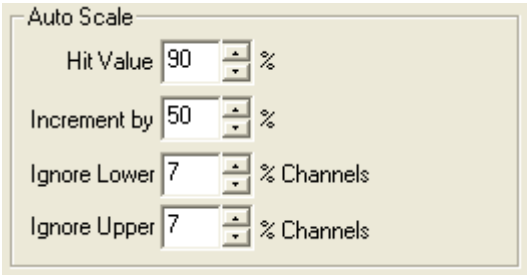

Hit Value refers to the maximum height (or % of counts) that the data's peak can reach in the histogram before the Y-axis is rescaled.

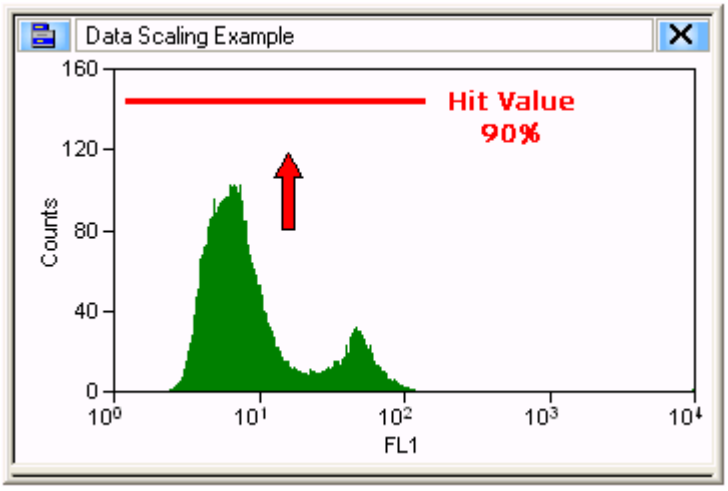

Increment by determines the degree by which the Y-axis is adjusted and the data is resized. The scale is incremented when the data's peak count reaches the assigned hit value in the histogram.

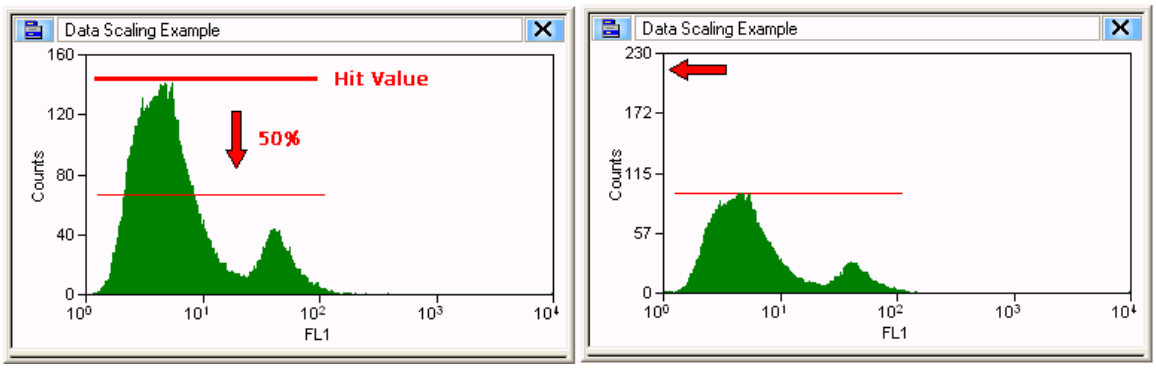

The **Ignore Lower % Channels** and **Ignore Upper % Channels** option is a useful aid for auto scaling. Keep in mind, when data is collected for a sample, all events that occur in all channels are collected and saved with the FCS file. However, when acquiring data, a percentage of lower and upper channels can be ignored when auto scaling. This option simply disregards any events in those channels when determining the proper Y-axis scale for displaying the data. (Again, all data in those channels is still collected and saved with the FCS file).

Why ignore a certain % of lower and upper channels when auto scaling?
Periodically when samples are run, a number of events are seen to buildup in either the first or last few channels. These events can be due to various factors such as sample debris, dead cells, or instrument noise. By ignoring the counts in these channels, auto scaling is set based on a maximum event count in a population(s) of interest.

The alternative is to have auto scaling based on the maximum event count in any channel. However, this method can present a problem for data display. As the sample is run, a number of counts could accumulate in the first or last few channels. Scaling in the histogram would then be based on the channel containing the maximum event number (for this example, the first channel). Histogram scaling would then be based on the tall peak in channel 1, thereby making the populations of interest appear unusually small (due to the low number of events in the population in comparison to the first channel).

The effect of the **Ignore Lower % Channels** and **Ignore Upper % Channels** feature (when activated and when turned off) can be seen in the two histograms below.

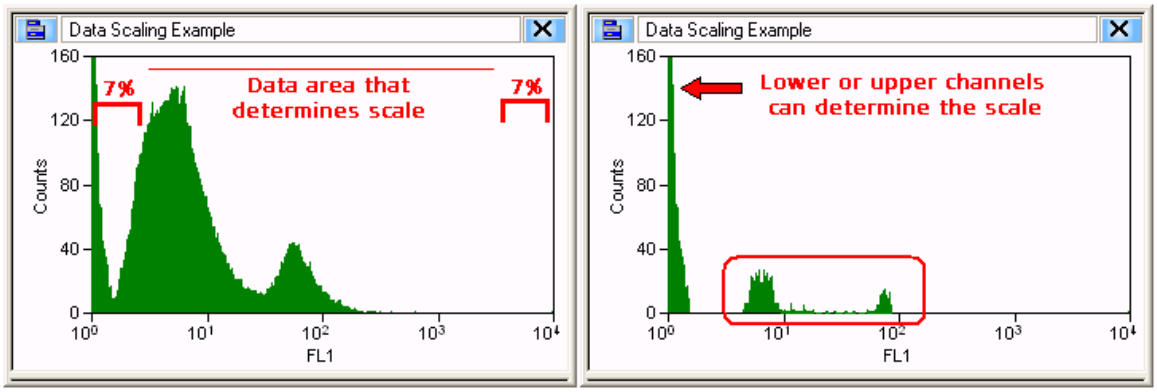

Subtraction Histograms

A subtraction histogram is an analysis tool that reports the fluorescent difference between a sample and a control tube for a particular parameter of interest. The calculated difference is displayed within the histogram and represents a "true" percentage of positively labeled events or cells. This population is mathematically determined by subtracting the control from the sample data.

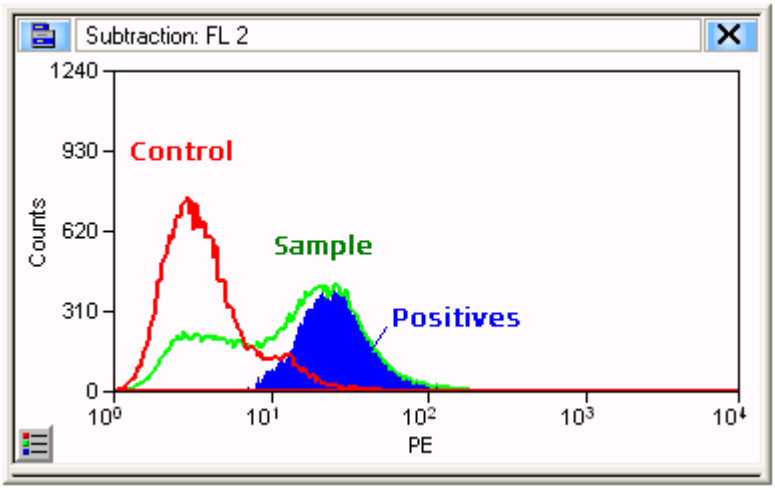

Controls Versus Samples

When working with subtraction histograms, it is important to properly designate which data set is the control and which represents the sample. Reversing these will result in the calculation of a different positive population. For example, the two subtraction histograms below contain the same two data sets, but the control and sample designations are switched. The outcome is a different positive population identified within the two histograms.

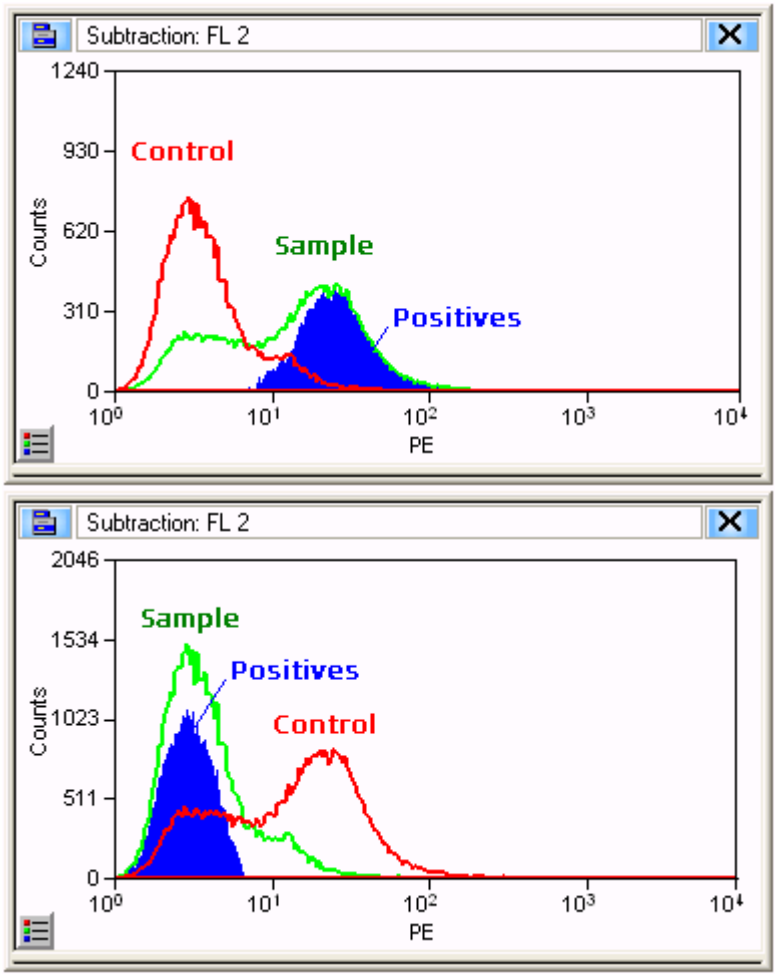

Analysis samples within a subtraction histogram, including the designated control, can be seen within the histogram's legend. To access this list, right-click within the subtraction histogram and select **Show Legend** from the popup menu.

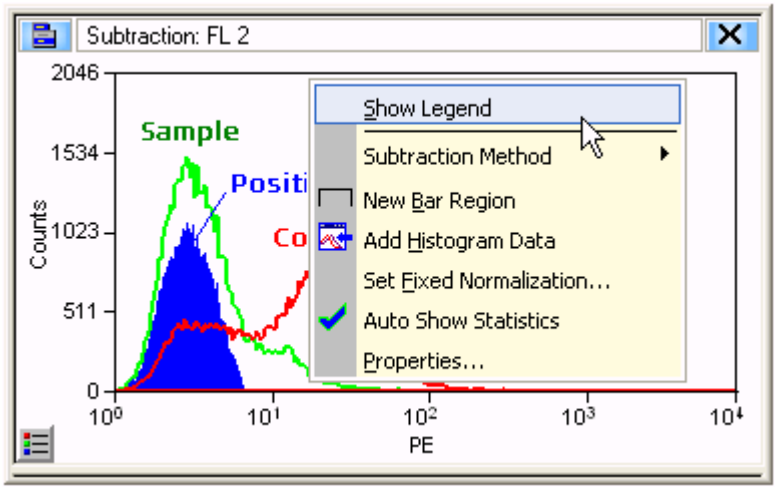

The legend will contain a list of data sets associated with the subtraction histogram with the designated control displayed in bold type. By default, the first data set added to a subtraction

histogram is designated as the control. Events for this data are then subtracted from all subsequently added samples to determine any "positive" events. If necessary, the sample designated as the control can be changed by right-clicking on a different sample and selecting **Control** from the popup menu.

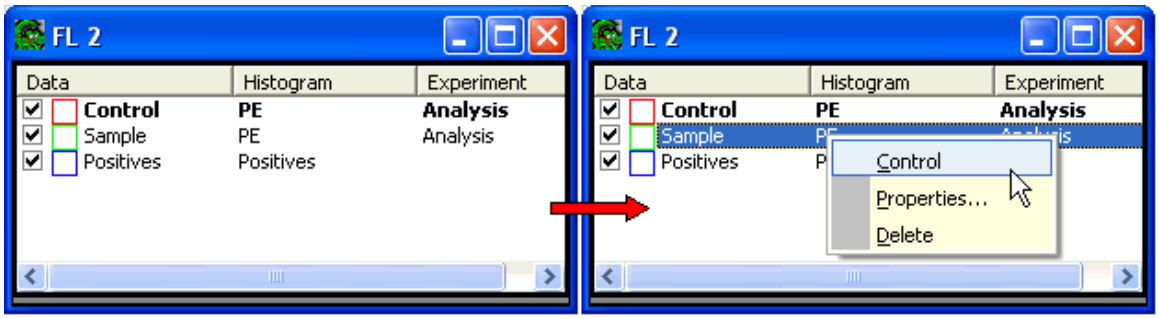

Subtraction Methods

Summit provides a couple of ways to calculate positive populations. The two available options, **Channel by Channel** and **Overton**, can be accessed by right-clicking within the subtraction histogram and selecting **Subtraction Method** from the popup menu.

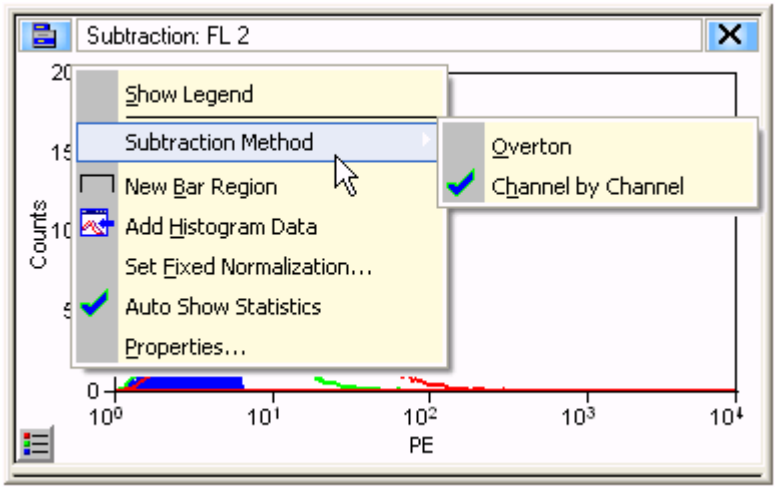

The **Channel by Channel** method subtracts all the collected events of the control from the sample data on a bin-by-bin (or channel-by-channel) basis. The event difference is then reported for all channels and represents the "true" positive population. Again, keep in mind that which data set is designated as the control and which is the sample will mathematically effect the reported difference in the two samples. For example, the following represents two subtraction data sets (the control and sample) for a given parameter. Events recorded for both groups are plotted within 6 channels and the calculated positive output is seen below. Control events are subtracted from sample events with any positive difference reported. Negative values are simply reported as "zero".

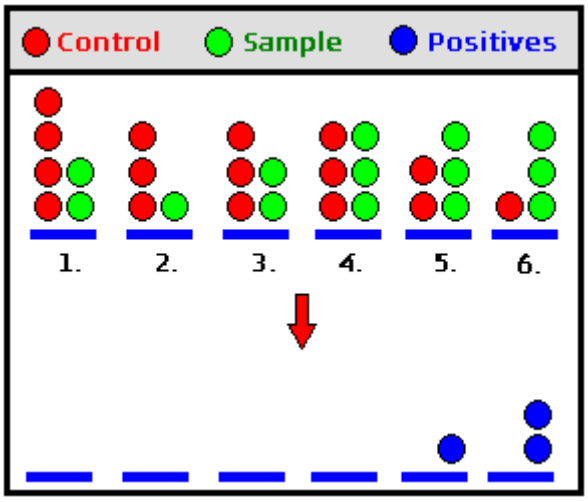

If we take the same two data sets, but reverse which is the control versus the sample, the following difference is reported (Again, sample events minus the control events on a per channel basis). Notice that in this case the calculated positives differ from the first example.

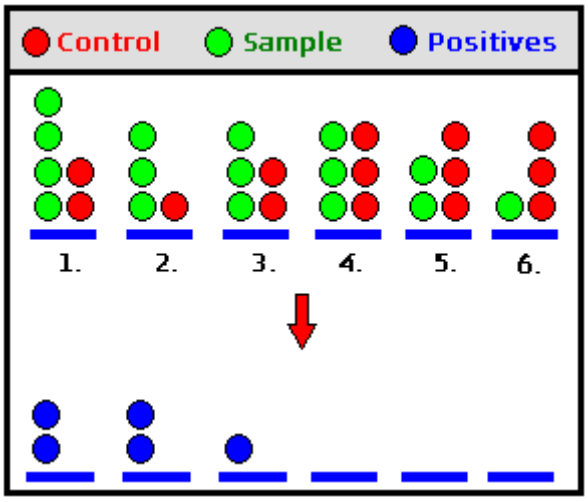

In practice, real data sets involve many more events per channel, but the same mathematical principles still apply. The following illustrates a subtraction histogram containing a single sample with a control. In this example, the positive population is identified as the following.

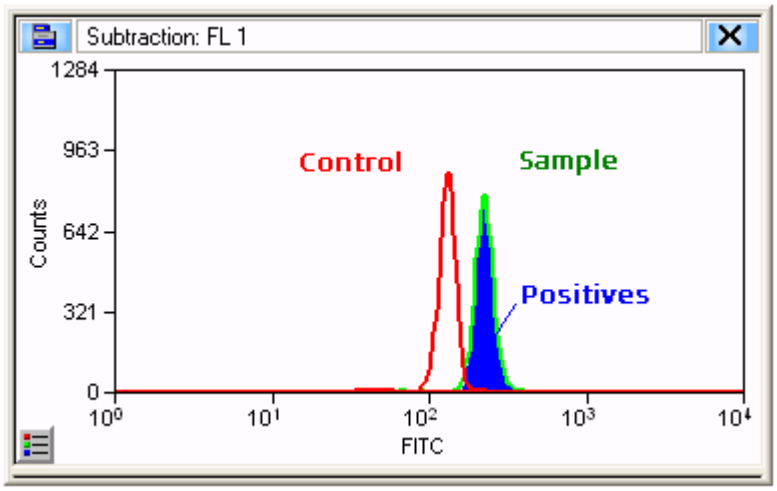

If the sample and control in this experiment are reversed, the following positive population is calculated.

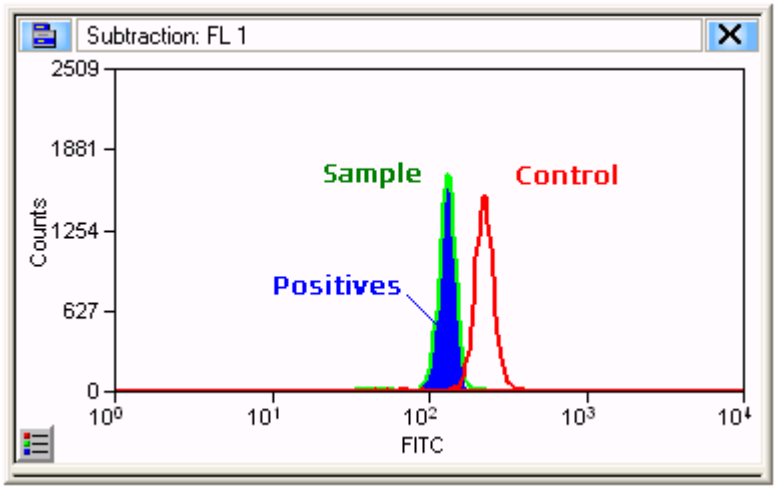

The **Overton** method calculates positive events on a percentage basis as a function of reverse cumulative distribution. This means that positive events reported within each sample channel are calculated by subtracting a number of control events based on that channel and all higher channels. Ultimately, this method helps to reduce the number of "false" positives and better reflects "true" biological differences. For example, using the Overton method below, the following positive population would be identified. In this case the result is the same as with the channel method.

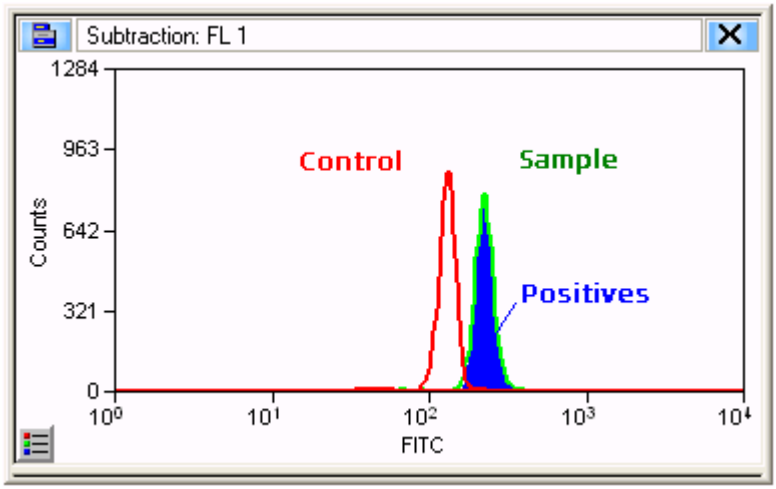

However, if the sample and control assignments are reversed, no positives are reported with the Overton method. Using the channel method, positives are reported under the "green" sample curve.

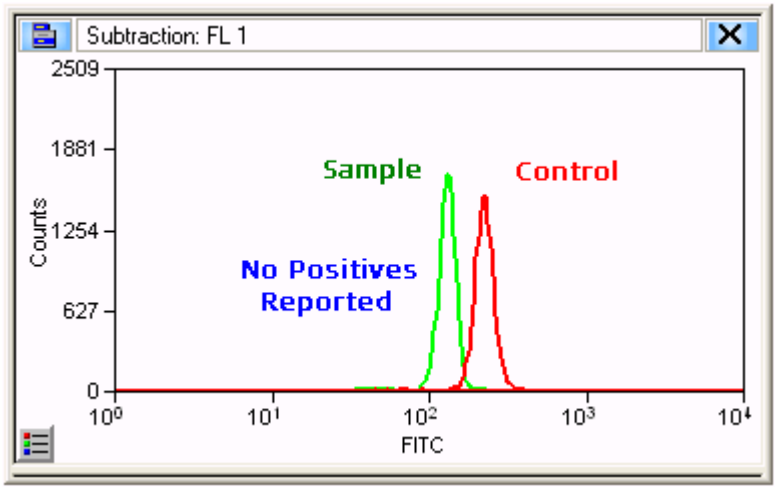

Experimental and Biological Relevance

The impact of using the Overton method for analyzing experimental data is demonstrated by the following example. Suppose data is first collected on a "true" FITC-negative control followed by a "potentially" FITC-positive sample. Data for the two samples is then added to a subtraction histogram to identify any "positive" events. Keep in mind that the events displayed within the histogram are binned and assigned to a channel based on an event's recorded intensity value for a particular parameter (in this case FITC). Thus for "true" FITC-positive events, one would expect a shift in the data to the right (or into a higher grouping of channels) i.e. a stronger signal is recorded from any FITC-positive cells, and subsequently, those events are assigned into higher channels within the histogram. With the Overton method, sample events falling "upstream" of the control are reported as "positives".

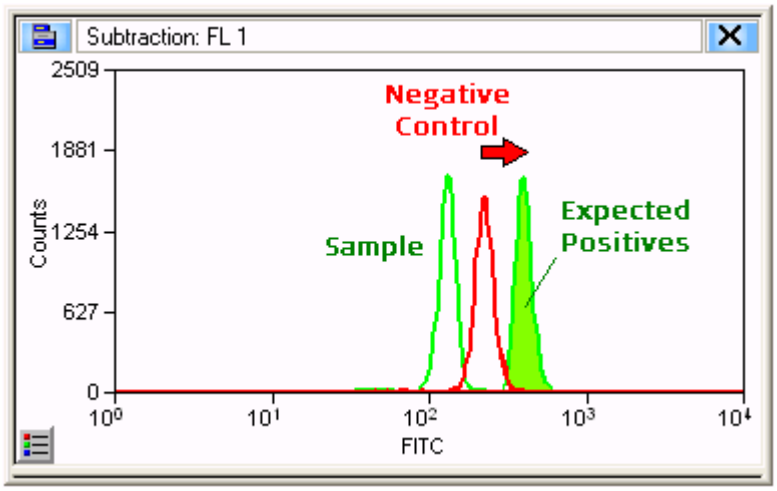

However, take a situation where a "potential" FITC-positive sample is analyzed and some or all of the data falls "equal to" or "below" the negative control. From an experimental perspective, it is unlikely that the sample is actually "FITC positive" since the recorded FITC signal is equivalent to or weaker than the non-FITC control (thus it is assigned to a lower set of channels). Using the Overton method, these events are not reported as positive since the algorithm also accounts for the control events present within higher channels (sample events per channel as a % of control events per channel and all higher channels).

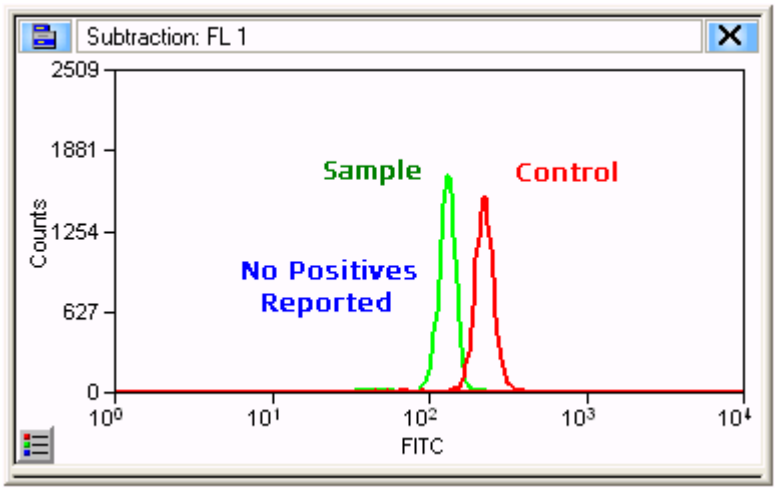

If the channel method were used in this case, the following positive population would be calculated and reported. However, it is very unlikely that these events actually represent "true" positives.

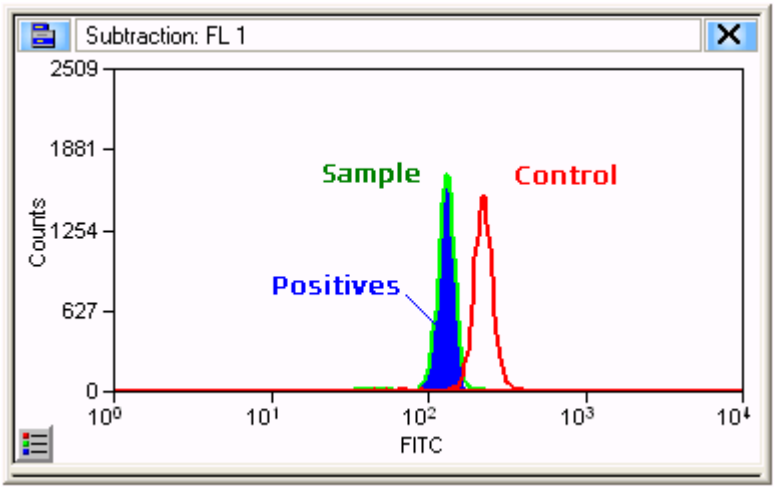

Another advantage of the Overton method is the reduction of "false positives" reported in the lower channels simply because more events were collected in those channels for a sample versus the control. This is especially evident when using subtraction histograms to compare data sets with different numbers of "total counts".

For example, the following is a subtraction histogram where the control contains 50,000 total events but the sample contains 100,000 events. Because the channel method reports "positives" based on the difference in the number of events between the sample and control on a per channel basis, many channels will report "positive" events simply because more events were collected on the sample tube (and thus are likely to predominate in number within certain channels than the control). The calculated "positives" in this case are not likely to represent "true" positives".

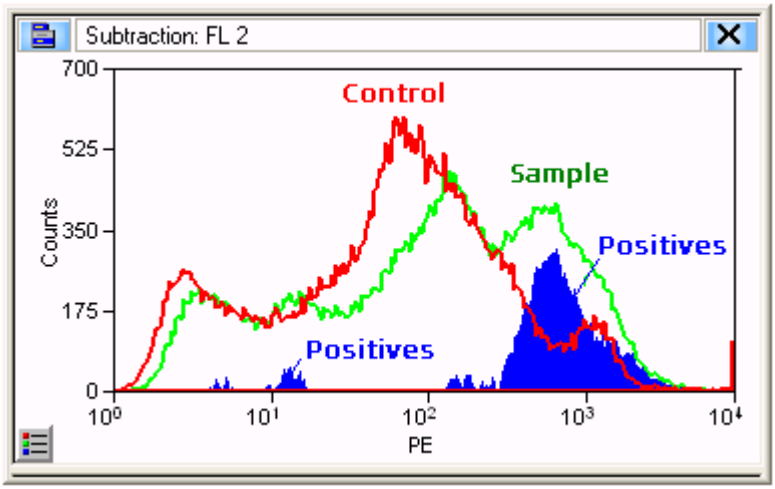

The Overton method helps to minimize these "false" positives that are reported within the lower channels. Again, this is done by calculating the "positive" events based on the control events within the equivalent and all higher channels.

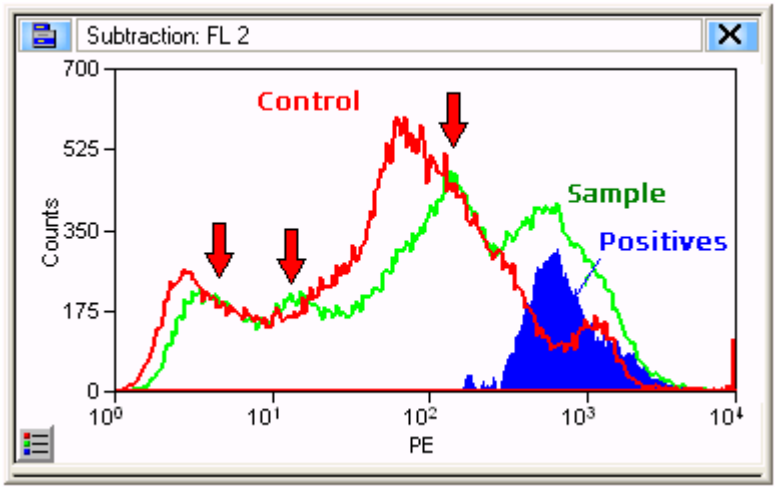

APPENDIX A

CYAN ADP CONSUMABLES

Table A.1:Calibration Particles

Code	Product
K0111	SpectrAlign™ - 3.0 µm, 1 x 10^7/mL, 2 mL/vial Single population of beads exciting and emitting across 351 nm, 405 nm, 488 nm, and 635 nm.
K0110	FluoroSpheres - 6-peak, 3.2 µm, 1 x 10^7/mL, 2 mL/vial
K0112	FluoroSpheres - 8-peak, 3.0 µm, 1 x 10^7/mL, 5 mL/vial
K0113	SpectraComp™ Kit 1 - Blank, FITC, PE, PE-Cy5, 3.2 µm, 1 x 10^7/mL, 1 mL/vial
K0114	SpectraComp™ Kit 2 - Blank, FITC, PE, PE-Cy5 & APC, 3.2 µm, 1 x 10^7/mL, 1 mL/vial
K0115	SpectraComp™ Kit 3 - Blank, FITC, PE, PE-TR, PE-Cy5, 3.2 µm, 1 x 10^7/mL, 1 mL/vial
K0116	SpectraComp™ Kit 4 - Blank, FITC, PE, PE-TR, PE-Cy5, PE-Cy7, APC & APC-Cy7, 3.2 µm, 1 x 10^7/mL, 1 mL/vial
K0117	SpectraComp™ Blank Particles, 5 mL/vial
K0118	SpectraComp™ FITC Particles, 1mL/vial
K0125	SpectraComp™ PE Particles, 1mL/vial
K0126	SpectraComp™ PE-TR Particles, 1mL/vial
K0121	SpectraComp™ PE-Cy5 Particles, 1mL/vial
K0124	SpectraComp™ PE-Cy7 Particles, 1mL/vial
K0123	SpectraComp™ APC Particles, 1mL/vial
K0124	SpectraComp™ APC-Cy7 Particles, 1mL/vial

Table A.2: Decontamination/Clean/Rinse Solutions

Code	Product
S2323	Solution, Clean & Rinse 5 Liter
S2324	Solution, Decontamination 5 Liter

To order CyAn ADP consumables, contact DakoCytomation Sales at 1.800.822.9902.

APPENDIX B

TECHNICAL AND INSTRUMENT SPECIFICATIONS

The technical and instrument specifications for the CyAn ADP are summarized in the following tables.

Table B.1: CyAn ADP UV Model Technical Specifications

Performance	
Acquisition rate	Up to 50,000 events/sec
Excitation Optics	
Optical parameters	2 scatter and 9 fluorescence
Beam geometry	Elliptical/Spherical
Number of excitation lines	3
Laser nominal operating output (See Coherent 621 Operator's Manual for more information.)	488 nm (150mW argon), UV (50mW argon), 635 nm (25mW semiconductor)
Laser maximum output value (Accessible in the interior of instrument)	488nm – 2W 351nm – 60mW 635nm – 27.5mW
Detectors and Filters (User-selected)	
488 nm Excitation	FL1-530/40 nm, FL2-575/25 nm, FL3-613/20 nm, FL4-680/30 nm, FL5-750 nm
UV Excitation	FL6-400/40 nm, FL7-450/50 nm
635 nm Excitation	FL8-665/20 nm, FL9-750 LP
Signal Processing	
Compensation	9 x 9 full matrix
Signal resolution	65536 (Summit displays up to 4096 channels on all parameters)

Data acquisition channels	11
Fluidics	
Fluidics control system	Software, hardware, and smart-sensor controls provide ease of use with RUN and PAUSE modes
Sample flow rate	Up to 300 µL/min
Sheath fluid	Maximum 1.03 bar (15 psi), nominal 0.41 bar (6 psi)
Quartz cuvette	UV-grade fused silica with 250 µm square-sectioned internal channel
Summit Workstation	
Platform	Windows® XP
Processor	1.7 GHz or faster
Memory	1 GB RAM (minimum)
Storage space	2 60 GB hard drives (minimum), CDRW
Monitor	17-inch LCD flat screen (dual monitor also available)
Network	High-speed Ethernet 10/100 MB/sec

Table B.2: CyAn ADP Technical Specifications

Performance	
Acquisition rate	Up to 50,000 events/sec
Excitation Optics	
Optical parameters	2 scatter and 9 fluorescence
Beam geometry	Elliptical
Number of excitation lines	3
Laser options nominal operating output (See Coherent OPSL Operator's Manual for more information.)	488 nm (20 mW Semiconductor), 635 nm (25 mW semiconductor), 405 nm (25 mW semiconductor)
Laser maximum output value (Accessible in the interior of instrument)	488nm - 20mW 635nm – 27.5mW 405 nm – 27.5mW
Detectors and Filters (User-selected)	
488 nm Excitation	FL1-530/40 nm, FL2-575/25 nm, FL3-613/20 nm, FL4-680/30 nm, FL5-750 nm
405 nm Excitation	FL6-450/50 nm, FL7-530/40
635 nm Excitation	FL8-665/20 nm, FL9-750 LP
Signal Processing	
Compensation	9 x 9 full matrix
Signal resolution	65536 (Summit displays up to 4096 channels on all parameters)
Data acquisition channels	11
Fluidics	
Fluidics control system	Software, hardware, and smart-sensor controls provide ease of use with RUN and PAUSE modes

Sample flow rate	Up to 300 µL/min
Sheath fluid	Maximum 1.03 bar (15 psi), nominal 0.41 bar (6 psi)
Quartz cuvette	UV-grade fused silica with 250 µm square-sectioned internal channel
Summit Workstation	
Platform	Windows® XP or NT
Processor	1.7 GHz or faster
Memory	1 GB RAM (minimum)
Storage space	2 60 GB hard drives (minimum), CDRW
Monitor	17-inch LCD flat screen (dual monitor also available)
Network	High-speed Ethernet 10/100 MB/sec

Table B.3: CyAn ADP Instrument Specifications

CyAn ADP Enclosure	
Type	Molded RIM polyurethane structural foam
Installation	Indoor only
UV Model Dimensions (not including Utility Cart, Heat Exchanger, or Summit Workstation)	Height 39.1cm (15.4 in) front cover closed 72.1cm (28.4 in) front cover open Width 119.4cm (47.0 in) 132.1cm (52.0 in) including clearance for cables Depth - 59.2cm (23.3 in) Weight - 86.5 kg (190 lbs)
Dimensions (not including Utility Cart or Summit Workstation)	Height 39.1cm (15.4 in) front cover closed 72.1cm (28.4 in) front cover open Width - 33.3cm (13.1 in) Depth 49.8cm (19.6 in) 62.5cm (24.6 in) including clearance for cables. Weight - 36.3 kg (80 lbs)
Auxiliary Components	
Laser Power Supply (UV Model)	Height – 19 cm (7.5 in) Width – 43 cm (17 in) Depth – 61 cm (24 in) Weight - 31 kg (68 lbs)
Sheath Management System (with casters): Houses sheath container, waste container, cleaner fluid container, air compressor, laser power supply, and vacuum	Height – 61.3 cm (24.2 in) Width - 73.3 cm (28.9 in) Depth – 61.9 cm (24.4 in) Weight – 52 kg (115 lbs)
Uninterruptible Power Supply	Height – 20.3 cm (7.9 in) Width – 14.7 cm (5.7 in) Depth – 44.5 cm (17.5 in) Weight – 20 kg (44 lbs)

Summit Workstation	Height - 42.9cm (16.9 in) Width - 19.1cm (7.5 in) Depth - 45.7cm (18.0 in) Weight - 10.5 kg (23 lbs)
External Transformer	Height – 19.1cm (7.5 in) Width - 31.2 cm (12.3 in) Depth - 19.1 cm (7.5 in) Weight - 11.4 kg (25 lbs)
Safety	
Interlock	The front cover is protected with dual magnetic positive-break (⊛) type interlock switch. Operates dual spring solenoid shutter actuators on all laser paths.
Laser product class	CLASS 1 LASER PRODUCT IEC/EN 60825 -1/A2:2001
Laser light leakage	Conforms to 21CFR1040.10 and 21CFR1040.11
Operating Environment	
Ambient temperature	15 to 30°C (59 to 86°F) For optimum performance maintain at +/- 2°C
Relative humidity	20 to 80% RH (non-condensing)
CyAn ADP System Utility Requirements & Fusing	
Power, UV Model (not including Enterprise II 621 Laser)	115 VAC +/- 10%, 60 Hz, single phase, 1.5A
Power, standard ADP	115 VAC +/- 10%, 60 Hz, single phase, 1.75A
Fuse	Type – 5x20mm, low breaking, high capacity, IEC. 115 VAC operation – 6.3A
Power, Sheath Management System	100-240 VAC , 50/60 Hz, single phase, 2A
Fuse, Sheath Management System	Type – 5x20mm, low breaking, high capacity, UL. 115 VAC operation – 3A

Power, Summit Workstation (not fused)	115 VAC +/- 10%, 60 Hz, single phase, 1A
Power, Summit Workstation Monitor (not fused)	115 VAC +/- 10%, 60 Hz, single phase, 2A
Power, External Transformer	Input: 230 VAC +/- 10%, 50/60 Hz, 5A Output: 15 VAC +/- 10%, 60 Hz, 8A
Fuse, External Transformer power	Type – 5x20mm, low breaking, high capacity, IEC, 115 VAC operation – 6.3A
CyAn ADP UV Model Laser System Utility Requirements	
Power, Coherent Enterprise II 621 Laser	208 – 240VAC, single phase, 50A
Cooling method	Water
Cooling load	4.5 kW (15,000 Btu/hr)
Cooling water pressure	138 – 414 kPa (20 – 60psi)
Cooling water inlet temperature	10 – 60 °C (50 – 140 °F)
Cooling water flow rate	8 – 11.6 l/min (2 – 3 gpm)
CyAn ADP UV Model Heat Exchanger Option	
Coherent LP5 Heat Exchanger	Height - 54.0cm (21.0 in) Width - 69.0cm (27.0 in) Depth - 44.0cm (17.0 in) Weight - 50 kg (110 lbs)
Power, Coherent LP5 Heat Exchanger	110/220 VAC +/- 10% 50/60 Hz, 10A
Fuse, Coherent LP5 Heat Exchanger power	Type – 5x25mm, fast acting, high capacity, IEC. 115 VAC operation – 5A 230 VAC operation – 2.5A
Cooling Method	Water-to-Air Heat Exchange
Heat Output	5 kW (17,000 Btu/hr)
Cooling water flow rate	8 – 9.5 l/min (2 – 2.5 gpm)
Maximum laser water return temperature	68 °C (154.4 °F)
Maximum ambient air temperature	40 °C (100 °F)

(heat exchanger only)	

APPENDIX C

FLOW CYTOMETRY REFERENCES

Researchers around the world and across many scientific disciplines rely on the MoFlo® High-Performance Cell Sorter and the CyAn™ ADP High-Performance Flow Cytometer. A partial list of peer-reviewed journal articles highlighting some of their cutting-edge science on the CyAn and MoFlo instruments follows.

Bacteria

Button, D. K., and B. R. Robertson. 2001. Determination of DNA content of aquatic bacteria by flow cytometry. *Appl Environ Microbiol 67:1636*.

Christmann, A., K. Walter, A. Wentzel, R. Kratzner, and H. Kolmar. 1999. The cystine knot of a squash-type protease inhibitor as a structural scaffold for *E. coli* cell surface display of conformationally constrained peptides. *Protein Engineering 12(9): 797-806.*

Edwards, R.A., and S.R. Maloy. 2001. Inside or outside: Detecting the cellular location of bacterial pathogens. *BioTechniques 30(2): 304.*

Gryllos, I., C. Cywes, M.H. Shearer, M. Cary, R.C. Kennedy, and M.R. Wessels. 2001. Regulation of capsule gene expression by group A *Streptococcus* during pharyngeal colonization and invasive infection. *Molecular Microbiology 42(1): 61-74.*

Robertson, B. R., D. K. Button, and A. L. Koch. 1998. Determination of the biomasses of small bacteria at low concentrations in a mixture of species with forward light scatter measurements by flow cytometry. *Appl Environ Microbiol 64:3900*.

Sierig, G., C. Cywes, M. R. Wessels, and C. D. Ashbaugh. 2003. Cytotoxic effects of Streptolysin O and Streptolysin S enhance the virulence of poorly encapsulated Group A Streptococci. *Infect. Immun. 71:446*.

Wehrman, T., B. Kleaveland, J. H. Her, R. F. Balint, and H. M. Blau. 2002. Protein-protein interactions monitored in mammalian cells via complementation of β-lactamase enzyme fragments. *PNAS 99:3469*.

Wentzel, A., A. Christmann, T. Adams, and H. Kolmar. 2001. Display of passenger proteins on the surface of Escherichia coli K-12 by the enterohemorrhagic E. coli intimin EaeA. *J Bacteriol 183:7273*.

Wentzel, A., A. Christmann, R. Kratzner, and H. Kolmar. 1999. Sequence requirements of the GPNG β-turn of the *Ecballium elaterium* trypsin inhibitor II explored by combinatorial library screening. *J Biol Chem 274(30) 21037-21043.*

Worden, A. Z., S. W. Chisholm, and B. J. Binder. 2000. In situ hybridization of Prochlorococcus and Synechococcus (marine cyanobacteria) spp. with RRNA-targeted peptide nucleic acid probes. *Appl Environ Microbiol 66:284*.

B Cell

Allman, D., R.C. Lindsley, W. DeMuth, K. Rudd, S.A. Shinton, and R.R. Hardy. 2001. Resolution of three nonproliferative immature splenic B cell subsets reveals multiple selection points during B cell maturation. *J Immunol 167: 6834-6840.*

Ansel, K.M., R. B.S. Harris, and J.G. Cyster. 2002. CSCL13 is required for B1 cell homing, natural antibody production, and body cavity immunity. *Immunity 16: 67-76.*

Arnold, L.W., S.K. McCray, C. Tatu, and S.H. Clarke. 2000. Identification of a precursor to phosphatidyl choline-specific B-1 cells suggesting that B-1 cells differentiate from splenic conventional B cell in vivo: Cyclosporin a blocks differentiation to B-1. *J Immunol 164: 2924-2930.*

Batten, M., J. Groom, T.G. Cachero, F. Quian, P. Schneider, J.Tschopp, J.L. Browning, and F. Mackay. 2000. BAFF mediates survival of peripheral immature B lymphocytes. *J Exp Med 192(10): 1453.*

Baumgarth, N., G.C. Jager, O.C. Herman, L.A. Herzenberg, and L.A. Herzenberg. 2000. CD4+ T cells derived from B cell-deficient mice inhibit the establishment of peripheral B cell pools. *PNAS 97(9): 4766.*

Baumgarth, N., O.C. Herman, G.C. Jager, L.E. Brown, L.A. Herzenberg, and J. Chen. 2000. B-1 and B-2 cell-derived immunoglobulin M antibodies are nonredundant components of the protective response to influenza virus infection. *J Exp Med 192(2): 271-280*.

Benschop, R.J., K. Aviszus, S. Zhang, T. Manser, J.C. Cambier, and L.J. Wysocki. 2001. Activation and anergy in bone marrow B cells of a novel immunoglobulin transgenic mouse that is both hapten specific and autoreactive. *Immunity 14(1): 33-43.*

Bross, L., Y. Fukita, F. McBlane, C. Demolliere, K. Rajewsky, and H. Jacobs. 2000. DNA double-strand breaks in immunoglobulin genes undergoing somatic hypermutation. *Immunity 13: 589*.

Bross, L., M. Muramatsu, K. Kinoshita, T. Honjo, and H. Jacobs. 2002. DNA double-strand breaks: Prior to but not sufficient in targeting hypermutation. *J Exp Med 195:1187.*

Clarke, S. H., and L. W. Arnold. 1998. B-1 cell development: evidence for an uncommitted immunoglobulin (Ig)M+ B cell precursor in B-1 cell differentiation. J *Exp Med 187:1325.*

Davis, R. S., H. Li, C.-C. Chen, Y.-H. Wang, M. D. Cooper, and P. D. Burrows. 2002. Definition of an Fc receptor-related gene (FcRX) expressed in human and mouse B cells. *Int. Immunol. 14:1075.*

Fleming, H.E., and C.J. Paige. 2001. Pre-B cell receptor signaling mediates selective response to IL-7 at the pro-B to pre-B cell transition via an ERK/MAP kinase-dependent pathway. *Immunity 15: 521-531*.

Gartner, F., F.W. Alt, R.J. Monroe, and K.J. Seidl. 2000. Antigen-independent appearance of Recombination Activating Gene (RAG)-positive bone marrow B cells in the spleens of immunized mice. *Journal of Experimental Medicine 192(12): 1745.*

Glazier, K. S., S. B. Hake, H. M. Tobin, A. Chadburn, E. J. Schattner, and L. K. Denzin. 2002. Germinal center B cells regulate their capability to present antigen by modulation of HLA-DO. *J Exp Med 195:1063.*

Gongora, R., R.P. Stephen, Z. Zhang, and M.D. Cooper. 2001. An essential role for Daxx in the inhibition of B lymphopoiesis by type I interferons. *Immunity 14(6): 727-737.*

Hayden, T. A., P. Riegert, and G. H. Kline. 2002. Detection of Functional VH81X Heavy Chains in Adult Mice with an Assessment of Complementarity-Determining Region 3 Diversity and Capacity to Form Pre-B Cell Receptor. *J Immunol 169:1970*.

Herblot, S., P.D. Aplan, and T. Hoang. 2002. Gradient of E2A activity in B-cell development. *Molecular and Cellular Biology 22(3): 886-900.*

Honczarenko, M., Y. Le, A. M. Glodek, M. Majka, J. J. Campbell, M. Z. Ratajczak, and L. E. Silberstein. 2002. CCR5-binding chemokines modulate CXCL12 (SDF-1)-induced responses of progenitor B cells in human bone marrow through heterologous desensitization of the CXCR4 chemokine receptor. *Blood 100:2321*.

Jin, L., P. A. McLean, B. G. Neel, and H. H. Wortis. 2002. Sialic acid binding domains of CD22 are required for negative regulation of B cell receptor signaling. *J Exp Med 195:1199*.

Kouro, T., K.L. Medina, K. Oritani, and P.W. Kincade. 2001. Characteristics of early murine B-lymphocyte precursors and their direct sensitivity to negative regulators. *Blood 97(9): 2708-2715.*

Lu, S.S., J. Tung, N. Baumgarth, O. Herman, M. Gleimer, L.A. Herzenberg, and L.A. Herzenberg. 2002. Identification of a germ-line pro-B cell subset that distinguishes the fetal/neonatal from the adult B cell development pathway. *PNAS 99(5): 3007-3012.*

Marchbank, K.J., C.C. Watson, D.F. Ritsema, and V.M. Hollers. 2000. Expression of human complement receptor 2 (CR2, CD21) in *Cr2*$^{-/-}$ mice restores humoral immune function. *J Immunol 165: 2354*.

Martin, F., A.M. Oliver, and J.F. Kearney. 2001. Marginal zone and B1 B cells unite in the early response against T-independent blood-borne particulate antigens. *Immunity 14(5): 617-629.*

Martin, F., and J.F. Kearney. 2000. Positive selection from newly formed to marginal zone B cells depends on the rate of clonal production, CD19 and *btk*. *Immunity 12: 39*.

Miller, J.P., D. Izon, W. DeMuth, R. Gerstein, A. Bhandoola, and D. Allman. 2002. The earliest step in B lineage differentiation from common lymphoid progenitors is critically dependent upon interleukin 7. *J Exp Med 196(5): 705-711.*

Ohdan, H., K.G. Swenson, H.S. Kruger Gray, Y.G. Yang, Y. Xu, A.D. Thall, and M. Sykes. 2000. Mac-1-negative B-1b phenotype of natural antibody-producing cells, including those responding to Galα1,3Gal epitopes in α1,3-galactosyltransferase-deficient mice. *J Immunol 165: 5518*.

Rolink. A.H., T. Brocker, H. Bluethmann, M.H. Kosco-Vilbois, J. Andersson, and F. Melchers. 1999. Mutations affecting either generation of survival of cells influence the pool size of mature B cells. *Immunity 10: 619-628.*

Rolink, A.H., T. Winkler, F. Melchers, and J. Anderson. 2000. Precursor B cell receptor-dependent B cell proliferation and differentiation does not require the bone marrow or fetal liver environment. *J Exp Med 191(1): 23-31.*

Rossi, M. I. D., T. Yokota, K. L. Medina, K. P. Garrett, P. C. Comp, A. H. Schipul, Jr, and P. W. Kincade. 2003. B lymphopoiesis is active throughout human life, but there are developmental age-related changes. *Blood 101:576.*

Sale, J.E., and M.S. Neuberger. 1998. TdT-accessible breaks are scattered over the immunoglobulin V domain in a constitutively hypermutating B cell line. *Immunity 9: 859-869.*

Seo, W.J., M.L. Fields, J.L. Buckler, A.J. Reed, L. Mandik-Nayak, S.A. Nish, R.J. Noelle, L.A. Turka, F.D. Finkelman, A.J. Caton, and J. Erickson. 2002. The impact of T helper and T regulatory cells on the regulation of anti-double-stranded DNA B cells. *Immunity 16: 535-546.*

Smith, K.G.C., D.M. Tarlinton, G.M. Doody, M.L. Hibbs, and D.T. Fearon. 1998. Inhitibition of the B cell by CD22: A requirement for Lyn. *J Exp Med 187(5): 807-811*.

Tatu, C., J. Ye, L.W. Arnold, and S.H. Clarke. 1999. Selection at multiple checkpoints focuses V_H12 B cell differentiation toward a single B-1 cell specificity. *J Exp Med 190(7): 903-914.*

Torres, R.M., and K. Hafen. 1999. A negative regulatory role for Ig-α during B cell development. *Immunity 11: 527-536.*

Wang, Y. H., R. P. Stephan, A. Scheffold, D. Kunkel, H. Karasuyama, A. Radbruch, and M. D. Cooper. 2002. Differential surrogate light chain expression governs B-cell differentiation. *Blood 99:2459*.

Xu, Y., S.-J. E. Beavitt, K. W. Harder, M. L. Hibbs, and D. M. Tarlinton. 2002. The activation and subsequent regulatory roles of Lyn and CD19 after B cell receptor ligation are independent. *J Immunol 169:6910*.

Cancer

Burchert, A., S. Wolfl, M. Schmidt, C. Brendel, B. Denecke, D. Cai, L. Odyvanova, T. Lahaye, M. C. Muller, T. Berg, H. Gschaidmeier, B. Wittig, R. Hehlmann, A. Hochhaus, and A. Neubauer. 2003. Interferon-α, but not the ABL-kinase inhibitor imatinib (STI571), induces expression of myeloblastin and a specific T-cell response in chronic myeloid leukemia. *Blood 101:259*.

Chen, J.S., E. Coustan-Smith, T. Suzuki, G.A. Neale, K. Mihara, C.H. Pui, and D. Campana. 2001. Identification of novel markers for monitoring minimal residual disease in acute lymphoblastic leukemia. *Blood 97(7): 2115-2120.*

Coleman, A.B., J. Momand, and S.E. Kane. 2000. Basic fibroblast growth factor sensitizes NIH 3T3 cells to apoptosis induced by Cisplatin. *Molecular Pharmacology 57: 324-333.*

Eischen, C.J., M.F. Roussel, S.J. Korsmeyer, and J.L. Cleveland. 2001. Bax loss impairs Myc-induced apoptosis and circumvents the selection of p53 mutations during Myc-mediated lymphomagenesis. *Molecular and Cellular Biology 21(22): 7653-7662.*

Ghia, P. P. Transidico, J.P. Veiga, C. Schaniel, F. Sallusto, K. Matsushima, S.e. Sallan, A.G. Rolink, A. Mantovani, L.M. Nadler, and A.A. Cardoso. 2001. Chemoattractants MDC and TARC are secreted by malignant B-cell precursors following CD40 ligation and support the migration of leukemia-specific T cells. *Blood 98(3): 533-540.*

Girardi, M., D.E. Oppenheim, C.R. Steele, J.M. Lewis, E. Glusac, R. Filler, P. Hobby, B. Sutton, R.E. Tigelaar, and A.C. Hayday. 2001. Regulation of cutaneous malignancy by $\gamma\delta$ T cells. *Science 294(5542): 605-609*.

Holash J., Maisonpierre, P.D., D. Compton, P. Boland, C.R. Alexander, D. Zagzag, G.D. Yancopoulos, and S.J. Wiegand. 1999. Vessel cooption, regression and growth in tumors mediated by angiopoietins and VEGF. *Science 284: 1994-1998.*

Holtz, M. S., M. L. Slovak, F. Zhang, C. L. Sawyers, S. J. Forman, and R. Bhatia. 2002. Imatinib mesylate (STI571) inhibits growth of primitive malignant progenitors in chronic myelogenous leukemia through reversal of abnormally increased proliferation. *Blood 99:3792*.

Lu, X., G. Magrane, C. Yin, D.N. Louis, J. Gray, and T. Van Dyke. 2001. Selective inactivation of p53 facilitates mouse epithelial tumor progression without chromosomal instability. *Molecular and Cellular Biology 21 (17): 6017-6030.*

Rego, E.M., Warrell, R.P., Z.G. Wang, and P.P. Pandolfi. 2000. Retinoic acid and As_2O_3 treatment in transgenic models of acute promyelocytic leukemia unravel the distinct nature of the leukemogenic process induced by the PML-RARα and PLZF-RARα oncoproteins. *PNAS 97(18): 10173.*

Schwieger, M., J. Lohler, J. Friel, M. Scheller, I. Horak, and C. Stocking. 2002. AML1-ETO inhibits maturation of multiple lymphohematopoietic lineages and induces myeloblast transformation in synergy with ICSBP deficiency. *J. Exp. Med. 196:1227*.

So, C. W., and M. L. Cleary. 2003. Common mechanism for oncogenic activation of MLL by forkhead family proteins. *Blood 101:633*.

Stripecke, R. A.A. Cardoso, K.A. Pepper, D.C. Skelton, X.J. Yu, L. Mascarenhas, K.I. Weinberg, L.M. Nadler, and D.B. Kohn. 2000. Lentiviral vectors for efficient delivery of CD80 and granulocyte-macrophage-colony-stimulating factor in human acute lymphoblastic leukemia and acute myeloid leukemia cells to induce antileukemic immune responses. *Blood 96(4): 1317-1326).*

Tomasson, M.H., I.R. Willliams, S. Li, J. Kutok, D. Cain, S. Gillessen, G. Dranoff, R.A. Van Etten, and D.G. Gilliland. 2001. Induction of myeloproliferative disease in mice by tyrosine kinase fusion oncogenes does not require granulocyte-macrophage colony-stimulating factor or interleukin-3. *Blood 97(5): 1435.*

Wulf, G.G., R.Y. Wang, I. Kuehnle, D. Weidner, F. Marini, M.K. Brenner, M. Andreeff, and M.A. Goodell. 2001. A leukemic stem cell with intrinsic drug efflux capacity in acute myeloid leukemia. *Blood 98(4): 1166-1173.*

Dendritic Cells

Barchet, W., M. Cella, B. Odermatt, C. Asselin-Paturel, M. Colonna, and U. Kalinke. 2002. Virus-induced interferon-α production by a dendritic cell subset in the absence of feedback signaling in vivo. *J Exp Med 195:507*.

Brawand, P., D. R. Fitzpatrick, B. W. Greenfield, K. Brasel, C. R. Maliszewski, and T. De Smedt. 2002. Murine plasmacytoid pre-dendritic cells generated from Flt3 ligand-supplemented bone marrow cultures are immature APCs. *J Immunol 169:6711*.

Briken, V., R. M. Jackman, G. F. M. Watts, R. A. Rogers, and S. A. Porcelli. 2000. Human CD1b and CD1c isoforms survey different intracellular compartments for the presentation of microbial lipid antigens. *J Exp Med 192:281*.

Edwards, A. D., S. P. Manickasingham, R. Sporri, S. S. Diebold, O. Schulz, A. Sher, T. Kaisho, S. Akira, and C. Reis e Sousa. 2002. Microbial recognition via toll-like receptor-dependent and -independent pathways determines the cytokine response of murine dendritic cell subsets to CD40 triggering. *J Immunol 169:3652*.

Fong, L., M. Mengozzi, N. W. Abbey, B. G. Herndier, and E. G. Engleman. 2002. Productive infection of plasmacytoid dendritic cells with human immunodeficiency virus type 1 is triggered by CD40 ligation. *J. Virol. 76:11033*.

Henri, S., J. Curtis, H. Hochrein, D. Vremec, K. Shortman, and E. Handman. 2002. Hierarchy of susceptibility of dendritic cell subsets to infection by Leishmania major: Inverse relationship to interleukin-12 production. *Infect Immun 70:3874*.

Le Bon, A., G. Schiavoni, G. D'Agostino, I. Gresser, F. Belardelli, and D. F. Tough. 2001. Type i interferons potently enhance humoral immunity and can promote isotype switching by stimulating dendritic cells in vivo. *Immunity 14:461*.

Montoya, M., G. Schiavoni, F. Mattei, I. Gresser, F. Belardelli, P. Borrow, and D. F. Tough. 2002. Type I interferons produced by dendritic cells promote their phenotypic and functional activation. *Blood 99:3263*.

Moron, G., P. Rueda, I. Casal, and C. Leclerc. 2002. CD8α- CD11b+ dendritic cells present exogenous virus-like particles to CD8+ T cells and subsequently express CD8α and CD205 molecules. *J Exp Med 195:1233*.

O'Keeffe, M., H. Hochrein, D. Vremec, J. Pooley, R. Evans, S. Woulfe, and K. Shortman. 2002. Effects of administration of progenipoietin 1, Flt-3 ligand, granulocyte colony-stimulating factor, and pegylated granulocyte-macrophage colony-stimulating factor on dendritic cell subsets in mice. *Blood 99(6): 2122-2130*.

O'Keeffe, M., H. Hochrein, D. Vremec, I. Caminschi, J. L. Miller, E. M. Anders, L. Wu, M. H. Lahoud, S. Henri, B. Scott, P. Hertzog, L. Tatarczuch, and K. Shortman. 2002. Mouse plasmacytoid cells: Long-lived cells, heterogeneous in surface phenotype and function, that differentiate into CD8+ dendritic cells only after microbial stimulus. *J. Exp. Med. 196:1307*.

O'Keeffe, M., H. Hochrein, D. Vremec, B. Scott, P. Hertzog, L. Tatarczuch, and K. Shortman. 2002. Dendritic cell precursor populations of mouse blood: Identification of the murine homologues of human blood plasmacytoid pre-DC2 and CD11c+ DC1 precursors. *Blood:2002*.

Qu, C., T. M. Moran, and G. J. Randolph. 2003. Autocrine type I IFN and contact with endothelium promote the presentation of influenza A virus by monocyte-derived APC. *J Immunol 170:1010*.

Reis e Sousa, C., G. Yap, O. Schulz, N. Rogers, M. Schito, J. Aliberti, S. Hieny, and A. Sher. 1999. Paralysis of dendritic cell IL-12 production by microbial products prevents infection-induced immunopathology. *Immunity 11:637*.

Riese, R. J., G. P. Shi, J. Villadangos, D. Stetson, C. Driessen, A. M. Lennon-Dumenil, C. L. Chu, Y. Naumov, S. M. Behar, H. Ploegh, R. Locksley, and H. A. Chapman. 2001. Regulation of CD1 function and NK1.1(+) T cell selection and maturation by cathepsin S. *Immunity 15:909*.

Schaniel, C., L. Bruno, F. Melchers, and A. G. Rolink. 2002. Multiple hematopoietic cell lineages develop in vivo from transplanted Pax5-deficient pre-B I-cell clones. *Blood 99:472*.

Vandenabeele, S., H. Hochrein, N. Mavaddat, K. Winkel, and K. Shortman. 2001. Human thymus contains 2 distinct dendritic cell populations. *Blood 97:1733*.

Villadangos, J. A., M. Cardoso, R. J. Steptoe, D. van Berkel, J. Pooley, F. R. Carbone, and K. Shortman. 2001. MHC class II expression is regulated in dendritic cells independently of invariant chain degradation. *Immunity 14:739*.

Vremec, D., J. Pooley, H. Hochrein, L. Wu, and K. Shortman. 2000. CD4 and CD8 expression by dendritic cell subtypes in mouse thymus and spleen. *Journal of Immunology 164: 2978-2986.*

Wang, Y., C. G. Kelly, J. T. Karttunen, T. Whittall, P. J. Lehner, L. Duncan, P. MacAry, J. S. Younson, M. Singh, W. Oehlmann, G. Cheng, L. Bergmeier, and T. Lehner. 2001. CD40 is a cellular receptor mediating mycobacterial heat shock protein 70 stimulation of CC-chemokines. *Immunity 15:971*.

Wu, L., A. D'Amico, K. D. Winkel, M. Suter, D. Lo, and K. Shortman. 1998. RelB is essential for the development of myeloid-related CD8α- dendritic cells but not of lymphoid-related CD8α+ dendritic cells. *Immunity 9:839*.

Yang. O.O., F.K. Racke, P.T. Nguyen, R. Gauslking, M.E. Severino, H.F. Horton, M.C. Byrne, J.L. Stroninger, and S. B. Wilson. 2000. CD1d on myeloid dendritic cells stimulates cytokine secretion from and cytolytic activity of Vα24JαQ T cells: A feedback mechanism for immune regulation. *J Immunol 165: 3756.*

Drosophila

Bryant, Z., L. Subrahmanyan, M. Tworoger, L. LaTray, C. R. Liu, M. J. Li, G. van den Engh, and H. Ruohola-Baker. 1999. Characterization of differentially expressed genes in purified Drosophila follicle cells: toward a general strategy for cell type-specific developmental analysis. *PNAS 96:5559.*

Hipfner, D. R., K. Weigmann, and S. M. Cohen. 2002. The bantam gene regulates Drosophila growth. *Genetics 161:1527*.

Noureddine, M. A., T. D. Donaldson, S. A. Thacker, and R. J. Duronio. 2002. Drosophila Roc1a encodes a RING-H2 protein with a unique function in processing the Hh signal transducer Ci by the SCF E3 ubiquitin ligase. *Dev Cell 2:757*.

Tapon, N., N. Ito, B. J. Dickson, J. E. Treisman, and I. K. Hariharan. 2001. The Drosophila tuberous sclerosis complex gene homologs restrict cell growth and cell proliferation. *Cell 105:345.*

Tseng, A.-S. K., and I. K. Hariharan. 2002. An overexpression screen in Drosophila for genes that restrict growth or cell-cycle progression in the developing eye. *Genetics 162:229.*

Fluorescent Proteins

Allenspach, E.J., P. Cullinan, J. Tong, Q. Tang, A.G. Tesciuba, J.L. Cannon, S.M. Takahashi, R. Morgan, J.K. Burkhardt, and A.I. Sperling. 2001. ERM-dependent movement of CD43 defines a novel protein complex distal to the immunological synapse. *Immunity 15: 739-750.*

Demo, S.D., E. Masuda, A.B. Rossi, B.T. Throndset, A.L. Gerard, E.H. Chan, R.J. Armstrong, B.P. Fox, J.b. Lorens, D.G. Pana, R.H. Scheller, and J.M. Fisher. 1999. Quantitative measurement of mast cell degranulation using a novel flow cytometric annexin-V binding assay. *Cytometry 36: 340-348.*

Dorris, D.R., and K. Struhl. 2000. Artificial recruitment of TFIID, but not RNA polymerase II holoenzyme, activates transcription in mammalian cells. *Molecular and Cellular Biology 20(12): 4350-4358.*

Eischen, C.J., M.F. Roussel, S.J. Korsmeyer, and J.L. Cleveland. 2001. Bax loss impairs Myc-induced apoptosis and circumvents the selection of p53 mutations during Myc-mediated lymphomagenesis. *Molecular and Cellular Biology 21(22): 7653-7662.*

Gartner, F., F.W. Alt, R.J. Monroe, and K.J. Seidl. 2000. Antigen-independent appearance of recombination activating gene (RAG)-positive bone marrow B cells in the spleens of immunized mice. *J Exp Med 192(12): 1745-1754.*

Kishimoto, J., R.E. Burgeson, et al. 2000. Wnt signaling maintains the hair-inducing activity of the dermal papilla. *Genes & Development 14(10): 1181-1185.*

Kishimoto, J., R. Ehama, L. Wu, S. Jiang, N. Jiang, and R.E. Burgeson. 1999. Selective activation of the versican promoter by epithelial-mesenchymal interactions during hair follicle development. *PNAS 96: 7336-7341.*

Lorens, J.B., M.K. Bennett, D.M. Pearsall, W.R. Throndset, A.B. Rossi, R.J. Armstrong, B.P. Fox, E.H. Chan, Y. Luo, E. Masuda, D.A. Ferrick, D.C. Anderson, D.G. Payan, and G.P. Nolan. 2000. Retroviral delivery of peptide modulators of cellular functions. *Molecular Therapy 1(5): 438-447.*

Mao, X., Y. Fujiwara, A. Chapdelaine, H. Yang, and S.H. Orkin. 2001. Activation of EGFP expression by Cre-mediated excision in a new ROSA26 reporter mouse strain. *Blood 97(1): 324.*

McGavin, M.K.H., K. Badour, L.A. Hardy, T.J. Kubiseksi, J. Zhang, and K.A. Siminovitch. 2001. The intersectin 2 adaptor links Wiskott Aldrich Syndrome protein (WASp)-mediated actin polymerization to T cell antigen receptor endocytosis. *J Exp Med 194(12): 1777-1787*.

Mohrs, M., K. Shinkai, K. Mohrs, and R.M. Locksley. 2001. Analysis of type 2 immunity in vivo with bicistronic IL-4 reporter. *Immunity 15(2): 303-311*.

Monroe, R. J., K.J. Seidl, F. Gaertner, S. Han, F. Chen, J. Sekiguchi, J. Wang, R. Ferrini, L. Davidson, G. Kelsoe, and F.W. Alt. 1999. RAG2:GFP knockin mice reveal novel aspects of RAG2 expression in primary and peripheral lymphoid tissues. *Immunity 11: 201-212.*

Nakamura, K., A. Malykhin, and K.M. Coggeshall. 2002. The Src homology 2 domain-containing inositol 5-phosphatase negatively regulates Fcγ receptor-mediated phagocytosis through immunoreceptor tyrosine-based activation motif-bearing phagocytic receptors. *Blood 100(9): 3374-3382.*

Olaso, E., K. Ikeda, F.J. Eng, L. Xu, L. Wang, H.C. Lin, and S.L. Friedman. 2001. DDR2 receptor promotes MMP-2-mediated proliferation and invasion by hepatic stellate cells. *J Clin Investigation 108(9): 1369-1378.*

Rada, C., J.M. Jarvis, and C. Milstein. 2002. AID-GFP chimeric protein increases hypermutation of Ig genes with no evidence of nuclear localization. *PNAS 99(10): 7003-7008.*

Rommel, C., B.A. Clarke, S. Zimmermann, L. Nunez, R. Rossman, K. Reid, K. Moelling, G.D. Yancopoulos, and D.J. Glass. 1999. Differentiation stage-specific inhibition of the Raf-MIK-ERK pathway by Akt. *Science 286: 1738-1741.*

Roncarati, R. N. Sestan, M.H. Scheinfeld, B.E. Berechid, P.A. Lopez, O. Meucci, J.C. McGlade, P. Rakic, and L. D'Adamio. 2002. The γ-secretase-generated intracellular domain of β-amyloid precursor protein binds Numb and inhibits Notch signaling. *PNAS 99(10): 7102-7107*.

Rosen, E.D., C. Husi, X. Wang, S. Sakai, M.W. Freeman, F.J. Gonzalez, and B.M. Spiegelman. 2002. C/EBPα induces adipogenesis through PPARγ: a unified pathway. *Genes & Development 16: 22-26.*

Scheinfeld, M.H., R. Roncarati, P. Vito, P.A. Lopez, M. Abdallah, and L. D'Adamio. 2002. Jun NH2-terminal kinase (JNK) interacting protein 1 (JIP1) binds the cytoplasmic domain of the Alzheimer's β-amyloid precursor protein (APP). *J Biol Chem 277(5): 3767-3775.*

Tomasson, M.H., I.R. Williams, S. Li, J. Kutok, D. Cain, S. Gillessen, G. Dranoff, R.A. Van Etten, and D.G. Gilliland. 2001. Induction of myeloproliferative disease in mice by tyrosine kinase fusion oncogenes does not require granulocyte-macrophage colony-stimulating factor or interleukin-3. *Blood 97(5): 1435.*

High-Throughput Screening

Ashcroft, R.G., and P.A. Lopez. 2000. Commercial high speed machines open new opportunities in high throughput flow cytometry. *Journal of Immunological Methods 243: 13.*

Battye, F.L., A. Light, and D.M. Tarlinton. 2000. Single cell sorting and cloning. *Journal of Immunol Methods 243: 25.*

Brenner, S., M. Johnson, J. Bridgham, G. Golda, D.H. Lloyd, D. Johnson, S. Luo, S. McCurdy, M. Foy, M. Ewan, R. Roth, D. George, S. Elitr, G. Albrecht, E. Vermaas, S.R. Williams, K. Moon, T. Burcham, M. Pallas, R.B. DuBridge, J. Kirchner, K. Fearon, J. Mao, and K. Corcoran. 2000. Gene expression analysis by massively parallel signature sequencing on microbead arrays. *Nature Biotechnology 18: 630-634.*

Brenner, S., S.R. Williams, E.H. Vermaas, T. Storck, K. Moon, C. McCollum, J. Mao, S. Luo, J.J. Kirchner, S. Eletr, R.B. DuBridge, T. Burcham, and G. Albrecht. 2000. In vitro cloning of complex mixtures of DNA on microbeads: Physical separation of differentially expressed cDNAs. *PNAS 97(4): 1665.*

Christmann, A., K. Walter, A. Wentzel, R. Kratzner, and H. Kolmar. 1999. The cystine knot of a squash-type protease inhibitor as a structural scaffold for *E. coli* cell surface display of conformationally constrained peptides. *Protein Engineering 12(9): 797-806.*

Daugherty, P.S., B.L. Iverson, and G. Georgiou. 2000. Flow cytometric screening of cell-based libraries. *Journal of Immunol Methods 243: 211.*

Demo, S.D., E. Masuda, A..B. Rossi, B.T. Throndset, A.L. Gerard, E.H. Chan, R.J. Armstrong, B.P. Fox, J.B. Lorens, D.G. Payan, R.H. Scheller, and J.M. Fisher. 1999. Quantitative measurement of mast cell degranulation using a novel flow cytometric annexin-V binding assay. *Cytometry 36: 340-348.*

Gubbels, M.-J., C. Li, and B. Striepen. 2003. High-throughput growth assay for Toxoplasma gondii using yellow fluorescent protein. *Antimicrob. Agents Chemother. 47:309*.

Kinsella, T. M., C. T. Ohashi, A. G. Harder, G. C. Yam, W. Li, B. Peelle, E. S. Pali, M. K. Bennett, S. M. Molineaux, D. A. Anderson, E. S. Masuda, and D. G. Payan. 2002. Retrovirally delivered random cyclic peptide libraries yield inhibitors of

interleukin-4 signaling in human B cells. *J. Biol. Chem. 277:37512*.

Lorens, J.B., M.K. Bennett, D.M. Pearsall, W.R. Throndset, A.B. Rossi, R.J. Armstrong, B.P. Fox, E.H. Chan, Y. Luo, E. Masuda, D.A. Ferrick, D.C. Anderson, D.G. Payan, and G.P. Nolan. 2000. Retroviral delivery of peptide modulators of cellular functions. *Molecular Therapy 1(5): 438-447.*

Shires, J., E. Theodoridis, and A. C. Hayday. 2001. Biological insights into TCR$\gamma\delta$+ and TCR$\alpha\beta$+ intraepithelial lymphocytes provided by serial analysis of gene expression (SAGE). *Immunity 15:419*.

Wehrman, T., B. Kleaveland, J.Her., R.F. Balint, and H.M. Blau. 2002. Protein-protein interactions monitored in mammalian cells via complementation of β-lactamase enzyme fragments. *PNAS 99(6): 3469-3474.*

Wentzel, A., A. Christmann, T. Adams, and H. Kolmar. 2001. Display of passenger proteins on the surface of Escherichia coli K-12 by the enterohemorrhagic E. coli intimin EaeA. *J Bacteriol 183:7273*.

Wentzel, A., A. Christmann, R. Kratzner, and H. Kolmar. 1999. Sequence requirements of the GPNG β-turn of the *Ecballium elaterium* trypsin inhibitor II explored by combinatorial library screening. *J Biol Chem 274(30) 21037-21043.*

Marine Biology and Limnology

Andreatta, S., M.M.Wallinger, T. Posch, and R. Psenner. 2001. Detection of subgroups from flow cytometry measurements of heterotrophic bacterioplankton by image analysis. *Cytometry 44(3): 218-225.*

Button, D.K., and B.R. Robertson. 2001. Determination of DNA content of aquatic bacteria by flow cytometry. *Appl Environ Microbiol 67(4): 1636-1645.*

DuRand, M. D., R. E. Green, H. M. Sosik, and R. J. Olson. 2002. Diel variations in optical properties of Micromonas pusilla (Prasinophyceae). *J. Phycol. 38:1132.*

Robertson, B.R., D.K. Button, et al. 1998. Determination of the biomasses of small bacteria at low concentrations in a mixture of species with forward light scatter measurements by flow cytometry. *Appl Environ Microbiol 64(10): 3900-3909.*

Worden, A.Z., S.W. Chisholm, and B.J. Binder. 2000. In situ hybridization of *Prochlorococcus* and *Synechococcus* with rRNA-targeted peptide nucleic acid probes. *Appl Environ Microbiol 66(1): 284*.

Monocytes

Deszo, E.L., D.K. Brake, K.A. Cengel, K.W. Kelley, and G.C. Freund. 2001. CD45 negatively regulates monocytic cell differentiation by inhibiting phorbol 12-myristate 13-acetate-dependent activation and tyrosing phosphorylation of protein kinase Cδ. *J. Biol. Chem. 276(13): 10212-10217.*

Eue, I., B. Pietz, J. Storck, M. Klempt, and C. Sorg. 2000. Transendothelial migration of 27E10+ human monocytes. *Int Immunol 12:1593.*

Qu, C., T. M. Moran, and G. J. Randolph. 2003. Autocrine type I IFN and contact with endothelium promote the presentation of influenza A virus by monocyte-derived APC. *J Immunol 170:1010.*

Wang, Y., C.G. Kelly, J.T. Karttunen, T. Whittail, P.J. Lehner, L. Duncan, P. MacAry, J.S. Younson, M. Singh, W. Oehlmann, G. Cheng, L. Bergmeier, and T. Lehner. 2001. CD40 is a cellular receptor mediating mycobacterial heat shock protein 70 stimulation of CC-chemokines. *Immunity 15: 971-983.*

NK Cells

Blanca, I.R., E.W. Bere, H.A. Young, and J.R. Ortaldo. 2001. Human B cell activation by autologous NK cells is regulated by CD40-CD40 ligand interaction: role of memory B cells and CD5+ B cells. *J Immunol 167(11): 6132-6139*.

Carayannopoulos, L. N., O. V. Naidenko, D. H. Fremont, and W. M. Yokoyama. 2002. Cutting edge: Murine UL16-binding protein-like transcript 1: A newly described transcript encoding a high-affinity ligand for murine NKG2D. J *Immunol 169:4079*.

Gosselin, P., L.H. Mason, J. Willette-Brown, J.R. Ortaldo, D.W. McVicar, and S.K. Anderson. 1999. Induction of DAP12 phosphorylation, calcium mobilization, and cytokine secretion by Ly49H. *J Leukocyte Biol 66(1): 165-171*.

Hoshino, T., R.H. Wiltrout, and H.A. Young. 1999. IL-18 is a potent coinducer of IL-13 in NK and T cells: A new potential role for IL-18 in modulating the immune response. *J Immunol 162: 5070-5077*.

Hoshino, T., R.T. Winkler-Pickett, A.T. Mason, J.R. Ortaldo, and H.A. Young. 1999. IL-13 production by NK cells: IL-13-producing NK and T cells are present in vivo in the absence of IFN-γ. *J Immunol 162: 51-59.*

Makrigiannis, A.P., J. Etzler, R. Winkler-Pickett, A. Mason, J.R. Ortaldo, and S.K. Anderson. 2000. Identification of the Ly49L protein: evidence for activating counterparts to inhibitory Ly49 proteins. *J Leukocyte Biol 68(5): 765-771*.

Makrigiannis, A.P., A.T. Pau, A. Saleh, R. Winkler-Pickett, J.R. Ortaldo, and S.K. Anderson. 2001. Class I MHC-binding characteristics of the 129/J Ly49 repertoire. *J Immunol 166(8): 5034-5043*.

Mason, L.H., J. Willette-Brown, A.T. Mason, D. McVicar, and J.R. Ortaldo. 2000. Interaction of Ly-49D^{+} NK cells with H-2D^{d} target cells leads to Dap-12 phosphorylation and IFN-γ secretion. *J Immunol 164: 603-611.*

McVicar, D. W., R. Winkler-Pickett, L. S. Taylor, A. Makrigiannis, M. Bennett, S. K. Anderson, and J. R. Ortaldo. 2002. Aberrant DAP12 signaling in the 129 strain of mice: Implications for the analysis of gene-targeted mice. *J Immunol 169:1721*.

Orange, J. S., N. Ramesh, E. Remold-O'Donnell, Y. Sasahara, L. Koopman, M. Byrne, F. A. Bonilla, F. S. Rosen, R. S. Geha, and J. L. Strominger. 2002. Wiskott-Aldrich syndrome protein is required for NK cell cytotoxicity and colocalizes with actin to NK cell-activating immunologic synapses. *PNAS 99:11351.*

Ortaldo, J.R., E.W. Bere, D. Hodge, and H.A. Young. 2001. Activating Ly-49 NK receptors: central role in cytokine and chemokine production. *J Immunol 166(8): 4994-4999*.

Ortaldo, J.R., A.T. Mason, R. Winkler-Pickett, A. Raziuddin, W.J. Murphy, and L.H. Mason. 1999. Ly-49 receptor expression and functional analysis in multiple mouse strains. *J Leukocyte Biol 66(3): 512-520.*

Ortaldo, J.R., R. Winkler-Pickett, and G. Wiegand. 2000. Activating Ly-49D NK receptors: expression and function in relation to ontogeny and Ly-49 inhibitor receptors. *J Leukocyte Biol 68(5): 748-756.*

Ortaldo, J.R., R. Winkler-Pickett, J. Willette-Brown, R.L. Wange, S.K. Anderson, G.J. Palumbo, L.H. Mason, and D.W. McVicar. 1999. Structure/function relationship of activating Ly-49D and inhibitory Ly-49G2 NK receptors. *J Immunol 163: 5269-5277.*

Schaniel, C., L. Bruno, F. Melchers, and A.G. Rolink. 2002. Multiple hematopoietic cell lineages develop in vivo from transplanted *Pax5*-deficient pre-B I-cell clones. *Blood 99(2): 472-478*.

Voehringer, D., M. Koschella, and H. Pircher. 2002. Lack of proliferative capacity of human effector and memory T cells expressing killer cell lectinlike receptor G1 (KLRG1). *Blood 100:3698*.

Parasites

Ellis, T. N., and B. L. Beaman. 2002. Murine polymorphonuclear neutrophils produce interferon-γ in response to pulmonary infection with Nocardia asteroides. *J Leukocyte Biol 72:373*.

Gao, W., H. H. Wortis, and M. A. Pereira. 2002. The Trypanosoma cruzi trans-sialidase is a T cell-independent B cell mitogen and an inducer of non-specific Ig secretion. *Int Immunol 14:299*.

Mayer, W. E., T. Uinuk-ool, H. Tichy, L. A. Gartland, J. Klein, and M. D. Cooper. 2002. Isolation and characterization of lymphocyte-like cells from a lamprey. *PNAS 99:14350*.

Stem Cells

Akashi, K., X. He, J. Chen, H. Iwasaki, C. Niu, B. Steenhard, J. Zhang, J. Haug, and L. Li. 2003. Transcriptional accessibility for genes of multiple tissues and hematopoietic lineages is hierarchically controlled during early hematopoiesis. *Blood 101:383*.

Asakura, A., P. Seale, A. Girgis-Gabardo, and M. A. Rudnicki. 2002. Myogenic specification of side population cells in skeletal muscle. *J. Cell Biol. 159:123*.

Bannert, N., M. Farzan, D. S. Friend, H. Ochi, K. S. Price, J. Sodroski, and J. A. Boyce. 2001. Human mast cell progenitors can be infected by macrophagetropic human immunodeficiency virus type 1 and retain virus with maturation in vitro. *J Virol 75:10808*.

Batten, M., J. Groom, T. G. Cachero, F. Qian, P. Schneider, J. Tschopp, J. L. Browning, and F. Mackay. 2000. BAFF mediates survival of peripheral immature B lymphocytes. *J Exp Med 192:1453*.

Burchert, A., S. Wolfl, M. Schmidt, C. Brendel, B. Denecke, D. Cai, L. Odyvanova, T. Lahaye, M. C. Muller, T. Berg, H. Gschaidmeier, B. Wittig, R. Hehlmann, A. Hochhaus, and A. Neubauer. 2003. Interferon-α, but not the ABL-kinase inhibitor imatinib (STI571), induces expression of myeloblastin and a specific T-cell response in chronic myeloid leukemia. *Blood 101:259*.

Chatterjee, S., W. Li, C. A. Wong, G. Fisher-Adams, D. Lu, M. Guha, J. A. Macer, S. J. Forman, and K. K. Wong, Jr. 1999. Transduction of primitive human marrow and cord blood-derived hematopoietic progenitor cells with adeno-associated virus vectors. *Blood 93:1882*.

Clarke, S. H., and L. W. Arnold. 1998. B-1 cell development: evidence for an uncommitted immunoglobulin (Ig)M+ B cell precursor in B-1 cell differentiation. *J Exp Med 187:1325*.

Dahl, A. M., C. Klein, P. G. Andres, C. A. London, M. P. Lodge, R. C. Mulligan, and A. K. Abbas. 2000. Expression of Bcl-XL restores cell survival, but not proliferation and effector differentiation, in CD28-deficient T lymphocytes. *J. Exp. Med. 191:2031*.

Fleming, H. E., and C. J. Paige. 2001. Pre-B cell receptor signaling mediates selective response to IL-7 at the pro-B to pre-B cell transition via an ERK/MAP kinase-dependent pathway. *Immunity 15:521*.

Ghia, P., P. Transidico, J. P. Veiga, C. Schaniel, F. Sallusto, K. Matsushima, S. E. Sallan, A. G. Rolink, A. Mantovani, L. M. Nadler, and A. A. Cardoso. 2001. Chemoattractants MDC and TARC are secreted by malignant B-cell precursors following CD40 ligation and support the migration of leukemia-specific T cells. *Blood 98:533*.

Goan, S. R., I. Junghahn, M. Wissler, M. Becker, J. Aumann, U. Just, G. Martiny-Baron, I. Fichtner, and R. Henschler. 2000. Donor stromal cells from human blood engraft in NOD/SCID mice. *Blood 96:3971*.

Gongora, R., R. P. Stephan, Z. Zhang, and M. D. Cooper. 2001. An essential role for Daxx in the inhibition of B lymphopoiesis by type I interferons. *Immunity 14:727*.

Habibian, H. K., S. O. Peters, C. C. Hsieh, J. Wuu, K. Vergilis, C. I. Grimaldi, J. Reilly, J. E. Carlson, A. E. Frimberger, F. M. Stewart, and P. J. Quesenberry. 1998. The fluctuating phenotype of the lymphohematopoietic stem cell with cell cycle transit. *J Exp Med 188:393*.

Henckaerts, E., H. Geiger, J. C. Langer, P. Rebollo, G. Van Zant, and H. W. Snoeck. 2002. Genetically determined variation in the number of phenotypically defined hematopoietic progenitor and stem cells and in their response to early-acting cytokines. *Blood 99:3947*.

Herblot, S., P. D. Aplan, and T. Hoang. 2002. Gradient of E2A activity in B-cell development. *Mol Cell Biol 22:886*.

Izon, D. J., J. C. Aster, Y. He, A. Weng, F. G. Karnell, V. Patriub, L. Xu, S. Bakkour, C. Rodriguez, D. Allman, and W. S. Pear. 2002. Deltex1 redirects lymphoid progenitors to the B cell lineage by antagonizing Notch1. *Immunity 16:231*.

Jackson, K. A., T. Mi, and M. A. Goodell. 1999. Hematopoietic potential of stem cells isolated from murine skeletal muscle. *PNAS U S A 96:14482*.

Jackson, K. A., S. M. Majka, H. Wang, J. Pocius, C. J. Hartley, M. W. Majesky, M. L. Entman, L. H. Michael, K. K. Hirschi, and M. A. Goodell. 2001. Regeneration of ischemic cardiac muscle and vascular endothelium by adult stem cells. *J Clin Invest 107:1395*.

Kaeser, P. S., M. A. Klein, P. Schwarz, and A. Aguzzi. 2001. Efficient lymphoreticular prion propagation requires PrP(c) in stromal and hematopoietic cells. *J Virol 75:7097*.

Kirby, S., W. Walton, and O. Smithies. 2000. Hematopoietic stem cells with controllable tEpoR transgenes have a competitive advantage in bone marrow transplantation. *Blood 95:3710*.

Kouro, T., K. L. Medina, K. Oritani, and P. W. Kincade. 2001. Characteristics of early murine B-lymphocyte precursors and their direct sensitivity to negative regulators. *Blood 97:2708*.

Kouro, T., V. Kumar, and P. W. Kincade. 2002. Relationships between early B- and NK-lineage lymphocyte precursors in bone marrow. *Blood 100:3672*.

Kubota, H., and L. M. Reid. 2000. Clonogenic hepatoblasts, common precursors for hepatocytic and biliary lineages, are lacking classical major histocompatibility complex class I antigen. *PNAS 97:12132*.

Kuehnle, I., M. H. Huls, Z. Liu, M. Semmelmann, R. A. Krance, M. K. Brenner, C. M. Rooney, and H. E. Heslop. 2000. CD20 monoclonal antibody (rituximab) for therapy of Epstein-Barr virus lymphoma after hematopoietic stem-cell transplantation. *Blood 95:1502*.

Lu, L. S., J. Tung, N. Baumgarth, O. Herman, M. Gleimer, and L. A. Herzenberg. 2002. Identification of a germ-line pro-B cell subset that distinguishes the fetal/neonatal from the adult B cell development pathway. *PNAS 99:3007*.

Majka, S. M., K. A. Jackson, K. A. Kienstra, M. W. Majesky, M. A. Goodell, and K. K. Hirschi. 2003. Distinct progenitor populations in skeletal muscle are bone marrow derived and exhibit different cell fates during vascular regeneration. *J Clin Invest 111:71*.

Manz, M. G., T. Miyamoto, K. Akashi, and I. L. Weissman. 2002. Prospective isolation of human clonogenic common myeloid progenitors. *PNAS 99:11872*.

Martin, F., and J. F. Kearney. 2000. Positive selection from newly formed to marginal zone B cells depends on the rate of clonal production, CD19, and btk. *Immunity 12:39*.

McKinney-Freeman, S. L., K. A. Jackson, F. D. Camargo, G. Ferrari, F. Mavilio, and M. A. Goodell. 2002. Muscle-derived hematopoietic stem cells are hematopoietic in origin. *PNAS 99:1341*.

Metcalf, D., L. Di Rago, and S. Mifsud. 2002. Synergistic and inhibitory interactions in the in vitro control of murine megakaryocyte colony formation. *Stem Cells 20:552*.

Mikkola, H. K. A., Y. Fujiwara, T. M. Schlaeger, D. Traver, and S. H. Orkin. 2003. Expression of CD41 marks the initiation of definitive hematopoiesis in the mouse embryo. *Blood 101:508*.

Moore, K. A., H. Ema, and I. R. Lemischka. 1997. In vitro maintenance of highly purified, transplantable hematopoietic stem cells. *Blood 89:4337*.

Nilsson, S. K., M. S. Dooner, and P. J. Quesenberry. 1997. Synchronized cell-cycle induction of engrafting long-term repopulating stem cells. *Blood 90:4646*.

Ogilvy, S., D. Metcalf, L. Gibson, M. L. Bath, A. W. Harris, and J. M. Adams. 1999. Promoter elements of vav drive transgene expression in vivo throughout the hematopoietic compartment. *Blood 94:1855*.

Okuno, Y., H. Iwasaki, C. S. Huettner, H. S. Radomska, D. A. Gonzalez, D. G. Tenen, and K. Akashi. 2002. Differential regulation of the human and murine CD34 genes in hematopoietic stem cells. *PNAS 99:6246*.

Okuno, Y., C. S. Huettner, H. S. Radomska, V. Petkova, H. Iwasaki, K. Akashi, and D. G. Tenen. 2002. Distal elements are critical for human CD34 expression in vivo. *Blood 100:4420*.

Pyatt, D. W., W. S. Stillman, Y. Yang, S. Gross, J. H. Zheng, and R. D. Irons. 1999. An essential role for NF-κB in human $CD34^+$ bone marrow cell survival. *Blood 93:3302*.

Radomska, H. S., D. A. Gonzalez, Y. Okuno, H. Iwasaki, A. Nagy, K. Akashi, D. G. Tenen, and C. S. Huettner. 2002. Transgenic targeting with regulatory elements of the human CD34 gene. *Blood 100:4410*.

Reddy, G. P., C. Y. Tiarks, L. Pang, J. Wuu, C. C. Hsieh, and P. J. Quesenberry. 1997. Cell cycle analysis and synchronization of pluripotent hematopoietic progenitor stem cells. *Blood 90:2293*.

Santulli-Marotto, S., M. W. Retter, R. Gee, M. J. Mamula, and S. H. Clarke. 1998. Autoreactive B cell regulation: peripheral induction of developmental arrest by lupus-associated autoantigens. *Immunity 8:209*.

Schaniel, C., L. Bruno, F. Melchers, and A. G. Rolink. 2002. Multiple hematopoietic cell lineages develop in vivo from transplanted Pax5-deficient pre-B I-cell clones. *Blood 99:472*.

Shih, C. C., M. C. Hu, J. Hu, J. Medeiros, and S. J. Forman. 1999. Long-term ex vivo maintenance and expansion of transplantable human hematopoietic stem cells. *Blood 94:1623*.

Shih, C. C., M. C. Hu, J. Hu, Y. Weng, P. J. Yazaki, J. Medeiros, and S. J. Forman. 2000. A secreted and LIF-mediated stromal cell-derived activity that promotes ex vivo expansion of human hematopoietic stem cells. *Blood 95:1957*.

Shih, C. C., Y. Weng, A. Mamelak, T. LeBon, M. C. Hu, and S. J. Forman. 2001. Identification of a candidate human neurohematopoietic stem-cell population. *Blood 98:2412*.

Spyridonidis, A., M. Schmidt, W. Bernhardt, A. Papadimitriou, M. Azemar, W. Wels, B. Groner, and R. Henschler. 1998. Purging of mammary carcinoma cells during ex vivo culture of $CD34^+$ hematopoietic progenitor cells with recombinant immunotoxins. *Blood 91:1820*.

Stewart, F. M., S. Zhong, J. Wuu, C. Hsieh, S. K. Nilsson, and P. J. Quesenberry. 1998. Lymphohematopoietic engraftment in minimally myeloablated hosts. *Blood 91:3681*.

Wright, D. E., E. P. Bowman, A. J. Wagers, E. C. Butcher, and I. L. Weissman. 2002. Hematopoietic stem cells are uniquely selective in their migratory response to chemokines. *J Exp Med 195:1145*.

Wulf, G. G., R. Y. Wang, I. Kuehnle, D. Weidner, F. Marini, M. K. Brenner, M. Andreeff, and M. A. Goodell. 2001. A leukemic stem cell with intrinsic drug efflux capacity in acute myeloid leukemia. *Blood 98:1166*.

Zhong, J. F., Y. Zhan, W. F. Anderson, and Y. Zhao. 2002. Murine hematopoietic stem cell distribution and proliferation in ablated and nonablated bone marrow transplantation. *Blood 100:3521*.

T Cells

Allenspach, E. J., P. Cullinan, J. Tong, Q. Tang, A. G. Tesciuba, J. L. Cannon, S. M. Takahashi, R. Morgan, J. K. Burkhardt, and A. I. Sperling. 2001. ERM-dependent movement of CD43 defines a novel protein complex distal to the immunological synapse. *Immunity 15:739*.

Avitahl, N., S. Winandy, C. Friedrich, B. Jones, Y. Ge, and K. Georgopoulos. 1999. Ikaros sets thresholds for T cell

activation and regulates chromosome propagation. *Immunity 10:333*.

Bachmann, M. F., A. Gallimore, S. Linkert, V. Cerundolo, A. Lanzavecchia, M. Kopf, and A. Viola. 1999. Developmental regulation of Lck targeting to the CD8 coreceptor controls signaling in naive and memory T cells. *J Exp Med 189:1521*.

Baumgarth, N., G. C. Jager, O. C. Herman, and L. A. Herzenberg. 2000. CD4+ T cells derived from B cell-deficient mice inhibit the establishment of peripheral B cell pools. *PNAS 97:4766*.

Baur, N., G. Nerz, A. Nil, and K. Eichmann. 2001. Expression and selection of productively rearranged TCR β VDJ genes are sequentially regulated by CD3 signaling in the development of NK1.1(+)αβT cells. *Int Immunol 13:1031*.

Briken, V., R. M. Jackman, G. F. M. Watts, R. A. Rogers, and S. A. Porcelli. 2000. Human CD1b and CD1c Isoforms Survey Different Intracellular Compartments for the Presentation of Microbial Lipid Antigens. *J. Exp. Med. 192:281*.

Buslepp, J., S. E. Kerry, D. Loftus, J. A. Frelinger, E. Appella, and E. J. Collins. 2003. High Affinity Xenoreactive TCR:MHC Interaction Recruits CD8 in Absence of Binding to MHC. *J Immunol 170:373*.

Cipriani, B., G. Borsellino, F. Poccia, R. Placido, D. Tramonti, S. Bach, L. Battistini, and C. F. Brosnan. 2000. Activation of C-C β-chemokines in human peripheral blood γδ T cells by isopentenyl pyrophosphate and regulation by cytokines. *Blood 95:39*.

Cunard, R., D. DiCampli, D. C. Archer, J. L. Stevenson, M. Ricote, C. K. Glass, and C. J. Kelly. 2002. WY14,643, a PPARα ligand, has profound effects on immune responses in vivo. *J Immunol 169:6806*.

Dahl, A. M., C. Klein, P. G. Andres, C. A. London, M. P. Lodge, R. C. Mulligan, and A. K. Abbas. 2000. Expression of Bcl-XL restores cell survival, but not proliferation and effector differentiation, in CD28-deficient T lymphocytes. *J. Exp. Med. 191:2031*.

Dorris, D. R., and K. Struhl. 2000. Artificial recruitment of TFIID, but not RNA polymerase II holoenzyme, activates transcription in mammalian cells. *Mol Cell Biol 20:4350*.

Doyle, A. M., A. C. Mullen, A. V. Villarino, A. S. Hutchins, F. A. High, H. W. Lee, C. B. Thompson, and S. L. Reiner. 2001. Induction of cytotoxic T lymphocyte antigen 4 (CTLA-4) restricts clonal expansion of helper T cells. *J Exp Med 194:893*.

Dyall, R., and J. Nikolic-Zugic. 1999. The final maturation of at least some single-positive CD4(hi) thymocytes does not require T cell receptor-major histocompatibility complex contact. *J Exp Med 190:757*.

Felix, N. J., W. J. Brickey, R. Griffiths, J. Zhang, L. Van Kaer, T. Coffman, and J. P. Ting. 2000. H2-DMα (-/-) mice show the importance of major histocompatibility complex-bound peptide in cardiac allograft rejection. *J Exp Med 192:31*.

Fiorini, E., I. Schmitz, W. E. Marissen, S. L. Osborn, M. Touma, T. Sasada, P. A. Reche, E. V. Tibaldi, R. E. Hussey, A. M. Kruisbeek, E. L. Reinherz, and L. K. Clayton. 2002. Peptide-induced negative selection of thymocytes activates transcription of an NF-κB inhibitor. *Mol Cell 9:637*.

Fowell, D. J., K. Shinkai, X. C. Liao, A. M. Beebe, R. L. Coffman, D. R. Littman, and R. M. Locksley. 1999. Impaired NFATc translocation and failure of Th2 development in Itk-deficient CD4+ T cells. *Immunity 11:399*.

Gartner, F., F. W. Alt, R. Monroe, M. Chu, B. P. Sleckman, L. Davidson, and W. Swat. 1999. Immature thymocytes employ distinct signaling pathways for allelic exclusion versus differentiation and expansion. *Immunity 10:537*.

Ghia, P., P. Transidico, J. P. Veiga, C. Schaniel, F. Sallusto, K. Matsushima, S. E. Sallan, A. G. Rolink, A. Mantovani, L. M. Nadler, and A. A. Cardoso. 2001. Chemoattractants MDC and TARC are secreted by malignant B-cell precursors following CD40 ligation and support the migration of leukemia-specific T cells. *Blood 98:533*.

Gibbons, D., N. C. Douglas, D. F. Barber, Q. Liu, R. Sullo, L. Geng, H. J. Fehling, H. von Boehmer, and A. C. Hayday. 2001. The biological activity of natural and mutant pTα alleles. *J Exp Med 194:695*.

Girardi, M., D. E. Oppenheim, C. R. Steele, J. M. Lewis, E. Glusac, R. Filler, P. Hobby, B. Sutton, R. E. Tigelaar, and A. C. Hayday. 2001. Regulation of cutaneous malignancy by γδ T cells. *Science 294:605*.

Gnjatic, S., Y. Nagata, E. Jager, E. Stockert, S. Shankara, B. L. Roberts, G. P. Mazzara, S. Y. Lee, P. R. Dunbar, B. Dupont, V. Cerundolo, G. Ritter, Y. T. Chen, A. Knuth, and L. J. Old. 2000. Strategy for monitoring T cell responses to NY-ESO-1 in patients with any HLA class I allele. *PNAS 97:10917*.

Goldrath, A. W., P. V. Sivakumar, M. Glaccum, M. K. Kennedy, M. J. Bevan, C. Benoist, D. Mathis, and E. A. Butz. 2002. Cytokine requirements for acute and basal homeostatic proliferation of naive and memory CD8+ T cells. *J. Exp. Med. 195:1515*.

Grogan, J. L., M. Mohrs, B. Harmon, D. A. Lacy, J. W. Sedat, and R. M. Locksley. 2001. Early transcription and silencing

of cytokine genes underlie polarization of T helper cell subsets. *Immunity 14:205*.

Hildeman, D. A., T. Mitchell, T. K. Teague, P. Henson, B. J. Day, J. Kappler, and P. C. Marrack. 1999. Reactive oxygen species regulate activation-induced T cell apoptosis. *Immunity 10:735*.

Hirst, C. E., M. S. Buzza, C. H. Bird, H. S. Warren, P. U. Cameron, M. Zhang, P. G. Ashton-Rickardt, and P. I. Bird. 2003. The intracellular granzyme B inhibitor, proteinase inhibitor 9, is up-regulated during accessory cell maturation and effector cell degranulation, and its overexpression enhances CTL potency. *J Immunol 170:805*.

Ho, I. C., D. Lo, and L. H. Glimcher. 1998. c-maf promotes T helper cell type 2 (Th2) and attenuates Th1 differentiation by both interleukin 4-dependent and -independent mechanisms. *J Exp Med 188:1859*.

Hori, S., M. Haury, A. Coutinho, and J. Demengeot. 2002. Specificity requirements for selection and effector functions of CD25+4+ regulatory T cells in anti-myelin basic protein T cell receptor transgenic mice. *PNAS 99:8213*.

Izon, D. J., J. A. Punt, L. Xu, F. G. Karnell, D. Allman, P. S. Myung, N. J. Boerth, J. C. Pui, G. A. Koretzky, and W. S. Pear. 2001. Notch1 regulates maturation of CD4+ and CD8+ thymocytes by modulating TCR signal strength. *Immunity 14:253*.
Kim, J. I., I. C. Ho, M. J. Grusby, and L. H. Glimcher. 1999. The transcription factor c-Maf controls the production of interleukin-4 but not other Th2 cytokines. *Immunity 10:745*.

Kita, H., S. Matsumura, X. S. He, A. A. Ansari, Z. X. Lian, J. Van de Water, R. L. Coppel, M. M. Kaplan, and M. E. Gershwin. 2002. Quantitative and functional analysis of PDC-E2-specific autoreactive cytotoxic T lymphocytes in primary biliary cirrhosis. *J Clin Invest 109:1231*.

Kochenderfer, J. N., S. Kobayashi, E. D. Wieder, C. Su, and J. J. Molldrem. 2002. Loss of T-lymphocyte clonal dominance in patients with myelodysplastic syndrome responsive to immunosuppression. *Blood 100:3639*.

Koehne, G., H. F. Gallardo, M. Sadelain, and R. J. O'Reilly. 2000. Rapid selection of antigen-specific T lymphocytes by retroviral transduction. *Blood 96:109*.

Koehne, G., K. M. Smith, T. L. Ferguson, R. Y. Williams, G. Heller, E. G. Pamer, B. Dupont, and R. J. O'Reilly. 2002. Quantitation, selection, and functional characterization of Epstein-Barr virus-specific and alloreactive T cells detected by intracellular interferon-γ production and growth of cytotoxic precursors. *Blood 99:1730*.

Lieberson, R., K. A. Mowen, K. D. McBride, V. Leautaud, X. Zhang, W. K. Suh, L. Wu, and L. H. Glimcher. 2001. Tumor necrosis factor receptor-associated factor (TRAF)2 represses the T helper cell type 2 response through interaction with NFAT-interacting protein (NIP45). *J Exp Med 194:89*.

McGavin, M. K., K. Badour, L. A. Hardy, T. J. Kubiseski, J. Zhang, and K. A. Siminovitch. 2001. The intersectin 2 adaptor links Wiskott Aldrich Syndrome protein (WASp)-mediated actin polymerization to T cell antigen receptor endocytosis. *J Exp Med 194:1777*.

Mohrs, M., K. Shinkai, K. Mohrs, and R. M. Locksley. 2001. Analysis of type 2 immunity in vivo with a bicistronic IL-4 reporter. *Immunity 15:303*.

Monroe, R. J., K. J. Seidl, F. Gaertner, S. Han, F. Chen, J. Sekiguchi, J. Wang, R. Ferrini, L. Davidson, G. Kelsoe, and F. W. Alt. 1999. RAG2:GFP knockin mice reveal novel aspects of RAG2 expression in primary and peripheral lymphoid tissues. *Immunity 11:201*.

Moron, G., P. Rueda, I. Casal, and C. Leclerc. 2002. CD8α- CD11b+ dendritic cells present exogenous virus-like particles to CD8+ T cells and subsequently express CD8α and CD205 molecules. *J Exp Med 195:1233*.

Nishizawa, K., C. Freund, J. Li, G. Wagner, and E. L. Reinherz. 1998. Identification of a proline-binding motif regulating CD2-triggered T lymphocyte activation. *PNAS 95:14897*.

Ohdan, H., Y. G. Yang, A. Shimizu, K. G. Swenson, and M. Sykes. 1999. Mixed chimerism induced without lethal conditioning prevents T cell- and anti-Gal α 1,3Gal-mediated graft rejection. *J Clin Invest 104:281*.

Ouyang, W., M. Lohning, Z. Gao, M. Assenmacher, S. Ranganath, A. Radbruch, and K. M. Murphy. 2000. Stat6-independent GATA-3 autoactivation directs IL-4-independent Th2 development and commitment. *Immunity 12:27*.

Pestano, G. A., Y. Zhou, L. A. Trimble, J. Daley, G. F. Weber, and H. Cantor. 1999. Inactivation of misselected CD8 T cells by CD8 gene methylation and cell death. *Science 284:1187*.

Poussier, P., T. Ning, D. Banerjee, and M. Julius. 2002. A unique subset of self-specific intraintestinal T cells maintains gut integrity. *J Exp Med 195:1491*.

Rengarajan, J., K. A. Mowen, K. D. McBride, E. D. Smith, H. Singh, and L. H. Glimcher. 2002. Interferon regulatory factor 4 (IRF4) interacts with NFATc2 to modulate interleukin 4 gene expression. *J Exp Med 195:1003*.

Reuther-Madrid, J. Y., D. Kashatus, S. Chen, X. Li, J. Westwick, R. J. Davis, H. S. Earp, C.-Y. Wang, and A. S. Baldwin, Jr. 2002. The p65/RelA subunit of NF-κB suppresses the sustained, antiapoptotic activity of Jun kinase induced by tumor necrosis factor. *Mol. Cell. Biol. 22:8175*.

Riese, R. J., G. P. Shi, J. Villadangos, D. Stetson, C. Driessen, A. M. Lennon-Dumenil, C. L. Chu, Y. Naumov, S. M. Behar, H. Ploegh, R. Locksley, and H. A. Chapman. 2001. Regulation of CD1 function and NK1.1(+) T cell selection and maturation by cathepsin S. *Immunity 15:909*.

Seo, S. J., M. L. Fields, J. L. Buckler, A. J. Reed, L. Mandik-Nayak, S. A. Nish, R. J. Noelle, L. A. Turka, F. D. Finkelman, A. J. Caton, and J. Erikson. 2002. The impact of T helper and T regulatory cells on the regulation of anti-double-stranded DNA B cells. *Immunity 16:535*.

Shires, J., E. Theodoridis, and A. C. Hayday. 2001. Biological insights into TCRγδ+ and TCRαβ+ intraepithelial lymphocytes provided by serial analysis of gene expression (SAGE). *Immunity 15:419*.

Strong, J., Q. Wang, and N. Killeen. 2001. Impaired survival of T helper cells in the absence of CD4. *PNAS 98:2566*.

Szmania, S., A. Galloway, M. Bruorton, P. Musk, G. Aubert, A. Arthur, H. Pyle, N. Hensel, N. Ta, L. Lamb, Jr, T. Dodi, A. Madrigal, J. Barrett, J. Henslee-Downey, and F. van Rhee. 2001. Isolation and expansion of cytomegalovirus-specific cytotoxic T lymphocytes to clinical scale from a single blood draw using dendritic cells and HLA-tetramers. *Blood 98:505*.

Teague, T. K., D. Hildeman, R. M. Kedl, T. Mitchell, W. Rees, B. C. Schaefer, J. Bender, J. Kappler, and P. Marrack. 1999. Activation changes the spectrum but not the diversity of genes expressed by T cells. *PNAS 96:12691*.

Teague, T. K., B. C. Schaefer, D. Hildeman, J. Bender, T. Mitchell, J. W. Kappler, and P. Marrack. 2000. Activation-induced inhibition of interleukin 6-mediated T cell survival and signal transducer and activator of transcription 1 signaling. *J Exp Med 191:915*.

Tibaldi, E. V., R. Salgia, and E. L. Reinherz. 2002. CD2 molecules redistribute to the uropod during T cell scanning: Implications for cellular activation and immune surveillance. *PNAS 99:7582*.

Usherwood, E. J., R. J. Hogan, G. Crowther, S. L. Surman, T. L. Hogg, J. D. Altman, and D. L. Woodland. 1999. Functionally heterogeneous CD8(+) T-cell memory is induced by Sendai virus infection of mice. *J Virol 73:7278*.

Vivien, L., C. Benoist, and D. Mathis. 2001. T lymphocytes need IL-7 but not IL-4 or IL-6 to survive in vivo. *Int Immunol 13:763*.

Voehringer, D., M. Koschella, and H. Pircher. 2002. Lack of proliferative capacity of human effector and memory T cells expressing killer cell lectinlike receptor G1 (KLRG1). *Blood 100:3698*.

Wagner, D. H., Jr., G. Vaitaitis, R. Sanderson, M. Poulin, C. Dobbs, and K. Haskins. 2002. Expression of CD40 identifies a unique pathogenic T cell population in type 1 diabetes. *PNAS 99:3782*.

Walker, L. S. K., L. J. Ausubel, A. Chodos, N. Bekarian, and A. K. Abbas. 2002. CTLA-4 Differentially Regulates T cell responses to endogenous tissue protein versus exogenous immunogen. *J Immunol 169:6202*.

Wang, B., A. Sharma, R. Maile, M. Saad, E. J. Collins, and J. A. Frelinger. 2002. Peptidic termini play a significant role in TCR recognition. *J Immunol 169:3137*.

Wen, R., D. Wang, C. McKay, K. D. Bunting, J. C. Marine, E. F. Vanin, G. P. Zambetti, S. J. Korsmeyer, J. N. Ihle, and J. L. Cleveland. 2001. Jak3 selectively regulates Bax and Bcl-2 expression to promote T-cell development. *Mol Cell Biol 21:678*.

Wilson, S. B., S. C. Kent, H. F. Horton, A. A. Hill, P. L. Bollyky, D. A. Hafler, J. L. Strominger, and M. C. Byrne. 2000. Multiple differences in gene expression in regulatory Vα 24JαQ T cells from identical twins discordant for type I diabetes. *PNAS 97:7411*.

Winandy, S., L. Wu, J. H. Wang, and K. Georgopoulos. 1999. Pre-T cell receptor (TCR) and TCR-controlled checkpoints in T cell differentiation are set by Ikaros. *J Exp Med 190:1039*.

Workman, C. J., K. J. Dugger, and D. A. A. Vignali. 2002. Cutting edge: Molecular analysis of the negative regulatory function of lymphocyte activation gene-3. *J Immunol 169:5392*.

Zhong, X.-P., E. A. Hainey, B. A. Olenchock, H. Zhao, M. K. Topham, and G. A. Koretzky. 2002. Regulation of T cell receptor-induced activation of the ras-ERK pathway by diacylglycerol kinase zeta *J. Biol. Chem. 277:31089*.

Viruses

Babcock, G. J., and D. A. Thorley-Lawson. 2000. Tonsillar memory B cells, latently infected with Epstein-Barr virus, express the restricted pattern of latent genes previously found only in Epstein-Barr virus-associated tumors. PNAS

97:12250.

Bannert, N., M. Farzan, D. S. Friend, H. Ochi, K. S. Price, J. Sodroski, and J. A. Boyce. 2001. Human Mast cell progenitors can be infected by macrophagetropic human immunodeficiency virus type 1 and retain virus with maturation in vitro. J Virol 75:10808.

Barchet, W., M. Cella, B. Odermatt, C. Asselin-Paturel, M. Colonna, and U. Kalinke. 2002. Virus-induced interferon-α production by a dendritic cell subset in the absence of feedback signaling in vivo. J Exp Med 195:507.

Baric, R. S., E. Sullivan, L. Hensley, B. Yount, and W. Chen. 1999. Persistent infection promotes cross-species transmissibility of mouse hepatitis virus. J Virol 73:638.

Baron, J. L., L. Gardiner, S. Nishimura, K. Shinkai, R. Locksley, and D. Ganem. 2002. Activation of a nonclassical NKT cell subset in a transgenic mouse model of hepatitis B virus infection. Immunity 16:583.

Baumgarth, N., O. C. Herman, G. C. Jager, L. Brown, and L. A. Herzenberg. 1999. Innate and acquired humoral immunities to influenza virus are mediated by distinct arms of the immune system. PNAS 96:2250.

Baumgarth, N., O. C. Herman, G. C. Jager, L. E. Brown, L. A. Herzenberg, and J. Chen. 2000. B-1 and B-2 Cell-derived Immunoglobulin M Antibodies Are Nonredundant Components of the Protective Response to Influenza Virus Infection. J. Exp. Med. 192:271.

Drexler, I., C. Staib, W. Kastenmuller, S. Stevanovic', B. Schmidt, F. A. Lemonnier, H.-G. Rammensee, D. H. Busch, H. Bernhard, V. Erfle, and G. Sutter. 2003. Identification of vaccinia virus epitope-specific HLA-A*0201-restricted T cells and comparative analysis of smallpox vaccines. PNAS 100:217.

Fong, L., M. Mengozzi, N. W. Abbey, B. G. Herndier, and E. G. Engleman. 2002. Productive infection of plasmacytoid dendritic cells with human immunodeficiency virus type 1 is triggered by CD40 ligation. J. Virol. 76:11033.

Gao, J., B. P. De, and A. K. Banerjee. 1999. Human parainfluenza virus type 3 up-regulates major histocompatibility complex class I and II expression on respiratory epithelial cells: involvement of a STAT1- and CIITA-independent pathway. J Virol 73:1411.

Gao, J., B. P. De, Y. Han, S. Choudhary, R. Ransohoff, and A. K. Banerjee. 2001. Human parainfluenza virus type 3 inhibits γinterferon-induced major histocompatibility complex class II expression directly and by inducing α/β interferon. J Virol 75:1124.

Gnjatic, S., Y. Nagata, E. Jager, E. Stockert, S. Shankara, B. L. Roberts, G. P. Mazzara, S. Y. Lee, P. R. Dunbar, B. Dupont, V. Cerundolo, G. Ritter, Y. T. Chen, A. Knuth, and L. J. Old. 2000. Strategy for monitoring T cell responses to NY-ESO-1 in patients with any HLA class I allele. PNAS 97:10917.

Gordadze, A. V., R. Peng, J. Tan, G. Liu, R. Sutton, B. Kempkes, G. W. Bornkamm, and P. D. Ling. 2001. Notch1IC partially replaces EBNA2 function in B cells immortalized by Epstein-Barr virus. J Virol 75:5899.

Johnson, J. A., and J. D. Gangemi. 1999. Selective inhibition of human papillomavirus-induced cell proliferation by (S)-1-[3-hydroxy-2-(phosphonylmethoxy)propyl]cytosine. Antimicrob Agents Chemother 43:1198.

Joseph, A. M., G. J. Babcock, and D. A. Thorley-Lawson. 2000. Cells expressing the Epstein-Barr virus growth program are present in and restricted to the naive B-cell subset of healthy tonsils. J Virol 74:9964.

Koehne, G., H. F. Gallardo, M. Sadelain, and R. J. O'Reilly. 2000. Rapid selection of antigen-specific T lymphocytes by retroviral transduction. Blood 96:109.

Koehne, G., K. M. Smith, T. L. Ferguson, R. Y. Williams, G. Heller, E. G. Pamer, B. Dupont, and R. J. O'Reilly. 2002. Quantitation, selection, and functional characterization of Epstein-Barr virus-specific and alloreactive T cells detected by intracellular interferon-γ production and growth of cytotoxic precursors. Blood 99:1730.

Kuehnle, I., M. H. Huls, Z. Liu, M. Semmelmann, R. A. Krance, M. K. Brenner, C. M. Rooney, and H. E. Heslop. 2000. CD20 monoclonal antibody (rituximab) for therapy of Epstein-Barr virus lymphoma after hemopoietic stem-cell transplantation. Blood 95:1502.

Laichalk, L. L., D. Hochberg, G. J. Babcock, R. B. Freeman, and D. A. Thorley-Lawson. 2002. The dispersal of mucosal memory B cells: Evidence from persistent EBV infection. Immunity 16:745.

Leon, R. P., T. Hedlund, S. J. Meech, S. Li, J. Schaack, S. P. Hunger, R. C. Duke, and J. DeGregori. 1998. Adenoviral-mediated gene transfer in lymphocytes. PNAS 95:13159.

Lewin, S. R., R. M. Ribeiro, G. R. Kaufmann, D. Smith, J. Zaunders, M. Law, A. Solomon, P. U. Cameron, D. Cooper, and A. S. Perelson. 2002. Dynamics of T cells and TCR excision circles differ after treatment of acute and chronic HIV infection J Immunol 169:4657.

Li, Y., L. Li, R. Wadley, S. W. Reddel, J. C. Qi, C. Archis, A. Collins, E. Clark, M. Cooley, S. Kouts, H. M. Naif, M. Alali, A. Cunningham, G. W. Wong, R. L. Stevens, and S. A. Krilis. 2001. Mast cells/basophils in the peripheral blood of allergic individuals who are HIV-1 susceptible due to their surface expression of CD4 and the chemokine receptors CCR3, CCR5, and CXCR4. Blood 97:3484.

Li, T., and J. Zhang. 2002. Intramolecular recombinations of Moloney murine leukemia virus occur during minus-strand DNA synthesis. J. Virol. 76:9614.

Mohri, H., A. S. Perelson, K. Tung, R. M. Ribeiro, B. Ramratnam, M. Markowitz, R. Kost, A. Hurley, L. Weinberger, D. Cesar, M. K. Hellerstein, and D. D. Ho. 2001. Increased turnover of T lymphocytes in HIV-1 infection and its reduction by antiretroviral therapy. J Exp Med 194:1277.

Okubo, E., J. M. Lehman, and T. D. Friedrich. 2003. Negative regulation of mitotic promoting factor by the checkpoint kinase Chk1 in simian virus 40 lytic infection. J. Virol. 77:1257.

Perez, O. D., G. P. Nolan, D. Magda, R. A. Miller, and L. A. Herzenberg. 2002. Motexafin gadolinium (Gd-Tex) selectively induces apoptosis in HIV-1 infected CD4+ T helper cells. PNAS 99:2270.

Qu, C., T. M. Moran, and G. J. Randolph. 2003. Autocrine type I IFN and contact with endothelium promote the presentation of influenza A virus by monocyte-derived APC. J Immunol 170:1010.

Simard, M. C., P. Chrobak, D. G. Kay, Z. Hanna, S. Jothy, and P. Jolicoeur. 2002. Expression of simian immunodeficiency virus nef in immune cells of transgenic mice leads to a severe AIDS-like disease. J Virol 76:3981.

Stripecke, R., A. A. Cardoso, K. A. Pepper, D. C. Skelton, X. J. Yu, L. Mascarenhas, K. I. Weinberg, L. M. Nadler, and D. B. Kohn. 2000. Lentiviral vectors for efficient delivery of CD80 and granulocyte-macrophage- colony-stimulating factor in human acute lymphoblastic leukemia and acute myeloid leukemia cells to induce antileukemic immune responses. Blood 96:1317.

Sutkowski, N., B. Conrad, D. A. Thorley-Lawson, and B. T. Huber. 2001. Epstein-Barr virus transactivates the human endogenous retrovirus HERV-K18 that encodes a superantigen. Immunity 15:579.

Szmania, S., A. Galloway, M. Bruorton, P. Musk, G. Aubert, A. Arthur, H. Pyle, N. Hensel, N. Ta, L. Lamb, Jr, T. Dodi, A. Madrigal, J. Barrett, J. Henslee-Downey, and F. van Rhee. 2001. Isolation and expansion of cytomegalovirus-specific cytotoxic T lymphocytes to clinical scale from a single blood draw using dendritic cells and HLA-tetramers. Blood 98:505.

Usherwood, E. J., R. J. Hogan, G. Crowther, S. L. Surman, T. L. Hogg, J. D. Altman, and D. L. Woodland. 1999. Functionally heterogeneous CD8+ T-cell memory is induced by Sendai virus infection of mice. J Virol 73:7278.

van Rij, R. P., H. Blaak, J. A. Visser, M. Brouwer, R. Rientsma, S. Broersen, A. M. de Roda Husman, and H. Schuitemaker. 2000. Differential coreceptor expression allows for independent evolution of non-syncytium-inducing and syncytium-inducing HIV-1. J Clin Invest 106:1039.

van Rij, R. P., J. A. Visser, R. M. van Praag, R. Rientsma, J. M. Prins, J. M. Lange, and H. Schuitemaker. 2002. Both R5 and X4 human immunodeficiency virus type 1 variants persist during prolonged therapy with five antiretroviral drugs. J Virol 76:3054.

Williams, O. M., K. W. Hart, E. C. Y. Wang, and C. M. Gelder. 2002. Analysis of CD4+ T-cell responses to human papillomavirus (HPV) type 11 L1 in healthy adults reveals a high degree of responsiveness and cross-reactivity with other HPV types. J Virol 76:7418.

Zhang, L., S. R. Lewin, M. Markowitz, H. H. Lin, E. Skulsky, R. Karanicolas, Y. He, X. Jin, S. Tuttleton, M. Vesanen, H. Spiegel, R. Kost, J. van Lunzen, H. J. Stellbrink, S. Wolinsky, W. Borkowsky, P. Palumbo, L. G. Kostrikis, and D. D. Ho. 1999. Measuring recent thymic emigrants in blood of normal and HIV-1-infected individuals before and after effective therapy. J Exp Med 190:725.

Yeast

Flattery-O'Brien, J.A., and I.W. Dawes. 1998. Hydrogen peroxide causes RAD9-dependent cell cycle arrest in G2 in S. cerevisiae whereas Mendadione causes G1 arrest independent of RAD9 function. J Biol Chem 273(15): 8564-8571.

Zheng, B., J. N. Wu, W. Schober, D. E. Lewis, and T. Vida. 1998. Isolation of yeast mutants defective for localization of vacuolar vital dyes. PNAS 95:11721.